3-D GEOPHYSICAL MODELLING OF CONFIRMED AND SUSPECTED IMPACT CRATERS IN SOUTHERN ONTARIO, CANADA: CONSTRAINING STRUCTURE ORIGIN, SUBSURFACE GEOLOGY AND POST-IMPACT MODIFICATION

By MARY-HELEN ARMOUR, MSc

A Thesis Submitted to the School of Graduate Studies in Partial Fulfilment

of the Requirements for the Degree Doctor of Philosophy

McMaster University

McMaster University DOCTOR OF PHILOSOPHY (2022) Hamilton, Ontario
(School of Earth, Environment and Society)

TITLE: 3-D geophysical modelling of terrestrial impact craters in southern Ontario, Canada: constraining structure origin, subsurface geology and post-impact modification

AUTHOR: Mary-Helen Armour
SUPERVISOR: Dr. Joseph I. Boyce
NUMBER OF PAGES: i, 216

Abstract

Impact cratering is a fundamental geomorphic process on planetary surfaces. More than 60% of known hypervelocity impact craters on Earth are either partially or completely buried beneath post-impact sediments and one-third have been discovered with geophysical methods. In this thesis, geophysical surveys (gravity, magnetics, seismic, bathymetric mapping) were conducted at the deeply buried (>400 m) Holleford impact crater (~2.35 km) and two probable impact structures (Charity Shoal, Skeleton Lake) in southern Ontario, Canada. 3-D potential field models were constructed to determine the subsurface geology and buried crater morphology, and to evaluate evidence for possible impact versus endogenic origins.

Holleford Crater is a deeply buried, Late Proterozoic-Early Cambrian (ca. 550 ±100 Ma) simple impact crater (~2.4 km) in southeastern Ontario, Canada. Land-based magnetic and gravity surveys and modelling were conducted in this study, recorded a ~ -3 mGal Bouguer anomaly and small (~30 nT) magnetic anomaly over the crater basin. 3-D gravity modelling revealed a deeply buried simple impact basin in Mesoproterozoic basement with an estimated rim-to-rim diameter (D) of 1.8-2 km, a residual rim height of ~20-30 m and true depth (d_t) >400 m. The southeast crater rim is dissected by a 150 m deep, 400 m wide erosional channel produced by fluvial rim dissection. The outflow is infilled by >50 m of Late Cambrian clastic sediments, indicating a probable Late Proterozoic to Early Paleozoic impact event.

Charity Shoal is a 1.2-km-diameter, 20 m deep, circular bedrock shoal in eastern Lake Ontario. Marine seismic profiling and total field magnetic surveys (140-line km) were conducted over a 9-km^2 area and combined with available multi-beam bathymetric data to evaluate the subsurface geology and structure origin. Seismic surveys revealed ~30 m of Quaternary sediments overlying Middle Ordovician (Trenton Group) carbonates in the central basin and evidence for folding and faulting of the structure rim. Magnetic surveys recorded an annular magnetic high (> 600 nT) and a central magnetic low (~500-600 nT) coincident with a ~-1.7 mGal Bouguer gravity anomaly. The continuity of Middle Ordovician bedrock below the structure rules out a post-Paleozoic

intrusion and a pre-Paleozoic intrusion is ruled out with the gravity anomaly. A deeply-buried (> 450 m) impact crater is the only scenario consistent with geophysical evidence. The crater has a rim-to-rim diameter of ~1.2 km, and rim height of ~15-20 m. A 100-m wide breach in the southwestern rim records a possible outflow channel.

Skeleton Lake is a suspected (~4.0 km) Paleozoic-age impact structure in Muskoka, Ontario. The lakebed morphology, subsurface structure and possible impact origin were investigated with high-resolution geophysical surveys (magnetics, bathymetry; ~140 line-km) and 3-D magnetic modelling. Bathymetric data reveal a deep (>65 m) central basin with arcuate (Paleozoic?) bedrock ridges that rise >30 m above the southwestern lakebed. Magnetic surveys recorded a >700 nT magnetic low, which truncates northwest-southeast regional magnetic trends. Low-amplitude, northwest-trending magnetic lineaments delineate basement shear zones below the basin centre. Through-going magnetic lineaments and lack of thermal alteration (e.g., dikes, fenitization) in Mesoproterozoic rocks indicate a volcanic origin is unlikely. A 1.2 km diameter volcanic plug with an Early Cambrian remanence (D = 82.2°, I = 82.7°) can reproduce some aspects of the magnetic anomaly but is at odds with the Bouguer gravity anomaly (~ -3 mGal). Forward modelling of a crater-form basin with induction and remanence magnetization yielded an estimated structure depth of ~1200 m. The basement surface model shows a complex basement topography with no apparent rim structure and elevated ‘pinnacles’ that may represent eroded remnants of a central uplift or a highly-dissected basement topography. The structure apparent diameter (> 4.2 km) and complex basement topography suggest a heavily-modified transitional crater, similar with the Gow (Saskatchewan, Canada) and Kärdla (Estonia) impact structures.

This thesis demonstrates the subsurface exploration of confirmed and suspected impact structures, integrating seismic, potential field (magnetics, gravity) and digital elevation data within a 3-D geophysical modelling workflow. The approach provides

important new insights into the surface and subsurface geology, morphology, and post-emplacement modification of the Holleford impact crater, and new geophysical constraints for evaluating two suspected impact structures. Geophysical data confirm that Charity Shoal and Skeleton Lake are deep-seated, crater-form depressions in Mesoproterozoic basement rocks. The weight of geophysical and geological evidence points to impact cratering processes as opposed to an endogenic (volcanic) origin for both structures.

Keywords: Hypervelocity impact craters; geophysical surveys, 3-D potential field models, geophysical surveys, digital elevation models, crater subsurface geometry, post-impact modification.

Acknowledgements

I wish to thank all those who have made this thesis possible, first, my supervisor Dr. Joe Boyce and committee members, Drs. Bill Morris, Janok Bhattacharya and Alan Dickin, who continued over the years it took to complete this.

I wish to thank the external reviewer Dr. Catherine Neish, whose comments helped to improve this work.

I wish to thank those who assisted in field work: Doug Hrvoic, Ilya Inozemtsev, David Zilkey, Zack Shulman and Chandler Podhorodeski, without which I could not have had the data to complete the extensive modelling in this work. I also wish to thank Dr. Hernan Ugalde for help with modelling advice and instruction with the Modelvision software.

And most of all, I would like to thank my husband Paul and children Victoria and Lucas for the patience in putting up over the time consuming and often stressful process of creating a doctoral thesis.

The research was supported through Natural Sciences and Engineering Council of Canada (NSERC) Discovery Grants (RGPIN-2014-05829, 2022-05333) to J.I. Boyce and a York University research grant to M.H. Armour. Thanks to Marine Magnetics Corp. for providing magnetometer equipment for survey work. Geophysical data processing was made possible through academic software grants from Markit (HIS Kingdom), Seequent Ltd. (Geosoft, Canada) and Teledyne Caris. We thank Sander Geophysics Ltd. (Ottawa) for providing marine gravity data.

Table of Contents

List of Figures

Chapter 1

Chapter 2

Chapter 3

Chapter 4

List of Tables

Chapter 1: Introduction

1.1 Overview

Impact cratering is an important geomorphic process on planetary surfaces (Pilkington and Grieve, 1992; French and Koeberl, 2010) and has played a significant role in the evolution of Earth's biosphere (Ganapathy, 1982; Sleep et al., 1989; Schmitz et al., 2008). Impact craters are abundant on planetary bodies with solid surfaces throughout the Solar System (e.g., the Moon, Mars, Ganymede) but have low preservation on Earth's surface due to removal by erosion, burial below sediments, and tectonic processes (Osinski and Pierazzo, 2013). About ~60 % of known terrestrial impact craters are partially or wholly buried and most buried structures are found within intracratonic basins preserved below epicontinental sediments (Kenkmann, 2021).

The study of terrestrial hypervelocity impact craters is important for understanding the past frequency of impact events and their role in planetary geological and biological processes (French and Koeberl, 2010). Impact craters are also host to important economic mineral deposits (e.g., Sudbury, Ontario) and hydrocarbon reservoirs (Grieve and Masaitis, 1994; Mazur et al., 2000; Reimold et al., 2005). To date, 202 terrestrial impact craters have been positively identified on Earth (PASSC, 2022) and many probable and suspected impact sites remain to be confirmed. A range of criteria are used to recognize terrestrial hypervelocity impact craters, including crater morphology, the presence of breccias and impactites, but alone these are not considered as definitive evidence of an impact origin (Osinski and Pierazzo, 2013). The current standard for confirmation of an impact origin is the identification of shock metamorphic effects (e.g., shatter cones, planar deformation features) or direct evidence of an impacting meteorite (French and Koeberl, 2010). In many suspected impact craters, direct geological evidence may be absent or difficult to retrieve due to post-impact erosion or deep burial of impact structures (Stewart, 2003). Exploration drilling to recover impact breccias and target

rocks may also be economically unfeasible for very deeply buried structures. In such circumstances, geophysical investigations (e.g., seismic methods, gravity, magnetic surveys) are important tools for identifying and investigating impact structures (Pilkington and Grieve, 1992; Kenkmann, 2021) and can provide evidence in support of an impact origin (Stewart, 2003).

About one-third of known impact structures on Earth have been discovered using geophysical methods (French, 1998). Chicxulub (Mexico) and Chesapeake Bay (USA) are examples of large impact structures discovered during regional magnetic and gravity exploration work. Other impacts structures such as Montagnais (Canada) (French, 1998) and the suspected Silverpit structure in the North Sea (Stewart and Allen, 2002; Stewart, 2003) have been discovered during offshore 3-D seismic surveying for oil and gas exploration. In some instances, geophysical data may be the only evidence available for evaluating deeply buried structures due to economics or regulatory limitations on drilling (Stewart, 2003; Tsikalas and Eldholm, 2018).

Geophysical modelling is an important tool in the investigation of impact craters (Pilkington and Grieve, 1992). 2-D forward magnetic and gravity profile modelling has been employed widely to estimate impact structure depth, geometry (i.e., crater base morphology) and the diameter of buried structures, particularly in cases where borehole data are limited or unavailable (e.g., Puura and Suuroja, 1992; Evangelatos et.al., 2009). 2-D geophysical models are typically constructed as 2-D profiles across the centre of impact basins (Evangelatos et al., 2009; Urbini et al., 2012). Direct imaging of the 3-D subsurface structure of impact craters and basin fill sediments can also be achieved using multi-channel seismic reflection methods (Mazur et al., 2000; Jõeleht et al., 2018). For example, Stewart and Allen (2005) used a 3-D marine seismic volume to investigate the origin of the proposed Silverpit structure.

Sophisticated 3-D potential field models, which incorporate a broad array of geophysical data (e.g., gravity, magnetics, seismic reflection) with geological and borehole constraints, are now employed widely in mineral resource and oil and gas exploration (Jessell, 2001; Pratt et al., 2001; Oldenburg and Pratt, 2007; Tschirhart et al., 2013). A common goal of 3-D modelling is to determine the subsurface 3-dimensional form and geometry of ore bodies and host rocks, and to determine rock physical properties (Caumon et al., 2009; Spicer et al, 2011). Geophysical inversion methods are often used to predict physical properties within 3-D subsurface models; for example, the prediction of magnetic parameters (magnetic susceptibility, NRM) or the density distribution (Tschirhart et al., 2013). 3-D modelling approaches have had more limited application in impact geology studies (Pilkington and Hildebrand, 2000; Ugalde et al., 2007; Batista-Rodríguez et al., 2013). Ebbing et al. (2001) employed gravity, seismic and borehole data in a 3-D model of the Chicxulub impact to determine the size of the central peak, ring structure and breccia depth. Their modelling also revealed deviations in the crater symmetry and 3-D density variations in the crater infill improving earlier 2-D models. Ugalde et al. (2007) investigated the Bosumtwi impact crater using 3-D potential field models. Their results showed that highly magnetic bodies in the crystalline target rocks were the source of anomalies rather than the highly-magnetized melt volume.

3-D subsurface geophysical models have also been applied in exploring and testing the origins of suspected impact structures (French, 1998). For example, Tsikalas and Eldholm (2018) employed 3-D geophysical modelling to compare the Mjolnir impact crater (Norway) with the suspected Malvinas structure on the Falklands Plateau. They developed a processing flow that integrates a range of geophysical data types (e.g., seismic, bathymetric, magnetic and gravity) in the construction of detailed 3-dimensional models.

An important advantage of 3-D models over 2-D profiles is that the subsurface geometry and lateral continuity of geological units can be explicitly defined in models, providing a greater degree of confidence in subsurface geological interpretations, particularly when multiple geophysical data are combined ('data-fused') in the modelling process (e.g., Tsikalas and Eldholm, 2018). 3-D modelling also provides a means for evaluating probable impact structures prior to drilling and retrieval of core samples. 3-D geophysical models can also be employed to better resolve the depth and geometry of known impact structures, and to evaluate post-emplacement crater modification by erosion and tectonic processes.

1.2 Objectives and Scope

In this thesis, geophysical methods and 3-D potential field modelling were employed to investigate the subsurface geology of a confirmed simple impact crater and two suspected impact structures in south-central Ontario, Canada (Fig 1.1). An overarching objective was to evaluate 3-D geophysical modelling as tool for investigating the subsurface geology of terrestrial impact craters. Three different structures, ranging in size from 1.2 to > 4 km diameter, were investigated: the 2.35 km diameter Holleford impact crater (Chapter 2), located near Kingston, Ontario, and two suspected impact craters - the Charity Shoal structure (CSS; Chapter 3) and the Skeleton Lake structure (SLS; Chapter 4) (Fig 1.1). The modelling approach (section 1.5.1) employed *multi-parameter* geophysical investigations, integrating magnetic, gravity, bathymetric/DEM and seismic data in the construction of 3-D subsurface geological models. The new geophysical data better resolve the subsurface structure of the Holleford crater and provide new constraints for evaluating the possible impact origin of Charity Shoal and Skeleton Lake (e.g., Waddington and Dence, 1979; Holcombe et al., 2013; Suttak, 2013).

The specific research objectives were:

1) to better resolve the depth, subsurface geometry and infill stratigraphy of the Holleford impact crater using a 3-D gravity model constrained with borehole data,
2) to investigate post-impact modification at Holleford by comparison of the subsurface crater morphology with scaling functions,
3) to investigate the subsurface geological structure of the Charity Shoal and Skeleton Lake suspected impact structures, and;
4) to evaluate their proposed impact and endogenic origins considering new subsurface data and modelling results.

The dissertation is formatted as a 'sandwich style' thesis comprising three standalone papers formatted for eventual journal publication. As such, some background material on the study sites presented here is also briefly summarized in the introduction to the individual papers. Chapter 2 summarizes the results of ground geophysical surveys and gravity modelling of the Holleford Crater. 3-D models provide important new insights into the crater subsurface structure and post-emplacement modification by erosion processes. In Chapter 3, a large multi-parameter geophysical database (seismic, magnetics, multi-beam bathymetry) was assembled and integrated within a 3-D model to evaluate the origin of the CSS as an impact structure (Holcombe et al., 2013) or a volcanic intrusive (Suttak, 2013). In Chapter 4, high-resolution lake-based magnetic and bathymetric studies were employed to investigate the SLS, to model the structure depth to basement and to evaluate the proposed impact origin (Waddington and Dence, 1979; Clarke, 1982). The modelling demonstrates a complex basement structure, which may provide evidence for a highly modified transitional crater.

1.3 Study Sites and Previous Work

Three study sites were chosen in southern Ontario for the evaluation of 3-D geophysical modelling methods and multi-parameter geophysical studies (Fig. 1.1). This section briefly summarizes the previous work at each site and the research questions addressed in this thesis. The regional and site-scale geology and physical setting of study areas are discussed in more detail within the individual results chapters.

1.3.1 Early work – The Dominion Observatory of Canada

The search for impact craters in Canada began with the pioneering work of the Dominion Observatory of Canada (Beals et al., 1956; Grieve, 2006). In the 1950's and 1960's, interest developed among geologists in terrestrial impact craters with the recognition of Meteor Crater in Arizona and Reis crater in Germany as products of hypervelocity impacts by extraterrestrial objects (Grieve, 2006). The first systematic studies of impact craters in Canada were conducted by V.B. Meen (Meen, 1950, 1951), following the discovery of the 3.4 km diameter Pingualuit (formerly Chubb and New Quebec) crater in northern Quebec (Meen, 1950, 1951; Millman, 1956). This was followed by recognition of the Brent crater in Algonquin Park in south-central Ontario (Fig. 1.1; Millman et al., 1960) and the Mereweather crater in northwestern Labrador (Meen, 1957). Following this early work, C.S. Beals of the Dominion Observatory of Canada recognized that the geologically stable Canadian Shield was a likely location to find impact structures. Some skepticism and lack of interest on the part of the Geological Survey of Canada (GSC) at the time led Beals to initiate a search to discover possible impact sites in Canada (Beals, et al., 1956; Grieve, 2006). Beginning in 1955, the Dominion Observatory conducted a systematic search for impact structures using available stereo air photos. This work led to the discovery of a number of potential terrestrial impact structures, including Holleford crater near Kingston, Ontario (Figs. 1.1,

1.2) (Beals, 1960) and the Skeleton Lake structure in Muskoka (Millman et al, 1960; Waddington and Dence, 1979).

Geophysical methods, including gravity and magnetic surveys were conducted in many of the early studies of Canadian impact craters (e.g., Clark, 1983). Much of this work was conducted by the Geological Survey of Canada (GSC) and led to pioneering work in understanding the geophysical signature of impact craters (Pilkington and Grieve, 1992). The original studies at Holleford included seismic refraction, gravity and aeromagnetic surveys (Beals, 1960; Beals and Innes, 1961).

1.3.2 Holleford Crater (Holleford, Ontario)

Holleford crater was first identified as a suspected impact structure in aerial photos in the 1950's and investigated with deep drilling and geophysical investigations (Beals, 1960) (Fig. 1.2). Three continuously cored boreholes were drilled to depths of over 430 m (Fig. 1.2A), establishing the presence of breccias below thick basin fill consisting of Paleozoic carbonates and clastic sedimentary rocks. Gravity surveys recorded a ~ 2-3 mGal central gravity low (Fig 1.2C) and gravity highs to the north and southwest of the structure. Beals (1960) estimated the crater diameter at 2.35 km based on the surface topographic expression of the buried crater rim. The drilling and geophysical investigations provided estimates of depths to basement from boreholes (Fig. 1.2C). The borehole nearest the centre of the structure did not penetrate to basement and so the crater true depth at the structure centre was not determined. Coesite was identified in breccia samples, confirming an impact origin (Bunch and Cohen, 1963).

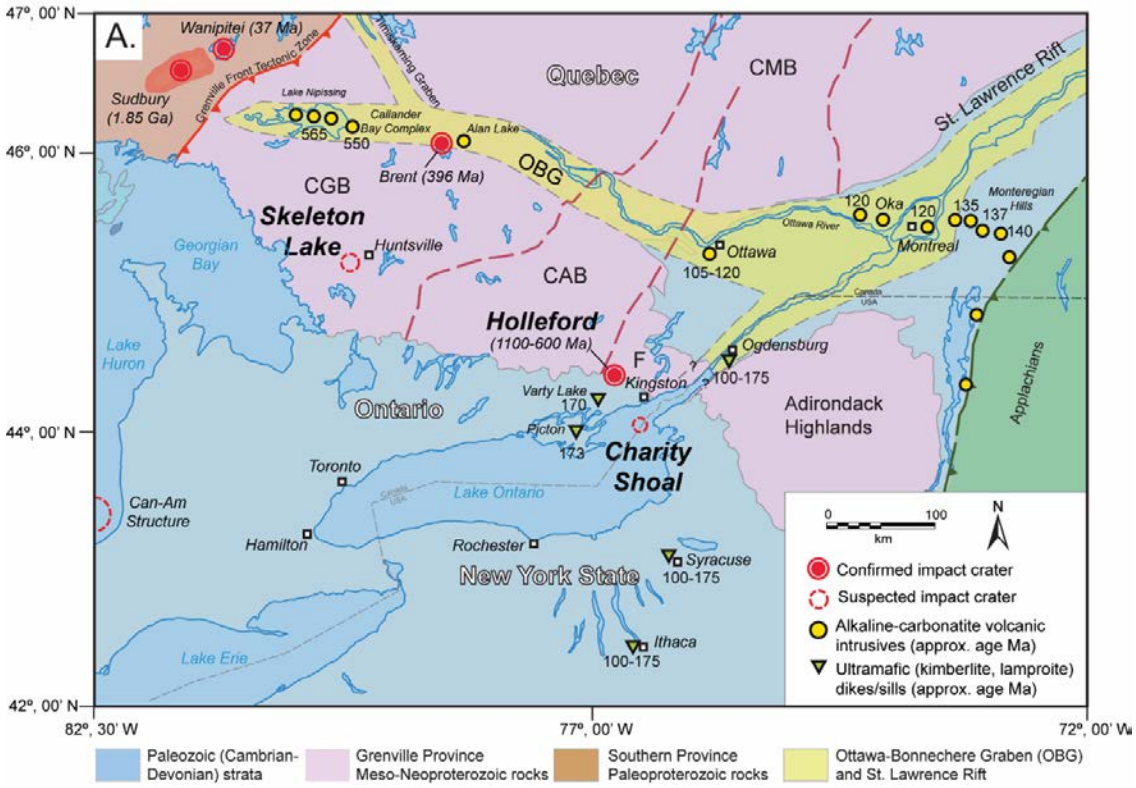

Figure 1.1. Regional bedrock geology map showing location of study sites (Holleford, Charity Shoal, Skeleton Lake). Locations of other confirmed impact structures and rift-related volcanic intrusive complexes also shown. OBG = Ottawa-Bonnechère graben, CGB = Central Gneiss Belt, CAB = Composite Arc Belt, CMB = Central Metasedimentary Belt, F = Frontenac Terrane.

St. John (1968) identified seven lithostratigraphic units within the crater basin fill, including Cambrian sandstones and clastic and carbonate sediments of the Middle Ordovician Black River Group. The sediments record Early Paleozoic fluvial and paleolacustrine environments and carbonate platform sedimentation in the Taconic foreland basin. The limited number of boreholes onsite prevented more detailed basin modelling of the crater infill stratigraphy. The details of the crater subsurface structure, as well as depth estimates, and the level of post-emplacement modification of the crater are unknown.

Andrieux and Clark (1969) conducted resistivity measurements along roadways and from the centre of the basin along a northeast-southwest line to the approximate location of the village of Holleford (Fig 1.2A). They estimated a structure depth of ~800 m and a basin fill consisting of 180 m of Paleozoic carbonate and clastic sedimentary rocks overlying the impact breccia. No further work has been completed at Holleford since that study.

The availability of a previous gravity and borehole data at Holleford (Figs. 1.2B, C), make this site a valuable location for testing 3-D geophysical modelling methods. Using 3-D gravity modelling, this study aimed to establish the subsurface crater structure to provide improved estimates of the buried crater basin morphology, depth, diameter and level of post-impact erosion and modification. The buried form of the crater and level of post-impact modification were investigated by reconstruction of the basement surface relief.

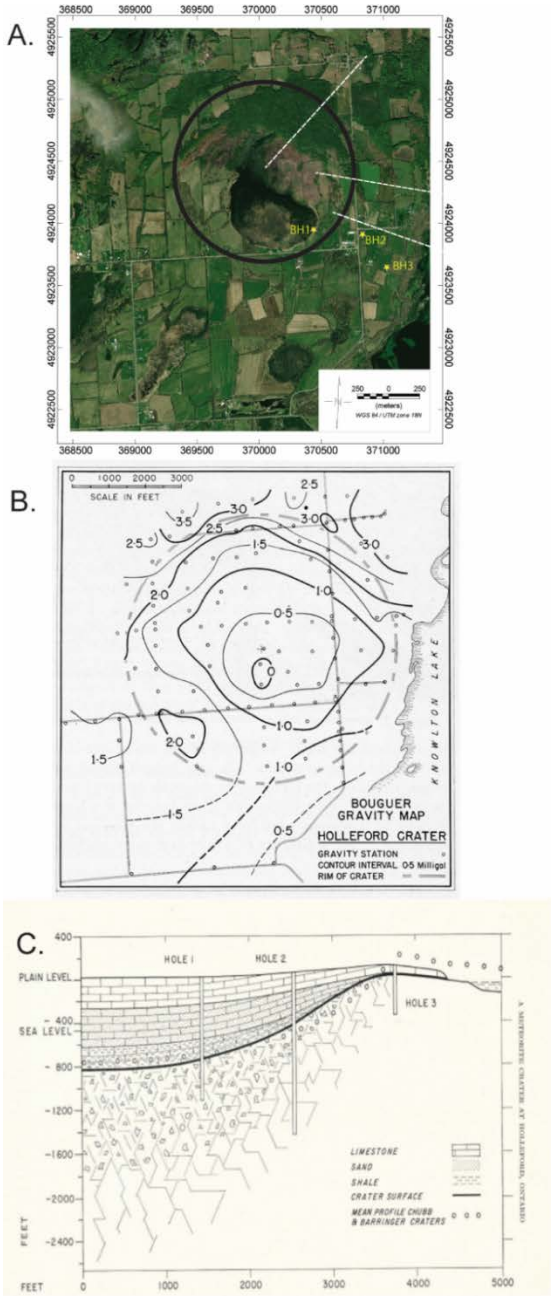

Figure 1.2. A. Aerial photo of Holleford crater with locations of three deep exploration boreholes (BH 1-3) (Beals, 1960) and resistivity surveys of Andrieux and Clark (1969). Bold line shows surface topographic expression of crater (after Beals, 1960). B. Bouguer gravity anomaly map (contour interval 0.5 mGal) with gravity station locations from Beals (1960). C. Geological cross-section of Holleford crater. Dotted surface shows mean profile of Pingualuit (formerly Chubb) and Barringer craters (from Beals, 1960).

1.3.3 Charity Shoal (Eastern Lake Ontario)

Charity Shoal was first identified in the late 1990's as a small (~1.2 km diameter), bedrock rimmed depression on the lakebed of eastern Lake Ontario (Virden et al., 1999). Holcombe et al. (2001) speculated on several possible origins including an impact structure and Holcombe et al. (2013) employed multi-beam bathymetric data (Fig. 1.3A) to examine the surface morphology and exposed bedrock structure. Holcombe et al. (2013) interpreted the annular Paleozoic bedrock rim as 'ring-anticline' structure, formed by draping of carbonate sediments across a buried impact crater rim (Fig 1.3B). They proposed a Middle Ordovician impact into marine sediments; however, no subsurface data were collected as part of the study and the crater depth and subsurface structure were not determined (Fig 1.3C). Suttak (2013) conducted the first geophysical surveys at Charity Shoal, including total field magnetics, high-frequency chirp seismic and bathymetric mapping. Magnetic surveys demonstrated a >1400 nT parabolic-shaped magnetic low over the central basin and annular magnetic high over the structure rim. Using 2-D forward modelling and Euler deconvolution of magnetic data, Suttak (2013) estimated a depth to basement of >600 m and parabolic crater-form basin with a raised rim. His modelling showed that a crater base in the Middle Ordovician carbonates (e.g., Holcombe et al., 2013; Fig. 1.3C) would not provide sufficient magnetic contrast to reproduce the large magnetic anomaly. His 2-D models demonstrated that the magnetic anomaly low could be produced by a 1.2 km diameter, crater-form basin in Mesoproterozoic basement, or by a Mesozoic maar-diatreme intruded into Paleozoic cover rocks. Chirp seismic profiling showed up to 25 m of sediment within the central basin overlying bedrock but did not provide penetration below the bedrock surface due to the limited penetration depth of the high-frequency seismic source. As a result, the presence of the proposed maar-diatreme below the Quaternary sediments could not be confirmed.

A primary aim of this study was to reconstruct the 3-dimensional form of the Mesoproterozoic basement surface and to determine the geometry (depth, extent, 3-D

form) of the crater-form basin identified by Suttak (2013). A key question was also the continuity of Middle Ordovician strata below the central basin (Fig. 1.3), as this was not determined in previous work; Holcombe et al. (2013) proposed a crater with a base in Paleozoic sediments and Suttak's (2013) volcanic model assumes that the Paleozoic cover rocks in the central basin are truncated by Jurassic-age ultrabasic maar-diatreme. The continuity of Paleozoic bedrock was investigated using low-frequency (1-4 kHz) marine seismic surveys and the buried crater structure determined by 3-D modelling of magnetic data. Seismic profiling and newly available multi-beam data (CHS, 2012) were also employed to investigate the rim structure and test the proposed ring-anticline model of Holcombe et al. (2013) (Fig. 1.3).

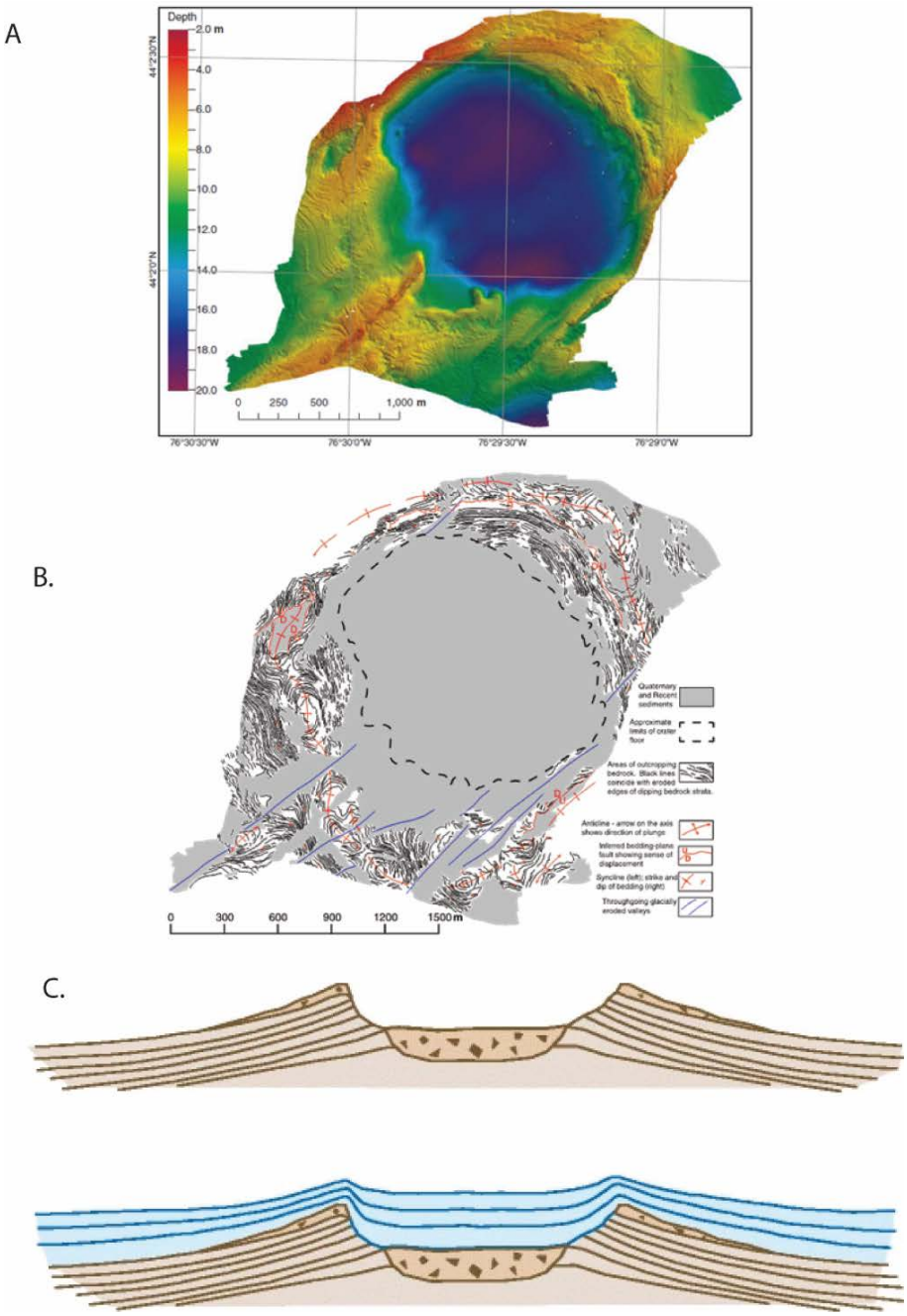

Figure 1.3. A. Multi-beam bathymetric map of Charity Shoal showing raised bedrock rim and 20-m-deep central basin (from Holcombe et al., 2013). B. Interpreted folding and bedding orientations in Paleozoic (Holcombe et al., 2013). C. Schematic cross-section showing impact crater Middle Ordovician marine sediments (top) and buried crater with proposed ring anticline structure (bottom) (Holcombe et al., 2013).

1.3.4 Skeleton Lake (Muskoka, Ontario)

Skeleton Lake was identified by Waddington and Dence (1979) as a probable 4-km-diameter impact structure with a modelled crater depth of ~1200 m based a -3 mGal gravity anomaly (Fig 1.4A) and the presence of autochthonous breccias on the northern edge of the lake. Clark (1982) employed aeromagnetic data and four north-south lake-based magnetic profiles (Fig 1.4B) to produce a magnetic model of the structure. The model suggests a ~ 3.5 km diameter structure but with a shallower depth of 800 m (Fig 1.4C). Petrographic analysis of the breccias did not find evidence for shock polymorphs (Waddington and Dence, 1979). No further work had been completed at Skeleton Lake since Clark's (1982) study.

High-resolution magnetic and bathymetry surveys were conducted at Skeleton Lake to determine the lakebed morphology and subsurface structure. 3-D magnetic models were constructed to investigate the subsurface structure and to evaluate the proposed impact origin (Waddington and Dence, 1979). The 3-D form of the buried Mesoproterozoic basement surface was reconstructed using magnetic modelling. The model shows a crater-form basin at a depth of >800-1200 m and a complex basement topography. Modelling constrains the structure size, indicating a > 4-km-diameter structure at the transition between a simple and complex crater (Waddington et al., 1979).

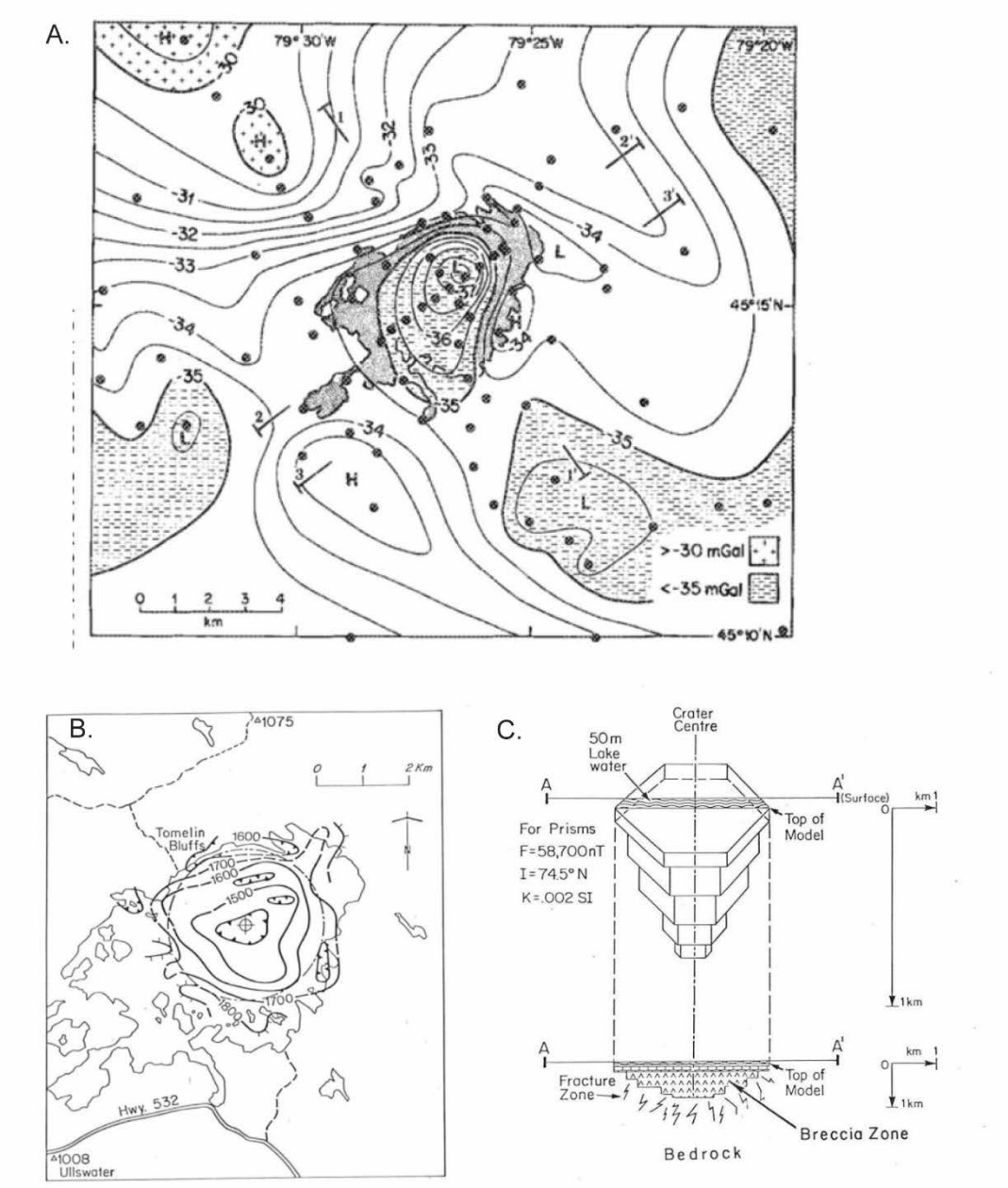

Figure 1.4. Previous geophysical surveys at Skeleton Lake. A. Bouguer gravity map showing -3 mGal gravity low (from Waddington and Dence, 1979). B. Residual magnetic intensity map showing a ~300 nT anomaly low and C. Magnetic model of impact crater from Clark (1982).

1.4 Background: hypervelocity impact craters

As a preamble to the results chapters, the following sections summarize the characteristics of terrestrial hypervelocity impact craters and outline the various geological and geophysical lines of evidence commonly used to determine an impact origin. These criteria include: 1) crater morphology, 2) geological evidence (micro- and macro-scale indicators of target rock deformation, shock metamorphism), and 3) geophysical signature.

1.4.1 Crater morphology

Hypervelocity impact craters are subdivided into two main types based on their morphology and geology: simple and complex (Melosh, 1989; Osinski and Pierazzo, 2013) (Figs. 1.5, 1.6). The transition from simple to complex crater types is a function of the target rock lithology (i.e., sedimentary vs. crystalline rocks) and the gravity of the planetary body. Craters are created through three main stages, 1) contact and compression, 2) excavation and 3) modification. After the initial contact where the ground surface is compressed, a transient crater is formed during the excavation phase from the combination of the outward shock wave and downward rarefaction wave. The final crater form results from gravitational forces that cause the collapse of the steep sides of the transient crater. This can result in uplift of the transient crater floor in larger impacts to produce a complex crater structure (Osinski and Pierazzo, 2013)

1.4.1.1 Simple impact craters

Simple craters typically have circular, uplifted rims and a central bowl-shaped depression with steeply dipping side slopes (Fig. 1.5) (Pilkington and Grieve, 1992; Osinski and Pierazzo, 2013). The central basin is overlain by an allochthonous breccia

layer, which may contain melt fragments. The target rocks are brecciated and fractured to some depth below the crater floor, leading to a lower density relative to host rocks (Pilkington and Grieve, 1992). An impact melt lens of higher density may or may not be present (Fig. 1.5). The uplifted rim height is due to ejecta deposits and structural uplift of the rim target rocks. The structure dips steeply into the basin, but much less steeply outside of the basin.

Simple craters on Earth typically have diameters of up to 2 km in sedimentary rocks and up to 4 km in crystalline rocks, with depth-to-diameter ratios of approximately 1:5 to 1:7 (Fig. 1.7) (Melosh, 1989; Osinski and Pierazzo, 2013). For simple impact craters, the size can be specified as both a rim-to-rim diameter D, and apparent diameter D_a (Fig. 1.5). In terrestrial craters, the D_a is typically measured, as post-impact erosion will reduce the original rim height. The rim height is measured as the height above the pre-existing surface elevation of the target rocks (Fig. 1.5). The crater true depth d_t is defined as the depth to basement from the pre-impact ground surface, and the apparent depth d_a, as the depth to the top of the allochthonous crater infill deposits (e.g., breccias) (Fig. 1.5).

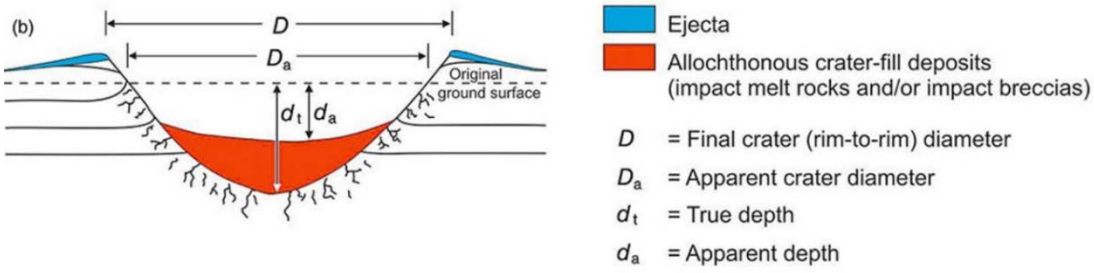

Figure 1.5. Simple impact crater in cross-section showing bowl-shaped basin with uplifted rim and morphologic parameters (D, D_a, d_t, d_a) used to define crater diameter and depth (from Osinski and Pierazzo, 2013). The basin fill consists of allochthonous breccias and may include thin melt sheet near the basin centre. Fracturing of autochthonous target rocks extends to depth below the final crater base.

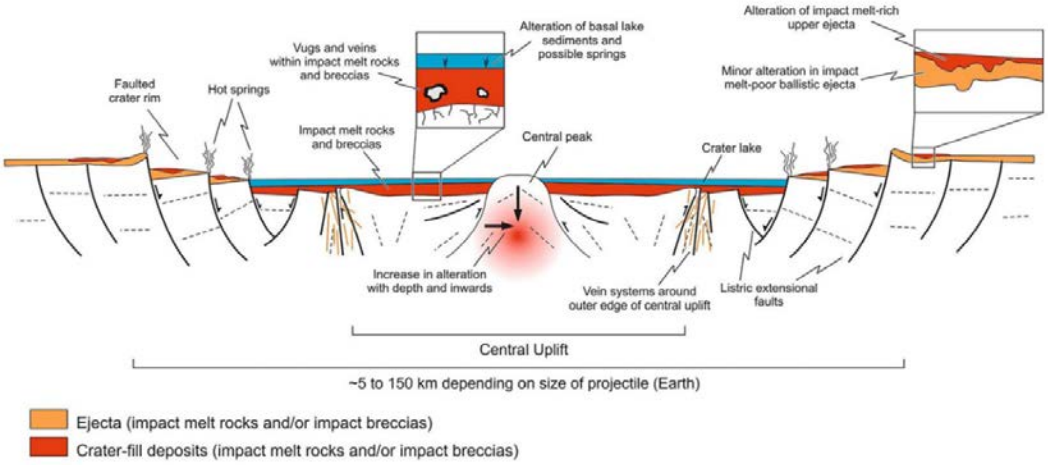

Impact Cratering: Processes and Products, First Edition. Edited by Gordon R. Osinski and Elisabetta Pierazzo.

Figure 1.6. Schematic cross-section through a complex impact crater, showing central uplift, crater-fill deposits. and ejecta layer. Complex craters are characterized by extensive faulting of the crater rim and basin producing central uplift and ring structures (from Osinski and Pierazzo, 2013).

1.4.1.2 Complex impact craters

Complex craters have a shallower impact basin with a central uplift and a down-faulted annular troughs (Fig.1.6) (Osinski and Pierazzo, 2013). The rim structures show evidence for dip-slip normal faulting and folding of rim strata. These more complex features form through modification of the transient crater by gravitational adjustments. Complex craters are significantly shallower than simple impact craters (Fig. 1.5) with depth-diameter ratios of 1:10 to 1:20 (Melosh, 1989). A general approximation gives the height of the central uplift as about 1/10 of the crater diameter (Osinski and Pierazzo, 2013). As the crater diameter increases, there is a transition from a central peak to concentric annular rings.

1.4.1.3‘Transitional’ impact craters

The diameter at which impact craters transition from simple to complex forms is dependent on the target rock types and the gravity of the planetary body, since the formation of a complex crater depends on gravitational adjustments of the initial (transient) crater. In sedimentary target rocks, the transition occurs at about 2 km diameter and at about 4 km in crystalline target rocks (Pilkington and Grieve, 1992). Recent work by Osinski et al. (2019) and Kenkmann (2021) has addressed the issue of transitional craters. According to Kenkmann (2021), the transition from simple to complex occurs at diameters of about 3-4 km in terrestrial craters (Fig 1.7).

Transitional crater structures can be ‘hybrid’ in structure, having features of both a simple and complex impact crater, such as terraces, but without a central uplift. The depth to diameter ratio for transitional craters is intermediate to that of a simple and complex impact structures (Kenkmann, 2021)

The Charity Shoal suspected impact structure and Holleford crater are approximately 1.2 and 2.35 km in diameter respectively and in the size range of simple impact structures (Figs. 1.2, 1.3). The Skeleton Lake structure has an apparent diameter of 3.5-4 km (Waddington and Dence, 1979; Clarke, 1982) and may represent a transitional crater, or possibly a heavily eroded complex crater.

1.4.2 Geological Evidence

1.4.2.1 Target rock deformation

Impact processes produce characteristic deformation structures in target rocks (French and Koerbel, 2010). Kumar and Kring (2008) discussed in detail the pattern of fractures and bedding plane deformation at Meteor (Barringer) Crater in Arizona. Structures at this crater include faults, fractures and rim uplift that changes the attitude of the bedding planes in and around the crater. The inner walls of Meteor Crater are well

exposed, so fracture planes can be measured. Kumar and Kring (2008) described a pattern of rim uplift and radial, conical, and concentric fractures from over 2500 structural measurements. Kumar (2005) also described the patterning of faults and uplift at the Lonar Crater in India, which includes radial, conical, and concentric fracturing. Kumar and Kring (2008) noted that although the fracture patterns of Meteor and Lonar crater are not the same, variation in the target lithologies (basalt at Lonar vs. sedimentary rocks at Meteor) likely account for these differences.

1.4.2.2 Mineralogical and geochemical indicators

At present, the only evidence accepted as 'diagnostic' of an impact structure are shock-metamorphic effects that are uniquely associated with the high temperature and pressure conditions resulting from an impact or elemental and chemical analysis that reveals elements thought to originate in non-terrestrial bodies (French and Koeberl, 2010). The high temperature and pressure conditions of an impact are not produced at Earth's surface through any known natural process. In its macroscopic form, this evidence consists of shatter cones, while in the microscopic form it takes the form of specific planar deformation features (PDF's), formation of high-pressure (diaplectic) glasses or high-pressure phase changes (e.g., coesite or stishovite) (French and Koeberl, 2010).

The survival of actual fragments of an impactor (i.e., meteorite) is diagnostic but rare. Chemical and isotopic signatures of impact processes have been found in about 45 of 175 identified craters (French and Koeberl, 2010). Elements that are considered diagnostic of impact processes are siderophile elements and platinum group elements that are in low abundance on Earth, the classic example being Ir found at the K-T boundary, indicating a large-scale impact. (French and Koeberl, 2010).

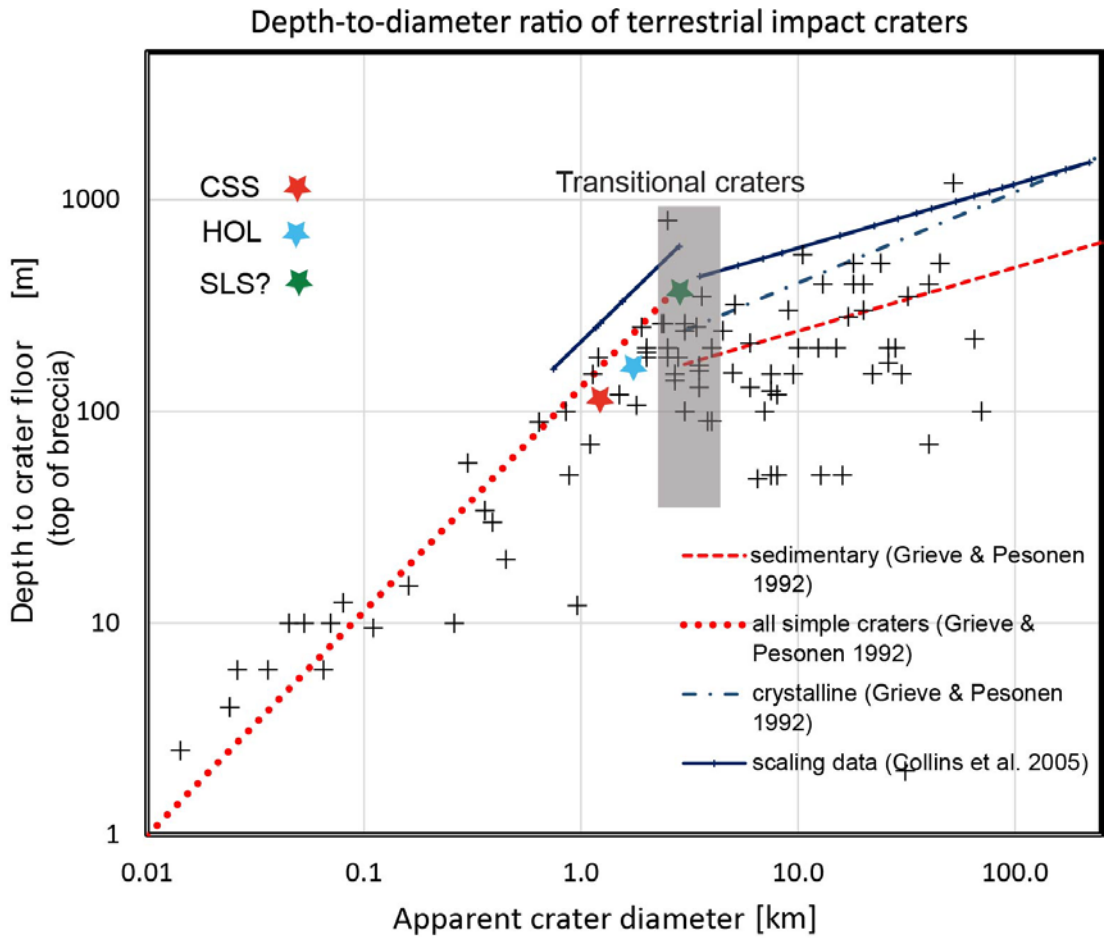

Figure 1.7. Apparent crater diameter versus depth to crater floor for terrestrial impacts (adapted from Kenkmann, 2021). The three structures investigated in this study are shown for comparison. Crater depth was estimated for the structures in this study using scaling equations (Pilkington and Grieve, 1992 ; Melosh, 1989) and existing estimates of structure diameter.

1.4.3 Geophysical signature of impact craters

Impact craters have characteristic geophysical signatures due to changes in the target rock physical properties (French and Koeberl, 2010). Contrasts in physical properties, particularly variations in density due to fracturing of the target rocks, and shock demagnetization produces characteristic gravity, magnetic and seismic signatures (Pilkington and Grieve, 1992).

1.4.3.1 Gravity

The gravity anomaly of impact craters results from the contrast in density between target rocks and overlying impact breccias and infill sediments (Fig. 1.8) (Pilkington and Grieve, 1992). Fracturing and brecciation results in a lower density and increased porosity of target rocks within the crater basin. Post-impact sediments deposited within the crater basin may have a strong density contrast with target rocks, particularly for crystalline target rocks.

Typically, the size of the gravity anomaly is proportional to the impact crater diameter (Pilkington and Grieve, 1992). Simple impact craters in the 1-3 km diameter range have gravity anomalies of a few mGal. For example, Holleford crater is defined by a 2-3 mGal gravity low and the Brent crater 5 mGal low (Fig. 1.1), while larger complex craters have anomalies up to ~ 30 mGal (Fig. 1.8). In the larger complex impact craters, the central uplift and melt sheet may have higher densities, so the largest anomaly is found in the ring around the central peak (e.g., Manicouagan; Fig. 1.8).

Holleford crater was investigated with gravity and magnetic surveys. Gravity surveys revealed ~ 2-3 mGal anomaly (Fig. 1.4B) (Beals, 1960; Pilkington and Grieve, 1992). Beals (1960) attributed the gravity low to the increased porosity of the fractured crystalline target rocks. The Skeleton Lake structure was also defined by ~3 mGal gravity low, which was attributed to the low density of infill sediments by Waddington and Dence (1979).

1.4.3.2 Magnetics

Magnetic anomalies produced by impact craters are typically more complex than the gravity signature, as they depend on both the magnetic susceptibility and remanent magnetizations of the target rocks and the impact-derived melt sheet and breccia deposits (Pilkington and Grieve, 1992). Simple craters are often marked by magnetic lows with anomalies on the order of a few tens to a few hundred nanoTeslas (nT) due to shock demagnetization of target rocks (Pilkington and Grieve, 1992; Morgan and Rebolledo-Vieyra, 2013). Magnetic anomalies are often recognizable because they locally disrupt regional magnetic trends, particularly in crystalline target rocks, as is the case at Skeleton Lake (Waddington and Dence, 1979). Pilkington and Grieve (1992) also emphasized that impact craters can acquire a shock remanent magnetization (SRM) at the time of impact, and that secondary components of magnetization at Meteor (Barringer) and Lonar craters may have been acquired this way.

Both ground and aeromagnetic surveys have been employed in the identification of impact structures. Ground magnetic surveys of the West Hawk structure (Manitoba) revealed a ~ 250 nT low over the impact structure (Grieve, 2006). Additional magnetic studies of craters have been done to map out specific features from their magnetic signal, such as at Ile Rouleau (Evangelatos, 2009). Ground magnetic surveys at Holleford crater determined a small magnetic anomaly over the north rim area, though overall the regional aeromagnetic surveys do not show a well-defined magnetic low corresponding with the impact basin (Beals, 1960). At Skeleton Lake, Clarke (1982) measured ~300 nT magnetic low in lake-based magnetic data collected along four separate north-south profiles.

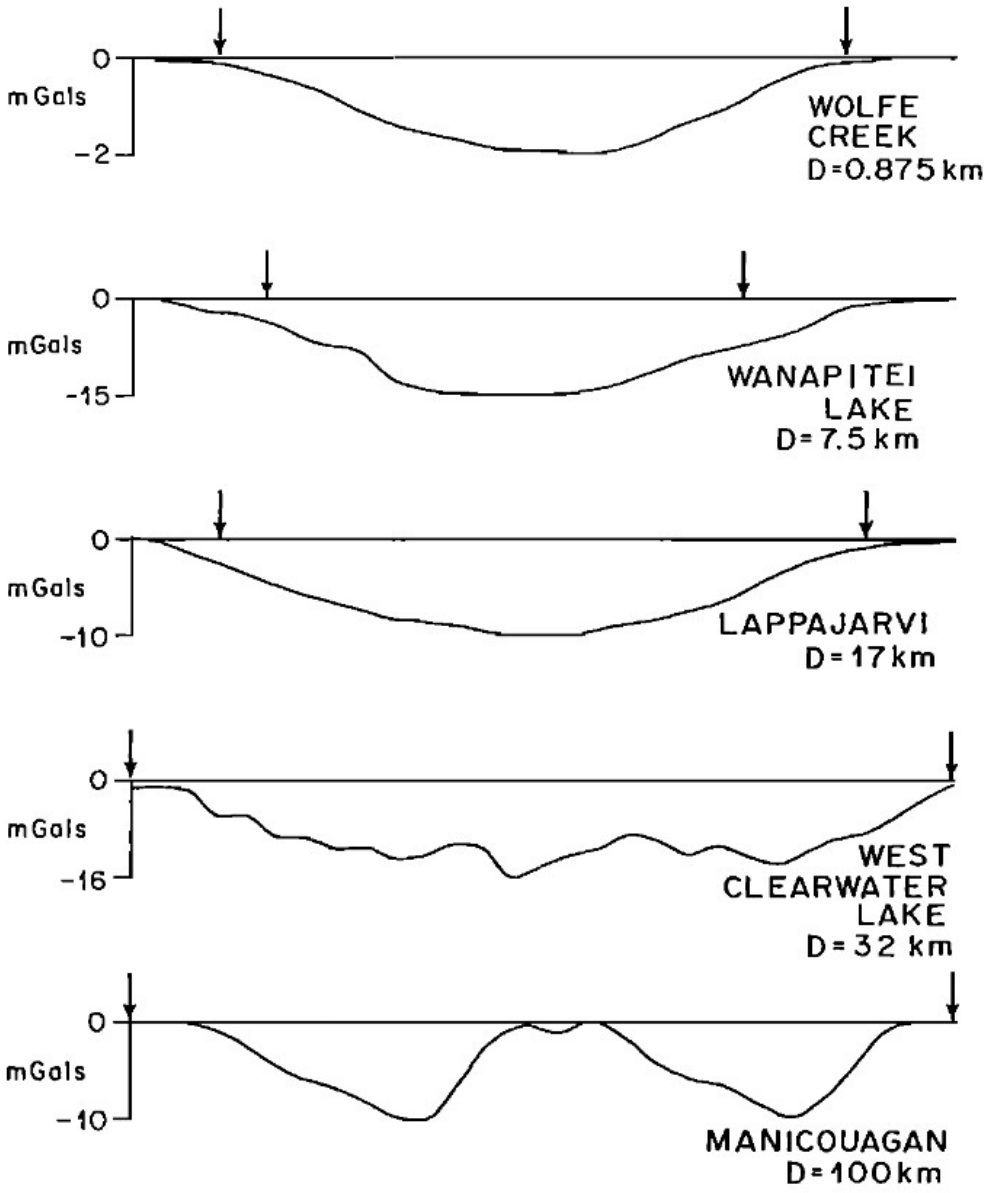

Figure 1.8. Examples of residual Bouguer gravity (mGals) profiles for selected impact structures (from Pilkington and Grieve, 1992). Arrows indicate location of structure rim. Wolfe Creek is a 0.9 km diameter simple impact structure, while all others are complex craters. The central gravity low in simple impact craters is due to lower density of infill sediments and breccias compared with target rocks. Large complex craters have a central gravity high (e.g., Manicouagan) due to the central uplift and surrounding annular trough filled with lower density crater infill sediments.

1.4.3.3 Seismic methods

Impact processes produce changes in the acoustic impedance (seismic velocity and density) of target rocks, which are detectable with seismic methods (Pilkington and Grieve, 1992). At Meteor crater for example, fracturing and brecciation of target rocks resulted in a 5% decrease in density and 50% decrease in the seismic velocity. Changes in acoustic impedance (i.e., at the crater base) produce reflection boundaries that can be detected in seismic reflection and refractions surveys. The impact melt lens will typically have a higher density than underlying fractured target rocks, producing a high contrast reflecting boundary. The contact between crystalline target rocks and post-impact sediments can also produce a significant impedance contrast detectable in seismic reflection surveys. Seismic reflection surveys can also provide detailed images of the basin infill sediments.

Seismic methods have been employed to investigate Meteor (Barringer) crater, one of the best-preserved examples of a simple impact crater. Roy and Stewart (2012) conducted near-surface seismic and gravity surveys over the crater to determine the seismic velocities and thickness of the ejecta blanket. Kumar et al. (2014) also used seismic methods in examining the structure of the rim and ejecta blanket surrounding the Lonar crater in India. Mazur et al. (2000) summarized the diagnostic seismic features of a simple impact crater. These include down-thrown slump blocks, uplifted rocks at the rim, breccia infill, melt sheets and zones of structural pinching. They show that seismic imaging can be used to delineate the overall structural size and would allow for the evaluation of the crater structure with respect to established crater scaling ratios and morphology. For complex craters, the central uplift, annular trough and faulting of target rocks can be resolved in seismic data.

3-D seismic surveys can provide high-resolution images of buried crater morphology. The Silverpit structure in the north Atlantic was discovered during offshore seismic exploration (Stewart and Allen, 2003, 2005). The 3-km-diameter crater-like structure is a multi-ring depression that has been interpreted as an impact crater (Stewart,

2003) or a synclinal basin formed by salt tectonics (Underhill, 2004). Stewart (2003) has argued that 3-D marine seismic can provide a reasonable amount of certainty of an impact origin when weighed against other endogenic origins. He addressed the issue of possible origins of different circular structures (i.e., salt diapirs, domal drape folds, impact structures) and how they vary in appearance in 3-D seismic data. Certain characteristics such as central peak in a complex crater, overall crater form, the regional geological context and other nearby structures are some of the factors he cites to consider in identifying an impact structure origin.

The CSS structure is submerged, which allows efficient collection of marine geophysical data as an areal survey with complete seismic coverage of the structure. Previous land-based seismic studies at Meteor and Lonar craters have only allowed investigation of limited segments of the crater (e.g., ejecta flaps). The most complete seismic surveys of impact craters collected to date are for deeply buried complex craters, such as the Chicxulub, Chesapeake, and Montagnais structures.

1.4.3.4 Digital elevation and bathymetric models

The increasing availability in the last decade of high-resolution digital elevation models (DEMs) and multi-beam bathymetric data has led to the discovery of several new suspected and confirmed impact craters (Herd et al., 2008; Holcombe et al., 2013; Lajeunesse et.al., 2013; Gottwald et al., 2017). Recent multi-beam mapping led to the discovery of the Corossol structure, a 4.1 km diameter and 185 m deep circular basin in the Gulf of St. Lawrence (Lajeunesse et al., 2013). Krøgli et al., (2007) describe an automated search routine to locate circular basins in digital elevation models as possible impact sites. However, there are many possible geological explanations for the origin of circular basinal structures for example: salt diapirs, karst sinkholes, maar-craters, kimberlites, and ring anticlines, so identification cannot be based on surface morphology alone. Geophysical survey data, when combined with digital elevation and bathymetric data, can provide additional constraints for evaluating an impact origin.

1.5 3-D Geophysical Models

1.5.1 Modelling approach

In this thesis, potential field models were constructed in Modelvision 17 (Tensor Geophysics Pty Ltd.) using total field magnetic intensity (TMI) or Bouguer gravity data. This section provides an overview of the modelling approach. A more detailed description of the modelling workflow is given in the Modelvision 17 user manual (Pratt et al., 2020).

Modelvision 17 offers several different methods for 2-D and 3-D modelling of potential field data with geological constraints (Pratt et al., 2020). The computation of the magnetic anomaly associated with the model allows for inversion and optimization of a full range of rock properties (e.g., density and magnetic parameters: κ, NRM, Q), model layer thickness and geometry. Due to the complexity of the geological models required in this study, Modelvision's profile modelling approach was employed (Fig. 1.9). This option allows modelling of complex, 3-dimensional structures, including multi-layered geological models with variable unit thicknesses and structural orientations, and incorporating faults (Fig. 1.9). Profile modelling was used to simulate both impact crater basins and volcanic structures (e.g., maar-diatreme), which could not be effectively reproduced using either single or multiple 'solid bodies' in Modelvision 17 (Pratt et al., 2020).

The modelling workflow involved the creation of a series of parallel 2-D profiles, with strike lengths that were consistent with geophysical survey line separations. Layer physical properties were assigned using field or laboratory measurements (e.g., density, magnetic susceptibility, NRM) or were estimated using inversion methods. Additional constraints on subsurface properties and layer geometry (e.g., layer thickness, depth) and near-surface geological structure were provided by seismic reflection profiles and multi-beam bathymetry data. High-resolution digital elevation models (DEMs) and

bathymetric data were also employed to constrain model surface topography and water depths.

The inversion routines in Modelvision 17 are ‘user-directed’ where the operator can select a range of model parameters and physical properties for inversion. After selecting a body type or shape (e.g., 2-D polygon), the vertices are typically adjusted manually to achieve an approximate fit with the observed magnetic or gravity signal and field strengths are forward calculated. The model is then refined by freeing one or more inversion parameters (e.g., rock properties) or node locations and using the inversion routines to optimize the model fit (Pratt et al., 2020). Typically, one inversion parameter is optimized at a time and constraints placed on the valid ranges for each parameter. For polygon nodes, constraints can be placed on the allowable displacement of the model layer surface during model iterations. Inversion can also be used to establish the regional field as well as to estimate the various physical properties, including density, magnetic susceptibility, NRM and the depth and horizontal extent of surfaces or bodies. The software includes several methods for remote remanence estimation (REE), including Helbig’s method and parametric methods which recover the resultant and remanent vectors using inversion (Pratt et al., 2014; Pratt et al., 2020). In this study, the parametric inversion was employed to determine the resultant and NRM magnetizations of source bodies in the Skeleton Lake study.

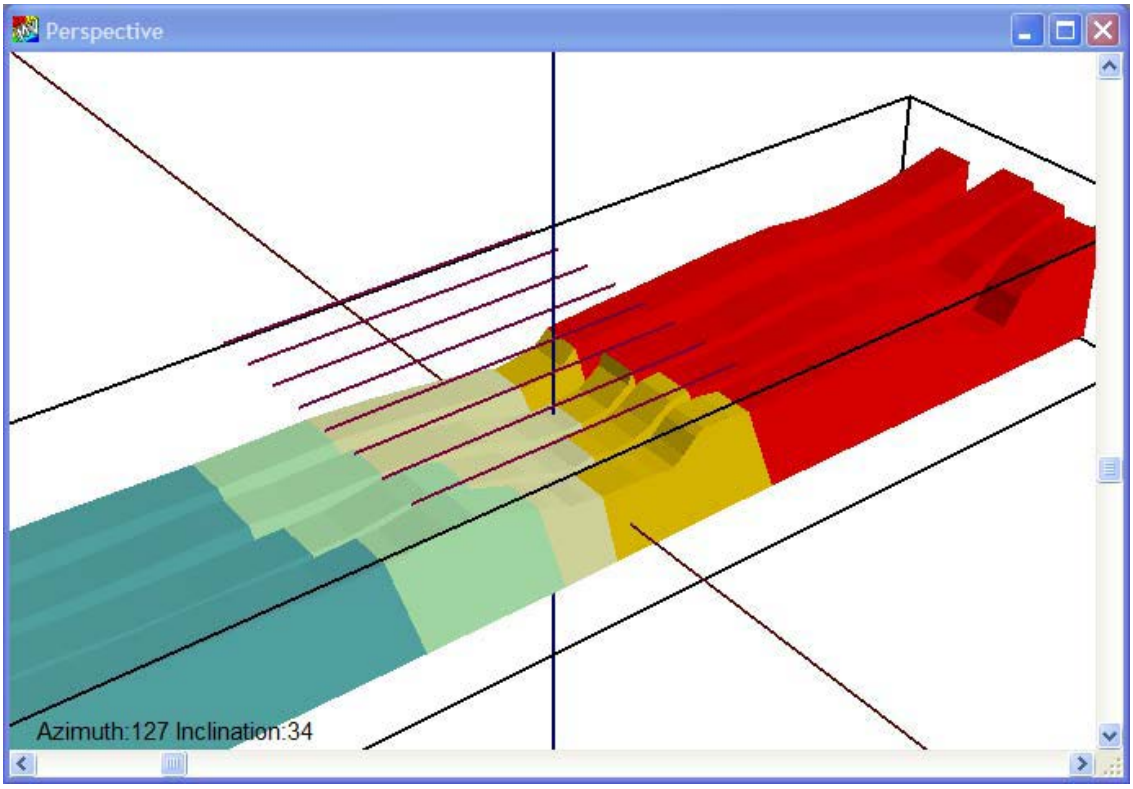

Figure 1.9. Example of multiple section model constructed with the profile modelling option in Modelvision 17. Complex models are produced using parallel profiles of a set width. The magnetic and gravity fields are calculated across the profiles to obtain the 3-D modelled potential fields (image source: Pratt et al., 2020).

1.5.2. Model algorithms

For profile modelling Modelvision 17 implements the Fortran-77 codes of Cady (1980) and Won and Bevis (1987). The gravity and magnetic response of 2-D polygonal source bodies are modelled as n-sided polygons as shown in Figure 1.10 using the methods originally developed by Talwani et al. (1959), Talwani and Ewing (1960) and Talwani (1965). The Talwani et al. (1959) approach calculates the gravitational field of an irregular shaped body represented by an n-sided polygon (Fig. 1.10). The polygons are constructed to approximate the shape of the geological source body and the vertical and horizontal components of gravity are calculated by summing the contributions from each side (Fig. 1.10).

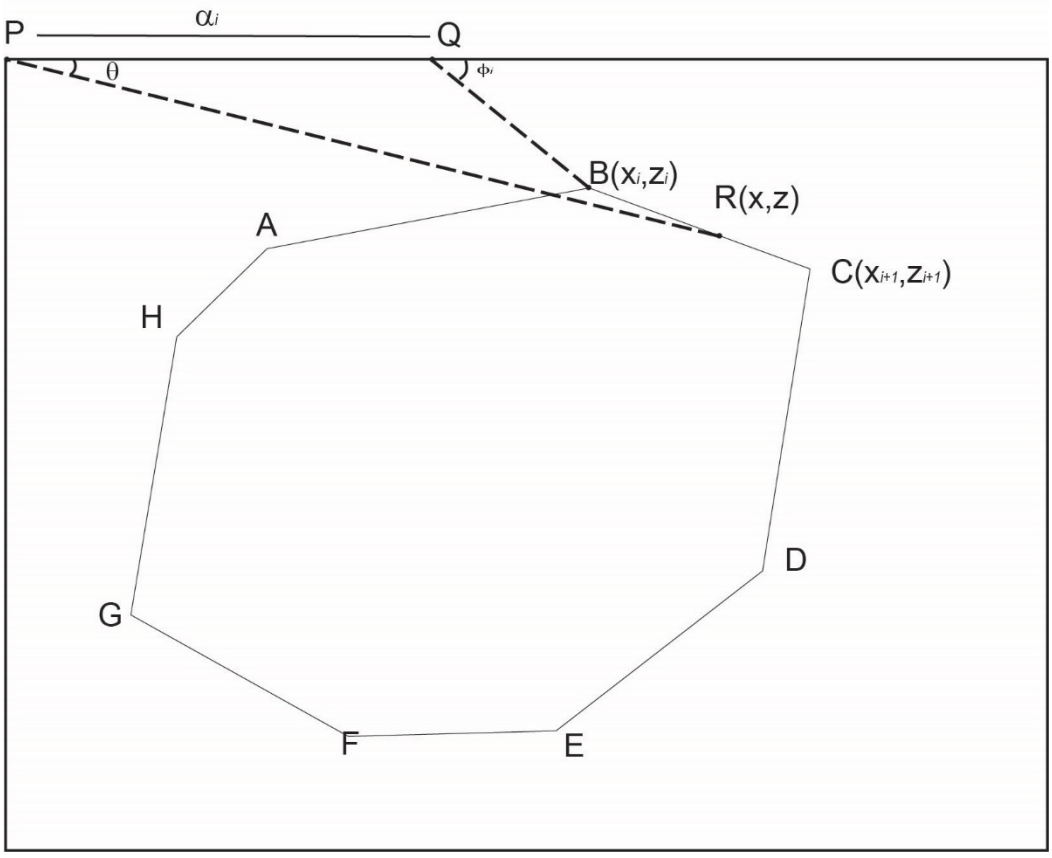

Figure 1.10. A polygonal source body in the x-z plane with varying side lengths (after Talwani et al., 1959). The horizontal and vertical components of gravity are evaluated using line integrals and summed for all n sides of the polygon (Hubbert, 1948).θ is angle from horizontal at point P to vertex on figure, ϕ is angle from point Q on horizontal to midway point R between points of polygon. α is distance between P and Q

As shown in Figure 1.10, the vertical and horizontal gravity attraction of an n-sided, 2-D dimensional polygon are calculated as:

$$Vertical\ component = 2G\rho \oint zd\theta$$

and similarly

$$Horizontal\ component = 2G\rho \oint xd\theta$$

where *G* is the universal gravitational constant and ρ is density of the body (Hubbert, 1948; Talwani et al., 1959).

The line integrals are calculated for each side of the polygon. The contribution for side *BC* of the polygon (Fig. 1.10) at a random point *R (x, z)* on this line is computed as:

$$z = xtan\theta$$

and for any point *R* on *BC*

$$z = (x - \alpha_i)tan\emptyset_i$$

This can be further simplified in terms of *z* to give

$$z = \frac{\alpha_i tan\theta tan\varphi_i}{tan\varphi_i - tan\theta}$$

or in terms of *x:*

$$x = \frac{\alpha_i tan\varphi_i}{tan\varphi_i - tan\theta}.$$

Integrating these terms gives the contribution for Z_i and X_i for each side of the polygon

$$\int_{BC} zd\theta = \int_B^C \frac{\alpha_i tan\theta tan\varphi_i}{tan\varphi_i - tan\theta} d\theta = Z_i$$

and

$$\int_{BC} x d\theta = \int_{B}^{C} \frac{\alpha_i tan\varphi_i}{tan\varphi_i - tan\theta} d\theta = X_i.$$

The vertical and horizontal components of the gravitational attraction for the whole polygon are then obtained by summation over *n* sides of the polygon:

$$V = 2G\rho \sum_i^n Z_i$$

and

$$H = 2G\rho \sum_i^n X_i.$$

Integrals are then solved for Z_i and X_i using the analytical functions described in Talwani et al. (1959).

Talwani and Heirtzler (1964) and Talwani (1965) adopted a similar approach to calculate the magnetic response above a uniformly magnetized body using 2-D polygonal bodies with a semi-infinite strike (Fig. 1.10). Kravchinsky et al. (2019) provide a detailed re-derivation of the original Talwani and Heirtlzer (1964) method and a modified algorithm for calculating the magnetic response of polygonal 2-D bodies.

In Modelvision 17, the methods of Talwani et al. (1959) and Talwani and Ewing (1960) are extended to 2.5-D for calculation of the gravity anomaly for source bodies with a polygonal cross-section and finite strike length using the method of Cady (1980) (Pratt et al., 2020). Cady (1980) further refined this approach, using the algorithm of Shuey and Pasquale (1973) to incorporate end corrections into the 2-D semi-infinite prisms for both magnetic and gravity anomalies. The 2-D profile is assumed to be centred between the ends of the source body and perpendicular to and at a finite distance along the strike.

For each profile, the outline of the polygonal geological bodies were created and adjusted to match the observed signal. Inversion was applied in all models to establish or verify regional trends, layer susceptibilities and densities. Point data is then extracted from the Modelvision and gridded in Sequeent Geosoft to produce depth surfaces for the different lithic units.

1.5.3 Modelling constraints and physical properties

Where available, borehole data and surface geological mapping were employed to determine the lithology and number of model layers and to constrain physical properties in geophysical models. Inversion was also employed to estimate model physical properties. At Holleford core lithology and physical property data (density, magnetic properties) were available from three continuously core, deep boreholes. Lithostratigraphic information was also available from a study of the basin infill sediments by St. John (1968).

At Charity Shoal, no borehole data were available and physical properties (magnetic susceptibility, NRM) were estimated from regional investigations (O'Dowd and Eaton, 2005). A previous study by Suttak (2013) provided some prior estimates of depth to basement and infill sediment thickness based on shallow seismic profiling. Multi-beam bathymetric maps available from the Canadian Hydrographic Service (CHS, 2011, 2012) were used to constrain water depth and to correct water-depth related change in magnetic intensity.

At Skeleton Lake, no borehole data were available but regional geological mapping had been conducted in two previous surveys (Hewitt, 1967; Lumbers and Vertolli, 2000). The structural orientations and lithology of modelled layers were determined using geological maps and available structural data. Magnetic properties were assigned using magnetic susceptibility measurements on outcrops and paleomagnetic data

(NRM) from a previous study of the Muskoka Domain (Symons and Chiasson, 1991; Alvarez and Dunlop 1998). The remanent magnetization of Mesoproterozoic bedrock units was also determined by inversion in Modelvision software. Structural measurements on outcrops (e.g., bedding and foliation orientations) were used to constrain the dip of model layers in cross-sections.

1.6 Author Contributions

This thesis is formatted as a 'sandwich style' thesis, comprising three full-length papers prepared for journal submission (Chapters 2-4) with an introductory and concluding chapter. In accordance with McMaster School of Graduates Studies policy, the author contributions to each of the chapters are summarized below.

Chapter 2: 3-D geophysical modelling of a deeply buried, simple impact crater: Holleford impact structure, Ontario, Canada

M.H. Armour, J.I. Boyce, D. Zilkey and Z. Shulman

(For submission to Meteoritics and Planetary Sciences)

MHA collected, analyzed, and processed geophysical data, produced 3-D gravity models and prepared the manuscript and drafted all figures. JIB supervised the research work, aided in field work and logistics, and edited the thesis manuscript. DZ and ZS assisted in the collection and processing of magnetic and gravity field surveys.

Chapter 3: 3-D subsurface geophysical modelling of the Charity Shoal Structure, a suspected 1.2 km diameter simple impact crater in eastern Lake Ontario, Canada

(For submission to Earth and Planetary Science Letters)

M.H. Armour, J.I. Boyce, P.A. Suttak, and D. Hrvoic

MHA collected and processed seismic and magnetic data, constructed 3-D models, and prepared the initial manuscript draft and all figures. JIB supervised the research work, aided in field work and logistics, and edited the thesis manuscript. PS and DH assisted with field data collection and processing of magnetic data.

Chapter 4: Geophysical investigation and 3-D modelling of the Skeleton Lake structure: A suspected (Late Proterozoic-Early Paleozoic?) transitional impact crater in Muskoka (Ontario, Canada)

(For submission to Earth and Space Science)

M.H Armour, J.I Boyce, C. Podhorodeski and I. Inozemtsev

MHA collected and processed geophysical data, produced 3-D geophysical models, prepared the initial draft manuscript and all figures. JIB supervised the research work, assisted with field work and logistics, and edited the thesis manuscript. CP and II assisted with field data collection and processing of geophysical data.

1.7 References

Alvarez V. C., and Dunlop D. J. 1998. A regional paleomagnetic study of lithotectonic domains in the Central Gneiss Belt, Grenville Province, Ontario. Earth and Planetary Science Letters, 157(1-2): 89-103. https://doi.org/10.1016/S0012-821X(98)00028-4

Andrieux P. and Clark J.F. 1969. Application des méthodes électriques de prospection à l'étude du cratère d'Holleford. *Canadian Journal of Earth Sciences*. 6(6): 1325-1337. https://doi.org/10.1139/e69-135

Batista-Rodríguez, J.A., Pérez-Flores, M.A. and Urrutia-Fucugauchi J. 2013. Three-dimensional gravity modeling of Chicxulub Crater structure, constrained with marine seismic data and land boreholes. *Earth, Planets and Space* 65(9): 973-983.

Beals C. S., Ferguson G. M., and Landau A. 1956. A search for analogies between lunar and terrestrial topography on photographs of the Canadian Shield *Journal of the Royal Astronomical Society* 50:258-259.https://doi.org/10.5047/eps.2013.05.015

Beals C.S. 1960. A probable meteorite crater of Precambrian age at Holleford, Ontario. *Publications of the Dominion Observatory* 24: 6 (Ottawa), 142 p. https://doi.org/10.4095/8727

Beals C. S. and Innes I. 1961. The study of fossil meteorite craters with the aid of geophysical and diamond drilling techniques. In Nordyke, Milo D. *Proceedings of the Geophysical Laboratory/Lawrence Radiation Laboratory Cratering Symposium*. United States. 44 p. https://doi.org/10.2172/1122567

Bunch T. E., and Cohen A. J. 1963. Coesite and shocked quartz from Holleford crater, Ontario, Canada. *Science* 142(3590): 379-381. https://doi.org/10.1126/science.142.3590.379

Cady J. W. 1980. Calculation of gravity and magnetic anomalies of finite-length right polygonal prisms. *Geophysics*, 45(10):1507-1512. http://dx.doi.org/10.1190/1.1441045

Caumon G., Collon-Drouaillet P., Le Carlier de Veslud C., Viseur, and Sausse, J. 2009, Surface-based 3-D modeling of geological structures: *Mathematical Geosciences*, 41: 927–945. https://doi.org/10.1007/s11004-009-9244-2

Clark J. F. 1982 Earth Physics Branch, Geomagnetic Report 81-2, 25 p. https://doi.org/10.4095/226536

Clark J.F. 1983. Magnetic survey data at meteoritic impact sites in North America. Geomagnetic Survey. Canadian Earth Physics Branch, Open File Report 83-5, 30 p. https://doi.org/10.4095/8903

CHS (2011). Digital bathymetric data, Charity Shoal. Canadian Hydrographic Service, Digital File No. 4013083.

CHS (2012). Digital bathymetric data, Charity Shoal. Canadian Hydrographic Service, Digital File No. 4013191.

Ebbing J., Janle P., Koulouris J. and Milkereit B. 2001. 3D gravity modelling of the Chicxulub impact structure. *Planetary and Space Science*, 49(6): 599-609. https://doi.org/10.1016/S0032-0633(01)00005-8

Evangelatos J., Butler K.E. and Spray J.G. 2009. A marine magnetic study of a carbonate-hosted impact structure: Ile Rouleau, Canada. *Geophysical Journal International* 179(1): 171-181. https://doi.org/10.1111/j.1365-246X.2009.04304.x

French B.M. and Koeberl C. 2010. The convincing identification of terrestrial meteorite impact structures: What works, what doesn't, and why. *Earth-Science Reviews* 98: 123-70 https://doi.org/10.1016/j.earscirev.2009.10.009

French B.M. 1998. Traces of Catastrophe: A Handbook of Shock-Metamorphic Effects in Terrestrial Meteorite Impact Structures. *LPI Contribution No.954*, Lunar and Planetary Institute, Houston. 120 p.

Ganapathy R. 1982. Evidence for a major meteorite impact on the Earth 34 million years ago: Implication for Eocene extinctions. *Science*, 216(4548): 885-886. https://doi.org/10.1126/science.216.4548.885

Gottwald M., Fritz T., Breit H., Schättler B. and Harris A. 2017. Remote sensing of terrestrial impact craters: The TanDEM-X digital elevation model. *Meteoritics and Planetary Science*, 52(7):1412-1427. https://doi.org/10.1111/maps.12794

Grieve R.A.F. 2006. Impact Structures in Canada. Geological Society of Canada, 210 p.

Grieve R. A. F. and Masaitis V. L., 1994, The economic potential of terrestrial impact craters, *International Geology Review*, 36, 105-151. https://doi.org/10.1080/00206819409465452

Herd C.D.K, Walton E.L., Herd E.P.K and Kofman R.S. 2008. The Discovery of a Late Holocene Impact Crater near Whitecourt Alberta *Meteoritics and Planetary Science Supplement* 43. https://ui.adsabs.harvard.edu/abs/2008MandPSA.43.5108H

Hewitt D. F. 1967. Geology and mineral deposits of the Parry Sound-Huntsville area. Department of Mines and Resources, 52.

Holcombe T.L., Warren J. S., Reid D. F., Virden W. T. and Divins D. L. 2001. Small Rimmed Depression in Lake Ontario: An Impact Crater? *Journal of Great Lakes Research* 27(4) : 510-517. https://doi.org/10.1016/S0380-1330(01)70664-8

Holcombe T.L., Youngblut S. and Slowey N. 2013. Geological structure of Charity Shoal crater, Lake Ontario, revealed by multi beam bathymetry. *Geo-Marine Letters* 33 (4): 245-252. https://doi.org/10.1007/s00367-013-0322-6

Hubbert M.K., 1948. A line-integral method of computing the gravimetric effects of two-dimensional masses. *Geophysics*, 13(2), pp.215-225.

Jessell M. 2001. Three-dimensional geological modelling of potential-field data. *Computers & Geosciences*, 27(4): 455-465.

Jõeleht A., Plado J. and Sarv K. 2018. Kärdla impact crater–transitional from simple to complex based on reflection seismics. *EPSC Abstracts*, 12.

Kenkmann T. 2021. The terrestrial impact crater record: A statistical analysis of morphologies, structures, ages, lithologies, and more. *Meteoritics & Planetary Science* 56(5), 1024-1070. https://doi.org/10.1111/maps.13657

Kravchinsky V. A., Hnatyshin D., Lysa B. and Alemie W. 2019. Computation of magnetic anomalies caused by two-dimensional structures of arbitrary shape: Derivation and Matlab implementation. *Geophysical Research Letters*, 46: 7345–7351. https://doi.org/10.1029/2019GL08276

Krøgli S. O., Dypvik H. and Etzelmüller B. 2007. Automatic detection of circular depressions in digital elevation data in the search for potential Norwegian impact structures. *Norwegian Journal of Geology/Norsk Geologisk Forening* 87. https://foreninger.uio.no/ngf/ngt/pdfs/NJG_87_157-166.pdf

Kumar P.S. 2005. Structural effects of meteorite impact on basalt: Evidence from Lonar crater, India. *Journal of Geophysical Research: Solid Earth* 110: B12402 https://doi.org/10.1029/2005JB003662

Kumar P.S. and Kring D.A. 2008. Impact fracturing and structural modification of sedimentary rocks at Meteor Crater, Arizona. *Journal of Geophysical Research: Planets* 113: E09009. https://doi.org/10.1029/2008JE003115

Kumar P.S., Prasanna Lakshmi K.J., Krishna N, Menon R., Sruthi U., Keerth, V., Senthil Kumar A., Mysaia, D., Seshunarayana T. and Sen M.K. 2014. Impact fragmentation of Lonar Crater, India: Implications for impact cratering processes in basalt. *Journal of Geophysical Research E: Planets* 119(9): 2029-2059. https://doi.org/10.1002/2013JE004543

Lajeunesse P., St-Onge G., Locat J., Duchesne M.J., Higgins M.D., Sanfaçon R. and Ortiz J. 2013. The Corossol structure: a possible impact crater on the seafloor of the northwestern Gulf of St. Lawrence, Eastern Canada. *Meteoritics and Planetary Science* 48(12): 2542-2558. https://doi.org/10.1111/maps.12224

Lumbers S.B. and Vertolli V.M. 2000. Precambrian geology, Bracebridge area; Ontario Geological Survey, Preliminary Map P.3411 -3414, scale 1:50 000.

Mazur M.J., Stewart R.R. and Hildebrand A.R. 2000. The seismic signature of meteorite impact craters. *CSEG Recorder* 25: 10-16.

Meen V.B. 1950. Chubb crater, Ungava, Quebec. *Journal of the Royal Astronomical Society of Canada* 44:169-180

Meen V.B. 1951. Chubb crater, Ungava Quebec. *Proceedings of the Geological Association of Canada* (4):49-67

Meen V.B. 1957. Merewether crater as a possible impact crater. *Proceedings of the Geological Association of Canada* (9):49-59

Millman P.M. 1956. A profile study of the New Quebec crater. *Publications of the Dominion Observatory* (18):61-82

Millman P. M., Liberty B. A., Clark J. F. Willmore P. L. and Innes M. J. S. 1960. *Publications of the Dominion Observatory* 24:1 https://doi.org/10.4095/8722

Melosh H.J. 1989. *Impact Cratering: A Geologic Process*. Oxford University Press, New York.

Morgan J. and Rebolledo-Vieyra M. 2013. Geophysical Studies of Impact Craters, *Impact Cratering: Processes and products* pp. 211-22: John Wiley and Sons, Ltd

O'Dowd C. and Eaton D. 2005. Field and laboratory measurements of magnetic properties and density, Central Metasedimentary Belt, Ontario. Current Research 2005-D2, Natural Resources Canada, Geological Survey of Canada, 13 p.

Oldenburg D. W. and Pratt D. A. 2007. Geophysical inversion for mineral exploration: A decade of progress in theory and practice. *In Proceedings of exploration* 7(5) :61-95. https://911metallurgist.com/blog/wp-content/uploads/2015/10/Geophysical-Inversion-for-Mineral-Exploration.pdf

Osinski G. R. and Pierazzo E. 2013. *Impact cratering: Processes and products*. John Wiley and Sons.

Osinski G. R., Silber E. A., Clayton J., Grieve R. A. F., Hansen K., Kalynn J. and Tornabene L. 2019.Transitional impact craters on the Moon: Insight into the effect of target lithology on the impact cratering process. *Meteoritics and Planetary Science* 54:573–591. https://doi.org/10.1111/maps.13226

PASSC, 2022. Earth Impact Database 2022. Planetary and Space Science Centre, University of New Brunswick, Fredericton NB. http://passc.net/EarthImpactDatabase/New%20website_05-2018/Index.html

Pilkington M. and Grieve R.A.F. 1992. The geophysical signature of terrestrial impact craters. *Reviews of Geophysics* 30: 161-81. https://doi.org/10.1029/92RG00192

Pilkington M. and Hildebrand A. R. 2000. Three-dimensional magnetic imaging of the Chicxulub crater. *Journal of Geophysical Research: Solid Earth*, 105(B10):23479-23491. https://doi.org/10.1029/2000JB900222

Pratt D. A., McKenzie K. B., White A. S., Foss C. A., Shamin A. and Shi Z. 2001. A user guided expert system approach to 3D interpretation of magnetic anomalies. *ASEG Extended Abstracts* 2001(1): 1-4. https://doi.org/10.1071/ASEG2001ab112

Pratt D. A., McKenzie K. B. and White T. S. 2014. Remote remanence estimation (RRE). *Exploration Geophysics*, 45(4):314-323. https://doi.org/10.1071/EG14031

Pratt D. A., White A. S., Parfre, K. L. and McKenzie K. B. 2020. ModelVision 17.0 User Guide. Tensor Research Pty Ltd., Grenwich, NSW, Australia, 596 p.

Puura V. and Suuroja K. 1992. Ordovician impact crater at Kärdla, Hiiumaa Island, Estonia. *Tectonophysics* 216(1-2): 143-156. https://doi.org/10.1016/0040-1951(92)90161-X

Reimold W.U., Koeberl C., Gibson R.L. and Dressler B.O., 2005. Economic mineral deposits in impact structures: a review. In, Koeberl C., Henkel H., Impact Tectonics, Springer, p.479-552.

Roy S. and Stewart R. 2012. Near-surface Seismic Investigation of Barringer (Meteor) Crater, Arizona. *Journal of Environmental and Engineering Geophysics* 17(3): 117-127. https://doi.org/10.2113/JEEG17.3.117

Schmitz B., Harper D.A., Peucker-Ehrenbrink B., Stouge S., Alwmark C., Cronholm,A., Bergström S.M., Tassinari M. and Xiaofeng W. 2008. Asteroid breakup linked to the Great Ordovician biodiversification event. *Nature Geoscience*, 1(1):49-53. https://doi.org/10.1038/ngeo.2007.37

Shuey R. T. and Pasquale A. S. 1973. End corrections in magnetic profile interpretation. *Geophysics* 38(3), 507-512. https://doi.org/10.1190/1.1440356

Sleep N.H., Zahnle K.J., Kasting J.F. and Morowitz H.J. 1989. Annihilation of ecosystems by large asteroid impacts on the early Earth. *Nature 342*: 139-42 https://doi.org/10.1038/342139a0

Spicer B., Morris B. and Ugalde H. 2011. Structure of the rambler rhyolite, Baie Verte Peninsula, Newfoundland: inversions using UBC-GIF Grav3D and Mag3D. *Journal of Applied Geophysics*, 75(1), pp.9-18. https://doi.org/10.1016/j.jappgeo.2011.06.013

St. John B. E. 1968. Paleolacustrine arenites in the Holleford meteorite crater, Ontario. *Canadian Journal of Earth Sciences* 5(4), 935-943. https://doi.org/10.1139/e68-090

Stewart S.A. and Allen P.J. 2002. A 20-km diameter multi-ringed impact structure in the North Sea. *Nature* 418:520-523 https://doi.org/10.1038/nature00914

Stewart S.A. and Allen P.J. 2005. 3D seismic reflection mapping of the Silverpit multi-ringed crater, North Sea. *GSA Bulletin* 117 (3-4): 354–368. https://doi.org/10.1130/B25591.1

Stewart S.A. 2003. How will we recognize buried impact craters in terrestrial sedimentary basins? *Geology* 31: 929-32, 31. https://doi.org/10.1130/G19853.1

Suttak P.A. 2013. High-resolution lake-based magnetic mapping and modeling of basement structures, with examples from Küçükçekmece Lagoon, Turkey and Charity Shoal, Lake Ontario. unpublished MS thesis, School of Geography and Earth Sciences, McMaster University, Hamilton, Ontario. 113 pp. http://hdl.handle.net/11375/13532

Symons D. T. A. and Chiasson A. D. 1991. Paleomagnetism of the Callander Complex and the Cambrian apparent polar wander path for North America. *Canadian Journal of Earth Sciences* 28:355–363 https://doi.org/10.1139/e91-032

Talwani M., Worzel J. L. and Landisman M. 1959. Rapid gravity computations for two-dimensional bodies with application to the Mendocino submarine fracture zone, *Journal of Geophysical Research* 64(1): 49– 59 https://agupubs.onlinelibrary.wiley.com/doi/10.1029/JZ064i001p00049

Talwani M. and Ewing M. 1960. Rapid computation of gravitational attraction of three-dimensional bodies of arbitrary shape. *Geophysic*s, 25(1): 203-225.

Talwani M. and Heirtzler J. R. 1964. Computation of Magnetic Anomalies Caused by Two Dimensional Bodies of Arbitrary Shape. In G. A. Parks (Ed.), *Computers in the Mineral Industries*, 1: 464-480. Stanford Univ. Publ., Geological Sciences 9.

Talwani M., 1965. Computation with the help of a digital computer of magnetic anomalies caused by bodies of arbitrary shape. *Geophysics*, 30(5): 797-817

Tschirhart V., Morris W. A., Jefferson C. W., Keating P., White J. C. and Calhoun L. 2013. 3D geophysical inversions of the north-east Amer Belt and their relationship to the geologic structure. Geophysical Prospecting, 61:547-560. https://doi.org/10.1111/j.1365-2478.2012.01098.x

Tsikalas F. and Eldholm O. 2018. Malvinas (Falkland) Plateau Structure versus Mjolnir crater: Geophysical workflow template for proposed marine impact structures. *Meteoritics and Planetary Sciences* 54(3): 544-557 https://doi.org/10.1111/maps.13227

Thomas M. D., Ford K. L. and Keating P. 2016. Exploration geophysics for intrusion-hosted rare metals. *Geophysical Prospecting,*64(5), 1275-1304. https://doi.org/10.1111/1365-2478.12352

Ugalde H., Danuor, S. K., and Milkereit B. 2007. Integrated 3-D model from gravity and petrophysical data at the Bosumtwi impact structure, Ghana. *Meteoritics and Planetary Science* 42(4-5), 859-866. doi: https://doi.org/10.1111/j.1945-5100.2007.tb01081.x

Underhill J.R. 2004. An alternative origin for the 'Silverpit crater'. *Nature,* 428(6980):1-2.

Urbini S., Nicolosi, I., Zeoli A., El Khrepy S., Lethy A., Hafez M., El Gabry M., El Barkooky A., Barakat A., Gomaa M. and Radwan A.M. 2012. Geological and geophysical investigation of Kamil crater, Egypt. *Meteoritics and Planetary Science* 47(11):1842-1868. https://doi.org/10.1111/maps.12023

Virden W.T., Warren J.S., Holcombe T.L., Reid D.F. and Berggren T.L. 1999. Bathymetry of Lake Ontario. National Geophysical Data Center, World Data Center A for Marine Geology and Geophysics, Boulder CO. Rept. MGG–14.

Waddington E. D. and Dence M. R. 1979. Skeleton Lake, Ontario - evidence for a Paleozoic impact crater. *Canadian Journal of Earth Sciences* 16(2): 256–263. https://doi.org/10.1139/e79-025

Won I. J. and Bevis M. 1987. Computing the gravitational and magnetic anomalies due to a polygon: Algorithms and Fortran subroutines. *Geophysics* 52: 232-238 https://doi.org/10.1190/1.1442298

Chapter 2: 3-D geophysical modelling of a deeply buried, simple impact crater:Holleford impact structure, Ontario, Canada

Abstract

Holleford Crater is a deeply buried, 2.35 km diameter Late Proterozoic-Early Cambrian (ca. 550 ±100 Ma) simple impact crater located in southeastern Ontario, Canada. Geophysical studies and drilling in the 1950's suggested a >450 m deep central basin and a -2.2 mGal gravity anomaly. We conducted ground-based geophysical surveys (magnetics, gravity) and potential field modelling to better resolve the buried crater depth and subsurface geometry. Geophysical surveys reveal a well-defined 2-3 mGal Bouguer gravity low over the crater basin and a <20 nT residual magnetic anomaly. The lack of a well-defined magnetic anomaly is attributed to the low magnetic contrast between Mesoproterozoic metasedimentary target rocks and overlying Paleozoic infill sediments.

The gravity model and reconstructed basement surface indicate a deeply buried (>200 m), heavily eroded simple impact crater with a rim-to-rim diameter (D) of 1.8-2 km, a residual rim height of about 20-30 m and a true depth (d_t)>400 m. The modelled basement surface identifies a rim breach and possible fluvial outflow channel in the southeast crater rim. The channel is up to 150 m deep, 400 m in width and is analogous to outlet channels produced by fluvial rim dissection of impact craters on Earth and 'tadpole craters' on Mars. Outflow channels are infilled by Cambrian-Early Ordovician sediments, indicating a probable Late Proterozoic-Early Paleozoic age for the structure.

Keywords: Holleford impact crater, microgravity, magnetic surveys, 3-D potential field modelling, post-impact erosion, rim breach, outlet channels

Highlights

- Buried simple impact crater with estimated 2.35 km diameter surface rim
- 3-D modelling of ground-based gravity survey data to determine crater depth, subsurface morphology
- Crater rim-to-rim diameter 1.8-2 km, residual rim height 20-30 m and true depth >400 m
- Evidence for crater modification by post-impact rim lowering and fluvial dissection
-

2.1. Introduction

The Holleford structure has been interpreted as a 2.35 km diameter, Late Proterozoic to Early Cambrian age (ca. 550 ±100 Ma) impact crater in southeastern Ontario, Canada (Fig. 2.1) (Beals, 1960; PASSC, 2022). The crater was first identified in the 1950's and confirmed by exploration drilling and recovery of impact breccias with shock polymorphs (Beals, 1960; Bunch and Cohen, 1963). Borehole and seismic refraction data suggested a deeply buried (>400 m) and heavily eroded simple impact crater with a -2.2 mGal gravity anomaly over the central basin (Beals, 1960). The gravity anomaly was attributed to low-density basin fill sediments and fracturing of target rocks (Beals, 1960; Beals and Innes, 1961; Innes, 1961). No further work has been completed at Holleford following the original 1960 studies. Advances in geophysical modelling since that time provide an opportunity to better resolve the crater subsurface morphology, geology and level of post-impact modification.

Geophysical modelling is an important tool in the discovery and investigation of terrestrial impact craters (Pilkington and Grieve, 1992; French and Koeberl, 2010; Morgan et al., 2013). 2-D forward gravity and magnetic models are often employed to estimate impact crater depth, diameter, and crater geometry (Puura and Suuroja, 1992; Evangelatos, 2009; Urbini et al., 2012; Suttak, 2013; Lamali et al., 2016). More

sophisticated, 3-D geophysical models can also reveal structural details and the three-dimensional subsurface morphology of buried impact structures. Geophysical studies and 3-D modelling have led to recognition of Chicxulub as a large multi-ring impact crater (Hildebrand et al., 1991; Pilkington et al., 1994; Pilkington and Hildebrande, 2000) and have been critical in mineral exploration of the Sudbury impact structure (Olaniyan et al., 2015).

3-D geophysical models have been applied in a small number of studies to investigate simple and transitional (< 4 km) terrestrial impact structures. Ugalde et al. (2007a) constructed a 3-D magnetic model for the Botsumi impact crater to determine the subsurface geology and magnetic source bodies. Ugalde et al., (2007b) employed a 3-D forward and inversion modelling of gravity data to determine density distribution and extent of fractured target rocks within the ~0.37 km diameter Monturaqui crater (Chile). Tsikalas and Eldholm (2018) advocated the use of 2-D and 3-D geophysical models in the investigation of suspected marine impact structures (Malvinas, Falklands Plateau) and developed a workflow template that integrates a range of geophysical data types (e.g., seismic, bathymetric, magnetic and gravity) in assessing possible impact origins.

In this paper, we report on the results of new ground-based geophysical surveys and 3-D potential field modelling of the Holleford impact crater (Fig. 2.1A, 2.2). A forward 3-D gravity model was employed to reconstruct the Precambrian basement surface and to investigate the buried crater morphology, depth, and geometry of infill sediments. 3-D modelling reveals a ~1.8-2.0 km diameter crater basin in Mesoproterozoic basement and evidence for erosional lowering and fluvial dissection of the buried crater rim. The rim breach has similar dimensions to fluvial channels produced by break-out floods in volcanogenic lakes (e.g., Lake Taupo, New Zealand) (Manville et al. 1999) and fluvial dissection of terrestrial impact craters (e.g., Talemzane crater, Algeria) (Grant and Schultz, 1993). The channel features may provide a possible ancient terrestrial analogue for outflow channels in Martian ‘pollywog’ craters (Goudge et al., 2021). The 3-D modelling techniques demonstrated here have a broader application to the subsurface

investigation of buried terrestrial impact craters and for evaluating post-impact modification processes (Grant and Schultz, 1993; Tsikalas et al., 2007).

2.2. Study Area

2.2.1 Physical setting and geology

The Holleford crater is located 30 km northwest of Kingston, in southeastern Ontario, Canada (Fig. 2.1A). The crater is defined by a ~2.4 km diameter, raised bedrock rim that encloses a shallow (< 30 m deep) central basin with an area of about 0.5 km^2 (Fig. 2.2) (Beals, 1960). Bedrock within the study area consists of Paleozoic clastic and carbonate sediments overlying Mesoproterozoic (ca. 1.4-1.1 Ga) metasedimentary rocks of the southwestern Grenville Province Frontenac Terrane (Easton, 2001; Carr et al., 2000) (Fig. 2.1B). The Frontenac Terrane includes abundant metacarbonates (e.g., marble) and siliciclastic metasedimentary rocks (quartzite, paragneiss), which are intruded by diorite and gabbro plutons (Fig. 2.1B) (Easton, 2001; Magnus and Easton, 2015). Within the Holleford study area, basement is composed of interbedded marble, quartzo-feldspathic gneiss, granulite, and amphibolite units that strike northwestward and dip southeastward. The western shoreline of Knowlton Lake marks the location of a major northeast-trending, down-to-the-east normal fault (Desert Lake-Canoe Lake Fault; Fig. 2.1B) (Easton, 2001; Dickin and Strong, 2021).

The Paleozoic cover strata (Fig. 2.1B) include Late Cambrian to Middle Ordovician carbonate and clastic sedimentary rocks of the Potsdam (Nepean) and Black River Groups (Beals, 1960; Kirwan, 1963; Brett et al., 2004; Sanford and Arnott, 2010; Brink et al., 2019). Paleozoic sediments have a total thickness >300 m within the crater basin (Beals, 1960; St. John, 1968) and thin rapidly northward of the crater, where Mesoproterozoic basement is exposed along the Paleozoic-Precambrian contact (Fig. 2.1B). Paleozoic strata form concentric bedrock outcrops around the crater rim and dip at

low angles (<2-5 °) into a broad syncline at the basin centre (Fig. 2.2A). Bedrock is mantled by thin (< 10 m thick) Quaternary glacial sediments and streamlined glacial landforms, including small drumlins and flutes. The southwestern bedrock rim of the crater forms part of a 1.5 km long, glacially streamlined 'crag-and-tail' feature formed below southwestward-flowing Laurentide ice (Sookhan et al., 2021) (Fig. 2.2A).

2.2.2 Previous work

The Holleford structure was first identified during a regional search of the Precambrian shield for impact craters conducted by the Dominion Observatory, Ottawa (Beals et al., 1956; Beals, 1958). The structure was investigated with geophysical surveys and drilling of three continuously cored boreholes to depths of >450 m (Figs. 2.2B, 2.3) (Beals, 1960; Innes, 1964; Dence, 1964). The deepest borehole BH-2 (453 m) intersected 125 m of Paleozoic strata, >100 m of polymictic impact breccias and Mesoproterozoic basement rocks at a depth of 240 m (Fig. 2.3). The basement rocks contained extensive calcite-filled fractures extending to a depth of >30 m and were interpreted by Beals (1960) as evidence for shock deformation and fracturing of target rocks. BH-1 (344 m), located near the basin centre (Fig. 2.2B), recorded 225 m of Paleozoic sediments and a minimum breccia thickness >100 m, but did not penetrate to basement (Fig. 2.3). In BH-3 (135 m) on the southeast crater rim, basement was reached at a shallow depth (~20 m) and no impact breccias were present (Fig. 2.3). Beals (1960) interpreted the elevated height of basement in BH-3 as a remnant of the southeastern crater rim. Citing the absence of Paleozoic clasts in the impact breccias, Beals (1960) proposed a Late Proterozoic to Early Cambrian age (600-500 Ma) for the crater. Petrographic studies by Dawson (1961) determined a polymictic breccia composition, consisting of angular marble, gneissic, amphibolite clasts within a fine-grained clay-rich matrix. Coesite and shocked quartz were subsequently identified in two breccia samples, confirming an impact origin (Bunch and Cohen, 1963).

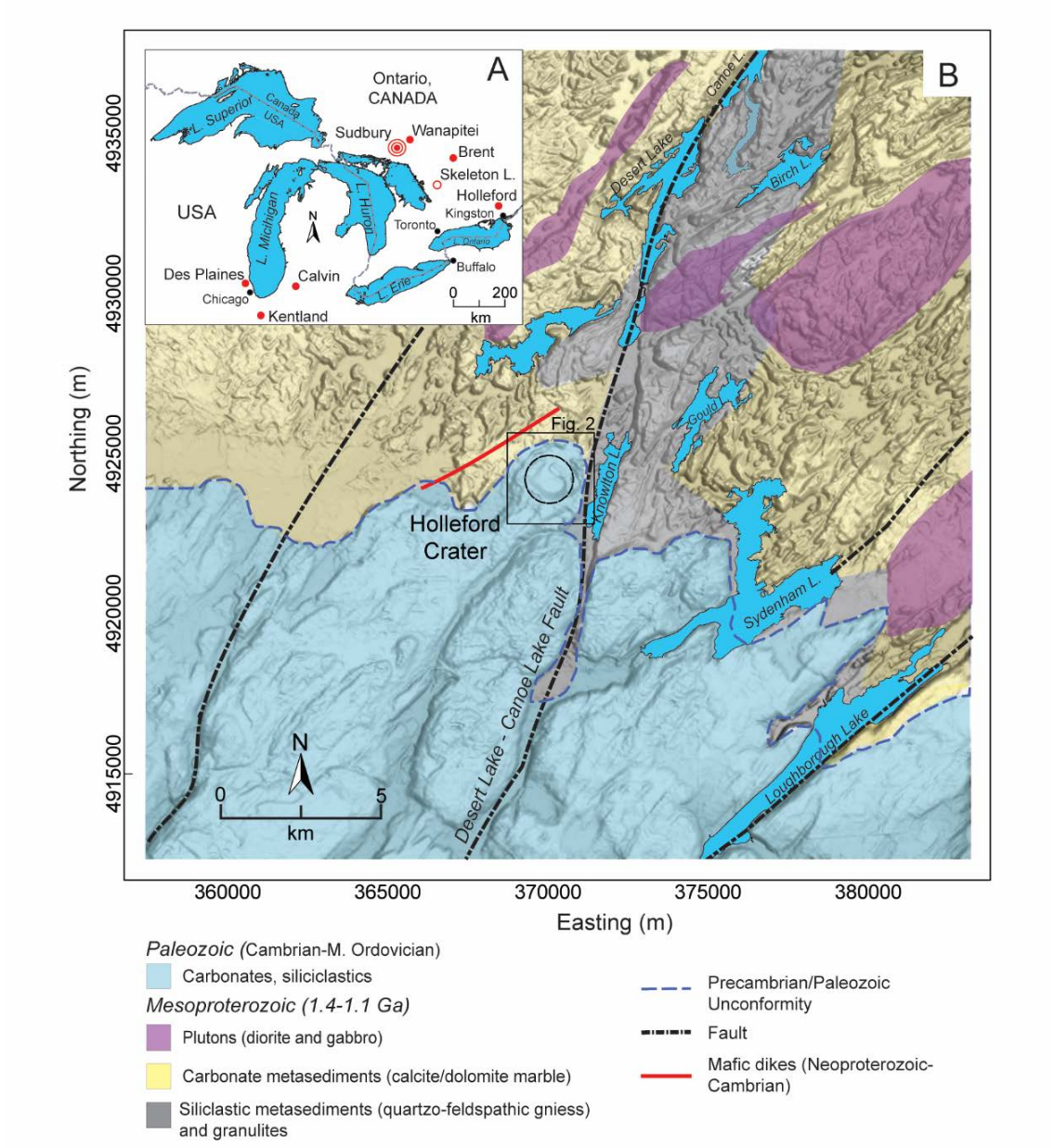

Figure 2.1. A. Location of the Holleford structure and other confirmed (red circles) and suspected (open red circle) impact craters in the Great Lakes region. B. Regional geology map showing location of Holleford study area (~9-km^2; Fig. 2.1). The crater lies close to the limit of Paleozoic cover and is underlain by Mesoproterozoic basement rocks of the Grenville Province Frontenac Terrane (modified from Magnus and Easton, 2015; Dickin and Strong, 2021). The Desert Lake-Canoe Lake fault marks a major normal basement fault that extends below Knowlton Lake.

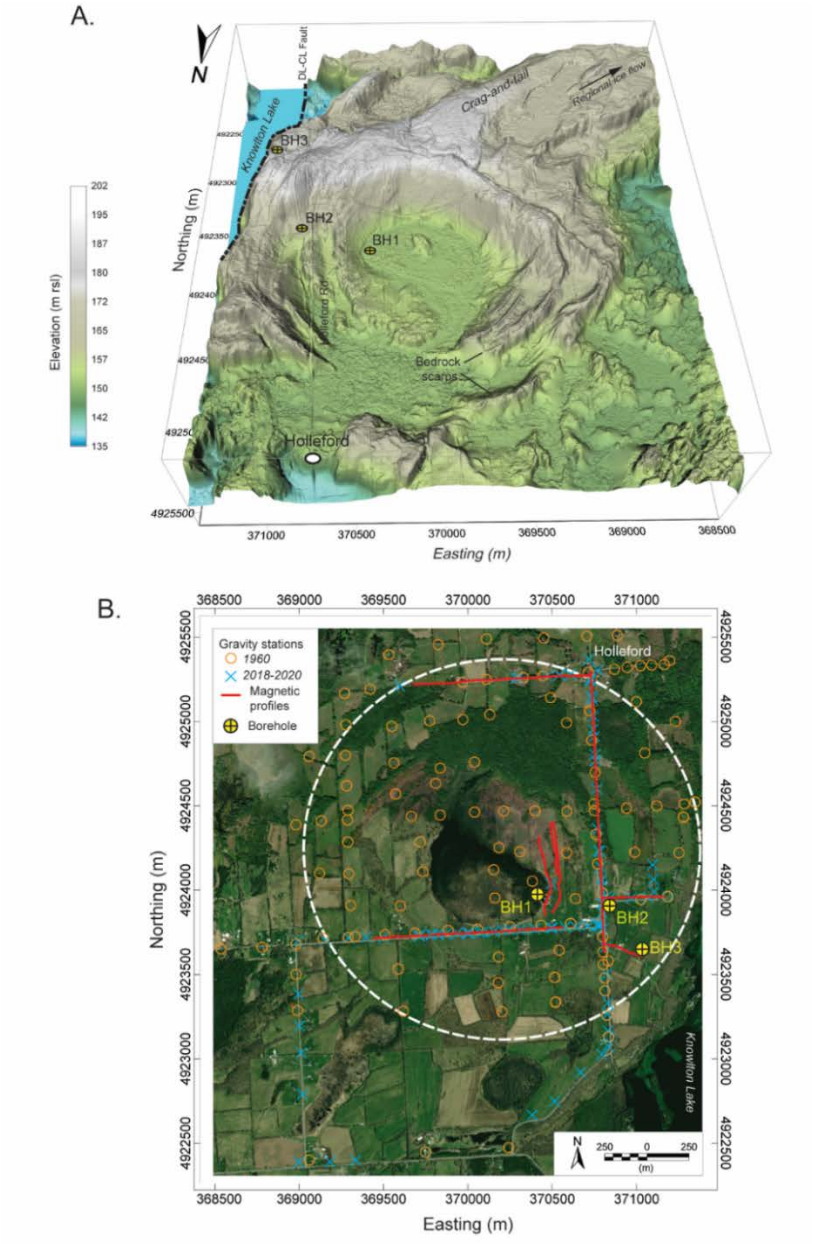

Figure. 2.2. A. Digital elevation model (DEM) of Holleford impact crater (2-m resolution; vertical exaggeration ~ 5 x, data source: LIO, 2014). Crater is defined topographically by concentric Paleozoic bedrock outcrops that dip (2-5°) into a syncline in the` basin centre. DL-CL = Desert Lake-Canoe Lake fault. B. Aerial image showing location of gravity stations, ground magnetic profiles and boreholes (BH1-3; Beals, 1960). Dashed circle indicates approximate crater rim (~2.4 km diameter) as interpreted from surface outcrop pattern by Beals (1960).

Gravity measurements (126 stations) collected as part of the 1960 study (Fig. 2.2B) revealed a 2.2 mGal central gravity low and a broad, annular gravity high corresponding with the structure topographic rim (Beals, 1960; Beals and Innes, 1961, Innes, 1961). Innes (1961) attributed the mass deficiency (3.4 $x10^{14}$ g), indicated by the gravity anomaly, to the presence of low-density infill sediments and breccias and estimated the total infill volume of ~1.5 $x10^{9}$ m^{3}. Andrieux and Clark (1969) conducted resistivity surveys across several transects and estimated a total crater depth of 800 +/- 120 m, including >180 m of Paleozoic sediments overlying thick impact breccias.

St. John (1968) identified seven distinct lithostratigraphic units within the crater basin fill (Fig. 2.3). The succession included an uppermost package of Middle Ordovician (Black River Group) dolomitic limestone, shale, and conglomerate (Units 6, 7) overlying Late Cambrian-age quartz arenite sandstones (Units 4, 5), calcareous shale, and limestone (Unit 3). The lowermost sediment package (Units 1, 2) consisted of thin basal conglomerate (< 5 m thick) overlying polymictic impact breccias (Fig. 2.3). The breccia was over 100 m thick in BH-2 and had a minimum thickness >120 m in BH-3 at the basin centre. BH-3 did not fully penetrate to basement, so the maximum thickness of the breccia was not determined (Beals, 1960; St. John, 1968). The Late Cambrian sandstones of Unit 4 were interpreted as paleolacustrine arenites deposited in a crater lake basin and separate from Potsdam Group (Nepean) fluvial sandstones, which are exposed to the south and northeast of the crater rim (St. John, 1968; Andrieux and Clark, 1969).

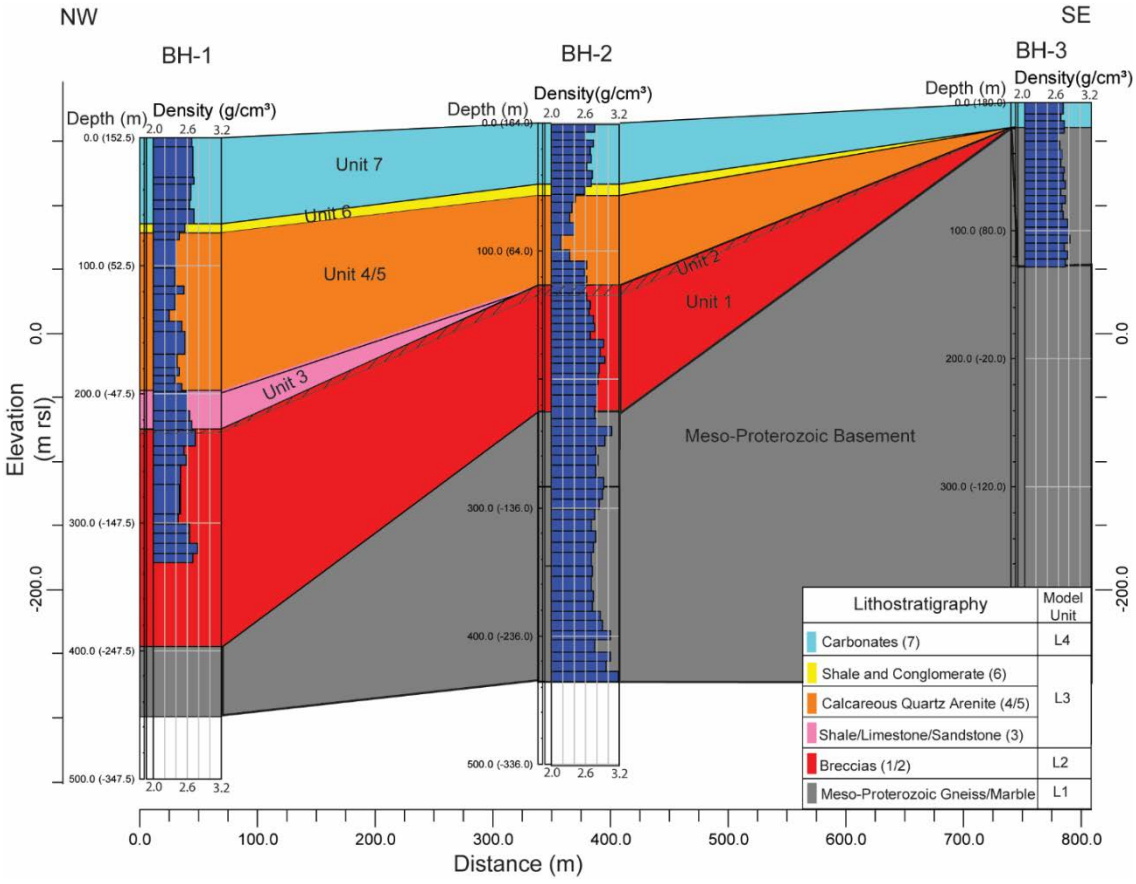

Figure 2.3. NW-SE Geological cross-section from basin centre to southeast crater rim showing basin fill lithostratigraphic units of St. John (1968) and assignment to model layers L1-L4. Core bulk densities (gcm^{-3}) compiled from Beals (1960). L1 = Mesoproterozoic basement (metasediments, gneiss), L2 = impact breccia and conglomerates (talus), L3 = Late Cambrian siliciclastic sediments and carbonates, L4 = Middle Ordovician (Black River Group) dolomitic limestone and shale.

2.3. Methods

2.3.1 Magnetic and gravity surveys

Ground-based magnetic and microgravity surveys were conducted over ~20 km^2 area at Holleford in 2018 and 2020 (Fig. 2.2B). Surveys were collected along existing roads and within open fields where access was granted (Fig. 2.2B). Total magnetic intensity (TMI) measurements (12-line-km) were acquired with an Overhauser magnetometer (GEM Systems GSM-19). The magnetometer sampled at 2 Hz and positioned using a differential GPS (D-GPS) with a horizontal positional accuracy of 0.1 m. A second basestation magnetometer was deployed onsite to record the diurnal magnetic variation at a 1 Hz rate. Magnetic data were processed in Geosoft Oasis software (Seequent Ltd.) following the general scheme outlined by Suttak (2013). Processing included application of diurnal corrections, statistical tie-line levelling and regional residual separation by subtraction of an upward continued (300 m) grid (Figs. 2.4 B, C). Ground magnetic surveys lines were combined with Provincial aeromagnetic data (Ontario Master Aeromagnetic Dataset; Reford et al., 1990) acquired at line spacing of 800 m and a flight elevation of 300 m. The data sets were merged by upward continuation of the land magnetic data to 300 m, followed by statistical tie-line levelling. The merged data were then gridded using minimum curvature with 50 m cells. A residual magnetic map was produced by subtraction of the regional field from the TMI grid (Luyendyk, 1997).

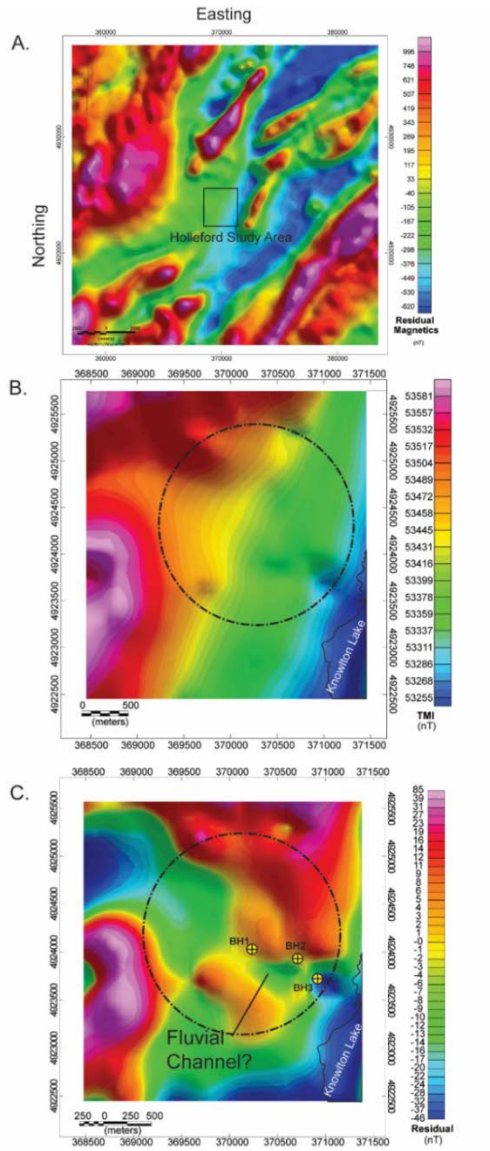

Figure 2.4. A. Residual aeromagnetic map for region around Holleford, showing northeast-trending magnetic fabric in Frontenac terrane Mesoproterozoic basement rocks (data source: Reford et al., 1990). Location of Holleford study area shown. High magnetic intensities correspond with plutonic rocks (diorite/gabbro) and migmatite, and low intensity 'troughs' with lower magnetic susceptibility carbonate and siliciclastic metasediments. B. Total magnetic intensity (TMI) map of Holleford study area. C. Residual magnetic map showing NW-SE trending magnetic low, corresponding with thickened Paleozoic infill strata and magnetic high around crater rim. Dashed circle indicates approximate outline of surface crater rim defined by Beals (1960). Borehole locations also shown.

Gravity measurements were acquired using a Lacoste and Romberg G128 land gravity meter and Scintrex CG-5 autolevelling gravimeter. A total of 74 gravity stations were measured at 150-200 m intervals adjacent to roadways and along two transects within the crater basin (Figure 2.2B). Diurnal and tidal gravity variations were recorded by re-occupation of a base station at 2-3 hr intervals. The station positions and elevations were measured using a D-GPS (Promark 3) with a horizontal and vertical positional error of <1 cm. Gravity data reduction included corrections for instrument drift, tidal variation, free-air, Bouguer cap using the methods outlined by Holum and Oldow (2007). The absolute Bouguer gravity was calculated with reference to measurements at a Canadian Gravity Standardization Network station (CGSN 9907-1999) located 30 km to the east at Gananoque. The new observations were merged with vintage gravity data (Fig. 2.2B; Beals, 1960) and levelled using a linear correction factor established where points from the two data sets overlapped. In a final step, the merged data were terrain corrected in Geosoft Oasis using a high-resolution (2-m graticule) digital elevation model (DEM) (LIO, 2014). Both the Bouguer cap and terrain corrections employed a density value of 2.67 gcm^{-3}. The terrain-corrected Bouguer gravity data were gridded and interpolated using ordinary Kriging with a 100 m grid cell size (Wackernagel, 2003).

2.3.2 3-D gravity model

A 3-D gravity model was constructed in ModelVision 17 (Tensor Geophysics Pty.) using the profile modelling option (Pratt et al., 2020), which implements the methods of Talwani and Ewing. (1960) and Cady (1980) to compute the gravity response of polygonal source bodies. The Bouguer gravity anomaly was forward modelled along NW-SE lines at 100 m separation and NE-SW crossing profiles at 400 m spacing (total 46 profiles; Fig. 2.6A). The crater geology was modelled as four separate layers (L1-L4; Table 2.1) using mean bulk density values from three boreholes (Fig. 2.3) (Beals, 1960). Mesoproterozoic basement rocks (L1) had a mean density of 2.99 ± 0.18 gcm^{-3} (Table

2.1) and overlying breccias (L2) were more variable (2.57-2.80 gcm^{-3}). The Late Cambrian siliciclastic sediments (lithostratigraphic units 3-6 of St. John, 1968; Fig. 2.3) were assigned to a single model layer (L3), as their densities were uniformly low (~2.44 ± 0.16 gcm^{-3}) (Table 2.1). The uppermost Black River limestones and shales (L4) had a mean bulk density of ~2.70 ± 0.03 gcm^{-3} (Table 2.1).

The bulk density data (Table 2.1; Fig. 2.3) demonstrate significant density contrasts at the contact between Late Cambrian clastic sediments (L3) and overlying Middle Ordovician carbonates (L4) (~0.25 gcm^{-3}) and at the top of the impact breccia layer (L2) (Fig. 2.3). There is also a large density contrast (~0.2-0.4 gcm^{-3}) between the impact breccias and the underlying Mesoproterozoic basement (L1). It was determined, however, that the model was less sensitive to the changes in the elevation of the breccia/basement (L2/L1) interface due to its greater depth when compared to the L3/L4 contact (Fig. 2.3).

As a first step, a NW-SE profile was constructed through the basin centre using borehole data to constrain the model layer thicknesses. Adjacent parallel profiles were then added to create a fully 3-D multi-section model (Pratt et al., 2020). The layer thicknesses and geometry were adjusted manually until the residual error between the observed gravity and modelled signal was minimized and typically < ±0.1-0.2 mGal RMS. The modelled layers surfaces were then exported and interpolated using minimum curvature to produce structure contour and isochore maps.

	n	Mean	Median	St. Dev
BH-1		g/cm^3	g/cm^3	g/cm^3
Middle Ordovician carbonates (L4)	11	2.70	2.71	0.03
Late Cambrian clastics (L3)	15	2.45	2.46	0.08
Impact breccia (L2)	17	2.57	2.50	0.12
Mesoproterozoic basement (L1)	n/a			
BH-2				
Middle Ordovician carbonates (L4)	8	2.69	2.70	0.05
Late Cambrian clastics (L3)	10	2.44	2.41	0.16
Impact breccia (L2)	15	2.80	2.78	0.15
Mesoproterozoic basement (L1)	25	2.99	3.02	0.18
BH-3				
Middle Ordovician carbonates (L4)	4	2.70	2.70	0.03
Late Cambrian clastics (L3)	n/a			
Impact breccia (L2)	n/a			
Mesoproterozoic basement (L1)	n/a			

Table 2.1. Tabulated borehole densities (gcm^{-3}) for model layers (L1-L4). Data compiled from Beals (1960). Model layers adapted from lithological units defined by St. John (1968) (Fig. 2.3).

2.4. Results

2.4.1 Magnetic survey

Regional aeromagnetic data show a well-defined northeast-trending magnetic fabric, consisting of linear magnetic highs and trough-like magnetic lows. (Figs. 2.4 A, B). The anomaly pattern is due to the alternation of low magnetic susceptibility Mesoproterozoic metacarbonate and siliciclastic gneiss units and more highly-magnetized plutonic rocks (diorite/gabbro) and migmatites (Fig. 2.1B). The crater is located within an area of low magnetic intensity, consistent with carbonate metasedimentary rocks (Figs. 2.1B, 2.4A). The Holleford crater TMI map (Fig. 2.4B) shows an overall low magnetic relief (300-400 nT) and a subtle magnetic low (~ 20-30 nT) below the crater that interrupts the regional northeast magnetic trend. The magnetic residual map shows that the anomaly low extends from the northwest crater rim southeast below Knowlton Lake (Fig. 2.4C).

The lack of a well-defined magnetic anomaly (Fig. 2.4B) can be attributed to the low contrast in magnetic susceptibility between Mesoproterozoic metasedimentary rocks and overlying Paleozoic cover strata (Magnus and Easton, 2015). Regionally, the Paleozoic sediments have a low magnetic susceptibility (mean $\kappa = 1.05\ 10^{-6}$ SI) and Mesoproterozoic metacarbonate rocks (i.e., marbles) have similarly low values (κ ~1.00-5.15 x 10^{-6} SI) (O'Dowd and Eaton, 2005). Plutonic and siliciclastic metasedimentary rocks in the Frontenac terrane, in contrast, have much greater values of up to 2.72 x 10^{-3} SI (O'Dowd and Eaton, 2005). The northwest-southeast trending magnetic low below the crater (Fig. 2.4C) is counter to the strike of Mesoproterozoic units (Fig. 2.1B). It may record changes in the relative thickness of low susceptibility Paleozoic cover rocks (L3, L4) over the crater infill breccia and Mesoproterozoic basement (section 2.4.3).

2.4.2 Gravity survey

The regional Bouguer gravity map shows that Holleford crater sits on the southeastern flank of a broad, northeast-trending gravity high (Fig. 2.5A). There is a general trend towards decreased gravity from the northwest to southeast, corresponding with the trend in magnetic intensity (Fig. 2.4A). The terrain-corrected Bouguer map shows a well-defined ~2-3 mGal gravity low over the basin centre (Figs. 2.5B, C), which clearly interrupts the regional gravity trend (Fig. 2.5A). The Bouguer gravity anomaly is consistent with Beals (1960) hand-contoured gravity map and better resolves short-wavelength components of the gravity signal in the southern and southeastern crater rim (Fig. 2.5B). Overlay of the Bouguer gravity on the DEM (Fig. 2.5C) shows gravity lows (~ 1.5 mGal) to the south of the crater rim and below Knowlton Lake where lower-density Paleozoic sediments thicken within a structural depression in the Precambrian basement surface. The gravity low below Knowlton Lake corresponds with a northwest-trending magnetic anomaly that defines the Canoe Lake-Desert Lake fault (Dickin and Strong, 2021) (Figs. 2.1B, 2.4A).

2.4.3 Gravity model

Forward-modelled gravity profiles with estimates of the crater dimensions (D, dt). are shown in Figures 2.6 and 2.7. The crater rim height was measured using the mean height of the Mesoproterozoic basement (~ 0 m rsl) as an approximation of the pre-impact surface elevation. The crater dimensions are minimum estimates, as the pre-impact basement surface topography and crater rim height have been reduced by post-impact erosion. Structure contour and isochore thickness maps for the model layers (L1-L4) are shown in Figures 2.8 and 2.9.

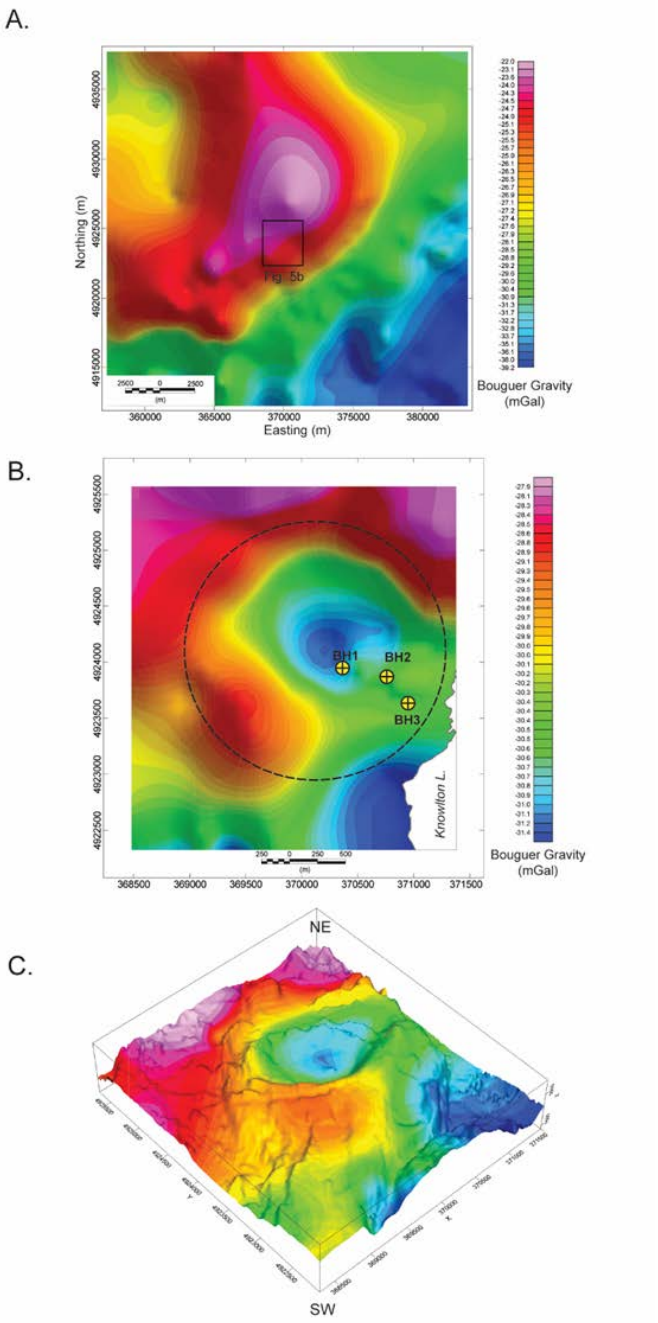

Figure 2.5. A. Regional Bouguer gravity map (data source: CGDB, 2020). B. Terrain-corrected Bouguer gravity map of Holleford compiled from 74 new gravity stations and vintage gravity data (Beals, 1960). Borehole locations also shown. C. Bouguer gravity anomaly draped on DEM (vertical exaggeration = 10). View from southwest.

Model profiles across the basin centre (Lines 12A, 26; Fig. 2.6) show central 2-3 mGal gravity low that generally parallels the crater surface topography (Figs. 2.6, 2.7). The estimated rim-to-rim diameter (D) as measured across the profiles is ~1.8-2.0 (±0.1) km (Fig. 2.8A). The basement surface map interpolated from the gravity profile data, shows a central deep basin with a maximum depth to basement >430 m and evidence for remnants of an upraised rim structure (Figs. 2.6, 2.7, 2.8A). The crater rim is discontinuous and dissected in the east by a southeast-trending 300-400 m wide channel feature that is up to 130 m in depth (Fig. 2.6B; Fig. 2.8A).

The overall crater fill thickness, as measured from the modern surface to basement, is ~580 m at the basin centre (Fig. 2.9A). Middle Ordovician sediments (L4) are thickest (~180 m) above the crater basement rim, forming an annular-shaped sediment body in the isochore map (Fig 2.9B). The Cambrian clastic sediments (L3) have a variable thickness, which is dependent on the relief on the upper surface of the breccia (L2) and underlying Mesoproterozoic basement (L1). Cambrian sediments reach a thickness >100 m within broad, northwest-southeast structural lows on the breccia top surface (Fig. 2.8B). The troughs follow the general northwest-southeast gradient on the basement surface and may record erosion of the crater basin by a post-impact fluvial drainage network. (Figs. 2.8C, 2.9). The trends are also evident in the residual magnetic map (Fig. 2.4C).

The breccia layer (L2) has a maximum thickness of ~350 m in the basin centre and thins radially outward towards the structure rim, consistent with the absence of breccia deposits in BH-3 (Figs. 2.3; 2.6B). Beals (1960) interpreted the absence of breccias in BH-3 as evidence for erosion of the crater rim.

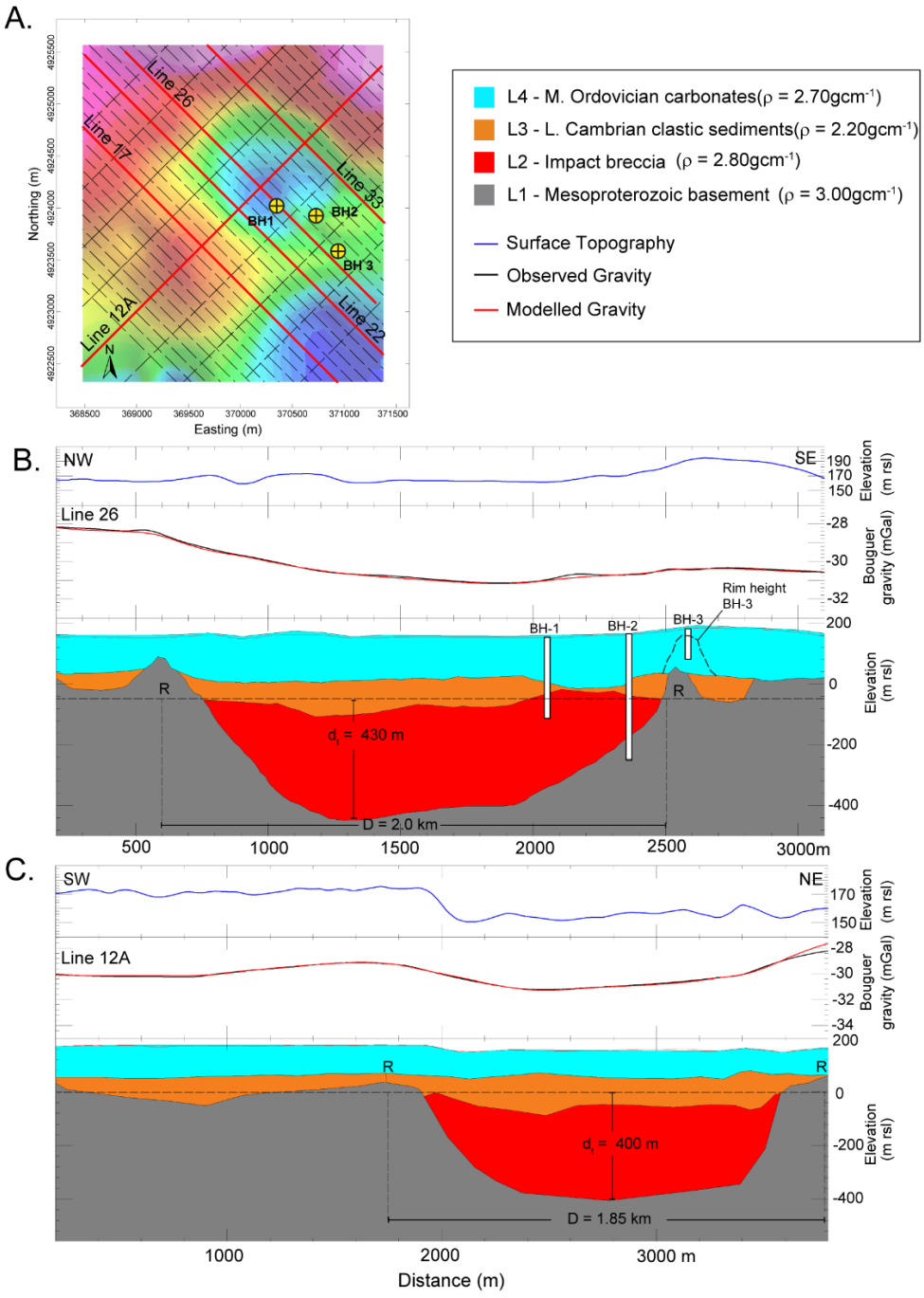

Figure 2.6. A. Model domain (9 km^2) showing model profiles and borehole locations. B. NW-SE gravity profile (Line 26) across basin centre. Boreholes shown projected onto section. C. SW-NE Gravity profile (Line 12A) parallel with basement regional strike. The interpreted crater rim (R), estimated rim-to-rim diameter (D) and true depth (d_t) are indicated on profiles.

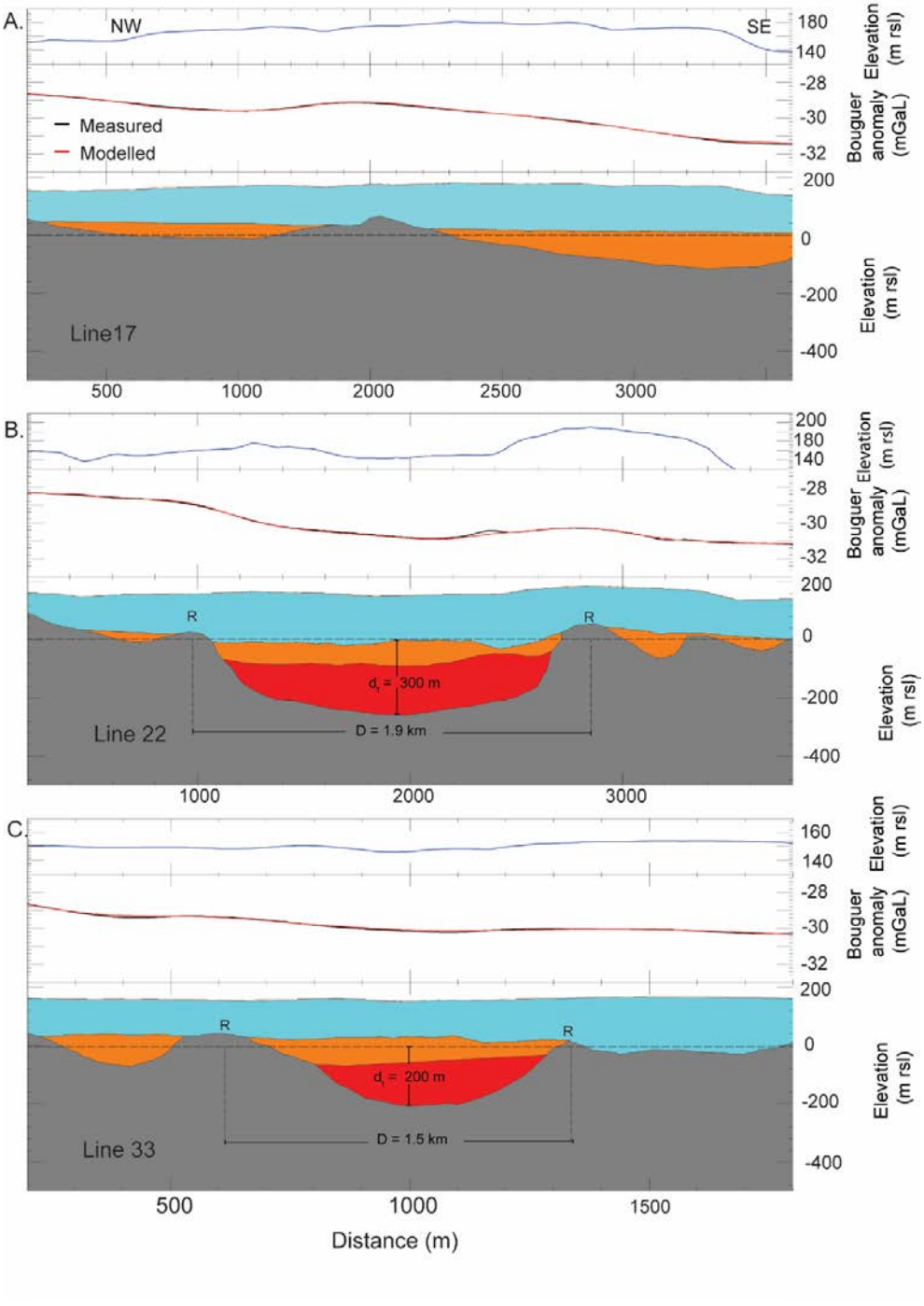

Figure 2.7. Forward modelled gravity profiles. A. Line 17. B. Line 22. C. Line 33. Profile locations shown in Fig. 2.6A. Estimated location of crater rim (R), rim-to-rim diameter (D) and true depth (d_t) indicated on profiles. Legend and regional map as from Fig. 2.6

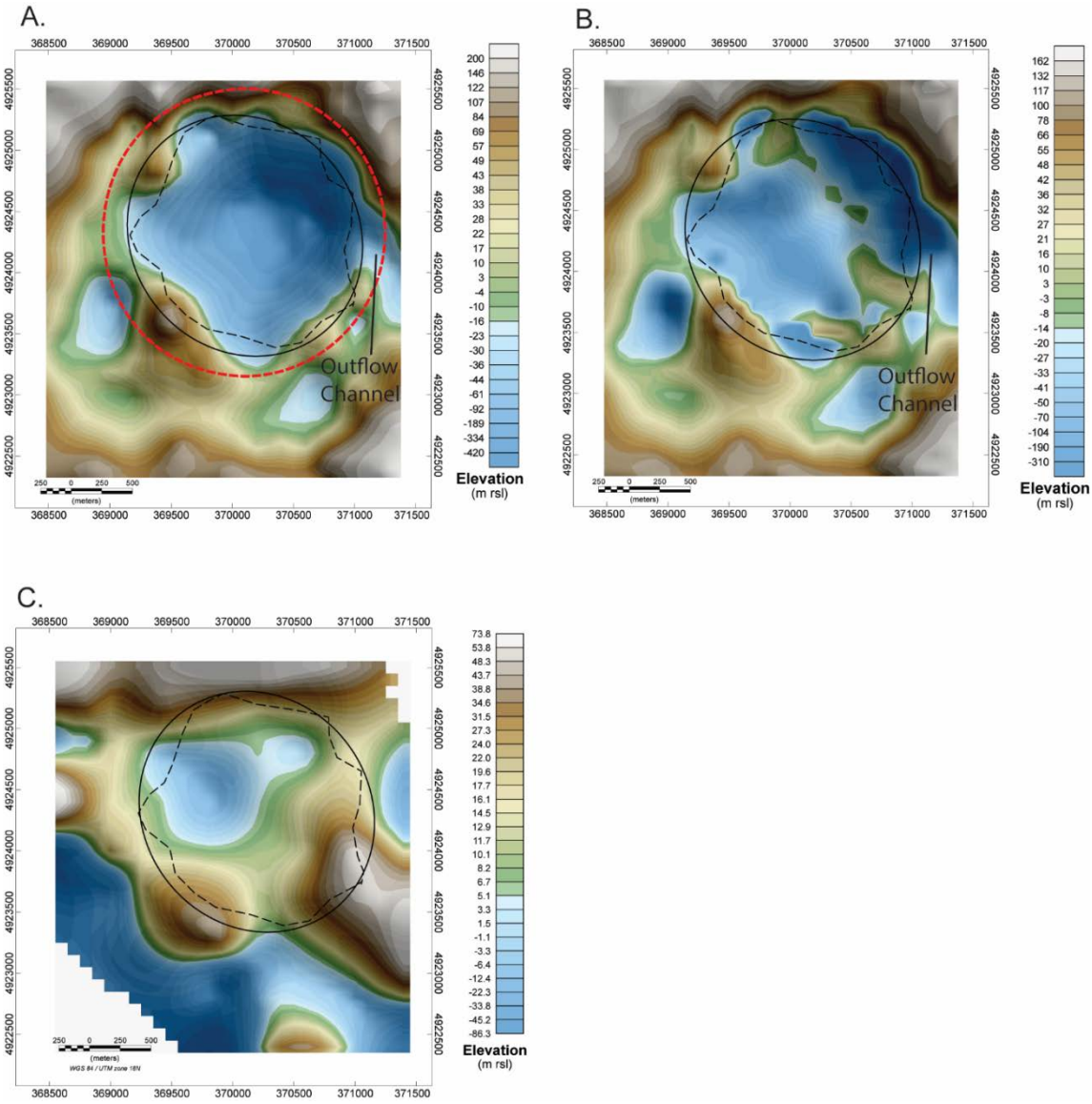

Figure 2.8. Structure contour maps for model layers (elevation in metres relative to sea level). A. Top of Mesoproterozoic basement (L1). Note possible outflow channel in eastern rim and depressions in basement surface outside southern crater rim. B. Top of breccia (L2). C. Top of Late Cambrian clastic sediments (L3). Red dashed circle indicates surface crater rim as mapped by Beals (1960) and solid black line is estimated basement rim-to-rim diameter (~1.8-2 km). Black dashed line indicates the approximate limit (zero thickness) of breccia.

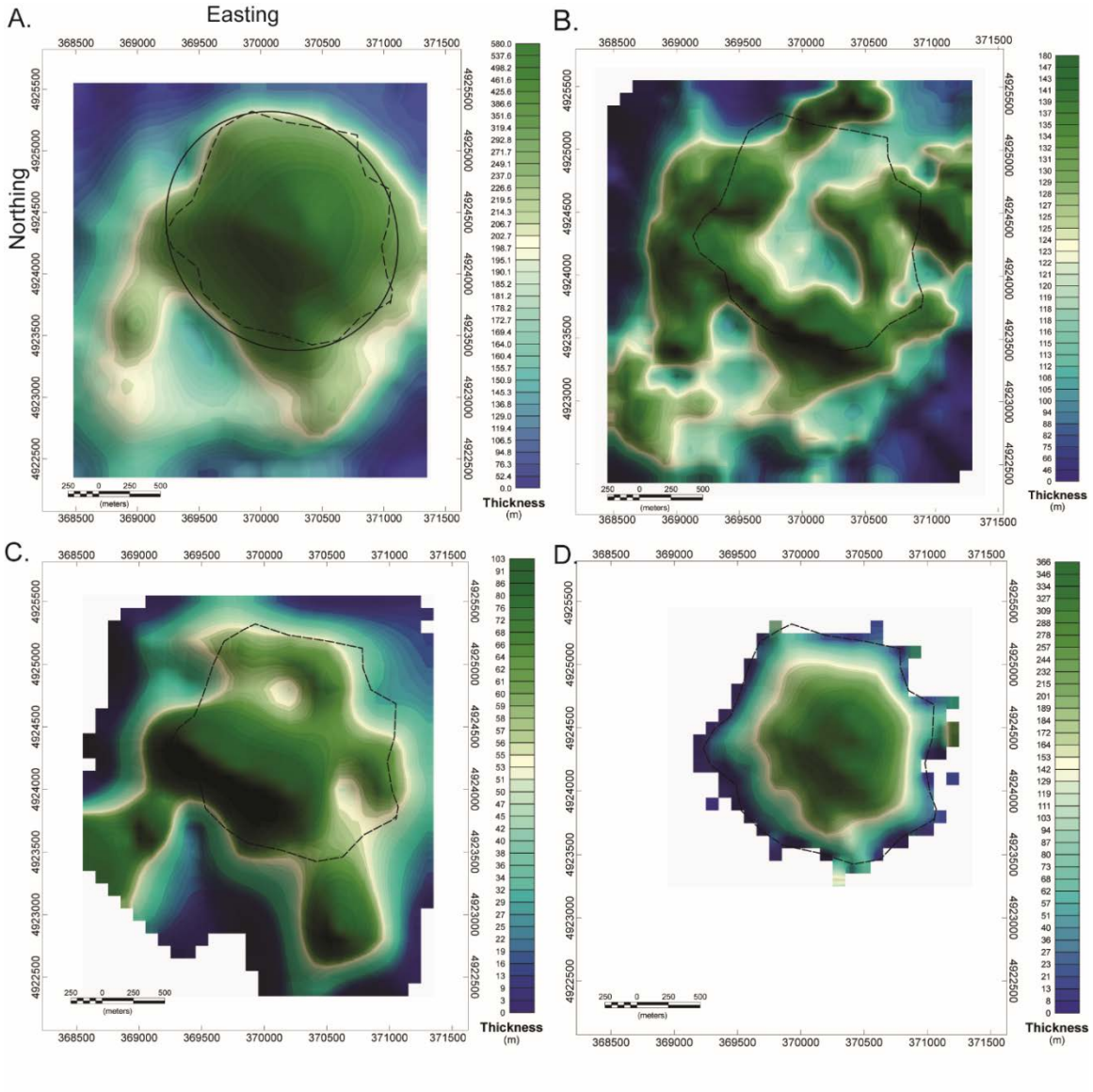

Figure 2.9. Isochore (sediment thickness) maps for model layers L2-L4. A. Total crater infill thickness. B. Middle Ordovician (Black River) carbonates (L4). L4 sediments are thickest over basement crater rim. C. Late Cambrian clastic sediments (L3). Cambrian sediments thicken within trough in upper surface of breccia (Fig. 2.8B). D. Impact breccia (L2). Breccia is >360 m thickness in central basin. Dashed line indicates limit (zero thickness) of breccia. Black circle shows modelled crater surface rim diameter (~2.00 km). Black dashed line indicates the approximate limit (zero thickness) of breccia.

2.5. Discussion

2.5.1 Crater morphology

The modelled basement surface (Figs. 2.8A, 2.10A) provides new details of the crater subsurface morphology. The crater basin is roughly circular in plan (1.8-2.0 km) with an estimated true depth >450 m (Fig. 2.6A). The basement rim is discontinuous and has a maximum height of about 30 m. The low rim height and dissection of the eastern rim suggests a heavily eroded simple impact crater. The basement rim diameter is about 15% smaller than Beals (1960) original estimate (2.35 km), which was based on the surface outcrop pattern of Paleozoic sediments (Fig. 2.2A).

The crater shape suggests possible basement structural controls on the crater morphology (Figs. 2.8A, 2.10A). The longest crater diameter (2.0 km) is in the approximate dip direction (northwest-southeast) strike of Mesoproterozoic basement rocks (Figs. 2.1, 2.4A, 2.6B) and the Desert Lake-Canoe Lake fault (Fig. 2.1B). The basement fault defines a major crustal boundary and broad zone of structural weakness in Mesoproterozoic rocks (Dickin and Strong, 2021). Structural analysis of target rocks at Meteor (Arizona) and Lonar (India) craters have shown that pre-existing fractures and other structural heterogeneities are important controls on target rock yield strength and crater morphology (Kumar, 2005; Kumar and Kring, 2008).

The high-relief surface topography of the Mesoproterozoic basement (Fig. 2.10A) may also have influenced the crater shape. As shown in Figure 2.6B, the crater basin is asymmetric, with a steeper gradient wall in the northwest. Krohn et al. (2014) for example, have demonstrated that impacts into high relief topography on the asteroid Vesta resulted in sharp craters rims on the upgradient side and smooth rim aspects on the downgradient slope. They also found that slopes tended to prevent the deposition of ejecta in the upslope direction.

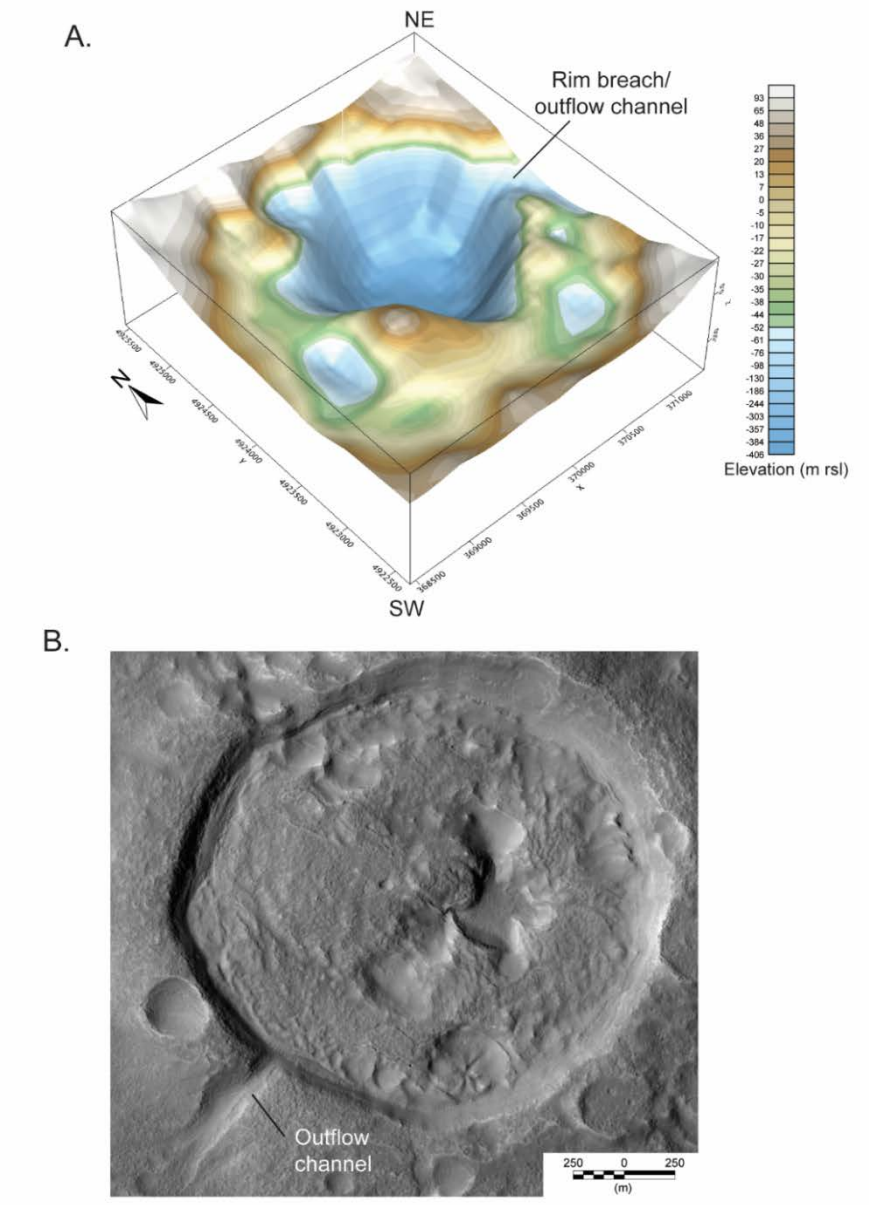

Figure 2.10. A. 3-D model of Mesoproterozoic basement surface showing crater basin morphology, rim breach and possible outflow channel in southeast rim (view from southwest). Channel feature is >150 deep and up to 400 m wide. Closed depressions in basement surface to the south of rim are mirrored in the modern surface topography (see DEM in Fig. 2a). B. HIRISE (High Resolution Imaging Science Experiment) image showing outflow channel in 2.3 km diameter 'pollywog' crater in northern Arabia Terra, Mars. Outflow channel is about 50-75 m in width (image source: NASA https://images.nasa.gov/details-PIA23738).

2.5.2 Infill sediments

St. John (1968) interpreted the crater basin fill as a succession of Late Cambrian paleolacustrine clastic sediments overlain by marine Middle Ordovician (Black River Group) clastic and carbonate sediments (Fig. 2.3). The model estimates a maximum infill sediment thickness of >580 m at the basin centre, comprising ~350 m of impact breccias (L2) and ~230 m of post-impact Paleozoic sediments (L3, L4; Fig. 2.9). Beals (1960) estimated a breccia thickness of 328 m assuming a mean density contrast of 0.16 gcm^3 between the breccia and unfractured target rocks. The estimated breccia thickness (350 m) is about 30% greater than predicted by scaling equations (240 m) for a 2-km-diameter impact crater (Table 2.2). This may indicate that the crater was originally larger in diameter and reduced in size by post-impact erosion, or that the model overestimates the breccia thickness. Terrestrial crater depth-diameter measurements show a significant scatter around the best fit scaling laws (Fig. 1.7), which indicates that a range of crater depths (and breccia layer thickness) are likely for crater of a given diameter (Fig. 1.7). Constraints on the breccia thickness are available from two boreholes – one that penetrated to Mesoproterozoic basement (BH-2), and a second borehole (BH-1) in the basin centre, which shows a minimum breccia thickness of 120 m (Fig. 2.3). The density contrast between breccias and basement target rocks is significant (~0.2-0.4 gcm^{-3}; Table 2.1) but borehole data show that the contact is transitional - the polymict breccias grade into heavily fractured and then in-situ Mesoproterozoic metasediments (Beals, 1960). The modelled-derived breccia thickness (Figs. 2.6, 2.7) thus likely includes a portion of the lower-density, fractured upper surface of Mesoproterozoic basement (Table 2.1).

The modelled basement surface shows evidence for fluvial dissection of the crater rim and thickening of Late Cambrian siliciclastics (L3) within local depressions on the basement surface (Figs. 2.9C, 2.10). The L3 sediments have a maximum thickness of ~100 m (Fig. 2.9C) at the basin centre and thicken within northwest-southeast trending structural lows on the L3/L4 surface (Figs. 2.3, 2.8A, 2.9C). The troughs may represent

remnants of a fluvial drainage system that developed following lake drainage and sub-aerial exposure of the crater basin (Fig. 2.11C).

The uppermost carbonate and siliciclastic succession (L4), records the inundation of the crater during the Middle Ordovician marine transgression and development of the Taconic foreland basin (St. John 1968; Brett et al., 2004) (Fig. 2.11 D). The increased thickness of L4 sediments over the crater rim suggests possible basement structural controls on carbonate sediment deposition (Fig. 2.9B). The increased thickness of L4 over the rim is in part due to differential erosion of the central basin (Fig. 2.2 A) but may reflect differences in carbonate sediment texture and facies. In southwestern Ontario, bioherms in Ordovician carbonates and Middle Silurian patch and pinnacle reefs occur on top of basement structural highs produced by faulting and tilting of the Precambrian basement rocks (Sanford et al., 1985; Bailey, 1986). Shallow water reef facies may include more erosion-resistant bioherm and rudite facies. The raised basement crater rim may have provided conditions favourable for the upgrowth of more erosion resistant bioherms, whereas the crater basin would have favoured carbonate mud and shale deposition (St. John, 1968). The upward and outward growth of carbonate reef facies would also explain the larger width of the surface rim when compared to the basement crater rim. This model could be tested by further detailed sedimentological and textural analysis of carbonate facies exposed in the crater basin and rim rocks (Fig. 2.2A).

The crater surface morphology of Holleford crater (Fig. 2.2A) is similar in many respects to the Charity Shoal structure, a proposed 1.2 km diameter impact crater in eastern Lake Ontario (Holcombe et al., 2013; Suttak, 2013; Chapter 3). Both structures have a raised bedrock rim that encloses a central synformal basin with Paleozoic carbonate strata dipping radially at low angles into the basin centre (Fig. 2.2A). The rim structure at Charity Shoal has been attributed to the conformal (drape) deposition of Middle Ordovician (Trenton Group) carbonate sediments over a buried impact crater and differential glacial erosion and plucking of dolomitic limestones (Holcombe et al., 2013). Both structures are examples of glacial craig-and-tail landforms, produced by erosional

streamlining of Paleozoic below southwest-flowing ice during the last (Late Wisconsinan) glaciation (Bukhari et al., 2021) (Fig. 2.2A).

2.5.3 Crater post-impact modification

The post-impact modification of terrestrial impact craters begins with the collapse of the transient crater cavity (Melosh and Ivanov, 1999; Osinski and Pierazzo, 2013) and is followed by degradation of the crater by surface geomorphic and tectonic processes (Grant and Shultz, 1993; Tsikalas and Faleide, 2007; Hergarten and Kenkman, 2015; Kenkman, 2021). On Earth, impact craters are modified by a range of surface processes (e.g., mass wasting, aeolian and fluvial erosion) but fluvial systems are the most effective agent of erosion (Grant and Shultz, 1993; Hergarten et al., 2014; Indu et al., 2021).

The post-impact modification and sedimentation history of Holleford crater is summarized in Fig. 2.11. The impact created a ~2 km diameter simple impact crater in Mesoproterozoic crystalline target rocks. The rim-to-rim diameter may be smaller than the original impact though as erosion can reduce the crater diameter (Forsberg-Taylor et al., 2004). The absence of Late Cambrian fragments within the impact breccia suggests a Late Proterozoic to Early Paleozoic impact event (ca. 550 Ma; Beals, 1960). The eroded upper surface of the breccia (L3) and presence of a thin conglomerate (Unit 2; Fig. 2.3) indicate a phase of sub-aerial erosion of the crater base. This was followed by development of a crater lake and deposition of thinly laminated quartz arenites (St. John, 1968). The heavily-dissected basement crater rim (Fig. 2.8A) suggests significant post-impact erosion of Holleford crater prior to burial below Paleozoic sediments (Fig. 2.11E). The level of erosion can be assessed by comparing the basement rim height and diameter with rim dimensions predicted by scaling equations (Table 2.2) (Melosh, 1989; Pilkington and Grieve, 1992; Collins et al., 2005). The rim (Figs. 2.8A, 2.10A) has maximum relief of about 30 m, which is <50% of the predicted rim height (~80 m),

indicating significant lowering of the rim by post-impact erosion. Rim erosion is also indicated by a ~400 m wide channel feature that dissects the eastern crater rim (Fig. 2.10A). The fluvial dissection of the rim structure may also explain the geometry of Late Cambrian clastics (L3), which thicken within the interpreted outflow channel in the southeastern rim (Fig. 2.11D).

Rim dissection and the development of outflow channels have been recognized in volcanic caldera lakes (e.g., Lake Taupo, New Zealand; Manville et al. 1999) and in terrestrial impact craters (Grant and Schultz; 1993; Komatsu et al., 2014). Grant and Schultz (1993) examined degradation processes at three young terrestrial craters (Meteor, Lonar and Talemzane crater) and compared them with selected Martian examples. They recognized a sequence of increasing degradation of crater form by fluvial, mass wasting and aeolian processes. At Talemzane crater (~3 Ma), rim breach channels with widths of 150-175 m wide were produced by headward erosion of crater drainage system. Modification by fluvial dissection can occur over relatively short geological time scales, as shown by the 1.8 km diameter Xiuyuan crater in northeast China (Chen, 2008; Chen et al. 2010). The Xiuyuan crater is a Late Pleistocene age (>0.05 Ma) simple impact basin formed in Proterozoic-age crystalline target rocks. The crater basin has a well-developed radial drainage pattern, which flows out through a 200 m wide and > 100 m deep channel in the northeastern rim (Chen, 2008). The crater floor is infilled by >107 m of Quaternary lacustrine sediments, indicating it was once a closed crater lake basin. The rim breach has not ascribed to lake outflow, but its dimensions and form are strikingly similar to the interpreted rim breach and channel at Holleford. Rim dissection by outflow from a paleolake basin is also an important process on Mars (Grant and Schultz,1993; Chen et al. 2010; Goudge et al. 2021) in the development of so-called ‘pollywog’ craters (e.g., 2.3 km diameter Arabia Terra crater; Fig. 2.10B).

Scaling equations		Parameters estimated from scaling equations			Model estimates (m)	Source
		Min (m)	Median (m)	Max (m)		
Rim-to-rim diameter (D)		1500	2000	2500	1800-2000	
True depth (basement)	$d_t = 0.28D^{1.02}$	486	651	819	430	Pilkington and Grieve (1992)
Apparent depth (top of breccia)	$D_a = 0.13D^{1.06}$	302	410	520	80-100	Pilkington and Grieve (1992)
Breccia Thickness	D_a-D_t	184	241	299	330-350	
Rim height	$H_r = 0.036D^{1.014}$	60	80	100	0 - 30	Melosh (1989)
Rim to basement depth	$H = D_t + H_r$	546	731	919	450	Melosh (1989)
Bolide diameter		107	125	148		
Apparent depth (top of breccia)	d_{fr}	325	425	537		Collins et.al. (2005)
Breccia thickness	t_{br}	150	197	249		Collins et.al. (2005)
Depth to basement	$d_t = d_{fr} + t_{br}$	475	622	886		

Table 2.2. Comparison of modelled crater dimensions with estimates from scaling equations (Melosh, 1989; Pilkington and Grieve, 1992) for crater rim-to-rim diameters (D) of 1.5, 2.0 and 2.5 km. Model estimates of rim-to-rim diameter D (1.8-2.0 km) from 2-D model profiles (Figs. 2.6, 2.7) and basement surface (Figs. 2.8A, 2.10A). Parameter estimates using the equations of Collins et al. (2005) assume a crystalline target wit\h an impact velocity of 20 m/s, 45 degree impact angle, and bolide density of 2.7 g/cm^3 (www.lpl.arizona.edu/impacteffects).

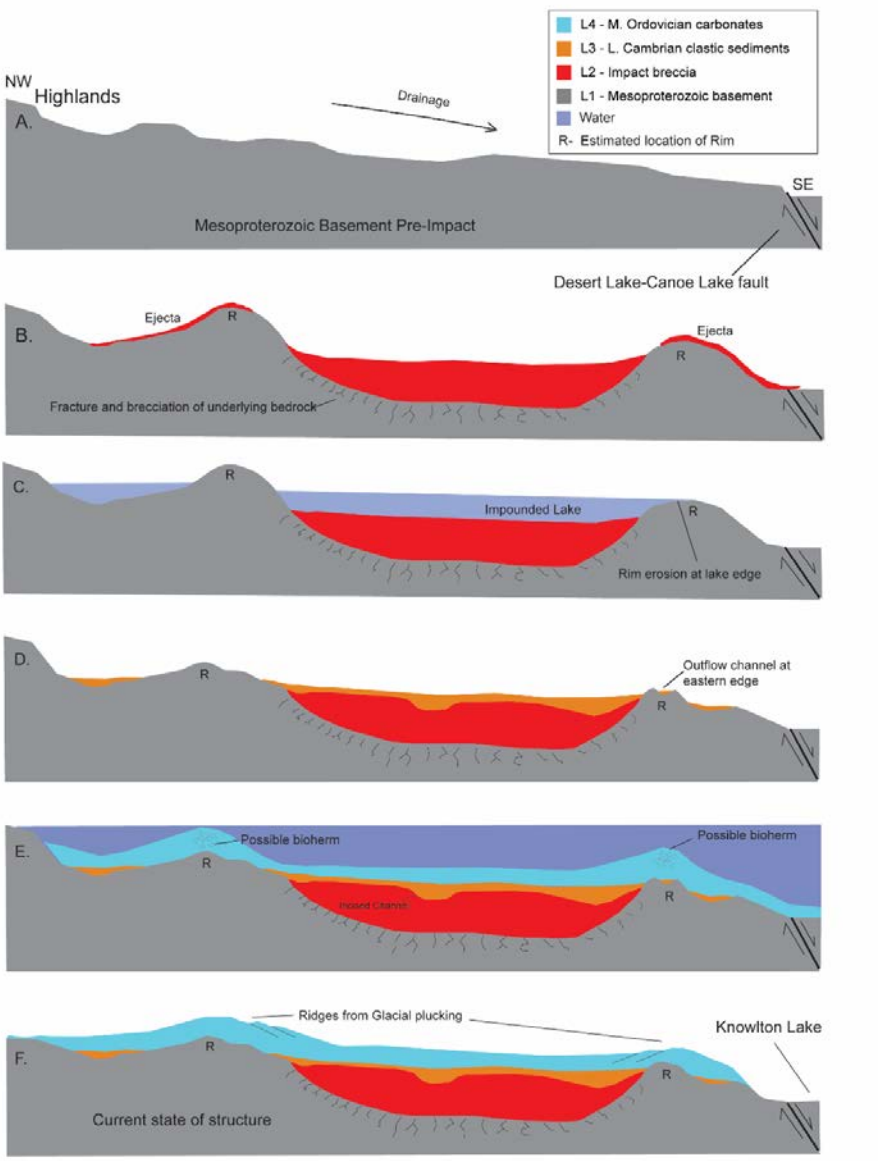

Figure 2.11. Post-impact modification and evolution of Holleford Crater. A. High-relief pre-impact surface with drainage from NW to SE. DL-CL = Desert Lake-Canoe Lake basement fault. B. Late-Proterozoic-Early Paleozoic simple crater (2 km diameter) with impact breccia (L2) and ejecta layers. Rim height (R) lower in southeast due to pre-existing basement topography. C. Impounded crater lake and deposition of Cambrian clastic sediments (L3). D. Lake drainage with breaching of SE crater rim by lake outflow, sub-aerial fluvial erosion of crater basin and rim. E. Middle Ordovician marine transgression and carbonate (L4) deposition. Upgrowth reef facies on upraised rim? F. Differential glacial erosion of crater rim and basin below southwest-ward flow ice.

The DEM model shows the surface crater has been modified significantly by glacial erosion (Figs. 2.2B; Fig. 2.11F). The 1.5-km long crag-and-tail landform on the down-flow side of southeastern rim records the streamlining of bedrock below southwestward-flowing Laurentide Ice during the last glacial cycle (Bukhari et al., 2021; Evans, 2021). The more extensive erosion on the northern crater rim (Fig. 2.2A) is due to preferential plucking of the exposed edges of southwest-dipping carbonate strata (Fig. 2.2A). The concentric gullies between the exposed Paleozoic bedrock scarps are due to the alternation of more erosion-resistant dolomitic limestones, with weaker shale units within the Trenton Group. A similar pattern of glacial erosion and craig-and-tail development has been identified at the Charity Shoal in northeastern Lake Ontario (Chapter 3; Fig. 3.1B).

2.6. Summary

This paper demonstrates the application of ground geophysical surveys and 3-D geophysical modelling to the investigation of the buried Holleford impact crater. The reconstructed basement surface (Figs. 2.10A) indicates a heavily-eroded, 1.8-2.0 km diameter (simple) impact crater with a maximum rim height of ~30 m (Figs. 2.6, 2.7). A > 100 m wide breach and channelized low in the southeast rim is interpreted as an outflow channel, produced by fluvial incision and downcutting of the basement rim (Figs. 2.6, 2.7). The feature has similar dimensions to outflow channels in terrestrial impact craters (Grant and Schultz, 1993) and may provide a terrestrial analog for paleolake outflow channels identified in Martian craters (Goudge et al., 2021; Warren et al., 2021).

The basement rim diameter is about 15-20% smaller than Beal's (1960) estimate (2.35 km), which was based on the surface outcrop pattern (Fig. 2.2). The basin shape suggests possible structural controls on the crater morphology by Mesoproterozoic rocks. The buried crater has an estimated true depth of ~430 m and maximum breccia thickness (Fig. 2.9D) of about 350 m, which is greater than expected for a 2-km-diameter simple impact crater. This could be due to post-impact erosion which has reduced the crater diameter (Forsberg –Taylor et al., 2004) The modelling confirms an earlier estimate by Beals and Innes (1961), which suggested a breccia thickness of about 1000 ft (305 m).

Holleford is an example of a simple impact crater with a complex history of erosional modification and deep burial below Cambrian-Ordovician lacustrine and marine shelf sediments (Beals, 1960; St. John, 1968). Deep burial has acted to preserve the crater structure (Beals, 1960; Grieve, 2001) and suggests the high potential for preservation of impact craters in the Precambrian surface below Paleozoic cover rocks in Ontario. Buried impact structures are likely to have surface expression (e.g., Fig. 2.2A) in areas where Paleozoic strata are thin (< 200-300 m), for example, along the Paleozoic-Precambrian contact in southern Ontario (Fig. 2.1B), and where cover strata are thinned over structural highs in the Precambrian basement (e.g., the Frontenac Arch; Hersi and Dix, 2000). More deeply buried structures are unlikely to have significant topographic

expression, as post-impact infill sedimentation progressively attenuates the crater topography and central synclinal basin structure (Fig. 2.2A). The presence of thick Quaternary sediments is also likely to mask crater topographic expression. The future discovery of deeply buried (e.g., > 500 m) craters below Paleozoic cover rocks will require both regional-scale exploration using (e.g. airborne gravity, electromagnetic, gravity surveys) and ground-truthing with site-scale geophysical searches (e.g., seismic reflection profiling, microgravity surveys) as demonstrated in this study. Detection of buried craters in aeromagnetic surveys may be complicated in the Central Metasedimentary Belt and other regions of the Grenville Province where the basement geology includes low magnetic susceptibility metasedimentary rocks (e.g., Frontenac Terrane, Fig. 2.1B).

High-resolution digital terrain models (Fig. 2.2A) and airborne geophysical data are increasingly available for large areas of southern Ontario and other regions across Canada. These emerging datasets provide a new opportunity to undertake renewed regional searches for impact structures (e.g., Beals, 1960). Several recent studies have demonstrated algorithms for automated detection of impact basins using high-resolution DEM's, which could be combined with geophysical data (e.g., high resolution aeromagnetic surveys) in the search for meteorite impact structures on Precambrian shields (e.g., Krøgli et al., 2007; Gottwald et al., 2017).

2.7 References

Andrieux P. and Clark J.F. 1969. Application des méthodes électriques de prospection à l'étude du cratère d'Holleford. *Canadian Journal of Earth Sciences* 6(6): 1325-1337. https://doi.org/10.1139/e69-135

Bailey S.M.B. 1986. A new look at the development, configuration, and trapping mechanisms of the Silurian Guelph reefs of southwestern Ontario. *Proceedings of the Ontario Petrology. Institute*, 25:1-28.

Beals C. S., Ferguson G. M. and Landau A. 1956. A search for analogies between lunar and terrestrial topography on photographs of the Canadian Shield *Journal of the Royal Astronomical Society* 50:258-259.

Beals C.S. 1958. Fossil meteorite impact craters. *Scientific American* 199, 33.

Beals C.S. 1960. A probable meteorite crater of Precambrian age at Holleford, Ontario. *Publications of the Dominion Observatory* 24:6 (Ottawa) https://doi.org/10.4095/8727

Beals C. S. and Innes I. 1961. The study of fossil meteorite craters with the aid of geophysical and diamond drilling techniques. In Nordyke, Milo D. Proceedings of the Geophysical Laboratory/Lawrence Radiation Laboratory Cratering Symposium. United States. 44 p. https://doi.org/10.2172/1122567

Bukhari S., Eyles N., Sookhan S., Mulligan R., Paulen R., Krabbendam M. and Putkinen N., 2021. Regional subglacial quarrying and abrasion below hard-bedded palaeo-ice streams crossing the Shield–Palaeozoic boundary of central Canada: the importance of substrate control. *Boreas*, 50(3):781-805. https://doi.org/10.2172/1122567

Brett C. E., McLaughlin P. I., Cornell S. R. and Baird G. C. 2004. Comparative sequence stratigraphy of two classic Upper Ordovician successions, Trenton Shelf (New York–Ontario) and Lexington Platform (Kentucky–Ohio): implications for eustasy and local tectonism in eastern Laurentia. *Palaeogeography, Palaeoclimatology, Palaeoecology* 210(2-4):295-329. https://doi.org/10.1016/j.palaeo.2004.02.038

Brink R., Mehrtens C. and Maguire H. 2019. Sedimentology and petrography of a lower Cambrian transgressive sequence: Altona Formation (Potsdam Group) in northeastern New York. *Bulletin of Geosciences* 94(3): 369-389.

Bunch T. E., and Cohen A. J. 1963. Coesite and shocked quartz from Holleford crater, Ontario, Canada. *Science* 142(3590): 379-381. https://doi.org/10.1126/science.142.3590.379

Cady J. W. 1980. Calculation of gravity and magnetic anomalies of finite-length right polygonal prisms. *Geophysics* 45(10):1507-1512. http://dx.doi.org/10.1190/1.1441045

Carr S.D., Easton R.M., Jamieson R.A. and Culshaw N.G. 2000. Geologic transect across the Grenville Orogen of Ontario and New York. *Canadian Journal of Earth Sciences* 37: 193-216. https://doi.org/10.1139/e99-074

Canadian Geodetic Survey (CGS). 2020. Canadian Gravity Database (CGDB).

Chen M. 2008 Impact-derived features of the Xiuyan meteorite crater. *Chinese Science Bulletin* 53: 392–395. https://doi.org/10.1007/s11434-008-0004-3

Chen M., Xiao W. and Xie X. 2010. Coesite and quartz characteristic of crystallization from shock-produced silica melt in the Xiuyan crater. *Earth and Planetary Science Letters*, 297(1-2):306-314. https://doi.org/10.1016/j.epsl.2010.06.032

Collins G. S., Melosh H. J.,and Marcus R. A. 2005. Earth impact effects program: A web-based computer program for calculating the regional environmental consequences of a meteoroid impact on Earth. *Meteoritics & Planetary Science* 40(6):817-840. https://doi.org/10.1111/j.1945-5100.2005.tb00157.x

Dawson K.R. 1961. The origin of the Holleford crater breccia. *Canadian Mineralogist* 6(5):634-636.

Dence M. R. 1964. A comparative structural and petrographic study of probable Canadian meteorite craters. *Meteoritics* 2(3):249-270. https://doi.org/10.1111/j.1945-5100.1964.tb01432.x

Dickin A. and Strong J. 2021. Nd isotope mapping of the Frontenac Terrane in southwestern Grenville Province. *Canadian Journal of Earth Sciences* 58(8):659-669. https://doi.org/10.1139/cjes-2020-0063

Easton R.M. 2001. Precambrian Geology, Tichborne Area (31 C/10). Ontario Geological Survey, Preliminary Map, 3442. Ministry of Energy, Northern Development and Mines.

Evangelatos J., Butler K.E. and Spray J.G. 2009. A marine magnetic study of a carbonate-hosted impact structure: Ile Rouleau, Canada. *Geophysical Journal International* 179(1): 171-181. https://doi.org/10.1111/j.1365-246X.2009.04304.x

Evans D. J. 2021. The Midland Valley: Ice-Moulded Lowlands. In Landscapes and Landforms of Scotland. Springer, Cham., p. 439-452.

French B.M. and Koeberl C. 2010. The convincing identification of terrestrial meteorite impact structures: What works, what doesn't, and why. *Earth-Science Reviews* 98: 123-70 https://doi.org/10.1016/j.earscirev.2009.10.009

Forsberg-Taylor N. K., Howard A. D. and Craddock R. A. 2004. Crater degradation in the Martian highlands: Morphometric analysis of the Sinus Sabaeus region and simulation modeling suggest fluvial processes. *Journal of Geophysical Research: Planets*, *109*(E5). https://doi.org/10.1029/2004JE002242

Gottwald M., Fritz T., Breit H., Schättler B. and Harris A. 2017. Remote sensing of terrestrial impact craters: The TanDEM-X digital elevation model. *Meteoritics& Planetary Science* 52(7):1412-1427. https://doi.org/10.1111/maps.12794

Goudge T.A., Morgan, A.M., Stucky de Quay, G. and Fassett C.I., 2021. The importance of lake breach floods for valley incision on early Mars. *Nature* 597: 645–649 https://doi.org/10.1038/s41586-021-03860-1

Grant J. A. and Schultz P. H. 1993. Degradation of selected terrestrial and Martian impact craters. *Journal of Geophysical Research: Planets* 98(E6):11025-11042. https://doi.org/10.1029/93JE00121

Grieve R.A.F. 2001. The Terrestrial Cratering Record. In: Accretion of Extraterrestrial Matter Throughout Earth's History edited by Peucker-Ehrenbrink B., Schmitz B. Springer, Boston, MA. https://doi.org/10.1007/978-1-4419-8694-8_19

Hergarten S., Robl J. and Stüwe K. 2014. Extracting topographic swath profiles across curved geomorphic features. *Earth Surface Dynamics*, 2(1):97-104. https://doi.org/10.5194/esurf-2-97-2014

Hergarten S. and Kenkmann T. 2015. The Terrestrial Impact Crater Inventory and Its Impact Beyond Impact Research. Bridging the Gap III: Impact Cratering in Nature, Experiments, and Modeling, 1861, p.1057.

Hersi O.S. and Dix G.R. 2000. Blackriveran (lower Mohawkian, Upper Ordovician) lithostratigraphy, rhythmicity, and paleogeography: Ottawa Embayment, eastern Ontario, Canada. *Canadian Journal of Earth Sciences*, 36(12):2033-2050. https://doi.org/10.1139/e99-087

Hildebrand A.R., Penfield G.T., Kring D.A., Pilkington M Camargo Z., Jacobsen S.B. and Boynton, W.V. 1991. Chicxulub crater: A possible Cretaceous-Tertiary boundary impact crater on the Yucatan peninsula, Mexico, *Geology*, 19:867-871. https://doi.org/10.5194/esurf-2-97-2014

Holcombe T.L., Youngblut S. and Slowey, N. 2013. Geological structure of Charity Shoal crater, Lake Ontario, revealed by multi beam bathymetry. *Geo-Marine Letters* 33 (4): 245-252. https://doi.org/10.1007/s00367-013-0322-6

Holom D. I. and Oldow J. S. 2007. Gravity reduction spreadsheet to calculate the Bouguer anomaly using standardized methods and constants. *Geosphere* 3(2): 86-90. https://doi.org/10.1130/GES00060.1

Indu G. K., James S., Chandran S.R. Aneeshkumar V., Keerthy S., Oommen T. and Sajinkumar K. S. 2021. Deriving a denudation index for terrestrial meteorite impact craters using drainages as proxies. *Geomorphology*, 397: 108007. https://doi.org/10.1016/j.geomorph.2021.108007

Innes M. J. S. 1961. The use of gravity methods to study the underground structure and impact energy of meteorite craters. *Journal of Geophysical Research*, 66(7): 2225-2239. https://doi.org/10.1029/JZ066i007p02225

Innes M.J.S. 1964. Recent advances in meteorite crater research at the Dominion Observatory, Ottawa, Canada. *Meteoritics* 2(3):219-241. https://doi.org/10.1111/j.1945-5100.1964.tb01430.x

Kenkmann T. 2021. The terrestrial impact crater record: A statistical analysis of morphologies, structures, ages, lithologies, and more. *Meteoritics & Planetary Science* 56(5): 1024-1070. https://doi.org/10.1111/maps.13657

Kirwan J. L. 1963. The age of the Nepean (Potsdam) sandstone in eastern Ontario. *American Journal of Science* 261(2):108-110. https://doi.org/10.2475/ajs.261.2.108

Komatsu G., Kumar P.S., Goto K., Sekine Y., Giri C. and Matsui, T. 2014. Drainage systems of Lonar Crater, India: Contributions to Lonar Lake hydrology and crater degradation. *Planetary and Space Science*, 95: 45-55. https://doi.org/10.1016/j.pss.2013.05.011

Krøgli S. O., Dypvik H. and Etzelmüller B. 2007. Automatic detection of circular depressions in digital elevation data in the search for potential Norwegian impact structures. Norwegian *Journal of Geology/Norsk Geologisk Forening, 87.* https://foreninger.uio.no/ngf/ngt/pdfs/NJG_87_157-166.pdf

Krohn K., Jaumann R., Elbeshausen D., Kneissl, T., Schmedemann N., Wagne, R., Voigt J., Otto K., Matz K.D., Preusker F., Roatsch T., Stephan K., Raymond C.A. and Russell, C. T. 2014. Asymmetric craters on Vesta: Impact on sloping surfaces. *Planetary and Space Science* 103:36-56. https://doi.org/10.1016/j.pss.2014.04.011

Kumar P. S. (2005), Structural effects of meteorite impact on basalt: Evidence from Lonar Crater, India, *Journal of Geophysical Resesearch*, 110: B12402 https://doi.org/10.1029/2005JB003662

Kumar P.S. and Kring D.A. 2008. Impact fracturing and structural modification of sedimentary rocks at Meteor Crater, Arizona. *Journal of Geophysical Research: Planets* 113: E09009 https://doi.org/10.1029/2008JE003115

Lamali A., Rochette P., Merabet N., Abtout A., Maouche S., Gattacceca J., Ferrière L., Hamoud, M., ASTER Team, Meziane E.H. and Ayache M. 2016. Geophysical and magneto-structural study of the Maâdna structure (Talemzane, Algeria): Insights on its age and origin. *Meteoritics & Planetary Science*, 51(12):2249-2273. https://doi.org/10.1111/maps.12715

LIO 2014. Digital Raster Acquisition Project Eastern (DRAPE) Ontario (2014). Land Information Ontario, Ontario. https://geohub.lio.gov.on.ca/documents/digital-raster-acquisition-project-eastern-ontario-drape-2014/about

Luyendyk A.P.J. 1997. Processing of airborne magnetic data. *AGSO Journal of Australian Geology and Geophysics* 17:31-38

Magnus S.J. and Easton R.M. 2015. Precambrian geology of eastern Ontario interpreted from aeromagnetic and compiled geological data—south sheet; Ontario Geological Survey, Preliminary Map P.3793, scale 1:100 000.

Manville V., White J.D., Houghton, B.F. and Wilson, C.J. 1999. Paleohydrology and sedimentology of a post–1.8 ka breakout flood from intracaldera Lake Taupo, North Island, New Zealand. *Geological Society of America Bulletin*, 111(10)): 1435-1447. https://doi.org/10.1130/0016-7606(1999)111%3C1435:PASOAP%3E2.3.CO;2

Melosh H.J. 1989. *Impact Cratering: A Geologic Process*. Oxford University Press, New York.

Melosh H.J. and Ivanov B.A. 1999. Impact crater collapse. *Annual Review of Earth and Planetary Sciences*, 27(1), pp.385-415. https://doi-org.libaccess.lib.mcmaster.ca/10.1146/annurev.earth.27.1.385

Morgan J., Rebolledo-Vieyra M., Osinski G.R. and Pierazzo, E. 2013. Geophysical studies of impact craters. In Osinski G. R. and Pierazzo E. Eds., Impact cratering processes and products, pp.211-22.

O'Dowd C. and Eaton D. 2005. Field and laboratory measurements of magnetic properties and density, Central Metasedimentary Belt, Ontario. Natural Resources Canada, Geological Survey of Canada.

Olaniyan O., Smith R.S. and Lafrance B. 2015. Regional 3-D geophysical investigation of the Sudbury Structure. *Interpretation*, 3(2): SL63-SL81. https://doi.org/10.1190/INT-2014-0200.1

Osinski, G. R. and Pierazzo E. 2013. Impact cratering: Processes and products. John Wiley and Sons.

PASSC 2022. Earth Impact Database 2022. Planetary and Space Science Centre, University of New Brunswick, Fredericton NB. http://passc.net/EarthImpactDatabase/New%20website_05-2018/Index.html

Pilkington M. and Grieve R.A.F. 1992. The geophysical signature of terrestrial impact craters. *Reviews of Geophysics* 30: 161-81 https://doi.org/10.1029/92RG00192

Pilkington M., Hildebrand A.R. and Ortiz A. 1994. Gravity and magnetic modeling and structure of the Chicxulub crater, Mexico, *Journal of Geophysical. Research*., 99 (13):147-162. https://doi.org/10.1029/94JE01089

Pilkington M. and Hildebrand A. R. 2000. Three-dimensional magnetic imaging of the Chicxulub crater. *Journal of Geophysical Research: Solid Earth*, 105(B10):23479-23491. https://doi.org/10.1029/2000JB900222

Pratt D. A., White A. S., Parfrey K. L. and McKenzie K. B. 2020. ModelVision 17.0 User Guide. Tensor Research Pty Ltd., Grenwich, NSW, Australia, 596 p.

Puura V. and Suuroja K. 1992. Ordovician impact crater at Kärdla, Hiiumaa Island, Estonia. *Tectonophysics* 216(1-2);143-156. https://doi.org/10.1016/0040-1951(92)90161-X

Reford S.W., Gupta V.K., Paterson N.R., Kwan K.C. and MacLeod I.N. 1990. Ontario master aeromagnetic grid: a blueprint for detailed compilation of magnetic data on a regional scale. In *SEG Technical Program Expanded Abstracts 1990, Society of Exploration Geophysicists* 617-61). https://doi.org/10.1190/1.1890282

Sanford B.V., Thompson F.J. and McFall G.H. 1985. Plate tectonics - a possible controlling mechanism in the development of hydrocarbon traps in southwestern Ontario. *Bulletin of Canadian Petroleum Geology*, 33:52-71. https://doi.org/10.35767/gscpgbull.33.1.052

Sanford B.V. and Arnott R.W.C. 2010. Stratigraphic and structural framework of the Potsdam Group in eastern Ontario, western Quebec and northern New York State; *Geological Survey of Canada, Bulletin 597* http://dx.doi.org/10.20381/ruor-13101

Sookhan S., Eyles, N., Bukhari S. and Paulen R. C. 2021. LiDAR-based quantitative assessment of drumlin to mega-scale glacial lineation continuums and flow of the paleo Seneca-Cayuga paleo-ice stream. *Quaternary Science Reviews* 263:107003. https://doi.org/10.1016/j.quascirev.2021.107003

St. John B. E.1968. Paleolacustrine arenites in the Holleford meteorite crater, Ontario. *Canadian Journal of Earth Sciences* 5(4): 935-943. https://doi.org/10.1139/e68-090

Suttak P.A. 2013. High-resolution lake-based magnetic mapping and modeling of basement structures, with examples from Küçükçekmece Lagoon, Turkey and Charity Shoal, Lake Ontario. unpublished MS thesis, School of Geography and Earth Sciences, McMaster University, Hamilton, Ontario. 113 pp. http://hdl.handle.net/11375/13532

Talwani M. and Ewing M. 1960. Rapid computation of gravitational attraction of three-dimensional bodies of arbitrary shape. *Geophysics*, 25(1): 203-225.

Tsikalas F. and Faleide J.I. 2007. Post-impact structural crater modification due to sediment loading: An overlooked process. *Meteoritics & Planetary Science*, 42(11): 2013-2029. https://doi.org/10.1111/maps.13227

Ugalde H., Danuor S. K. and Milkereit B. 2007a. Integrated 3-D model from gravity and petrophysical data at the Bosumtwi impact structure, Ghana. Meteoritics & Planetary Science, 42(4-5): 859-866. https://doi.org/10.1111/j.1945-5100.2007.tb01081.x

Ugalde H., Valenzuela M., Milkereit B. 2007b. An integrated geophysical and geological study of the Monturaqui impact crater, Chile. Meteoritics & Planetary Science, 42(12):2153-2163. https://doi.org/10.1111/j.1945-5100.2007.tb01015.x

Urbini S., Nicolosi I., Zeoli A., El Khrepy S., Lethy, A., Hafez M., El Gabry M., El Barkooky A., Barakat A., Gomaa M. and Radwan A.M 2012. Geological and geophysical investigation of Kamil crater, Egypt. *Meteoritics & Planetary Science* 47(11):1842-1868. https://doi.org/10.1111/maps.12023

Wackernagel, H., 2003. Ordinary kriging. In Multivariate Geostatistics. Springer, Berlin, Heidelberg. p. 79-88.

Warren A. O., Holo S., Kite E. S. and Wilson S. A. 2021. Overspilling small craters on a dry Mars: Insights from breach erosion modeling. *Earth and Planetary Science Letters* 554: 116671. https://doi.org/10.1016/j.epsl.2020.116671

NASA ID PIA23738 Pollywog crater on Mars NASA/JPL-Caltech/University of Arizona. https://images.nasa.gov/details-PIA23738

Chapter 3: 3-D subsurface geophysical modelling of the Charity Shoal structure: a probable (Late Proterozoic-Early Paleozoic) simple impact crater in eastern Lake Ontario

Abstract

The Charity Shoal structure (CSS) is a 1.2 km diameter, 20 m deep, bedrock-rimmed depression located in eastern Lake Ontario. The structure has been proposed as a possible Middle Ordovician-age impact crater or volcanic intrusion. We conducted seismic and magnetic surveys over a 9-km^2 area to better resolve the subsurface geology and origin of the CSS. The rim structure was evaluated using multi-beam bathymetric data and single channel (1-4 kHz) seismic profiling. We constructed 3-D forward geophysical models to evaluate possible origins as a deeply buried impact crater in Mesoproterozoic basement, a maar-diatreme, or a cylindrical zoned volcanic plug intruded below Middle Ordovician cover rocks.

Seismic and multi-beam data show 25-30 m of Quaternary sediments overlying Middle Ordovician (Trenton Group) carbonate bedrock and evidence for normal faulting and complex, 3-dimensional folding of the structure rim. Magnetic surveys recorded an annular magnetic high over the structure rim (> 600 nT) and a central magnetic low (~500-600 nT) that is coincident with a ~-1.7 mGal Bouguer gravity anomaly. The continuity of Middle Ordovician strata rules out a previously proposed Mesozoic maar-diatreme intruded into Paleozoic cover rocks. A zoned intrusive with an inner pipe diameter of ~800-1000 m (κ = 0.05 SI) and outer zone radius of 100-200 m (κ = 0.02 SI) can be fitted to the magnetic anomaly but is incompatible with the observed Bouguer gravity low. Magnetic modelling predicts a structure depth of 450-500 m, a rim-to-rim diameter of ~1.2 km and rim height of ~15-20 m. A 100-m wide and 50 m deep channel in the Mesoproterozoic basement may record breaching and fluvial dissection of the southwestern rim. Previously proposed Middle Ordovician and Younger Dryas (ca. 12.9 Ka) impact events at Charity Shoal are not supported by new geophysical results. A deeply buried (>450 m), simple impact crater is the origin most compatible with all

available geophysical data, suggesting a probable Mesoproterozoic-Early Paleozoic impact event at Charity Shoal.

Keywords: Charity Shoal, 3-D potential field modelling, suspected impact crater, magnetics, Bouguer gravity, seismic profiling, Middle Ordovician, Trenton Group

Highlights

- 1.2 km diameter, crater-like bedrock shoal in northeastern Lake Ontario
- Previously proposed as a Middle Ordovician impact crater or maar-diatreme
- 3-D potential field modelling of subsurface structure and geometry using magnetic, seismic and gravity data
- Coincident magnetic (-600 nT) and gravity (-1.7 mGal) anomalies over central basin
- Deeply-seated (>450 m) structure in Mesoproterozoic basement, probable Mesoproterozoic-Early Paleozoic impact event.

3.1. Introduction

Impact cratering is an important geological process on planetary surfaces (French and Koeberl, 2010; Osinski and Pierazzo, 2013). Confirmation of an impact crater on Earth requires evidence of meteoritic materials, impactites or shock metamorphic effects in target rocks (French and Koeberl, 2010; Reimold et al., 2014). Where primary physical evidence is lacking, geophysical data can assist in evaluating a possible impact origin (Pilkington and Grieve, 1992; French, 1998; Evangelatos, 2009; Urbini et al.,2012; Lajeunesse et al., 2013; Gottwald et al., 2017; Tsikalas and Eldhom, 2018). About one-third of confirmed impact structures on Earth have been discovered using geophysical methods (French, 1998) (e.g., land- and marine-based seismic, gravity, magnetic, electromagnetic and resistivity measurements). Geophysical methods have also been applied in the investigation of suspected and confirmed impact craters (Pilkington and Grieve, 1992; French, 1998; Tsikalas and Eldhom, 2018). 2-D profile modelling of potential field data (i.e., gravity, magnetics) is used widely in estimating impact structure depth and geometry, particularly for deeply buried structures in which borehole data is often unavailable (Puura and Suuroja, 1992; Evangelatos et.al., 2009; Urbini et al., 2012). Potential field modelling of gravity and magnetic data can also assist in evaluating suspected impact craters, where direct physical evidence of impact origin may be absent or inaccessible due to deep subsurface burial or removal by post-impact tectonic and geomorphic processes (Clark, 1982; Waddington and Dence, 1979).

Sophisticated 3-D potential field models and multi-parameter surveys are now conventional tools in exploration geophysics and resource geology (Wellman and Caumon, 2018) and are gaining increasing application in the study of impact craters (Pilkington and Hildebrand, 2000; Ugalde et al., 2007a, b; Batista-Rodríguez et al., 2013). Ebbing et. al. (2001) integrated gravity, seismic and borehole data in a 3-D model of the Chicxulub impact to delimit the central peak, ring structure and breccia thickness. Ugalde et al. (2007a) investigated the Bosumtwi impact crater using 3-D magnetic models to determine the magnetic source bodies. 3-D potential field modelling has also been employed as a tool for investigating the origin of suspected impact structures. For

example, Tsikalas and Eldholm (2018) employed 3-D geophysical modelling to compare the Mjolnir impact crater in Norway with the suspected Malvinas structure on the Falklands Plateau. They developed a processing flow that integrates a range of geophysical data (e.g., seismic, bathymetric, magnetic and gravity) in the construction of detailed, 3-dimensional subsurface models.

In this paper, we present the results of geophysical surveys and 3-D potential field modelling of the Charity Shoal structure (CSS), a suspected ~1.2 km diameter impact crater in eastern Lake Ontario (Fig. 3.1A) (Holcombe et al., 2013; Suttak, 2013). Charity Shoal was first identified in 1999 as a crater-like bedrock shoal on the northern margin of the St. Lawrence channel (Virden et al., 1999; Holcombe et al., 2001) (Fig. 3.1B). Several origins were proposed, including a volcanic intrusive, glacial erosion, a karst sinkhole and meteorite impact crater (Holcombe et al., 2001; Holcombe et al., 2013; Suttak, 2013) (Fig. 3.2). Holcombe et al. (2013) mapped the bedrock rim using multi-beam bathymetric data and interpreted the structure as a 'ring-anticline', formed by successive draping of Paleozoic sediments over a buried simple impact crater (Fig. 3.2A). They proposed a Middle Ordovician impact event in marine shelf sediments (Fig 3.2A) but no subsurface or geophysical data were provided in support of their interpretations. Suttak (2013) conducted magnetic and chirp seismic surveys at CSS and used 2-D

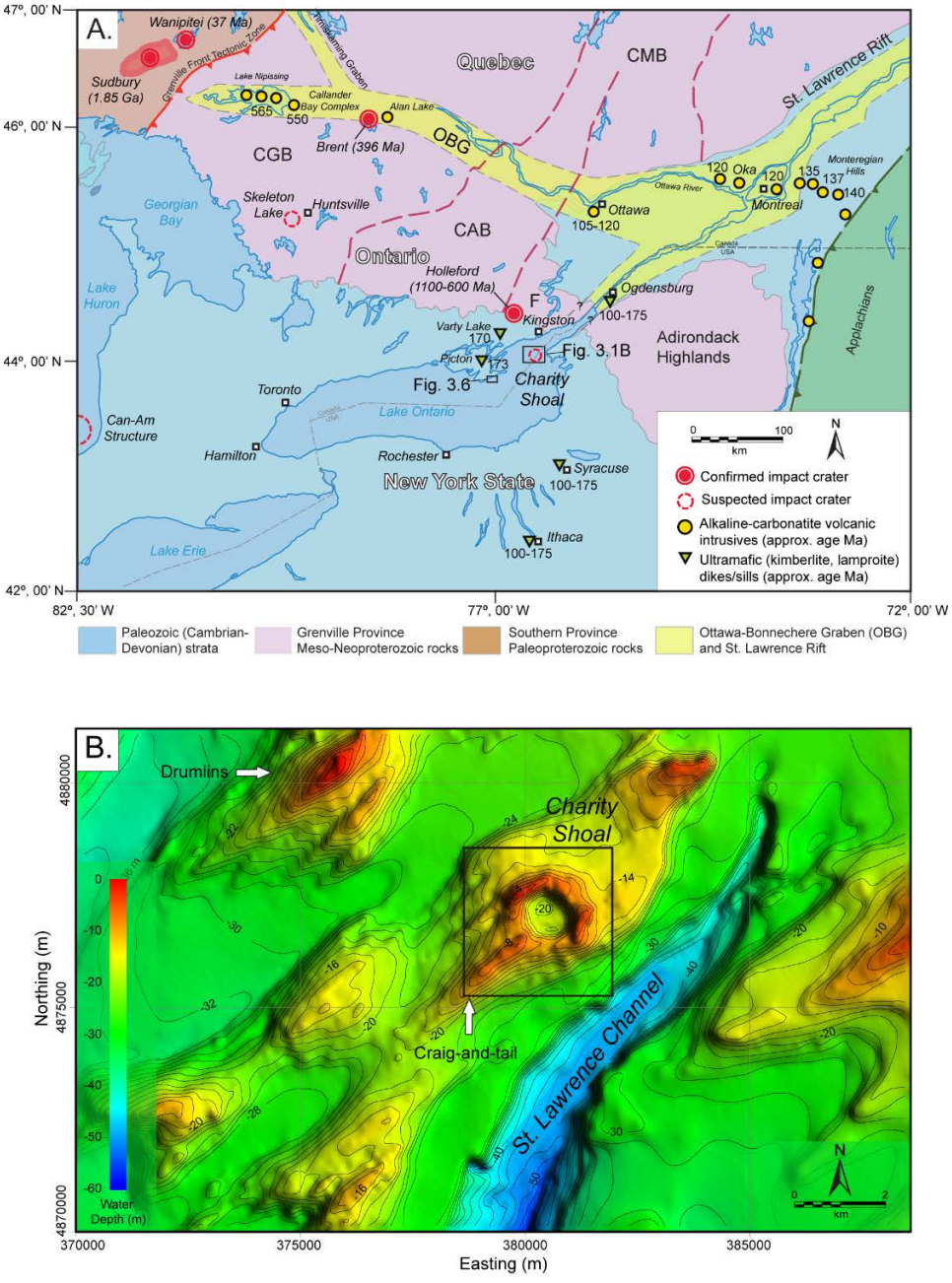

Figure 3.1. A. Regional geology map showing location of Charity Shoal in eastern Lake Ontario and locations of confirmed and suspected impact structures and rift-related volcanics. OBG = Ottawa-Bonnechère graben (OBG), CGB = Central Gneiss Belt, CAB = Composite Arc Belt, CMB = Central Metasedimentary Belt. B. Bathymetric map showing CSS on north margin of the St. Lawrence Channel (contour interval 2 m) (data source: Virden et al., 1999).

magnetic modelling and Euler deconvolution to estimate the structure depth and geometry. His results ruled out glacial erosion, basement structural depression or a karst sinkhole as likely origins, as these type of structures could not reproduce the annular ring high and central low over the basin. Suttak (2013) showed that the >1400 nT magnetic anomaly could be reproduced by a volcanic maar-crater at shallow depth (Fig. 3.2B), or deeply buried (> 500 m) simple impact crater in the Mesoproterozoic basement (Fig. 3.2C). The impact crater model best matched Euler depth-to-basement estimates, which indicated a parabolic-shaped basement depression at a depth of >500 m (Fig. 3.2D).

In this paper, we present new details of the subsurface geology and bedrock structure of Charity Shoal and evaluate previously proposed geological models with 3-D geophysical modelling. We evaluate possible origins as a simple impact crater (Holcombe, 2011; 2013), and endogenic origins as either a maar-diatreme (Suttak, 2013) or zoned volcanic (carbonatite- alkalic) pipe intruded into Mesoproterozoic basement rocks. The modelling approach, combining magnetic, gravity, seismic and multi-beam data, has broader application to the investigation of suspected and confirmed impact structures in lakes and marine environments (e.g., Tsikalas and Eldholm, 2018), where water depth and deep burial may limit the possibility for exploration drilling and recovery of physical evidence of impact origins (e.g., Stewart, 2003).

3.2. Study Area and Geologic Setting

Charity Shoal is an anomalous, circular bedrock shoal located in northeastern Lake Ontario, about 25 km southwest of Kingston (Fig. 3.1A). The structure straddles the Canada-US border and was first discovered during bathymetric mapping of the Duck-Galloo Sill (Fig. 3.1B) in the late 1990's (Virden et al., 1999; Holcombe et al., 2001). The 1-1.2 km diameter raised bedrock rim encloses a roughly circular basin with a maximum water depth of about 20 m (Fig. 3.1B) (Holcombe et al., 2013). The bedrock

rim consists of Middle Ordovician dolomitic limestone and shales of the Trenton-Black River Group (Sanford and Baer, 1981; Johnson et al., 1992; McFall, 1993; Suttak, 2013). The Paleozoic strata have a low regional dip (~0.5) towards the southwest and are between 200-260 m in thickness in nearby Prince Edward County (McFall and Allam, 1991; McFall, 1993). At Charity Shoal, the Paleozoic sediment thickness has been estimated at >200 m, based on magnetic depth-to-basement modelling (Suttak, 2013) (Fig. 3.2D). The Paleozoic bedrock surface is draped by a variable thickness of Late Pleistocene glacial and post-glacial sediments (Gilbert and Shaw, 1992; Anderson and Lewis, 2012; Suttak, 2013). Chirp seismic surveys conducted by Suttak (2013) indicate >20 m of Quaternary sediments in the central basin, but the bedrock surface was not imaged due to limited seismic penetration. The Paleozoic bedrock strata lie unconformably over Grenville Province Mesoproterozoic (ca. 1.1 Ga) metasedimentary rocks (Easton, 1992, 2001; McFall, 1993). In eastern Lake Ontario, the basement rocks include metacarbonates (e.g., marble), siliciclastic metasediments (quartzite, paragneiss), and plutonic rocks of the Frontenac Terrane (Fig. 3.1B) (Easton, 2001; Magnus and Easton, 2015).

The regional geology of eastern Lake Ontario includes Early Paleozoic to Mesozoic-age volcanic intrusive rocks emplaced during several phases of post-Grenville rift volcanism. These include thin (< 2 m) kimberlite and lamprophyre dikes in Paleozoic limestones near Picton and Varty Lake (Fig. 3.1A) (Barnett et al., 1984). Mesozoic dikes are typically < 30 cm wide but pipes up to 60 m in diameter have been identified in upper New York State (Van Fossen and Kent, 1993; Bailey and Lupulescu, 2015) (Fig. 3.1A). Other intrusive rocks in south-central Ontario include alkalic-carbonatite intrusions associated with post-Grenville, rift-related volcanism in the Ottawa-Bonnechère Graben (OBG; Fig. 3.1A) (Gittens et al., 1967; Symons and Chiasson, 1991). Carbonatite-alkalic volcanic complexes range in age from ~550 Ma at the western end of the OBG (Nipissing Complex) to 125-130 Ma for the Monteregian intrusives in the eastern rift segment (Fig. 3.1A) (Gold, 1986; Foland et al 1986; Symons and Chiasson, 1991).

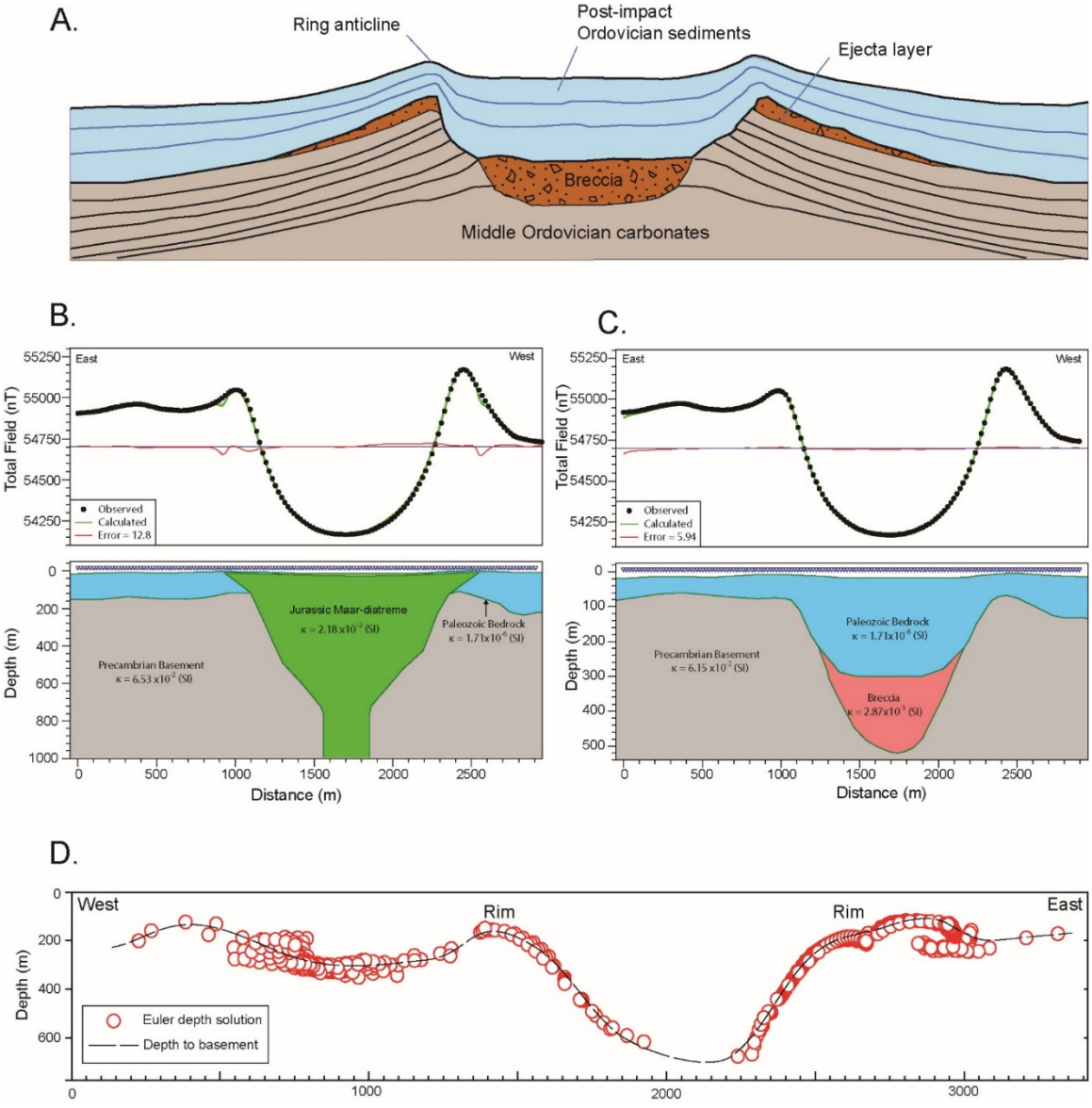

Figure 3.2. A. Holcombe et al. (2013) model for impact crater in Middle Ordovician marine sediments. Ring-anticline formed by drape deposition of carbonates sediment over impact crater rim. B. 2-D forward magnetic model for Jurassic-age maar-diatreme (kimberlite) with remanence magnetization opposing modern field direction (Suttak, 2013). C. 2-D forward magnetic model for simple impact crater in Precambrian basement (Suttak, 2013). D. Euler depth to basement profile (Suttak, 2013). Estimated basement depth in structure centre > 660 m.

3.3. Methods

3.3.1 Geophysical surveys

A digital bathymetric model (DBM) was constructed using high-resolution multi-beam datasets available from the Canadian Hydrographic Service (CHS, 2010, 2011). Multi-beam data were imported into Geosoft Oasis^{TM} (Seequent Ltd.) and gridded using minimum curvature with a 1-m grid cell spacing (Briggs, 1974). The strike and dip of well-exposed bedding planes were measured on the exposed bedrock rim using the DBM. Bedding orientations were measured on individual exposed bedding planes in multi-beam images by calculating the change in bedding plane surface height (gradient) along the direction of maximum dip. Single-channel seismic profiles (>110 line-km) were acquired over a 9-km^2 area using a 100 J boomer seismic source (1-4 kHz; C-boom Ltd.) and 8-element hydrophone array (Fig. 3.3A). Seismic profiles were collected along north-south and west-east lines and along two additional NE-SE lines over the glacial crag-and-tail feature extending from the southwestern rim (Fig. 3.3A). The survey navigation was recorded with an onboard D-GPS (horizontal accuracy ± 0.5 m) and the seismic array positioned using a layback correction. The seismic processing flow included picking of water bottom first breaks, bandpass filtering (200-3500 Hz) and application of time-varying gain (TVG) in Vista 2D/3D^{TM} software. In a final step, a zero-offset correction was applied to suppress water-bottom multiples using Radexplorer^{TM} software (Gaynanov, 2010). Depth scales on the seismic sections were estimated using a water column velocity of 1450 ms^{-1} and 1600 ms^{-1} for the unconsolidated sediments above bedrock.

Magnetic surveys were acquired using a marine Overhauser magnetometer (Marine Magnetics Seaspy^{TM}) towed 60 m behind the survey vessel. A total of ~180 line-km of total magnetic intensity (TMI) data were collected over a 9-km^2 area with a nominal line separation of 50 m (N-S) and tie lines at 100 m (W-E) (Fig. 3.3A). The sensor was cycled at 2 Hz, providing ~2 samples per metre at a survey speed of 5 kmh^{-1}.

The diurnal magnetic variation was recorded using a submersible base station magnetometer (Marine Magnetics Sentinel^{TM}) deployed in ~2 m water depth on the structure rim. Magnetic survey data processing included corrections for diurnal variation, sensor layback and tie-line leveling using an iterative least squares algorithm (Suttak, 2013). The levelled TMI data were gridded using minimum curvature interpolation (Briggs, 1974) at 25 m cell size. A residual magnetic map was produced by upward continuation (200 m) and subtraction from the TMI grid and the 1st vertical derivative and the amplitude of analytic signal (ASA) were calculated on the TMI grid (Roest et al., 1992; MacLeod et al., 1993).

Two marine gravity profiles were available from a survey conducted at Charity Shoal in 2009 (Sander Geophysics Ltd.) (Fig. 3.3B). The marine gravity survey was acquired NW-SE across the structure using a Scintrex SeaGrav^{TM} gravimeter and the data provided as terrain-corrected Bouguer gravity profiles (Fig. 3.3B).

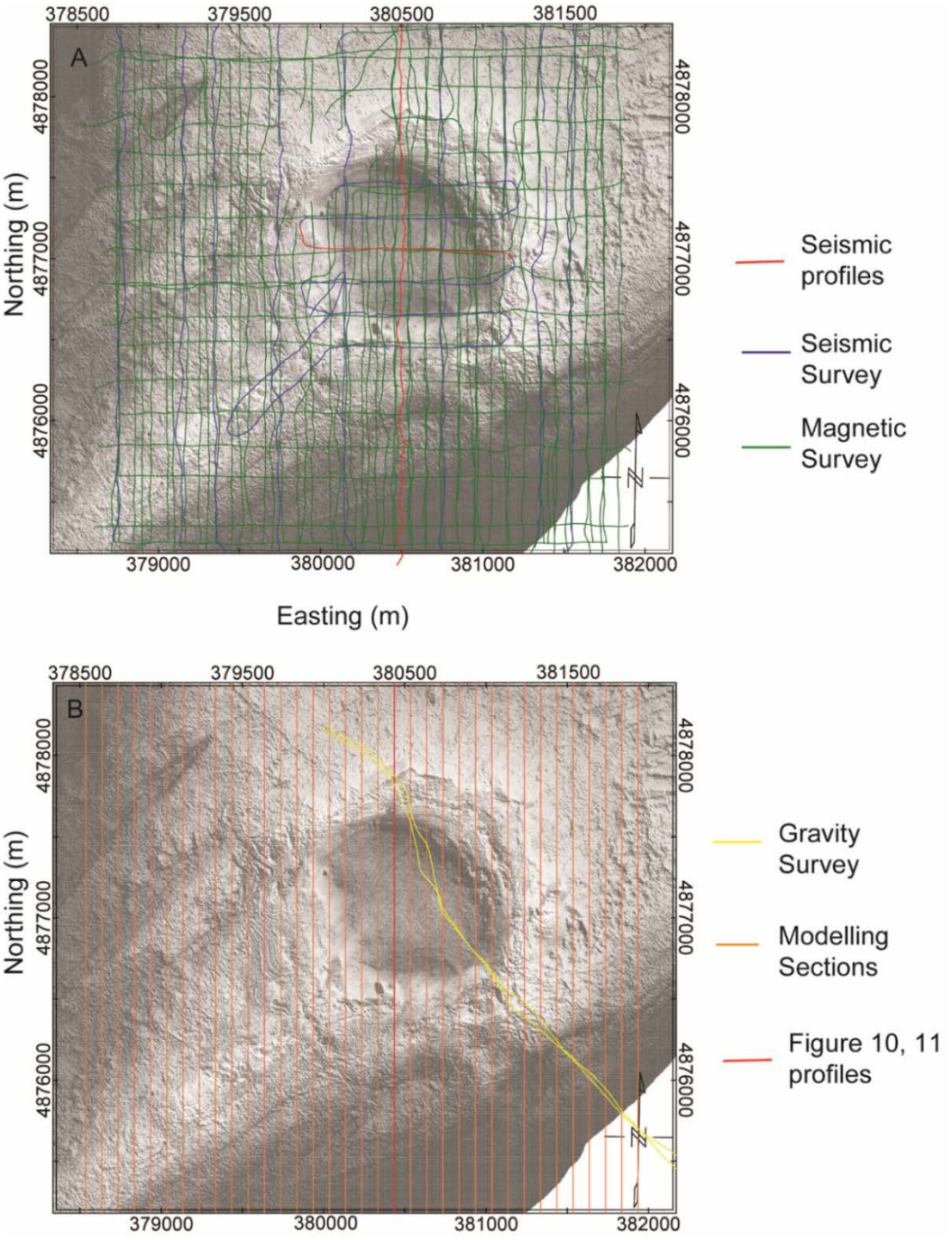

Figure 3.3. A. Geophysical survey area (~9 km^2) showing magnetic survey and boomer seismic (1–4 kHz) tracklines. Locations of seismic profiles in Fig. 3.7 shown. B. 3-D model domain showing modelled magnetic profiles and gravity survey tracklines (gravity data source: Sander Geophysics, Ltd.).

3.3.2 3-D modelling

3-D forward magnetic models were constructed in Modelvision 17 (Tensor Geophysics Pty.) using the profile modelling option (Pratt et al., 2020), which implements Talwani's method to compute the magnetic response of 3-dimensional source body prisms (Talwani and Heirtzler, 1964; Talwani, 1965; Cady, 1980; Won and Bevis, 1987). Three geological scenarios were modelled: 1) a maar-crater, 2) a cylindrical volcanic plug and 3) a simple impact crater in Mesoproterozoic basement.

The TMI grid was imported to Modelvision and profiles constructed at 100 m and 200 m line intervals over a 9-km^2 model domain (Fig. 3.3B). A central reference profile was constructed using 2-D polygons to represent the model layers and the source bodies were replicated in adjacent sections. Polygon vertices were adjusted manually to achieve an initial fit, and in a second step, an inversion routine was used to optimize the model fit and reduce residual errors (Oldenburg and Pratt, 2007). The final profiles had an RMS error of $<\pm$ 10 nT in the central part of the model and <50 nT at the model edges. $\chi 2$ was also calculated for the central profiles of all three models. The model goodness-of-fit was assessed using the root-mean-square of the model residuals and by comparison of the chi-squared statistic (Pratt D.A. 2020; Pearson, 1900).

Two volcanic models were investigated based on a review of post-Grenville volcanic intrusive types in the region (Satterly, 1970; Thomas et al., 2016) (Fig. 3.1A). Mode 1 simulated a broad (> 1 km), funnel-shaped maar-crater (diatreme) and feeder pipe below Middle Ordovician strata. Model magnetic susceptibilities for Paleozoic cover rocks and breccia were set using estimates from O'Dowd and Eaton (2005) and Suttak (2013) respectively (Table 3.1). Model 2 simulated a zoned cylindrical volcanic plug (~1-km diameter) intruded below Paleozoic cover rocks modelled after zoned carbonatite-alkalic intrusives (e.g., Oka) in south-central Ontario (Thomas et al., 2016). The pipe was modelled with a high susceptibility outer ring (κ = 0.05 SI) and lower susceptibility (κ = 0.02 SI) inner pipe and susceptibilities optimized by inversion (Table 3.1).

Model	Basement k (SI)	Paleozoic Cover k (SI)	Breccia k (SI)	Diatreme k (SI)	Outer Zone k (SI)	Remanence vector	Sources
Simple impact crater	0.05-0.1	$1.7x10^{-6}$	0.003	n/a	n/a	n/a	Suttak (2013) O'Dowd and Eaton (2005)
Maar-diatreme	0.07	$1.7x10^{-6}$	n/a	0.02	n/a	I = -70° D = 167°	Suttak (2013) O'Dowd and Eaton (2005) Model Inversion
Zoned intrusive	0.07	$1.7x10^{-6}$	n/a	0.02	0.05	n/a	O'Dowd and Eaton (2005) Model Inversion

Table 3.1: Modelling parameters used in 2-D and 3-D forward geophysical modelling

Model 3 simulated a simple impact crater with four model layers: 1) Mesoproterozoic target rocks, 2) impact breccia, 3) Paleozoic strata, 4) Quaternary sediments. Magnetic susceptibility (κ) values were assigned using available regional magnetic property data (O'Dowd and Eaton, 2005) (Table 3.1). The κ value for Mesoproterozoic basement rocks was varied (0.05-0.1 SI) to determine the effect on the modelled basin depth and geometry. The final 3-D model employed mean values for the Mesoproterozoic basement (κ = 0.07 SI) and Paleozoic sedimentary rocks ($\kappa = 1.7 \times 10^{-6}$ SI) (O'Dowd and Eaton, 2005). Quaternary sediments were assigned $\kappa = 2.6 \times 10^{-3}$ SI as an estimate for coarse-grained glacial deposits (e.g., till, outwash) (Gravenor and Stupasky, 1974). The initial thickness of the breccia deposits was set using the scaling equation for a 1.2 km diameter simple impact crater (Melosh, 1989) and optimized using model inversion (Table 3.2). The breccia magnetic susceptibility (κ = 0.003 SI) was assigned using the estimate of Suttak (2013). For the impact models, the crater geometric parameters (rim-to-rim diameter, D; true depth, d_t; apparent depth, d_a, rim height, H_r and rim-to-basement depth, H) were estimated using the crater scaling equations of Melosh (1989) and Pilkington and Grieve (1992).

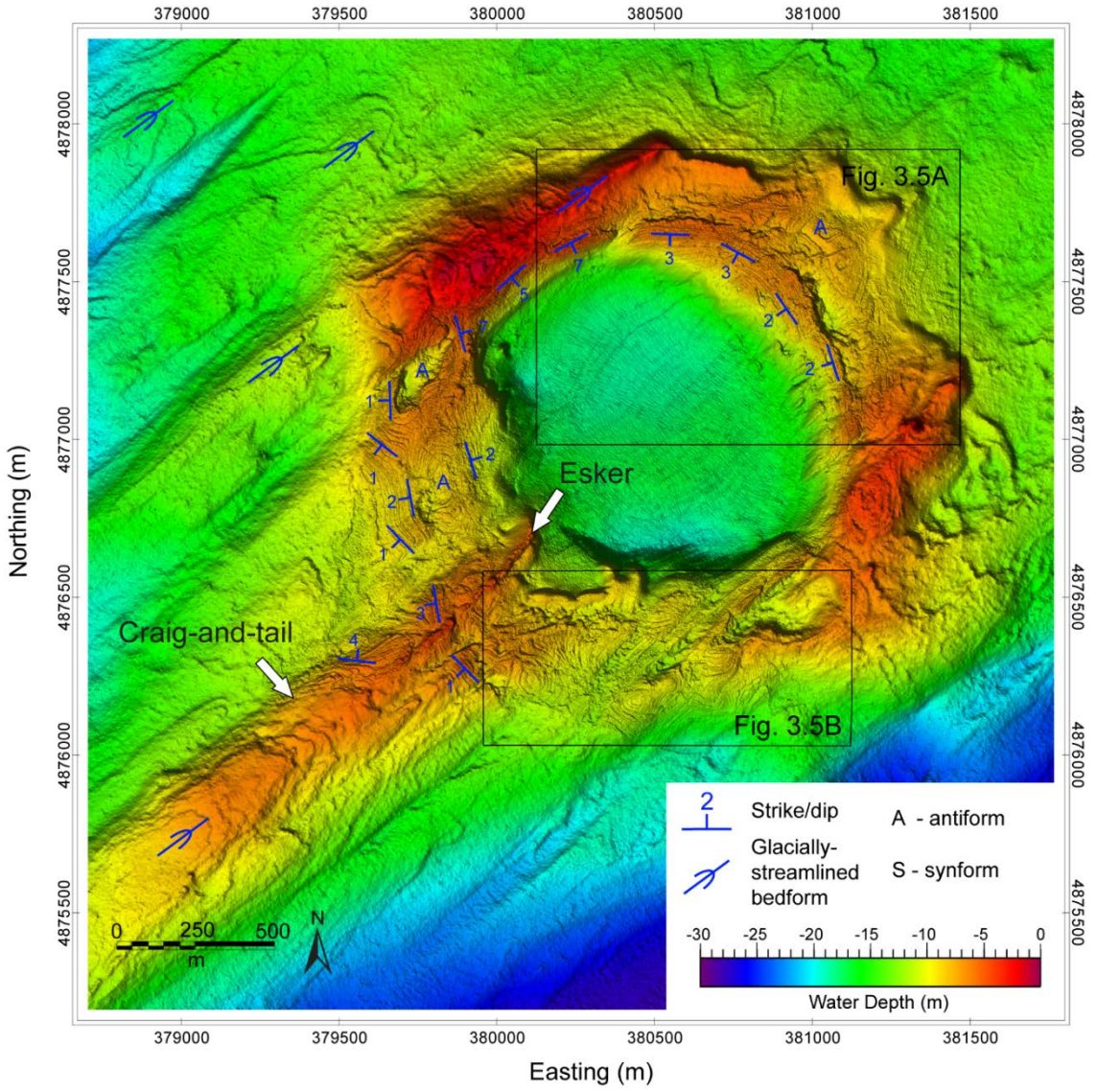

Figure 3.4. A. Digital bathymetric model (DBM) of Charity Shoal compiled from 1-m resolution multi-beam data (data sources: CHS, 2011, 2012). Location shown in Fig. 3.1B. Bedding orientations of Middle Ordovician (Trenton Group) carbonates indicated by strike and dip symbols. The Paleozoic bedrock rim forms part of a glacially streamlined crag-and-tail feature that extends 3 km to the southwest.

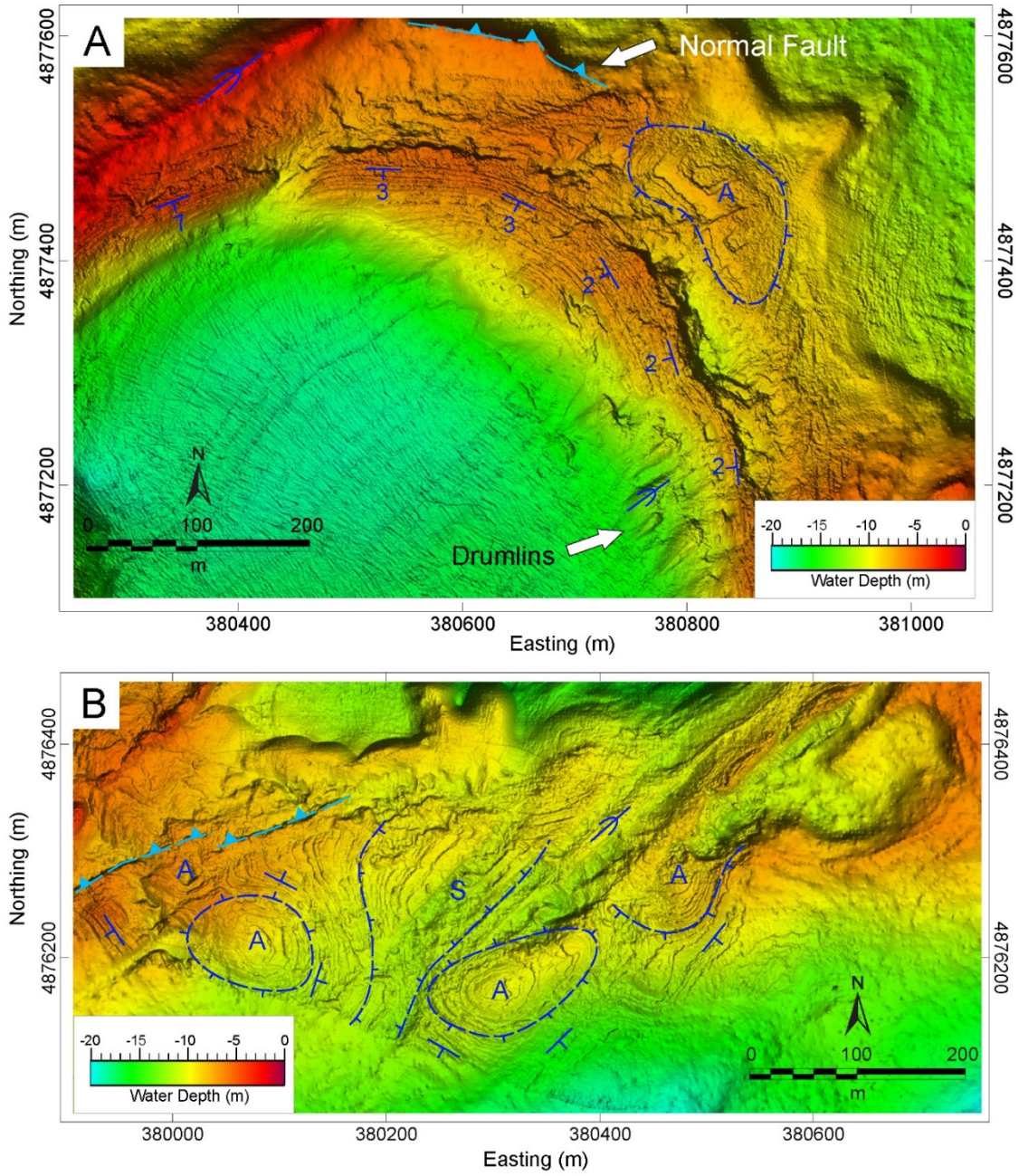

Figure 3.5. A. Multi-beam bathymetric map of northeastern rim (1-m resolution), showing radial dip of Trenton Group strata into central basin (2-7°) and 3-dimensional folding of Paleozoic strata on rim. B. Complex 3-dimensional folding on southeastern rim defined by antiforms (A) and synforms (S). Similar folding can be observed elsewhere in the Trenton Group carbonates where they are exposed along the shoreline of Lake Ontario (see Fig. 3.6)

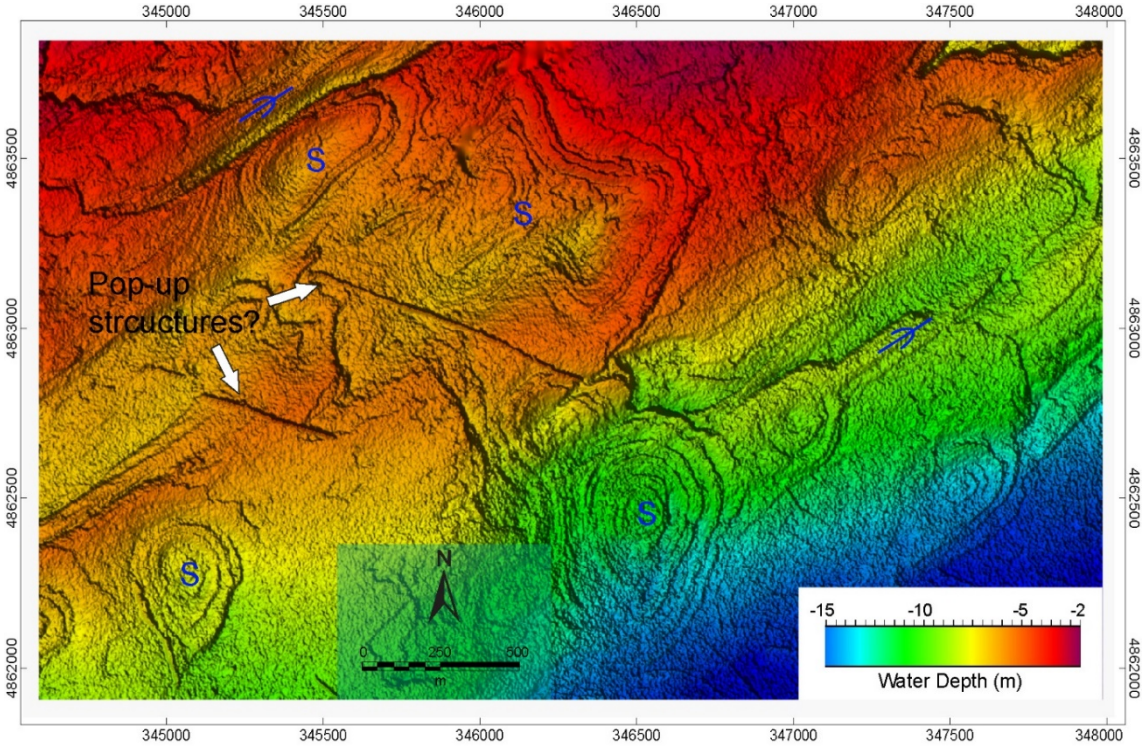

Figure 3.6. Multi-beam bathymetric map showing complex 3-dimensional folding of Trenton Group (Verulam Fm.) limestones on the north shore of Lake Ontario (Prince Edward County) (Fig. 3.1A). Northwest-trending linear features are likely bedrock 'pop-up' structures in Paleozoic bedrock (McFall, 1993). Low amplitude synforms (S) and antiforms are a regional feature of Trenton Group strata, recording low amplitude, syndepositional, soft sediment deformation of carbonate shelf sediments.

3.4. Results

3.4.1 Multi-beam bathymetry

Multi-beam bathymetric maps of Charity Shoal are shown in Figures 3.4 and 3.5. Charity Shoal is defined by a 1.2-1.5 km diameter circular bedrock shoal that encloses a central basin with a maximum water depth of about 20 m (Fig. 3.4). The rim rises within 2 m of the lake surface and is composed of fossiliferous Trenton Group dolomitic limestones (Suttak, 2013). On the northeast rim, concentric bedding planes dip uniformly at 2-7° into the basin centre (Fig. 3.5A). Elsewhere on the rim, the Paleozoic bedding is more complex and contorted by low-amplitude, 3-dimensional folding (Fig. 3.5A, B). 3-dimensional folds are most abundant on the southern and western rim, consisting of elliptical antiforms and synforms, which range in scale from 100 to > 250 m in diameter (Fig. 3.5). The antiforms in many cases have been 'unroofed' by glacial erosion (e.g., Fig. 3.5B) exposing Trenton bedrock in concentric outcrops (Fig. 3.4). Antiformal folds are most common and have fold axes that generally parallel the bedrock rim (Fig. 3.5A). In other locations, fold axes are more randomly oriented (Fig. 3.5B).

Complex, 3-dimensional folding of the rim at Charity Shoal is a regional feature of Trenton Group sediments (Figs. 3.5, 3.6). CHS multi-beam bathymetric data from the north shore of Lake Ontario (Prince Edward County) show similar folding patterns in Trenton Group sediments (Fig. 3.6). The fold structures are up to 800 m in diameter with local dips of >5°. The fold structures are analogous to the Charity Shoal rim folds that have been 'unroofed' by glacial erosion, exposing Trenton bedrock in concentric outcrops (Figs. 3.4C, 3.5).

Multi-beam images show that the exposed Charity Shoal bedrock rim has been heavily modified by glacial erosion and plucking. A broad (> 100 m) linear sediment ridge (flute) extending ~650 m from the southwest rim (Fig. 3.4) is a 'craig-and-tail' feature, formed by streamlining of glacial sediments in the lee of the rim bedrock high (Evans, 2021; Bukhari et al., 2021). Small drumlins and flutes are present in the Quaternary basin fill sediments inside the northeastern basin rim (Fig. 3.5A) and linear grooves on bedrock record glacial erosion below southwestward flowing ice. The drumlins and craig-and-tail feature likely record a final readvance of Ontario lobe of the Laurentide Ice Sheet into the Lake Ontario basin (Barnett, 1991; Gilbert and Shaw, 1992; Sookhan et al., 2018). A 30-40 m wide sinuous ridge at the northeast end of the craig-and-tail is an esker formed during ice retreat.

3.4.2. Seismic profiles

The low-frequency boomer seismic system provided a penetration of >30 m in Quaternary sediments and imaged the upper surface of Trenton Group bedrock (Fig. 3.7). The top of the bedrock surface is represented by a distinct, high-amplitude reflection that can be traced continuously below the structure and forms the water bottom reflection on the structure rim (Fig. 3.7). Seismic penetration below the top of bedrock was limited to < 10 m. The top of the Trenton Group (TTG; Fig. 3.7) represents acoustic basement, except in the central part of the basin, where several parallel, intraformational reflection events are recognized within bedrock (Figs. 3.6B, 3.7A). The contoured upper surface of bedrock, obtained by interpolation of the seismic reflection, shows a roughly circular bedrock basin with northwest-southeast diameter of ~1200 m (Fig. 3.8A).

The Quaternary infill sediments are up to 30 m thick at the basin centre and overlie a faulted, high-relief bedrock surface (Figs. 3.7, 3.8). Three distinct seismostratigraphic units (SU I-III) were identified in the basin fill based on reflection geometry, continuity and stacking patterns (Fig. 3.7). The uppermost unit SU-I consists of 1-5 m thick parallel seismic reflections interpreted as laminated Holocene muds

(Lewis and Todd, 2019). SU-II is thick package (> 25 m) of discontinuous reflections with numerous point diffractions that are interpreted as coarse-grained glacial deposits (Fig. 3.7B). SU-III is a wedge-shaped package of clinoformal reflections with internal point diffractor that onlaps the bedrock along the northwestern rim (Fig. 3.7A). The geometry and presence of point diffractors in SU-III suggests that it is likely coarse-grained glaciofluvial sediments (sub-aqueous fan?) deposited over bedrock.

Normal faults are present at several locations on the bedrock rim and basin floor, as indicated by offsets in the bedrock reflection (Fig. 3.7). On the northeastern rim, a ~5 m high, west-east trending bedrock scarp in the bathymetry marks a down-to-the-north normal fault that is visible in N-S seismic profiles (Fig. 3.7B). The fault has an apparent displacement in seismic data of at about 5-6 metres (Fig. 3.7B). Other bedrock normal faults, representing small horst and graben structures, and linear fracture zones are present on the southwestern rim margin, as indicated by discontinuities in the Trenton Group bedrock surface (Fig. 3.5B, 3.7A).

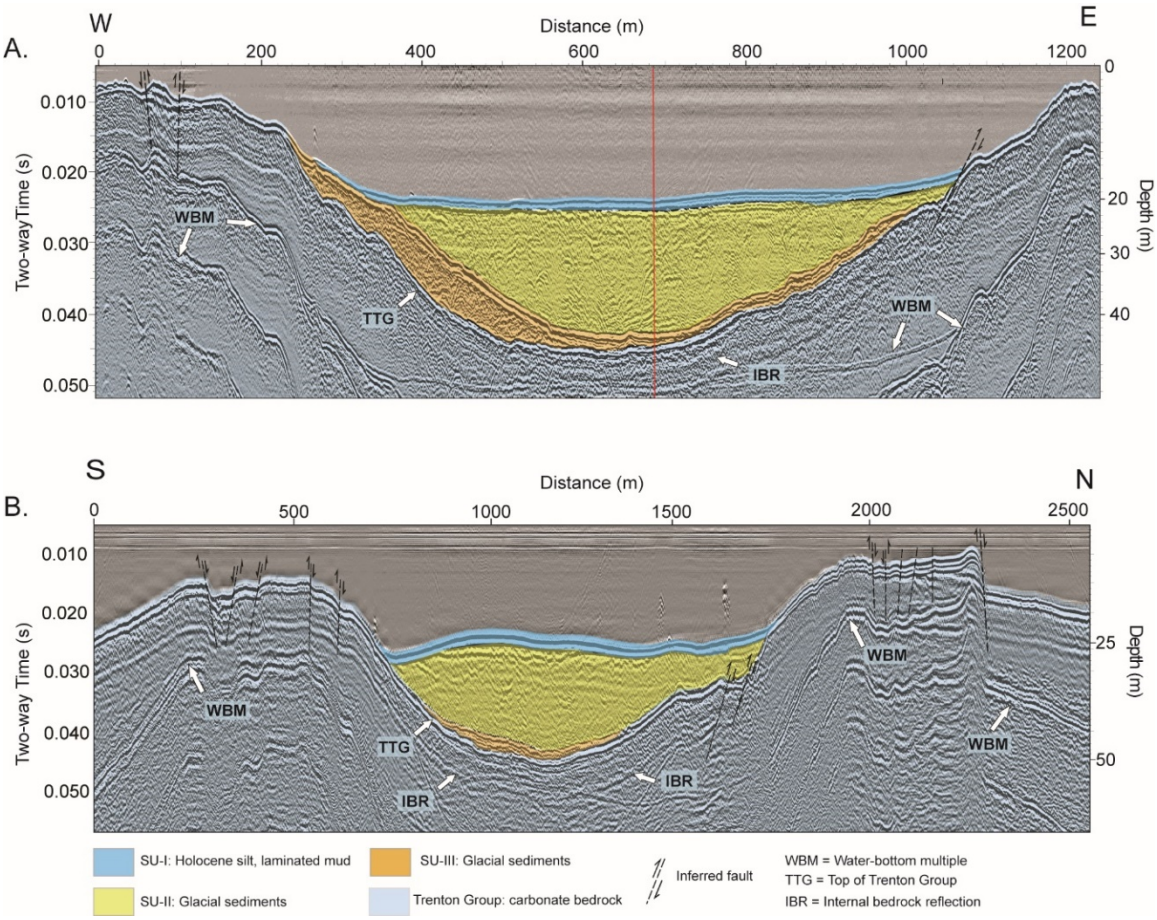

Figure 3.7. A. W-E single-channel seismic profile across Charity Shoal showing basin fill sediments and bedrock B. N-S profile. The Trenton Group (TTG) bedrock surface is indicated by high-amplitude reflections on structure rim and can be traced as a continuous interface below Quaternary sediment. The bedrock rim is offset by normal faults with apparent displacement of up to 5 m. Quaternary infill sediments are up to 30 m thick and contain three seismostratigraphic units (I-III). IBR = internal bedrock reflection, WBM = water-bottom multiple.

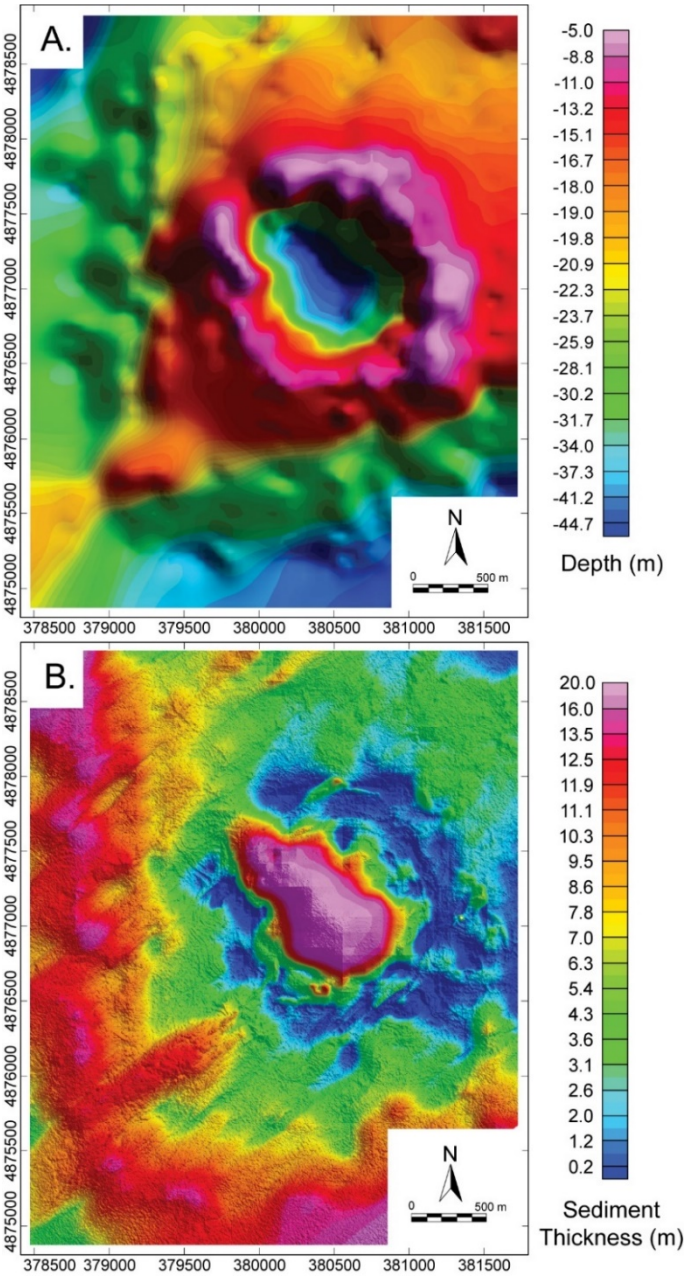

Figure 3.8. A. Seismic horizon map showing interpolated upper surface of Trenton Group bedrock (TTG; Fig. 3.7) using depth estimations as in section 3.3.1. B. Isochore map showing Quaternary sediment thickness over Paleozoic bedrock. Quaternary sediments are > 20 m thick within central basin. The Paleozoic bedrock rim is exposed in shallow water (< 5 m) and overlain by thin Quaternary sediments in water depths 5-10 m (Fig. 3.5). Note elliptical shape of central basin and structure rim.

3.4.3. Magnetics and gravity

The results of the magnetic and gravity surveys are shown in Figures 3. 9 and 3.10. The total magnetic intensity (TMI) variation across the study site is >1400 nT (Fig. 3.9A). The CSS is defined in the residual magnetic map by a ~ 600 nT magnetic low over the basin centre and annular magnetic high (>600 nT) coinciding with the structure rim (Fig. 3.9B). The 1st vertical derivative and analytic signal amplitude (ASA) maps (Fig. 3.9C, D) indicate source bodies below the surface bedrock rim. The annular anomaly is interrupted in the southwest by a southwestward-trending magnetic low.

Figure 3.10 compares 2-D profiles for bathymetry, Bouguer gravity, TMI, residual, first vertical derivative, and analytic signal along a NW-SE line across the structure (Fig. 3.3B) The variation in TMI, residual, first vertical derivative and analytic signal coincide with the variation in depth as can be seen from the 2-D profiles.

The marine gravity profile shows a general trend to decreasing Bouguer gravity over the central basin (~ 1.7 mGal) and increased gravity over the structure rim, following in general the TMI intensity (Figure 3.10 B, C). In the SE part of the profile, two gravity highs coincide with peaks in the TMI and vertical 1st derivative. The Bouguer gravity anomaly is consistent with an increased depth to basement and increased thickness of Quaternary and Paleozoic sediments below the central basin.

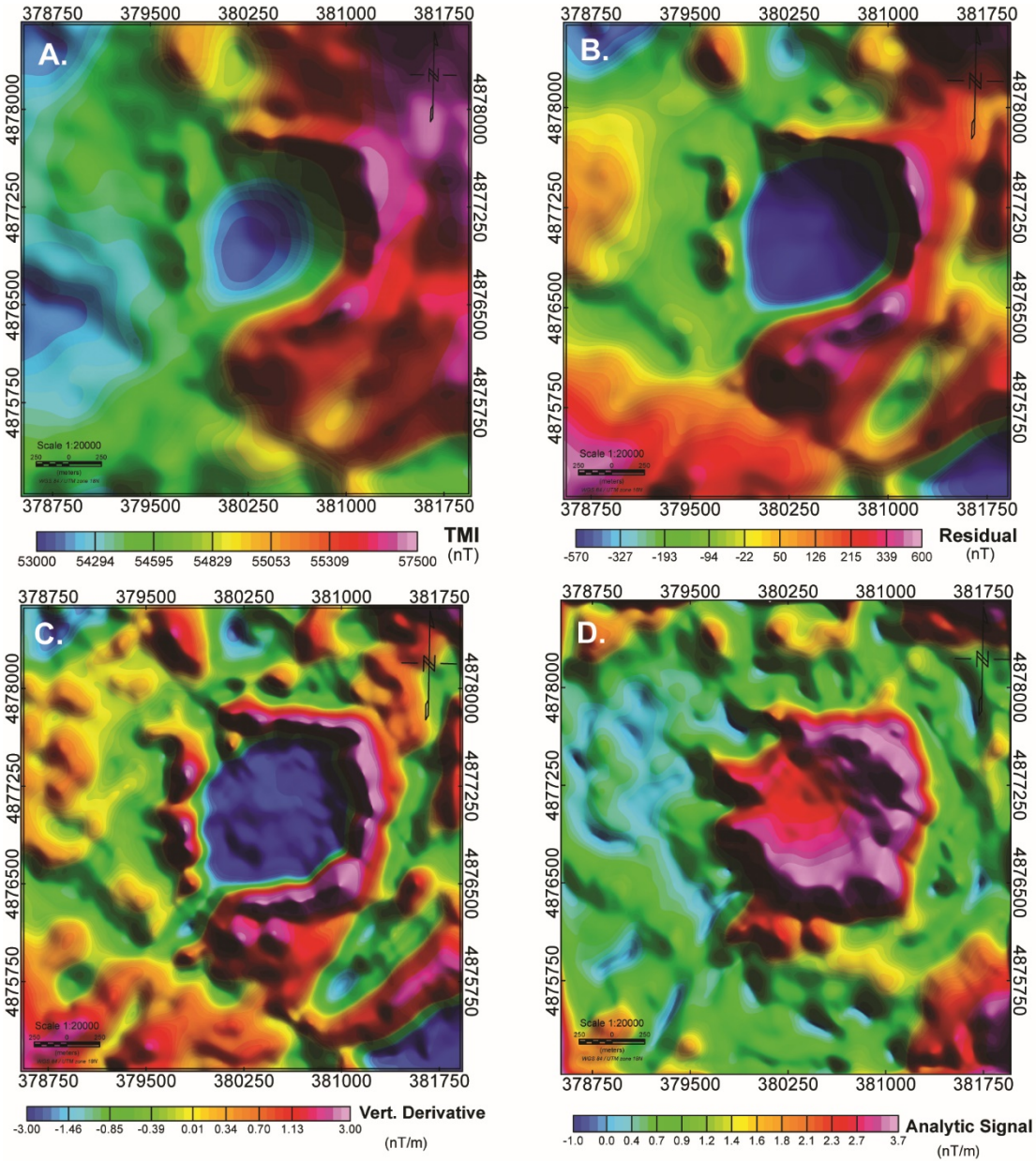

Figure 3.9. Magnetic survey results: A. Total magnetic intensity (TMI), B. Residual magnetic intensity, C. 1st vertical derivative. D. Analytic signal amplitude (ASA).

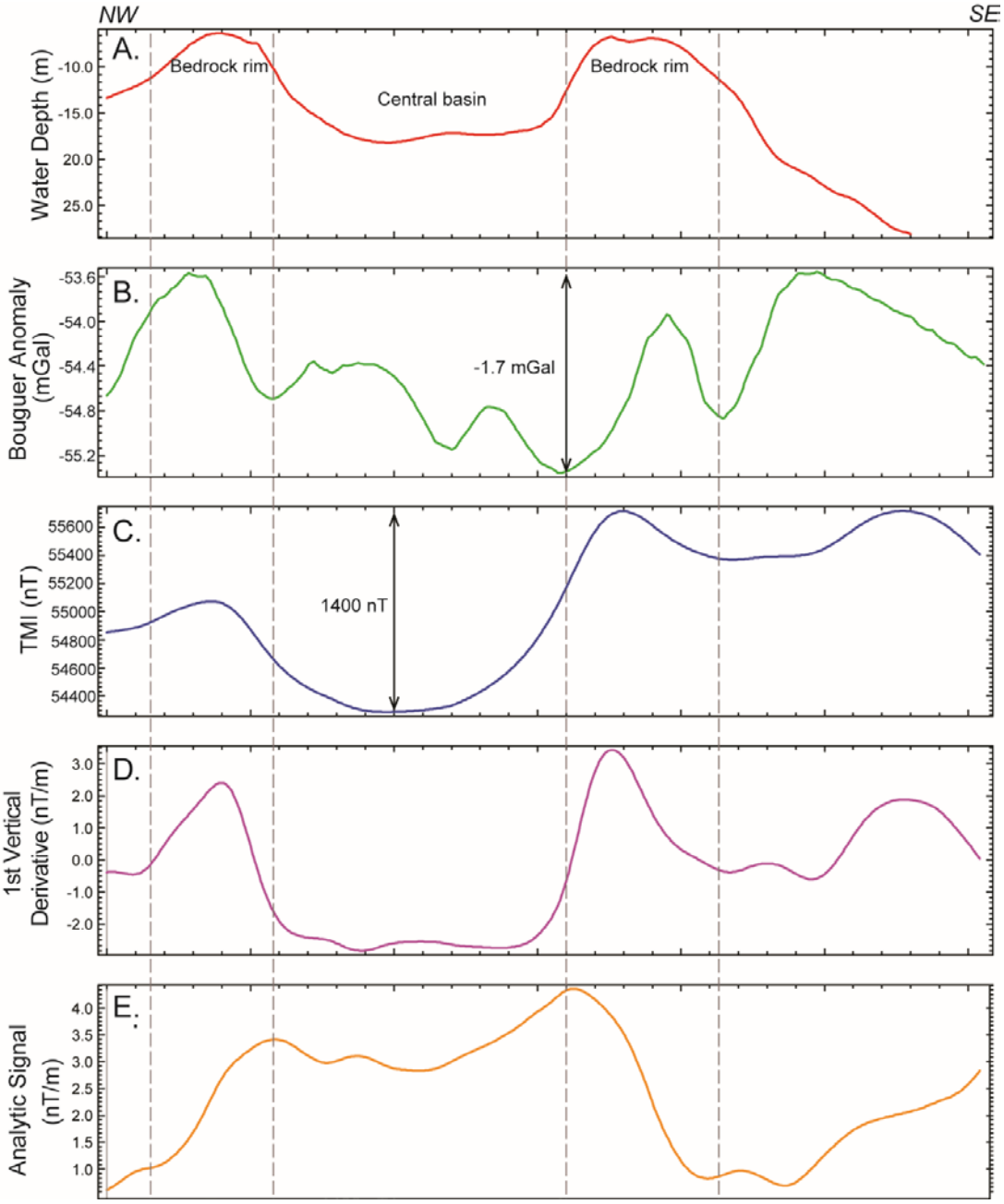

Figure 3.10. Bathymetry, gravity, and magnetic profiles along NW-SE transect across central basin (Fig. 3.3B). A. Water depth. B. Terrain-corrected Bouguer gravity (data source: Sander Geophysics Ltd.). C. Total magnetic intensity (TMI). D. Magnetic1st vertical derivative. E. Analytic signal amplitude (ASA). Note parabolic magnetic anomaly low (~1400 nT) corresponds with decrease in Bouguer gravity (~1.7 mGal) across basin centre.

3.4.4 3-D Geophysical Models

3.4.2.1 Volcanic models

t can be seen that both the RMS of the central profile is 15 and the chi-squared is 11.2. This is better than the maar-diatreme, but still a poorer fit than the impact structure.

3.4.2.2 Impact crater model

Prior to 3-D modelling, 2-D profiles were constructed across the central basin with varying basement magnetic susceptibility (κ = 0.05, 0.07, 0.1 SI) (Fig. 3.12). Modelling by Suttak (2013) had determined κ = 0.07 SI for basement rocks, to achieve a basement height that matched Euler depth-to-basement estimates (Fig. 3.2D). For 2-D profile, a value of 0.05 SI resulted in a shallow structure with thin Paleozoic cover (Fig. 3.12A) and crater true depth of ~250-300 m. A susceptibility value of 0.07 SI produced a d_t of ~450 metres, which was most consistent with crater scaling equations. A value of 0.1 SI (Fig. 3.12C) produced an extremely deep structure, >800 m depth, which is inconsistent with the crater scaling equation for a structure of this size (Table 3.2). In all three scenarios, the magnetic susceptibility had little or no effect on crater diameter. Changes in the thickness of the Quaternary sediments produced a negligible change in the model magnetic response and depth to basement due to the low κ of sediments.

Profile 3.12B is a 2-D section across the centre of the structure, and Figure 3.14A shows the modelled top of basement. The crater-form basin has a rim-to-rim diameter of ~1.2 km, (Fig 3.12B) and a rim height of 15-20 m. The diameter should be taken as a minimum value as post-emplacement modification of the rim may have reduced the

structure diameter. The depth to basement at the structure centre is ~500 metres with an estimated true depth d_t of ~ 450 metres relative to the pre-impact ground surface (~50 m below lake level) (Fig 3.12B). The basement rim has been removed on the north end of the structures, with heights of no more than 20 metres elsewhere on the rim (Fig 3.14A). Table 3.2 gives values for crater dimensions based on modelling and scaling equations. From Table 3.3 it can be seen that the RMS of the central profile is 4.2 and the chi-squared is 9.2. This is the best fit of any of the 3 models approaches in this work.

	Scaling Equation	Min (m)	Average (m)	Max (m)	Model estimate (m)	Source
Rim-to-rim diameter (D)	n/a	1000	1200	1400	1200	
True depth (d_t)	$d_t = 0.28D^{1.02}$	321	387	453	400	Pilkington and Grieve (1992)
Apparent depth (top of breccia)	$D_a = 0.13D^{1.06}$	196	238	281	n/a	Pilkington and Grieve (1992)
Rim height	$H_r = 0.036D^{1.014}$	40	48	56	15-20	Melosh (1989)
Rim to basement depth	$H = d_t + H_r$	361	435	509	450-500	Melosh (1989)
Bolide diameter		90	96	103		
Apparent Depth (top of breccia)	d_{fr}	214	253	298		Collins et.al. (2005)
Breccia thickness	t_{br}	99	117	138		Collins et.al. (2005)
Depth to Basement	$d_t = d_{fr} + t_{br}$	313	370	537		

Table 3.2: Crater dimensions and breccia thickness estimated from scaling functions (Melosh, 1989; Pilkington and Grieve, 1992) and Collins et al., (2005) for comparison with geophysical model estimates.(Fig. 3.12B) For the equations from Collins et al.,(2005), an impact velocity of 20 m/s, impact angle of 45 degrees and density of bolide of 2.7 g/cm^3 are assumed with crystalline basement rock as the target from www.lpl.arizona.edu/impacteffects .

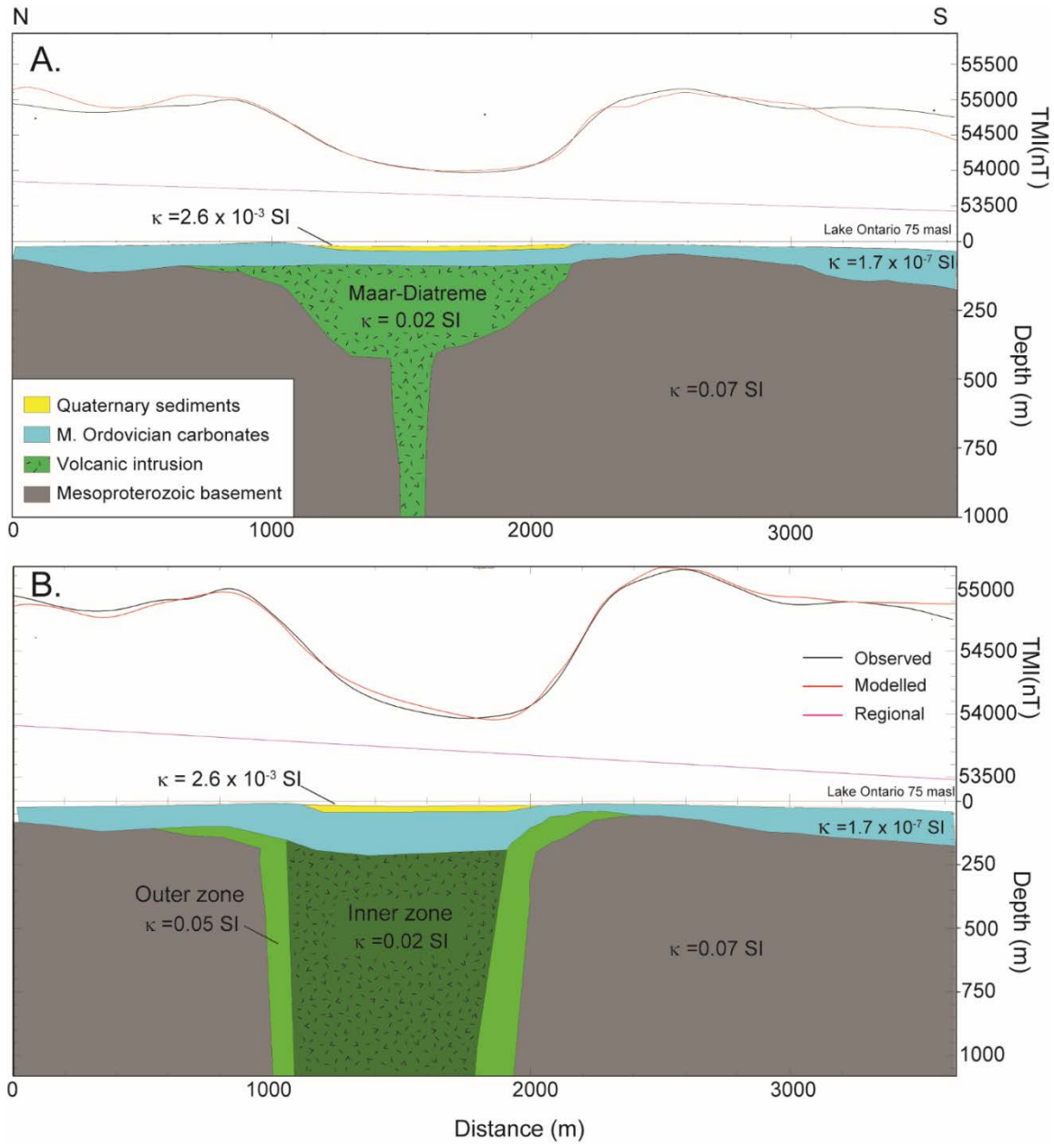

Figure 3.11. Forward magnetic models for volcanics intruded below Paleozoic cover rocks . A. 1.2-km-diameter maar-diatreme. B. Zoned volcanic intrusive with central pipe (κ = 0.02 SI) and outer zone of higher susceptibility (κ = 0.05 SI). Model depths relative to lake level datum (~75 masl).

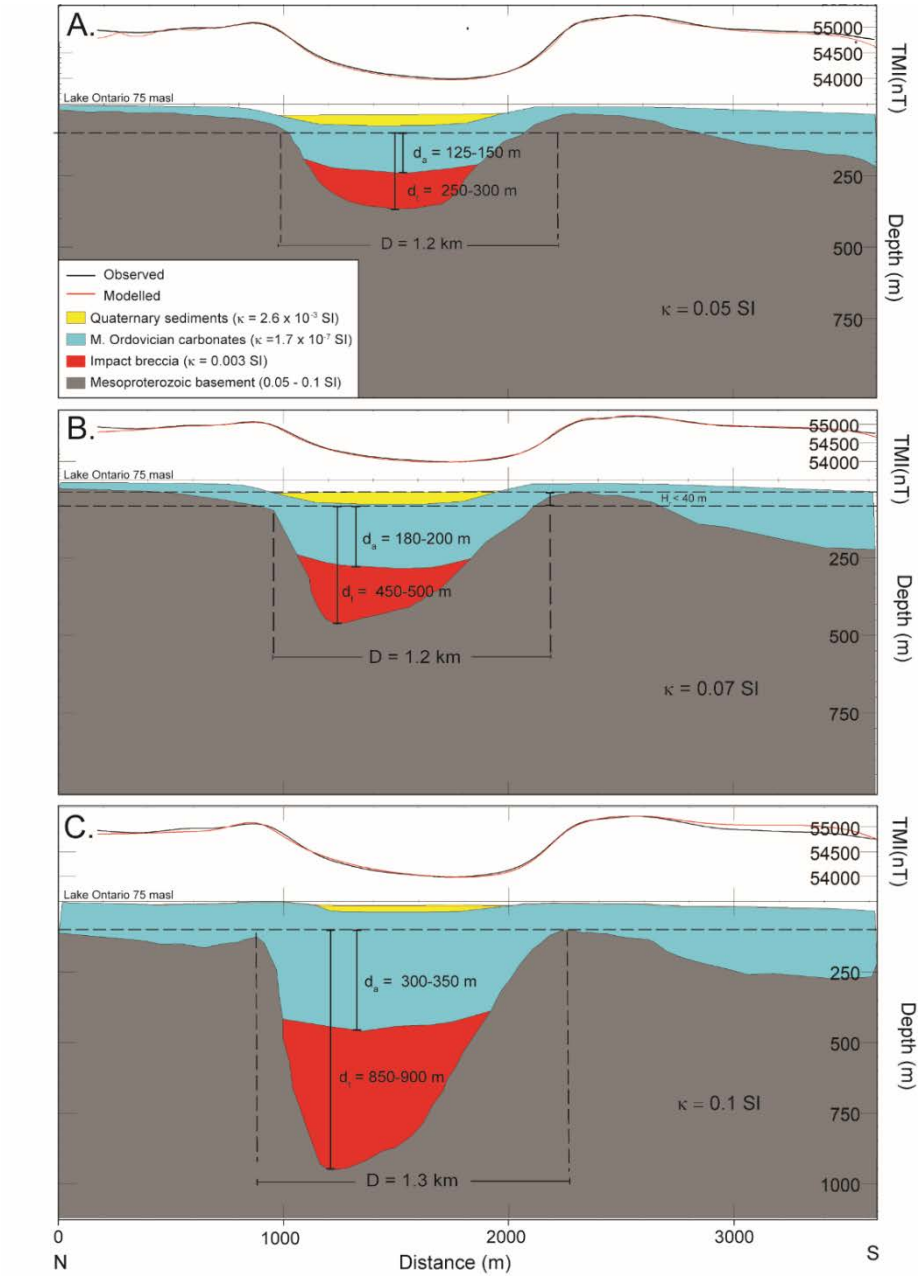

Figure 3.12. 2-D model profiles for simple impact structure with varying basement magnetic susceptibility (locations Fig. 3.3B). Initial breccia thickness estimated from scaling equations (Table 3.2) and determined by inversion. Estimated crater dimensions: d_a = apparent depth, d_t = true depth, H_r = rim height. A. κ = 0.05 SI. B. κ = 0.07 SI. C. κ = 0.1 SI. Layers above basement were assigned constant κ values (impact breccia κ = 0.003 SI, Paleozoic strata κ = 1.7 x 10^{-6}, Quaternary sediments κ = 2.6 x 10^{-3} SI). Model depths are relative to lake level datum (~75 m above sea level).

Model	**χ^2 Central profiles**	**RMS error (nT)**
Maar-Diatreme	94.2	>50
Zoned Intrusive	11.2	15.0
Impact Crater	9.2	4.2

Table 3.3 - Chi-squared statistic (χ^2) and RMS residual error values for central model profiles of kimberlite pipe (Fig. 3.11A), zoned intrusive (Fig. 3.11B) and impact crater (Fig 3.12B) models.

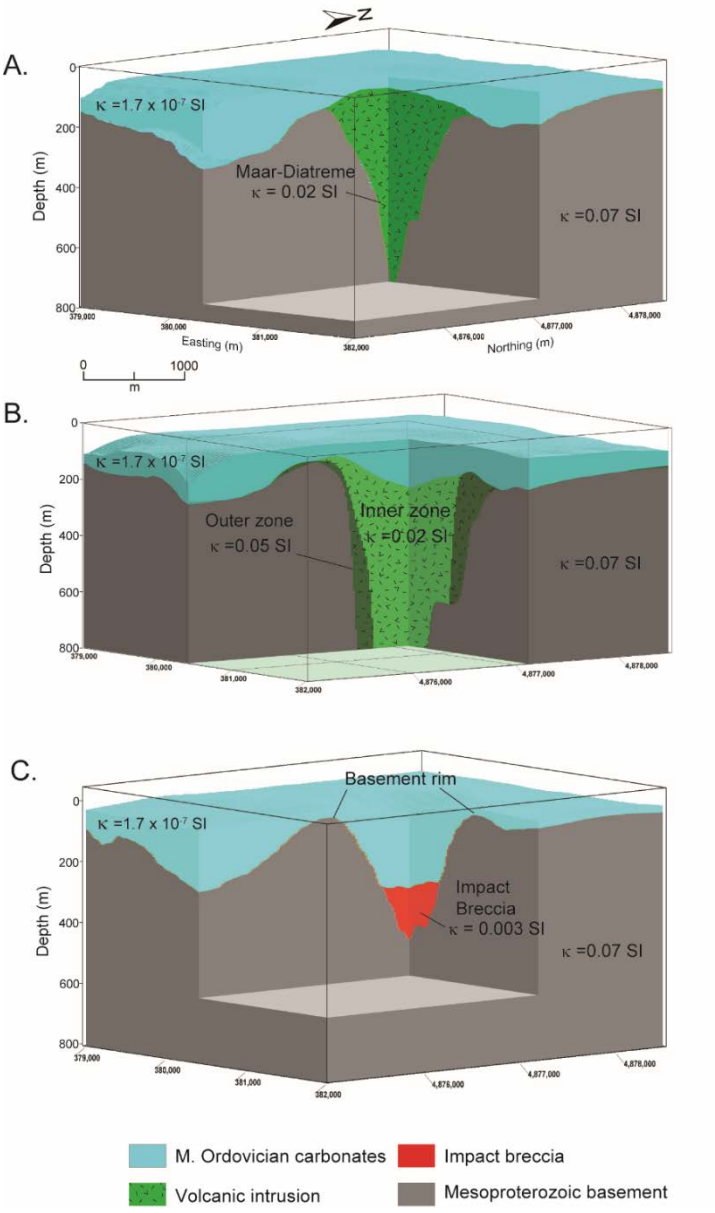

Figure 3.13. 3-D voxel models for volcanic intrusive and crater-form basin. A. Maar-diatreme (κ = 0.02 SI) intruded below Paleozoic cover. B. Zoned cylindrical volcanic plug with inner low magnetic susceptibility pipe (i.e., carbonatite; κ = 0.02 SI) and higher susceptibility outer zone (κ = 0.05 SI). C. Simple impact crater in Mesoproterozoic basement with low magnetic susceptibility basin infill (breccia κ = 0.003 SI, Paleozoic carbonate sediments κ = 1.7 x 10^{-6} SI). Model depths relative to lake level datum (~75 m above sea level).

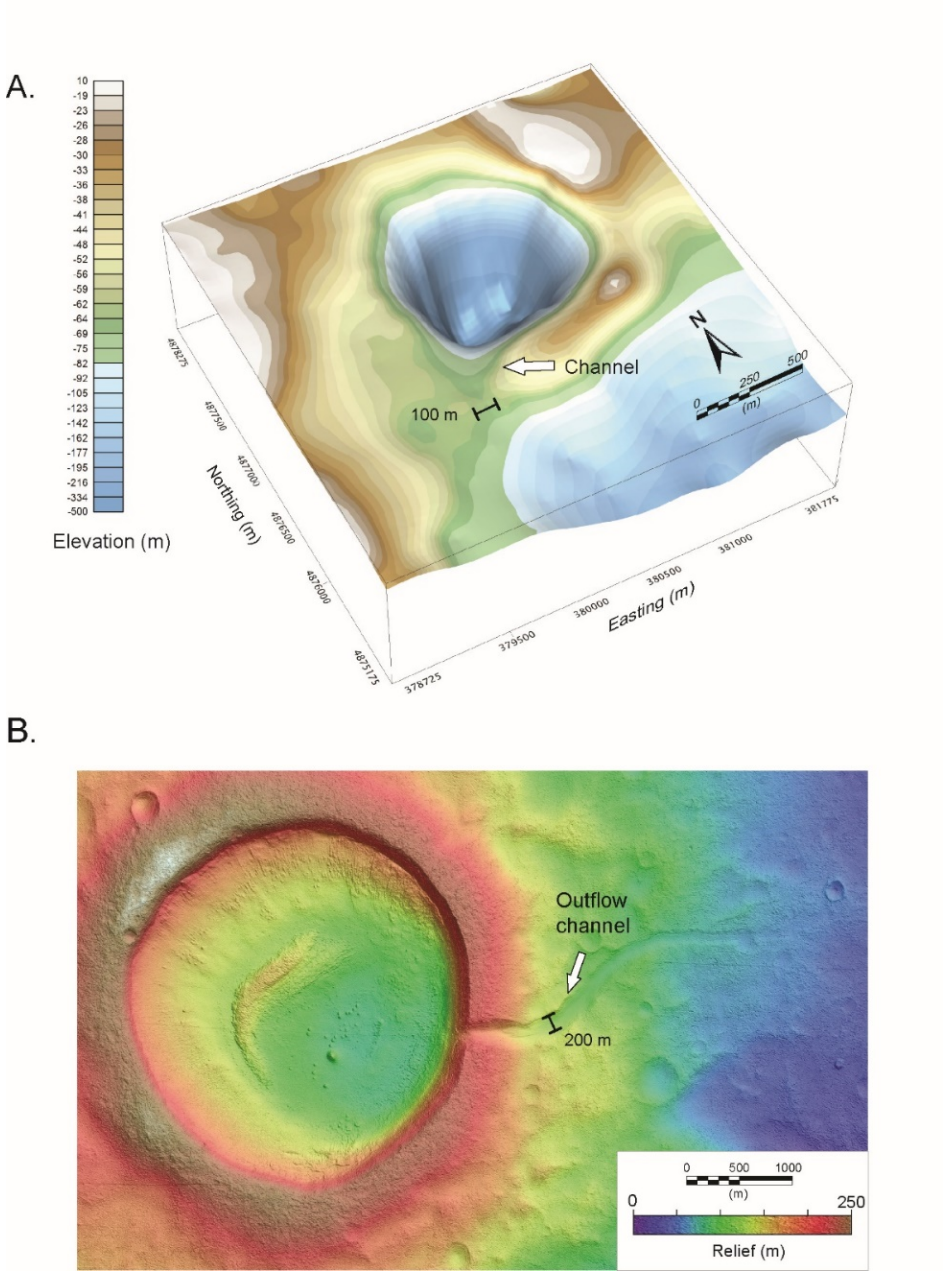

Figure 3.14. A. Modelled top of Mesoproterozoic basement (impact crater model, κ = 0.07 SI) showing raised rim and broad (>100 m) channel-like feature in southwest rim. Channel likely records sub-aerial erosion and fluvial incision of structure rim by outflow from a paleolake basin inside the crater. Elevations are relative to lake level datum (~75 m above sea level). B. For comparison, Mars Reconnaissance Orbiter digital terrain model of "tadpole crater" showing well-defined exit breach and outlet channel produced by paleolake outflow (Dehouck et al., 2010; data source: NASA/JPL/University of Arizona; stereo ESP 053222 2150).

3.5. Discussion

3.5.1 Volcanic origin?

Two previous studies have proposed a volcanic origin for Charity Shoal (Holcombe et al., 2001; Suttak, 2013). Holcombe et al. (2001) speculated on a possible volcanic cone or 'inhomogeneity' in the Precambrian basement. Suttak (2013) proposed a Mesozoic maar-diatreme intruded into Paleozoic cover rocks (Fig. 3.2A). We tested two volcanic models (Fig. 3.11) simulating a maar-diatreme and zoned carbonatite-alkalic intrusion below Paleozoic cover rocks (Figs. 3.11A, 3.13.A). The maar-diatreme model simulated a 1.3-1.4 km maar crater intruded at shallow depth below Paleozoic cover (Figs. 3.11A). This model required a reversed remanent magnetization to reproduce the observed -600 nT magnetic low and had the largest residual error (> 50 nT RMS, 94.2 chi-squared value) of the three modelled scenarios. As noted by Suttak (2013), the tapering edges of a maar-crater produce short wavelength magnetic anomalies, which are absent in the observed TMI signal (Fig. 3.11A). The gravity anomaly low (~ 1.7 mGal; Fig. 3.10B) is also inconsistent with the typical positive gravity signature of ultramafic intrusives and carbonatite-alkalic complexes (Kamara, 1981; Thomas et al., 2016). A further problem is that no pre-Paleozoic or Mesozoic ultramafic maar craters of this size are known in the region. The largest described Mesozoic kimberlite pipe from upper state New York State is 60 m in diameter (Van Fossen and Kent, 1993).

The zoned intrusive (Model 2), simulating a cylindrical volcanic plug intruded below the Paleozoic cover, has an overall better fit with the TMI compared with the maar-diatreme model with RMS ~ 15, and chi-squared of 11.2 (Fig. 3.11B, 3.13B, Table 3.3). The zoned intrusive model better reproduces the annular magnetic anomaly of the structure rim (Fig. 3.11 B) and has dimensions comparable with rift-related alkaline-carbonatite complexes in the Ottawa-Bonnechère Graben and St. Lawrence Rift system (Gittens, 1967; Symons and Chiasson, 1991) (Fig. 3.1A). Wallach (2002) previously proposed the extension of St. Lawrence rift structures into eastern Lake Ontario (Fig.

3.1A), which might support a possible carbonatite-alkalic intrusion related to Iapetan rifting.

Bouguer gravity profiles, however, show a relative gravity low (1.7 mGal) over the basin centre, indicating a mass deficit relative to the Mesoproterozoic basement (Fig. 3.10). Carbonatites in Ontario typically have densities of 2.8-3.5 g/cm^3 and are associated with positive gravity anomalies due to the large density contrast with host rocks (Thomas et al., 2016). For example, the Oka carbonatite complex has a +15 mGal anomaly and St. Honoré a gravity high of +30 mGal (Thomas et al., 2016). The 1.7 mGal gravity low over the CSS is not consistent with an origin as a carbonatite-alkalic intrusive body.

3.5.2 Impact crater?

The simple impact crater model (Figs. 3.12B, 3.13C) had the highest degree of fit and was the only geological scenario compatible with all available geophysical data. From Table 3.3, we see that the RMS and chi-squared values also produce the best fit of all three models. The RMS of 4.2, is the best fit of all three, while the chi-squared of 9.2, though closer in the value to the zoned intrusive model of 11.2, is still overall the best fit.

The magnetic model produces a depth to basement of ~500 m with an estimated true depth d_t ~450 m, a basement rim-to-rim diameter of ~1.2 km and rim height of 10-20 m (Table 3.2). The basement crater reproduces the annular magnetic high over the structure rim and parabolic-shaped, magnetic low over the central basin (Fig. 3.10B). The model is also consistent with the -1.7 mGal Bouguer anomaly, which indicates a mass deficiency below the central basin (Fig. 3.10B) and is consistent with thickening of lower density Paleozoic strata within the central basin. The crater true depth is in the range predicted by scaling equations for a 1.2 km simple impact crater (Table 3.2). The rim height, however, is lower compared with the predicted value (~50 m; Table 3.2),

which suggests post-emplacement erosion of the impact structure prior to deep burial (see 3.5.2.1 below).

The CSS has some similarities to other deeply buried impact structures in crystalline Precambrian target rocks, including the Kärdla, Granby and Tvären impact craters in Scandinavia (Suuroja et al., 2002; Henkel et al., 2010). These structures are Proterozoic to early Paleozoic impact craters buried below Paleozoic sediments. The ~4 km diameter Kärdla impact structure in Finland is defined by an 800 nT annular magnetic high over the crater rim, and a central magnetic low in the crater basin (Puura and Suuroja, 1992; Suuroja et al., 2002). The crater is buried below Paleozoic limestones, which dip into a broad syncline in the basin centre (Suuroja et al., 2002). Suuroja et al. (2002) speculated that the synclinal architecture of the Paleozoic infill was due to post-impact compaction of low porosity impact breccias. The synclinal basin structure at Charity Shoal may indicate draping of carbonate sediments across a high-relief basement surface and the differential compaction of breccias below more than 450 m of Paleozoic sediments (Fig. 3.6). The less-well studied Granby and Tvären simple impact structures may be better analogs for the CSS. In both these structures, 2-D sections through these structures based on seismic profiles and drill holes (Henkel et al., 2010) show a very similar structure to Figures 3.7, 3.12B. Both Granby and Tvären have raised bedrock rims with limestone infill in the crater.

Suttak (2013) noted that the CSS has a similar morphology to the ~2.4 km diameter Holleford impact crater, located 30 km to the north (Fig. 3.1A). Holleford was identified as a probable early Paleozoic (ca. 550 Ma) impact crater in 1960 and confirmed by exploratory drilling and recovery of impact breccias with shock polymorphs (Beals, 1960; Bunch et al., 1963) (Chapter 2). The crater is buried below >200 m of Cambrian-Middle Ordovician sediments, which form a central synclinal basin with an upraised (>40 m) bedrock rim. The rim structure has been heavily modified by glacial erosion and forms a bedrock crag-and-tail feature that is morphologically very similar to the CSS. Like Charity Shoal, the Holleford crater has a central gravity low of ~-2 mGal, which

Beals (1960) attributed to the low-density impact breccias and infill sediments. In contrast to the CSS, however, Holleford has no significant magnetic signature, as the metasedimentary Frontenac terrane target rocks at that locality have low magnetic magnetic contrast with the Paleozoic crater infill sediments (e.g., marble). Holleford crater may therefore represent a structural analogue for the CSS as a heavily modified and deeply buried simple impact crater but has significant differences in its magnetic signature.

3.5.2.1 Structure age?

Holcombe et al. (2013) have proposed Charity Shoal as a marine impact crater in Middle Ordovician shelf sediments (Fig. 3.2A). They interpret the bedrock rim as a ring anticline formed by the drape deposition of carbonate sediments across a simple impact crater (Fig. 3.2A). The geophysical and 3-D model results reported here, indicate a much more deeply buried structure (>450 m) seated in Mesoproterozoic basement rocks (Fig. 3.12B). As argued by Suttak (2013), the Charity Shoal magnetic anomaly (>1400 nT) cannot be reproduced with a crater base in the low magnetic susceptibility (~10^{-6} SI) Paleozoic carbonate rocks. The proposed ring anticline model (Fig. 3.2A; Holcombe et al., 2013), with sediments dipping into and away from a buried crater rim, is not supported by multi-beam bathymetric data (Figs. 3.4, 3.5). Multi-beam images show a much more complex pattern of 3-dimensional folding and faulting of the rim Paleozoic strata (Fig. 3.5A, C). Low-amplitude 3-D folding, consisting of synforms and antiforms, is a regional feature of Trenton Group sediments in eastern Lake Ontario (Fig. 3.6). Folding likely records soft sediment deformation and liquefaction associated with co-seismic ground shaking (i.e., seismites) and foundering of carbonate shelf sediments on the tectonically active Taconic shelf margin (McLaughlin and Brett, 2004; Oruche and Dix, 2020). The structural relief on the basement crater rim (Fig. 3.14) may have been a factor leading to sediment instability, triggering submarine mass movements, and passive folding of unconsolidated shelf sediments (McLaughlin and Brett, 2004) (Fig. 3.4). The raised structure rim (Fig. 3.4), could also represent a carbonate build-up, produced by

preferential growth of reef bioherms on top of basement structural high. Seismic and drill core data from southwestern and central Ontario have shown an association between Precambrian basement topographic highs (i.e., the Algonquin Arch) and the location of bioherms and pinnacle reefs in overlying Paleozoic rocks (Bailey, 1986). The reef rocks typically include massive corals and rudite facies, which are more erosion resistant than micritic limestones, and tend to form upstanding bioherms (Brett, 1985).

Charity Shoal has been identified as the site of a possible Late Pleistocene-age comet impact that triggered the Younger Dryas (ca. 12.9 Ka) cooling event and the extinction of Pleistocene megafauna (Firestone et al. 2007; Wu et al., 2013; Van Hoesel et al., 2014). Wu et al. (2013) have proposed several possible impact sites in eastern North America, including Charity Shoal, but other workers have strongly criticized the reproducibility of their field data and results (French and Koeberl, 2010; Paquay et al., 2009; Kerr, 2010; Van Hoesel et al., 2014). Our geophysical data and modelling demonstrate that Charity Shoal is a deep-seated, crater-form structure in Grenville Mesoproterozoic basement rocks infilled by Middle Ordovician-age sediments, which rules out a Late Pleistocene-age comet strike (Holcombe et al., 2013).

3.5.2.2 Post-emplacement modification

The modelled basement surface (Fig. 3.13C, 3.14A) allows estimates of crater dimensions and assessment of the level of post-impact modification (Kenkmann, 2021). The crater has a true depth (d_t) of >450 m and rim height of about 10-20 m (Fig. 3.12B). The basement rim height is less than half that predicted by scaling equations (~50 m; Table 3.2) for a 1.2 km diameter simple impact crater, suggesting significant post-emplacement erosion of the basement structure rim. Rim erosion is also indicated by a 50-m deep and 100 m wide channel feature in the southwest rim (Fig. 3.14A). The feature may record fluvial dissection by outflow from a lake or marine embayment impounded within the crater basin (Fig. 3.14A). Outflow and fluvial rim dissection has been

recognized in terrestrial impact craters such as Tamelzane in Algeria (Grant and Schultz, 1993; Lamali et al., 2016; Indu et al., 2021) and in volcanic calderas on Earth (e.g., Lake Taupo, New Zealand). Outflow channel incision is also an important rim modification process in Martian impact craters (Goudge et al., 2015; Fig. 3.14B).

3.6. Summary and Conclusions

Geophysical surveys and 3-D magnetic modelling demonstrate that Charity Shoal is a 1.2-km-diameter crater-form basin in the Mesoproterozoic basement rocks of eastern Lake Ontario (Fig. 3.13C, 3.14A). A proposed Mesozoic-age maar-diatreme (Suttak, 2013) can be ruled out, as Middle Ordovician sediments are continuous below the structure (Fig. 3.7). A pre-Paleozoic age maar-diatreme or zoned intrusive pipe is also unlikely, as there are no known kimberlites of this size or age in the region (Van Fossen and Kent, 1993; Bailey and Lupulescu, 2015). A zoned volcanic plug below Paleozoic cover strata (Fig. 3.11B) can reproduce the annular magnetic anomaly but is at odds with gravity data, which show a ~1.7 mGal gravity low, indicating a mass deficit below the basin centre.

Of the three geological models considered, an impact crater is the only origin compatible with all available geophysical data (Fig. 3.13). The >1400 nT parabolic-shaped magnetic anomaly and gravity low (~ 1.7 mGal) are consistent with a simple impact crater in Mesoproterozoic basement rocks at a depth of >450 m (Fig. 3.12B). The structure rim height (10-20 m) and diameter (~ 1.2 km) suggest a simple impact crater that has undergone significant post-impact erosion prior to deep burial. Rim erosion rim is indicated by a >100 m wide channel in the southwestern rim (Fig. 3.14A). The channel may record fluvial incision by outflow from a crater lake. The channel dimensions are comparable to drainage outflow channels observed in terrestrial and Martian impact craters of similar dimensions (Goudge et al., 2015; Indu et al., 2021).

A marine impact structure with a base in Middle Ordovician sediments, as proposed by Holcombe et al. (2013), is at odds with the Charity Shoal magnetic anomaly (>1200 nT), which indicates a deeply-seated structure; magnetic modelling indicates a parabolic crater-form basin Mesoproterozoic basement at depth of > 450 m. Their proposed ring-anticline model for the structure rim is not supported by multi-beam bathymetric images and seismic data, which show a more complexly folded rim structure (Fig. 3.4, 3.5). Complex 3-dimensional folding is a regional feature of the Trenton Group sediments and likely records slumping of carbonate sediments on a tectonically active shelf margin.

As demonstrated in this paper, multi-parameter geophysical surveys and 3-D geophysical models can assist in evaluating competing geological models for suspected impact craters, where direct geological evidence for impact origin is lacking. Confirmation of an impact origin for Charity Shoal will ultimately require deep exploration drilling and sampling and recovery of impact products (e.g., impact breccias, pdf's, shock features) (French and Koeberl, 2010). Offshore drilling, however, is currently banned in the Great Lakes under US law and is subject to strict regulation in Canada (Hall, 2011). Due to these restrictions and the high costs of offshore drilling, marine seismic investigations are a more viable option. Future work could employ high-energy, low-frequency seismic sources (e.g., airguns) to enable seismic imaging of the entire Paleozoic section and top surface of basement (Stewart, 2003).

3.7 References

Anderson T.W. and Lewis C.F.M. 2012. A new water-level history for Lake Ontario basin: evidence for a climate-driven early Holocene lowstand. *Journal of Paleolimnology* 47: 513–530 https://doi.org/10.1007/s10933-011-9551-8

Bailey D.G. and Lupulescu M.V. 2015. Spatial, temporal, mineralogical, and compositional variations in Mesozoic kimberlitic magmatism in New York State, *Lithos* 212–215: 298-310. https://doi.org/10.1016/j.lithos.2014.11.022

Bailey S.M.B. 1986. A new look at the development, configuration, and trapping mechanisms of the Silurian Guelph reefs of southwestern, Ontario. *Proceedings of Ontario. Petrological. Institute*. 25:1– 28.

Barnett R.L., Arima M., Blackwell J.D., Winder C.G., Palmer H.C. and Hayatsu A. 1984. The Picton and Varty Lake ultramafic dikes: Jurassic magmatism in the St. Lawrence Platform near Belleville, Ontario. *Canadian Journal of Earth Sciences* 21: 1460-72 https://doi.org/10.1139/e84-151

Barnett P.J. 1991. Quaternary Geology of Ontario. *Geology of Ontario Special Volume 4* Part 2: 1001-1090.

Batista-Rodríguez J. A., Pérez-Flores M. A. and Urrutia-Fucugauchi J. 2013. Three-dimensional gravity modeling of Chicxulub Crater structure, constrained with marine seismic data and land boreholes. *Earth, Planets and Space*, 65(9):973-983. https://doi.org/10.5047/eps.2013.05.015

Beals C.S. 1960. A probable meteorite crater of Precambrian age at Holleford, Ontario. *Publications of the Dominion Observatory* 24:6 (Ottawa) https://doi.org/10.4095/8727

Brett C. E. 1985. Pelmatozoan echinoderms on Silurian bioherms in western New York and Ontario. *Journal of Paleontology* :820-838. https://www.jstor.org/stable/1304932

Briggs I. C. 1974. Machine contouring using minimum curvature. *Geophysics*, 39(1):39-48.

Bunch T. E. and Cohen A. J. 1963. Coesite and shocked quartz from Holleford crater, Ontario, Canada. *Science,* 142:379-381.

Bukhari S., Eyles N., Sookhan S., Mulligan R., Paulen R., Krabbendam M. and Putkinen N. 2021. Regional subglacial quarrying and abrasion below hard-bedded palaeo-ice streams crossing the Shield–Palaeozoic boundary of central Canada: the importance of substrate control. *Boreas*, 50(3):781-805. https://doi.org/10.2172/1122567

Cady J. W. 1980. Calculation of gravity and magnetic anomalies of finite-length right polygonal prisms. *Geophysics*, 45(10):1507-1512. http://dx.doi.org/10.1190/1.1441045

CHS (2011). Digital bathymetric data, Charity Shoal. Canadian Hydrographic Service, Digital File No. 4013083.

CHS (2012). Digital bathymetric data, Charity Shoal. Canadian Hydrographic Service, Digital File No. 4013191.

Clark J. F. 1982 Earth Physics Branch, Geomagnetic Report 81-2, 25 pages https://doi.org/10.4095/226536

Collins G. S., Melosh H. J. and Marcus R. A. 2005. Earth impact effects program: A web-based computer program for calculating the regional environmental consequences of a meteoroid impact on Earth. *Meteoritics & Planetary Science* 40(6):817-840. https://doi.org/10.1111/j.1945-5100.2005.tb00157.x

Dehouck E., Mangol N., Le Mouélic S., Ansan V. and Poulet F. 2010. Ismenius Cavus, Mars: A deep paleolake with phyllosilicate deposits. *Planetary and Space Science*, 58(6):941-946. https://doi.org/10.1016/j.pss.2010.02.005

Easton R.M. 1992 The Grenville Province and Proterozoic History of Central and Southern Ontario *Geology of Ontario Special Volume 4* Part 2: 715-906.

Eaton R.M. 2001. Precambrian Geology, Tichborne Area (31 C/10). Ontario Geological Survey, Preliminary Map, 3442. Ministry of Energy, Northern Development and Mines.

Ebbing J., Janle P., Koulouris J. and Milkereit B. 2001. 3D gravity modelling of the Chicxulub impact structure. *Planetary and Space Science*, 49(6):599-609 https://doi.org/10.1016/S0032-0633(01)00005-8

Evangelatos J., Butler K.E. and Spray J.G. 2009. A marine magnetic study of a carbonate-hosted impact structure: Ile Rouleau, Canada. *Geophysical Journal International* 179(1): 171-181. https://doi.org/10.1111/j.1365-246X.2009.04304.x

Evans D. J. 2021. The Midland Valley: Ice-Moulded Lowlands. In *Landscapes and Landforms of Scotland.* Springer, Cham., p. 439-452.

Firestone R.B., West A. and Kennett J.P. 2007. Evidence for an extraterrestrial impact 12,900 years ago that contributed to the megafaunal extinctions and the Younger Dryas cooling. *Proceedings of the National Academy of Sciences of the United States of America* 104: 16016-21 https://doi.org/10.1073/pnas.0706977104

Foland K.A., Gilbert L.A., Sebring C.A. and Jiang-Feng C. 1986. $^{40}Ar/^{39}Ar$ ages for plutons of the Monteregian Hills, Quebec: Evidence for a single episode of Cretaceous magmatism. *GSA Bulletin*: 97 (8): 966–974. https://doi.org/10.1130/0016-7606(1986)97%3C966:AAFPOT%3E2.0.CO;2

French B.M. 1998. Traces of Catastrophe: A Handbook of Shock-Metamorphic Effects in Terrestrial Meteorite Impact Structures. LPI Contribution No.954, Lunar and Planetary Institute, Houston. 120 p.

French B.M. and Koeberl C. 2010. The convincing identification of terrestrial meteorite impact structures: What works, what doesn't, and why. *Earth-Science Reviews* 98: 123-70. https://doi.org/10.1016/j.earscirev.2009.10.009

Gaynanov V.G. 2010. Acoustic profiling data processing software. *Oceanology* 50: 131–138. https://doi.org/10.1134/S0001437010010157

Gilbert R. and Shaw J. 1992. Glacial and early postglacial lacustrine environment of a portion of northeastern Lake Ontario. *Canadian Journal of Earth Sciences*. 29(1):63-75. DOI: https://doi.org/10.1139/e92-008

Gittens J., MacIntyre R.M. and York D. 1967. The ages of carbonatite complexes in eastern Canada. *Canadian Journal of Earth Sciences*, 4: 651-5. https://doi.org/10.1139/e67-042

Gold D. P. 1986. Carbonatites, diatremes and ultra-alkaline rocks in the Oka area, Quebec. Geological Association of Canada.

Gottwald M., Fritz T., Breit H., Schättler B. and Harris A. 2017. Remote sensing of terrestrial impact craters: The TanDEM-X digital elevation model. *Meteoritics & Planetary Science*, 52(7):1412-1427. https://doi.org/10.1111/maps.12794

Goudge T. A., Aurel K. L., Head J. W., Fassett C. I. and Mustard J. F. 2015. Classification and analysis of candidate impact crater-hosted closed-basin lakes on Mars. *Icarus*, 260, 346-367. https://doi.org/10.1016/j.icarus.2015.07.026

Grant J. A. and Schultz P. H. 1993. Degradation of selected terrestrial and Martian impact craters. *Journal of Geophysical Research: Planets*, 98(E6):11025-11042. https://doi.org/10.1029/93JE00121

Gravenor C.P. and Stupavsky M. 1974 Magnetic susceptibility of the surface tills of Southern Ontario. *Canadian Journal of Earth Sciences,* 11(5): 658-663. https://doi.org/10.1139/e74-063

Hall N.D. 2011. Oil and freshwater don't mix: transnational regulation of drilling in the Great Lakes. *Environmental Affairs and Law Review*, 38: 305-314.

Henkel H., Ekneligoda T. C. and Aaro S. 2010. The extent of impact induced fracturing from gravity modeling of the Granby and Tvären simple craters. *Tectonophysics*:485(1-4):290-305. https://doi.org/10.1016/j.tecto.2010.01.008

Holcombe T.L., Warren J. S., Reid D. F., Virden W. T. and Divins D. L. 2001 Small rimmed depression in Lake Ontario: An impact crater? *Journal of Great Lakes Research*. 27(4): 510-517. https://doi.org/10.1016/S0380-1330(01)70664-8

Holcombe T.L., Youngblut S. and Slowey N. 2013. Geological structure of Charity Shoal crater, Lake Ontario, revealed by multi beam bathymetry. *Geo-Marine Letters*. 33 (4): 245-252. https://doi.org/10.1007/s00367-013-0322-6

Johnson M.D., Armstrong D.K, Sanford B.V., Telfor, P.G. and Rutka M.A. 1992. Paleozoic and Mesozoic geology of Ontario. In: Geology of Ontario. *Ontario Geological Survey* Special Volume 4:907-1008.

Kamara A.Y.S 1981 Review: geophysical methods for kimberlite, prospecting. *Bulletin of the Australian Society of Exploration Geophysics* 12(2): 43-51 https://doi.org/10.1071/EG981043

Kenkmann T. 2021. The terrestrial impact crater record: A statistical analysis of morphologies, structures, ages, lithologies, and more. *Meteoritics & Planetary Science,* 56(5):1024-1070. https://doi.org/10.1111/maps.13657

Kerr R.A. 2010. Mammoth-killer impact flunks out. *Science* 329 (5996) :1140-1141 https://doi.org/10.1126/science.329.5996.1140

Indu G. K., James S., Chandran S.R. Aneeshkumar V., Keerthy S., Oommen T. and Sajinkumar K. S. 2021. Deriving a denudation index for terrestrial meteorite impact craters using drainages as proxies. *Geomorphology*, 397: 108007. https://doi.org/10.1016/j.geomorph.2021.108007

Lajeunesse P., St-Onge G., Locat, J., Duchesne M.J., Higgins M.D., Sanfaçon R. and Ortiz J. 2013. The Corossol structure: a possible impact crater on the seafloor of the northwestern Gulf of St. Lawrence, Eastern Canada. *Meteoritics & Planetary Science*, 48(12)2542-2558. https://doi.org/10.1111/maps.12224

Lamali A., Rochette P., Merabet N., Abtout A., Maouche, S., Gattacceca J., Ferrière L., Hamoudi, M., ASTER Team, Meziane E.H. and Ayache M. 2016. Geophysical and magneto-structural study of the Maâdna structure (Talemzane, Algeria): Insights on its age and origin. *Meteoritics & Planetary Science*, 51(12):2249-2273. https://doi.org/10.1111/maps.12715

Lewis C. M. and Todd B. J. 2019. The Early Lake Ontario barrier beach: evidence for sea level about 12.8–12.5 cal. Ka BP beneath western Lake Ontario in eastern North America. *Boreas*, 48(1):195-214. https://doi.org/10.1111/bor.12351

MacLeod I. N., Jones K. and Dai T. F. 1993. 3-D analytic signal in the interpretation of total magnetic field data at low magnetic latitudes. *Exploration Geophysics*, 24(4):679-688. https://doi.org/10.1071/EG993679

Magnus S.J. and Easton R.M. 2015. Precambrian geology of eastern Ontario interpreted from aeromagnetic and compiled geological data—south sheet; Ontario Geological Survey, Preliminary Map P.3793, scale 1:100 000.

McFall G. H. 1993. Structural elements and neotectonics of Prince Edward County, southern Ontario. *Geographie physique et Quaternaire*, 47(3): 303-312. https://doi.org/10.7202/032959ar

McFall G.H. and Allam A. 1991. Neotectonic Investigations in Southern Ontario Prince Edward County – Phase II. A research report prepared for the Atomic Energy Control Board Ottawa, Canada, Project No. 3.131. (INFO–0343-2).

McLaughlin P. I. and Brett C. E. 2004. Eustatic and tectonic control on the distribution of marine seismites: examples from the Upper Ordovician of Kentucky, USA. *Sedimentary Geology*, 168(3-4)165-192. https://doi.org/10.1016/j.sedgeo.2004.02.005

Melosh H.J. 1989 Impact Cratering: A Geologic Process. Oxford University Press, New York.

O'Dowd C. and Eaton D. 2005. Field and laboratory measurements of magnetic properties and density, Central Metasedimentary Belt, Ontario. Natural Resources Canada, Geological Survey of Canada.

Oldenburg D.W. and Pratt D.A. 2007. Geophysical inversion for mineral exploration: A decade of progress in theory and practice. In *Proceedings of exploration* 7(5):61-95 https://911metallurgist.com/blog/wp-content/uploads/2015/10/Geophysical-Inversion-for-Mineral-Exploration.pdf

Oruche N.E. and Dix G.R., 2021. Sequence stratigraphy of a Middle to Upper Ordovician foreland succession (Ottawa Embayment, central Canada): Evidence for tectonic control on sequence architecture along southern Laurentia. *Basin Research*, 33(1):779-808. https://doi.org/10.1111/bre.12495

Osinski G. R. and Pierazzo E. 2013. Impact cratering: Processes and products. John Wiley & Sons.

Paquay F.S., Goderis S., Ravizza G., Vanhaeck F., Boy M., Surovell T.A., Holliday V.T., Haynes C.V. and Claeys P., 2009. Absence of geochemical evidence for an impact event at the Bølling–Allerød/Younger Dryas transition. *Proceedings of the National Academy of Sciences,* 106(51):21505-21510 https://doi.org/10.1073/pnas.0908874106

Pearson K. 1900. On the criterion that a given system of deviations from the probable in the case of a correlated system of variables is such that it can be reasonably supposed to have arisen from random sampling. Philosophical Magazine, 50, 157–172. https://doi.org/10.1080/14786440009463897

Pilkington M. and Hildebrand A. R. 2000. Three-dimensional magnetic imaging of the Chicxulub crater. *Journal of Geophysical Research: Solid Earth*, 105(B10):23479-23491. https://doi.org/10.1029/2000JB900222

Pilkington M. and Grieve R.A.F. 1992. The geophysical signature of terrestrial impact craters. *Reviews of Geophysics* 30: 161-81 https://doi.org/10.1029/92RG00192

Pratt D. A., White A. S., Parfrey K. L. and McKenzie K. B., 2020. ModelVision 17.0 User Guide. Tensor Research Pty Ltd., Grenwich, NSW, Australia, 596 p.

Puura V. and Suuroj K. 1992. Ordovician impact crater at Kärdla, Hiiumaa Island, Estonia. *Tectonophysics*, 216(1-2):143-156. https://doi.org/10.1016/0040-1951(92)90161-X

Reimold W.U., Ferrière L., Deutsch A. and Koeberl C. 2014. Impact controversies: Impact recognition criteria and related issues. *Meteoritics & Planetary Science* 49(5): 723-731. https://doi.org/10.1111/maps.12284

Roest W.R., Verhoef, J. and Pilkington M. 1992. Magnetic interpretation using the 3-D analytic signal. *Geophysics*, 57(1):116-125. https://doi.org/10.1190/1.1443174

Sanford B.V. and Baer A.J. 1981. Geological Map of Southern Ontario, GEOLOGICAL ATLAS 1:1,000,000 (R. J. W. Douglas, coordinator), Geological Survey of Canada, map 1335A, sheet 30S.

Satterly J. 1970. Aeromagnetic maps of carbonatite-alkalic complexes in Ontario: Ontario Department of Mines and Northern Affairs, Preliminary map no. P452.

Sookhan S., Eyles N., Arbelaez-Moreno L. 2018. Converging ice streams: a new paradigm for reconstructions of the Laurentide Ice Sheet in southern Ontario and deposition of the Oak Ridges Moraine. *Canadian Journal of Earth Sciences*, 55(4): 373-396. https://doi.org/10.1139/cjes-2017-0180

Stewart S.A. 2003. How will we recognize buried impact craters in terrestrial sedimentary basins? *Geology* 31: 929-32, 31. https://doi.org/10.1130/G19853.1

Suttak P.A. 2013. High-resolution lake-based magnetic mapping and modeling of basement structures, with examples from Küçükçekmece Lagoon, Turkey and Charity Shoal, Lake Ontario. Unpublished MSc thesis, School of Geography and Earth Sciences, McMaster University, Hamilton, Ontario. 113 pp. http://hdl.handle.net/11375/13532

Symons D. T. A. and Chiasson A. D. 1991. Paleomagnetism of the Callander Complex and the Cambrian apparent polar wander path for North America. *Canadian Journal of Earth Sciences* 28:355–363 https://doi.org/10.1139/e91-032

Talwani M. and Heirtzler J. R. 1964. Computation of magnetic anomalies caused by two dimensional bodies of arbitrary shape. In G. A. Parks (Ed.), Computers in the Mineral Industries, Part 1, Stanford Univ. Publ., *Geological Sciences*, 9: 464-480.

Talwani M. 1965. Computation with the help of a digital computer of magnetic anomalies caused by bodies of arbitrary shape. *Geophysics*, 30(5):797-817.

Thomas M. D., Ford K. L. and Keating P. 2016. Exploration geophysics for intrusion-hosted rare metals. *Geophysical Prospecting*, 64(5): 1275-1304. https://doi.org/10.1111/1365-2478.12352

Tsikalas F. and Eldholm O. 2018. Malvinas (Falkland) Plateau Structure versus Mjolnir crater: geophysical workflow template for proposed marine impact structures. *Meteoritics & Planetary Sciences* 54(3): 544-557 https://doi.org/10.1111/maps.13227

Ugalde H., Danuor S. K. and Milkereit B. 2007a. Integrated 3-D model from gravity and petrophysical data at the Bosumtwi impact structure, Ghana. *Meteoritics & Planetary Science*, 42(4-5): 859-866. https://doi.org/10.1111/j.1945-5100.2007.tb01081.x

Ugalde H., Valenzuela M., Milkereit B. 2007b. An integrated geophysical and geological study of the Monturaqui impact crater, Chile. *Meteoritics & Planetary Science*, 42(12):2153-2163. https://doi.org/10.1111/j.1945-5100.2007.tb01015.x

Urbini S., Nicolosi I., Zeoli, A., El Khrepy S., Lethy A., Hafez M., El Gabr M., El Barkooky A., Barakat A., Gomaa M. and Radwan A.M 2012. Geological and geophysical investigation of Kamil crater, Egypt. *Meteoritics & Planetary Science*, 47(11): 1842-1868. https://doi.org/10.1111/maps.12023

Van Fossen M.C. and Kent D.V. 1993. Palaeomagnetic Study of 143 Ma Kimberlite Dikes In Central New York State, *Geophysical Journal International*, 113(1): 175–185. https://doi.org/10.1111/j.1365-246X.1993.tb02538.x

Van Hoesel A., Hoek W.Z., Pennock G.M. and Drury M.R. 2014. The Younger Dryas impact hypothesis: a critical review. *Quaternary Science Reviews*, 83: 95-114. https://doi.org/10.1016/j.quascirev.2013.10.033

Virden W.T., Warren J.S., Holcombe T.L., Reid D.F., and Berggren T.L. 1999. Bathymetry of Lake Ontario. National Geophysical Data Center, World Data Center A for Marine Geology & Geophysics, Boulder CO. Rept. MGG–14.

Waddington E. D. and Dence M. R. 1979. Skeleton Lake, Ontario - evidence for a Paleozoic impact crater. *Canadian Journal of Earth Sciences*, 16(2): 256–263. https://doi.org/10.1139/e79-025

Wallach J.L. 2002. The presence, characteristics, and earthquake implications of the St. Lawrence fault zone within and near Lake Ontario (Canada–USA). *Tectonophysics*, 353(1-4):45-74. https://doi.org/10.1016/S0040-1951(02)00285-8

Wellmann F. and Caumon G. 2018. 3-D structural geological models: concepts, methods, and uncertainties. *Advances in Geophysics*, 59: 1-121. https://doi.org/10.1016/bs.agph.2018.09.001

Won I. J. and Bevis M. 1987. Computing the gravitational and magnetic anomalies due to a polygon: Algorithms and Fortran subroutines. *Geophysics* 52: 232-238 https://doi.org/10.1190/1.1442298

Wu Y., Sharma M., Lecompte M.A., Demitroff M.N. and Landis J.D. 2013. Origin and provenance of spherules and magnetic grains at the Younger-Dryas boundary. *Proceedings of the National Academy of Science* 110(38): E3557-E3566 https://doi.org/10.1073/pnas.1304059110

Chapter 4: 3-D geophysical modelling of the Skeleton Lake structure: A possible (Late Proterozoic-Early Paleozoic?) transitional impact crater in Muskoka (Ontario, Canada)

Abstract

Skeleton Lake is a suspected 4.0 km diameter, Paleozoic-age impact structure in central Ontario (Muskoka) Canada. The lake has a roughly circular shoreline that cuts across the regional topographic trends and a deep central basin (>60 m). Surveys in the 1970's identified a central gravity low (3.3 +/- 0.7 mGal) and autochthonous breccias within Grenville Province Mesoproterozoic (~1.46 Ga) basement rocks, but no evidence for shock polymorphs or other indicators of an impact origin. We conducted high-resolution, total magnetic intensity (TMI) and bathymetry surveys (~140 line-km) to investigate the lakebed morphology and subsurface structure and 3-D magnetic models were constructed to evaluate possible origins as an impact crater or volcanic intrusive plug. Model parameters were estimated using magnetic susceptibility measurements (n > 400) and paleomagnetic data from previous works.

The digital bathymetric model (DBM) revealed a roughly circular lake basin (maximum water depth 69 m) and arcuate (Paleozoic?) bedrock ridges that rise >30 m above the southwestern lakebed. TMI surveys recorded a >700 nT magnetic low, which truncates the northwest-southeast regional magnetic trends in the Mesoproterozoic basement. The anomaly has a distinct dipole component, indicating a component of remanence magnetization in basement rocks. Low-amplitude, northwest-trending magnetic lineaments below the basin centre delineate basement shear zones (amphibolite gneiss) that outcrop on the lake shoreline. The through-going basement magnetic lineaments and lack of evidence for thermal alteration (e.g., dikes, fenitization) in Mesoproterozoic rocks indicate a volcanic origin is unlikely. The magnetic anomaly can be reproduced by 1.2 km diameter volcanic plug with an Early Cambrian remanence (D = 82.2°, I = 82.7°) but is at odds with the Bouguer gravity anomaly (~ -3 mGal). Forward modelling of a crater-form basin with induction and remanence magnetization yielded an

estimated structure depth of ~1200 m and reveals a complex basement topography with no apparent rim structure. Elevated ‘pinnacles’ in the basement surface may indicate eroded remnants of a central uplift or highly dissected basement topography. Magnetic and gravity data are most compatible with an origin as an impact crater, which has excavated the Mesoproterozoic basement to ~1200 m depth. The estimated structure diameter (> 4.2 km) and complex basement topography suggest that Skeleton Lake is likely a heavily modified transitional crater, similar to the Gow (Saskatchewan, Canada) and Kärdla (Estonia) impact structures. The geomagnetic poles reconstructed from the tilt-corrected NRM vectors are consistent with previous paleomagnetic studies and plot on the Late Proterozoic apparent polar wander path (~ 980 Ma). The new geophysical data provide new details of the subsurface structure of Skeleton Lake and support an origin as a probable Late Proterozoic to early Paleozoic impact crater.

Keywords: Skeleton Lake, suspected impact crater, geophysical survey, 3-D geophysical modelling, magnetic lineaments, crater subsurface geometry, remanence.

Highlights

- Suspected Late Proterozoic-Early Paleozoic, >4.2 km diameter impact crater with a -3 mGal magnetic anomaly
- 3-D magnetic modelling to estimate depth, subsurface structure
- High-relief, complex basement surface with no apparent rim structure
- Heavily modified and deeply buried (> 1200 m) crater-form basin
- Probable Late Proterozoic-Early Paleozoic transitional impact crater

4.1 Introduction

Skeleton Lake is a proposed 4.0 km diameter Paleozoic-age impact crater in south-central Ontario, Canada (Fig. 4.1A) (Waddington and Dence, 1979). The structure was first identified in the 1960's in aerial photos and investigated with geophysical and petrographic studies in the mid-1970's (Dence et al., 1968; Waddington and Dence, 1975, 1979; Clark, 1982). Gravity surveys revealed a central gravity anomaly (-3.3 ± 0.7 mGal) and a corresponding magnetic anomaly low (~300 nT) in aeromagnetic data (Waddington and Dence, 1979; Clark, 1982). Autochthonous, monomict breccias were identified at two localities (Opal Island, Tomelin Bluffs) on the northwest shore (Fig. 4.1B). The breccias consisted of angular fragments of Mesoproterozoic gneiss within a fine-grained chloritized matrix but lacked diagnostic petrographic evidence of shock metamorphism (Waddington and Dence, 1979). Waddington and Dence (1979) concluded that Skeleton Lake was a possible eroded remnant of a Paleozoic-age impact crater buried below Ordovician-age sediments. No further work has been conducted at Skeleton Lake since these initial investigations.

The geophysical characteristics of Skeleton Lake are consistent with an impact origin (Waddington and Dence, 1979; Pilkington and Grieve, 1992) but the structure cannot be conclusively identified as an impact crater without evidence for shock effects in target rocks (e.g., planar deformation features, shatter cones, impact melt bearing breccias, or other diagnostic features) (French and Koeberl, 2010). For many suspected impact structures such as Skeleton Lake, conclusive geological evidence of an impact origin may be difficult to obtain due to post-impact erosion and burial of the crater and target rocks (Kenkmann, 2021). Exploration drilling and coring can provide positive identification of an impact origin (e.g., Beals, 1960) but may not be feasible for economic or other reasons (e.g., restricted site access, environmental considerations). Geophysical surveys and numerical modelling can assist in identifying the remnants of heavily-eroded impact craters (Pilkington and Grieve, 1992; Kenkmann, 2021) and can provide

geophysical constraints for evaluating suspected impact structures (Tsikalas and Eldholm, 2018).

In this study, we conducted detailed, lake-based geophysical surveys and 3-D potential field modelling to investigate the subsurface structure and origin of Skeleton Lake. We evaluated possible origins as an impact crater (Waddington and Dence, 1979; Clark, 1982) and a volcanic plug intruded into Mesoproterozoic basement rocks (e.g., Currie and Shafiqullah, 1967). A volcanic origin was investigated as Skeleton Lake lies 125 km south of the Ottawa-Bonnechère Graben (OBG), which was associated with several phases of post-Grenville (< 1.1 Ga) rift volcanism (Currie and Ferguson, 1971; Hogarth et al., 1988, Gittens and Lumbers, 1972; Symons and Chiasson, 1991). OBG rift volcanics include the Callander Bay alkaline complex in Lake Nipissing and the Allan Lake carbonatite (Fig. 4.1A) (Symons and Chiasson, 1991; Rimando and Benn, 2005). We employed the general approach outlined by Tsikalas and Eldholm (2018), which advocates the integration of a broad range of geophysical survey data (bathymetry, magnetic and gravity surveys) in the subsurface modelling and analysis of suspected marine impact structures. The geophysical modelling methods demonstrated in this paper can be applied more broadly in the investigation of confirmed and suspected impact craters and are highly relevant for ancient Precambrian impact craters, where erosion and subsequent deep burial have significantly modified the original crater morphology and surface expression.

4.2 Physical and Geologic Setting

The Skeleton Lake structure (SLS) is located 17 km west of Huntsville, in the Muskoka district of south-central Ontario, Canada (Fig 4.1A). The structure was first investigated in 1968 by the Dominion Observatory (Ottawa) during a regional search for impact craters (Dence et al., 1968). In contrast with other shallow (<30 m), linear lakes in the region (e.g., Barnes Lake; Fig. 4.1B) Skeleton Lake has a deep central basin (> 60 m)

and a roughly circular shoreline that cuts across the regional topographic relief (Fig. 4.1B). (Waddington and Dence, 1979).

The study area (16-km^2) is located within the Central Gneiss Belt (CGB) of the Grenville structural province of south-central Ontario (Fig. 4.1B, 4.2) (Hewitt, 1967; Easton, 1992). The bedrock in the region consists of Mesoproterozoic (<1.46 Ga) crystalline rocks, including gneiss, migmatite and plutonic intrusive rocks (< 1.1 Ga). Skeleton Lake sits on a major lithotectonic boundary and thrust fault separating the Seguin and Rosseau domains (Fig. 4.2) (Schwerdtner et al., 1987; Dickin et al., 2017).

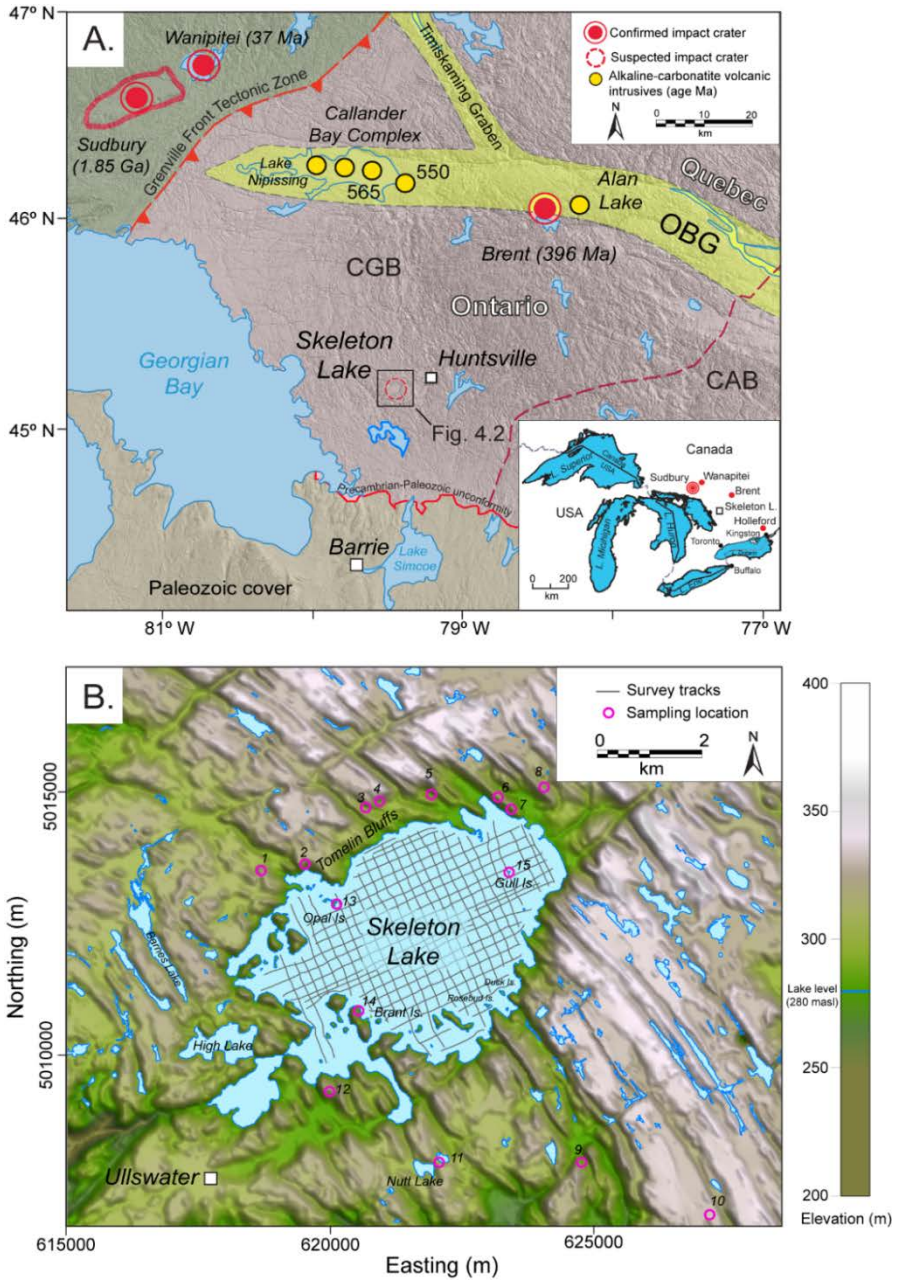

Figure 4.1. A. Map showing location of Skeleton Lake structure (SLS) in the Central Gneiss Belt (CGB) of the Grenville Province. The structure lies 125 km south of the Ottawa- Bonnechère Graben (OBG) and Nipissing alkaline volcanic complex. CAB = Composite Arc Belt. B. Digital elevation model of Skeleton Lake with geophysical survey track lines (141-line km) and locations of outcrop magnetic susceptibility measurements. The lake basin truncates the northwest-southeast ridge-and-swale topography defined by the strike of Mesoproterozoic units.

The local basement rocks include three main lithologies: 1) grey orthogneiss (>1.46 Ga), 2) monzonite and quartzo-feldspathic gneiss (1.46-1.43 Ga) and 3) monzonitic and amphibolite gneiss (1.46-1.43 Ga) (Lumbers and Vertolli, 2000). The Mesoproterozoic units strike northwest-southeast and dip northeastward (~25-75°) forming part of the southern limb of the Seguin synform (Fig. 4.2) (Hewitt, 1967; Schwerdtner et al., 2016). Mesoproterozoic basement is overlain by thin Quaternary glacial sediments (Waddington and Dence, 1979; Clark, 1982).

Monomict, autochthonous breccias are exposed on the northwestern shore of the lake at Tomelin Bluffs and on Opal Island (Waddington and Dence, 1979; Lumbers and Vertolli, 2000) (Fig. 4.2). The breccias consists of angular, unaltered gneissic and amphibolite clasts up to 0.05 m in diameter within a finer chloritized matrix. Petrographic studies conducted by Waddington and Dence (1979) found no evidence for shock metamorphic effects in breccias.

Skeleton Lake lies about 125 km south of the Ottawa-Bonnechère graben (OBG; Fig. 4.1A), a Neoproterozoic (Iapetan) rift, which extends ~700 km eastward of Ottawa to Lake Nipissing (Fig. 4.1A) (Kumarapeli and Saull, 1966; Rimando and Benn, 2005). The rift is associated with extensive Grenville dike swarms and alkalic-carbonatitic volcanism, including the Callander Bay (Symons and Chiasson, 1991), Manitou Island, and Seabrook Lake intrusive complexes (Cullers and Medaris, 1977; Kamo et al., 1995) (Fig. 4.1A). Callander Bay (Fig.4. 1A) is a circular (~3 km diameter) volcanic pipe that intrudes the Mesoproterozoic basement rocks of the CGB (Cullers and Medaris, 1977; Symons and Chiasson, 1991). The structure is a zoned intrusive, consisting of layered concentric sheets of nepheline syenite and carbonatites (Currie and Ferguson, 1971) intruded into Grenville gneiss during the early Cambrian (575 ±5 <Ma) and is associated with widespread development of radial lamprophyre and carbonatite dikes and fenitization of host rocks (Symons and Chiasson, 1991; Elliot et al., 2018).

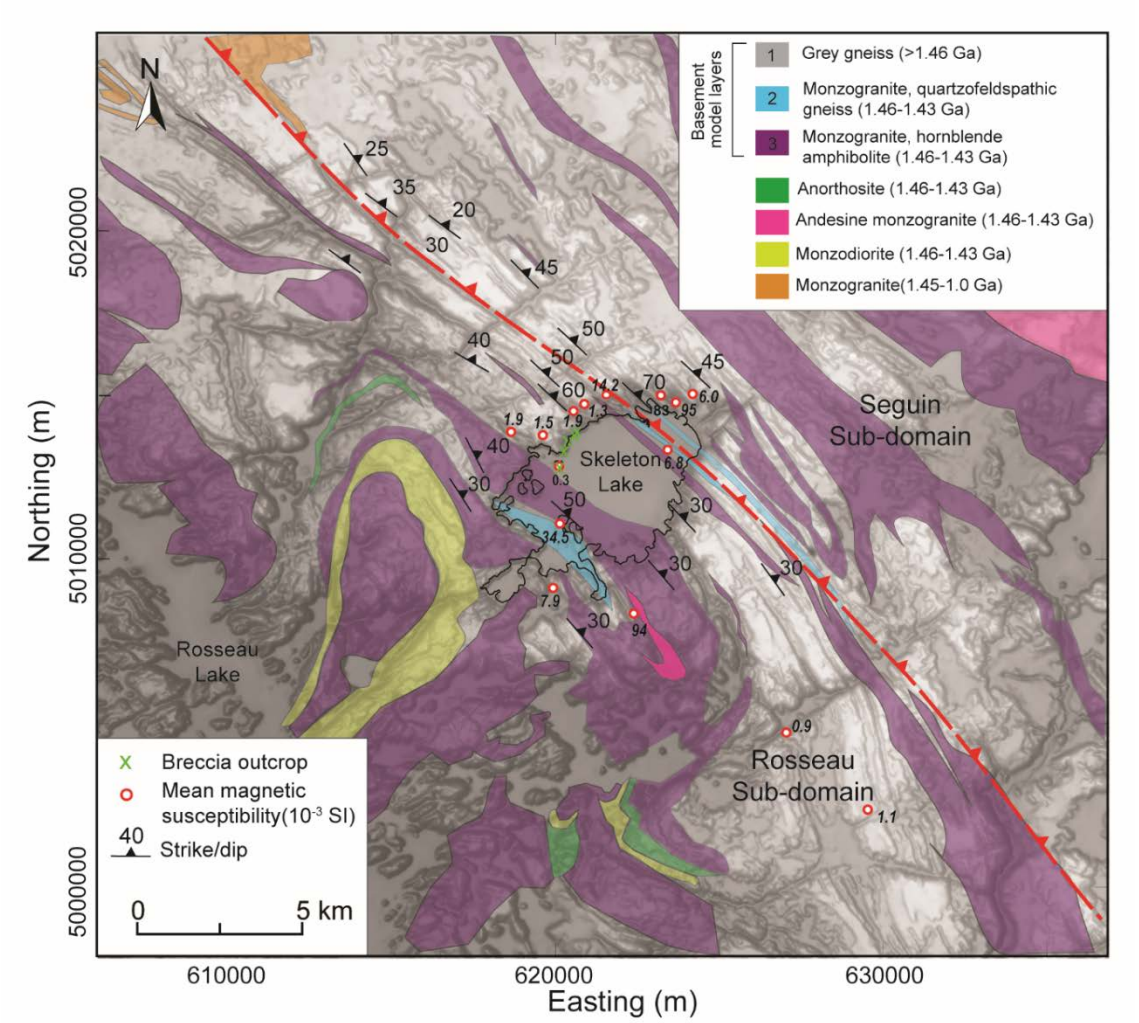

Figure 4.2. Precambrian geology of study area (adapted from Lumbers and Vertolli, 2000) showing locations of breccia outcrops (Opal Island, Tomelin Bluffs) and mean magnetic susceptibility values (10^{-3} SI). Skeleton Lake lies on a major lithotectonic boundary separating the Rosseau and Seguin sub-domains of the Mesoproterozoic (ca. 1.5 –1.0 Ga) Muskoka Domain (Dickin et al., 2017). The boundary is defined by a steeply-dipping, northeastward-dipping shear zone (red dashed line) (Schwerdtner et al., 1987).

4.2.1 Previous work

Gravity surveys (total 73 stations) were conducted on the lake ice and in an area extending to 10 km beyond the shoreline in 1970-71 (Waddington and Dence, 1979). The surveys recorded a circular Bouguer gravity anomaly of -3.3 +/- 0.7 mGal over the central lake basin. A forward gravity model for a parabolic impact basin using the method of Talwani and Ewing (1960) produced a depth to crater base of 1200 m and a ~4 km diameter structure (Waddington and Dence, 1979). Assumed fracturing and brecciation of the country rock was interpreted to have lowered the density at the edges of the structure giving a possible diameter as small as 3.5 km. The estimated diameter places the breccia outcrops on Opal Island and Tomelin Bluffs (Fig. 4.2) near the northwest limit of structure rim. Clark (1982) modelled Skeleton Lake as a parabolic impact crater using four marine magnetic profiles and aeromagnetic data. His modelling suggested an ~3.5 km diameter structure with a depth to basement of ~750 m.

4.3. Methods

4.3.1 Bathymetry and magnetic surveys

Marine geophysical surveys (~140 line-km; Fig. 4.1B) were conducted across the main lake basin (6 km^2) using an Overhauser magnetometer (Marine Magnetics SeaSPY2; resolution 0.01 nT/√Hz) and differential GPS (D-GPS) with sub-meter positioning. The magnetometer was towed 30 m behind an inflatable boat and cycled at 2 Hz, providing ~1 m inline sample spacing at an average boat speed of 10 kmh^{-1}. The survey was collected along a grid pattern of northeast-southwest (~70-250°) lines across strike and orthogonal tie lines (~157°-337°) at 200 m separation (Fig. 4.1B). The diurnal magnetic variation was recorded with a second basestation magnetometer (GEM Systems GSM-19) located onshore.

Processing of magnetic data included diurnal corrections, tie line levelling and corrections for changes in TMI due to water depth (Cordell, 1985; Paterson et al., 1990). The TMI grid was interpolated using minimum curvature with a 40 m grid cell spacing. A magnetic residual map was produced by subtraction of the upward continued grid (100 m) from the TMI. In a final step, the 1st vertical and horizontal magnetic derivatives were calculated from the fully levelled TMI grid to enhance imaging of linear magnetic trends. Maps of the regional aeromagnetic residual magnetic field intensity and Bouguer gravity were produced using available datasets (OGS, 1999; CGS, 2021) for comparison with the lake-based, high-resolution magnetic data. The aeromagnetic data were collected at nominal line spacing of 800 m and 300 m flight elevation. Aeromagnetic and gravity point data were gridded using minimum curvature with 200 m and 500 m grid cell spacing respectively (Briggs, 1974).

Bathymetry profiles were recorded with a 200-kHz sonar transducer mounted on the magnetometer. Bathymetry data were combined with available onshore digital elevation data (3 m resolution; LIO, 2019) and gridded using a minimum curvature and 20 m grid cell spacing (Briggs, 1974) to create a digital bathymetric model (DBM) (Sonnenburg et al., 2012).

To provide constraints for modelling and interpretation of magnetic data, the volume magnetic susceptibilities (κ) of Mesoproterozoic basement rocks and the breccia were measured at 12 outcrop locations. Outcrop measurements were made using a hand-held magnetic susceptibility probe (MPP probe, GDD Instruments) and 10 block samples from Opal, Brant, and Gull islands measured using a Bartington MS2-E probe (Fig. 4.1B). The remanence magnetic properties (NRM, vector direction) for the Mesoproterozoic rocks from a previous paleomagnetic study (Alvarez and Dunlop, 1998) were used to initialize the models and optimized by inversion (Table 4.2, 4.3; section 4.3.2) (Pratt et al., 2020).

4.3.2 3-D modelling

3-D geophysical models were constructed in Modelvision 17 (Tensor Geophysics Pty.) using profile modelling (Pratt et al., 2020). In this approach, the magnetic response of 2-D polygonal source bodies is calculated across a series of parallel (across-strike) profiles using Talwani's method (Talwani and Heirtzler, 1964; Cady, 1980) to produce a fully 3-dimensional model (Oldenburg and Pratt, 2007). The model allows for inversion and optimization of full range of rock magnetic properties (κ, NRM, Q; Table 4.2,4.3), model layer thickness and geometry.

3-D magnetic models were constructed for three scenarios: 1) an impact structure in Mesoproterozoic basement with induction magnetization only, 2) an impact structure with induction and remanent magnetization, and 3) a volcanic plug with both induction and remanent magnetization. The model layer strike and dip (~25-60°) were assigned using bedding orientations measured in the field and from regional mapping (Fig. 4.2) (Lumbers and Vertolli, 2000). The κ values were initially assigned using field measurements (Table 4.1) and optimized by model inversion (Pratt et al., 2014) (Table 4.2). Remanence parameters (J_r, I, D, Q) were estimated using paleomagnetic data for the Muskoka Domain (Table 4.2) (Alvarez and Dunlop, 1998). The model goodness-of-fit was assessed using the root-mean-square of the model residuals and by comparison of the chi-squared statistic (Pratt D.A. 2020; Pearson, 1900).

The basement geology in all models was replicated using three layers representing the primary Mesoproterozoic basement rock types: Layer 1: grey orthogneiss (κ = 0.04 SI), Layer 2: quartzo-feldspathic gneiss (κ =0.01-0.02 SI), and Layer 3: amphibolite gneiss (κ = 0.09 SI) (Fig. 4.2). The model layer magnetic susceptibilities were set initially using field measurements and optimized in the model using an inversion routine (Table 4.1).

Outcrop Location	Lithology	Mean Magnetic Susceptibility (10^{-3} SI)	n	St. Dev.	Model Layer
1	GO	1.9	39	2.0	1
2	GO	1.5	15	0.7	1
3	GO	1.9	56	1.4	1
4	GO	1.3	18	1.2	1
5	GO	14.2	94	15.2	1
6	AG	83.1	53	42.3	3
7	AG	94.8	40	44.9	3
8	GO	6.0	21	5.9	1
9	GO	0.9	38	0.5	1
10	GO	1.1	37	0.7	1
11	AG	93.8	64	100.4	3
12	GO	7.9	17	3.3	1
13. Opal Island*	B	0.30	20	0.3	n/a
14. Brant Is.*	AG	34.5	20	21.2	3
15. Gull Is.*	QFG	6.8	20	6.0	2

Table 4.1. Volume magnetic susceptibility (κ) measured on outcrops and hand samples (* = laboratory measurements on block samples). Locations shown in Fig. 4.1B. GO = grey orthogneiss (layer 1), QFG = quartzo-feldspathic gneiss (layer 2), AG = amphibolite gneiss (layer 3), B = monomict breccia. Model layer assignment indicated in last column.

Model	Modelled Layers	Magnetic Susceptibility, κ (SI)	Remanence Direction (Inversion)	NRM intensity, J_r (A/m)	Q
Impact crater (induction only)	1	0.04	n/a	n/a	n/a
	2	0.01 to 0.02	n/a	n/a	n/a
	3	0.09	n/a	n/a	n/a
	Breccia	0.0003	n/a	n/a	n/a
	Infill sediments	0.0001-0.0003	n/a	n/a	n/a
Impact crater (induction + remanence)	1	.04	Inc. -60 Dec. 202	1.0	0.58
	2	0.01 to 0.02	Inc. -69 Dec. 48*	0.12	0.14
	3	0.09	Inc. -69 Dec. 48	3.00	0.78
	Breccia	0.0003	n/a	n/a	n/a
	Infill sediments	0.0001-0.0003	n/a	n/a	n/a
Slab Model (SM)	3	0.09 (background 0.04)	Inc. -67 Dec. 50	4.00	1.1
Slab Model (SMR)	3	0.09 (background 0.04)	Inc. -73 Dec. 45	4.50	1.2
Volcanic intrusive (induction + remanence)	Volcanic Intrusive	0.01 to 0.02	Inc. 82.7 Dec. 82.2	1.00	2.3
	1	0.04	Inc. -69 Dec. 202	1.0	0.14
	2	0.01-0.02	Inc. -69 Dec. 48	0.12	0.78
	3	.09	Inc. -69 Dec. 48	3.0	0.58
	Infill sediments	0.0001-0.0003	n/a	n/a	n/a

Table 4.2. Summary of magnetic parameters employed in three model scenarios. Model magnetic susceptibility (κ SI) values obtained by field measurements (Table 4.1) and optimized through model inversion. NRM intensity (J_r) and direction for basement (layers 1-3) were initialized using regional NRM paleomagnetic vector for Muskoka Domain (Alvarez and Dunlop, 1998) and optimized in model. Remanence for volcanic intrusive set using NRM from Callander Bay Complex (Symons and Chiasson, 1991). Paleozoic and Quaternary infill sediment magnetic susceptibility estimated from O'Dowd and Eaton (2005). *Model layer 2 remanence direction vector set to inverted values from layer 3.

The fully corrected TMI grid was imported to ModelVision 17, and the regional field estimated by model inversion. In each model, 20 across-strike (SW-NE) profiles were constructed over a 9 km^2 model domain with 200 m profile widths. A central reference profile was constructed first, and the layer geometries adjusted manually to achieve an initial fit with the TMI. The layer thicknesses and κ values were then optimized using linear inversion (Pratt et al., 2020).

For the induction-remanence models, the resultant magnetization vector and remanence (NRM) directions were estimated using parametric modelling in Modelvision (Pratt et al., 2020). Three methods were used to determine remanence parameters: Helbig's method, direct remanence inversion of model layers, and remanence inversion on a simple dipping slab model with an orientation and thickness based on the local geology (Pratt et al., 2014; Clark, 2014). For the slab model, remanence estimation was conducted on a large (>200 nT) dipole anomaly at the contact between the layer 3 amphibolite and layer 1 orthogneiss. The modelled NRM vectors were then corrected for bedding tilt (~50° NE) (Morris et al., 2007) and the paleopole directions calculated for comparison with the Proterozoic apparent polar wander paths (APWP's) for regional Grenville rocks (Hyodo and Dunlop, 1993; Alvarez and Dunlop, 1998; Brown and McEnroe, 2012). The virtual geomagnetic poles (VGP) were then calculated to provide an estimate of the timing of NRM acquisition and subsequent tilting of Mesoproterozoic strata (Morris et al., 2007).

For the impact crater models, the breccia and overlying Paleozoic and Quaternary crater infill were modelled as a single layer with a uniformly low magnetic susceptibility determined from the mean of breccia samples (κ = 0.0003 SI) (Table 4.1). Experimentation with a range of κ values for Quaternary and Paleozoic sediments showed that the models were relatively insensitive to changes in magnetic contrast in the upper 100-400 m of the model. The strong magnetic susceptibility contrast between the basement and overlying breccia-infill sediments (κ = 0.007-0.090 SI; Table 4.2) was the main control on the basement height and thus the crater depth estimates.

The volcanic pipe model simulated an elliptical (plan view) plug with a homogeneous remanence and magnetic susceptibility. Remanence values (NRM vector, J_r) were set initially using values from the Callander Bay complex (Symons and Chaisson, 1991) and the regional Proterozoic basement (Alvarez and Dunlop, 1998; Table 4.2). Regionally, alkaline-carbonatite complexes show significant variation in magnetic properties (Thomas et al., 2016). To address this, the model κ values were determined by inversion. An induction-only model was also constructed but a reasonable fit (< 50 nT RMS) with the observed TMI could not be obtained. The infill above the intrusive body was assumed to be low susceptibility (κ = 0.0001 SI), Paleozoic and Quaternary sediments.

A single forward 2-D gravity model was calculated along a central southwest-northeast line across the lake basin for comparison with the previous 2-D gravity model of Waddington and Dence (1979). The gravity profile used the basement layer geometry obtained in the impact crater model (induction/remanence) and the layer densities assigned were from Waddington and Dence (1979).

4.4. Results

4.4.1 Bathymetry

The DBM shows a roughly circular lake basin with a maximum water depth of 69 m (Fig. 4.3). The lake basin clearly truncates the northwest-southeast trending ridge-and-swale topographic relief (Fig. 4.1B). The north-northeastern portion of the shoreline defines a semi-circular arc defined by the Tomelin bluffs, and in the south, the shoreline forms a number of northwest-oriented embayments between topographic ridges. The central lake basin is relatively low relief except for three arcuate ridges in the southwest (Fig. 4.3A). The ridges are up to 1400 m in length and rise 20-30 m above the surrounding lakebed (Fig. 4.3B). The ridges are steep sided with side slopes of up 10°, which suggests that they are likely bedrock and not unconsolidated Quaternary sediment or lake deposits. Paleozoic limestone clasts have been identified in Quaternary drift

deposits to the south of Skeleton Lake (Waddington and Dence, 1979). Clark (1982) described Ordovician limestone pebbles in glaciofluvial gravels in the Nutt Lake area (Fig. 4.1B), 1.5 km south of Skeleton Lake. There are no known Paleozoic outliers to the north of Skeleton Lake, which indicates the possible outlier within the lake basin (Clark, 1982). Steep sided pinnacles of Mesoproterozoic basement form small islands (e.g., Rosebud, Duck islands) along the south shore (Figs. 4.1B, 4.3A).

On the western edge of the main basin, a 15-20 m deep channel feature extends from Opal Island between the arcuate ridges and opens to the south into the deepest part of the lake. This channel likely records glacial or meltwater erosion of bedrock and overlying sediments and can be traced on land to the north and southeastward in the DEM (Fig. 4.1B). In the east, several small islands (e.g., Gull Island) mark the transition from a steep basin slope to a shallower shelf margin at the eastern end of the lake. The western edge of the basin is interrupted by a circular arc of islands (Fig. 4.3A) with shallower water depths (< 15 m, Fig 4.3B) to the west.

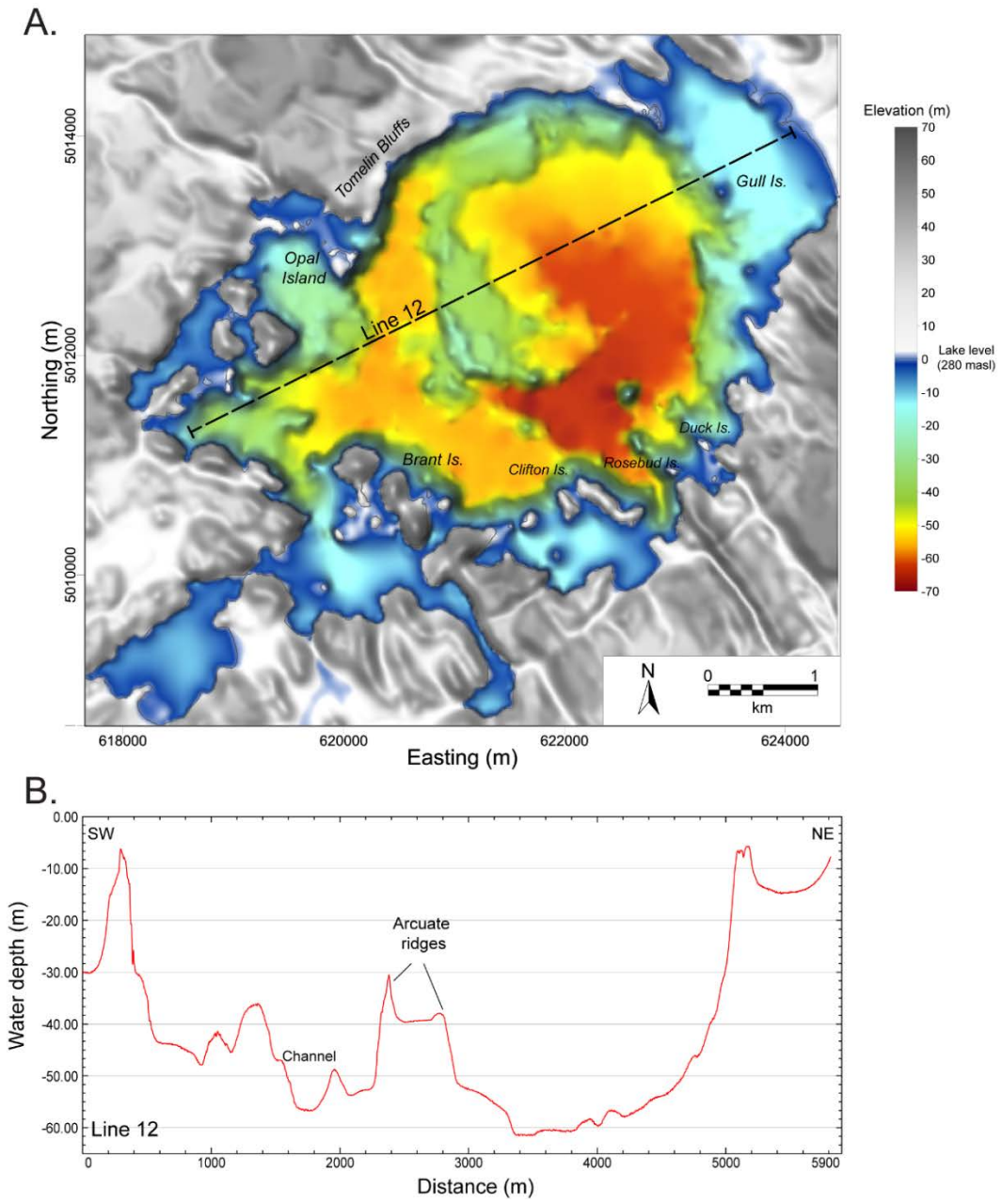

Figure 4.3. A. Digital bathymetric model (DBM) of Skeleton Lake (topographic data source: LIO, 2019). Elevations relative to sea level datum (lake level ~280 m asl). Arcuate ridges in southwestern basin indicate (Paleozoic-age?) bedrock scarps that are cut by a northwest-southeast trending channel feature. Red line (WD) indicates location of Waddington and Dence (1979) gravity profile shown in Fig. 4.12. B. Bathymetric profile (Line 12; Fig. 4.1B) showing 20-30 m high, arcuate bedrock ridges and channel feature in southwestern lake basin.

4.4.2 Magnetic surveys

In regional aeromagnetic maps, the SLS is indicated by a broad magnetic anomaly low that interrupts the northwest-southeast regional magnetic trends in Mesoproterozoic basement (Fig. 4.4A). In the high-resolution TMI and residual magnetic maps (Fig. 4.5 A, B), the central lake basin corresponds with a roughly circular, ~700 nT magnetic anomaly. Several northwest-trending, high amplitude linear magnetic anomalies mark the location of a broad shear zone at Rosseau-Seguin domain boundary (Figs 4.2., 4.5A, B). In the west, the TMI anomaly has a distinct dipole component (Fig. 4.5A) with a peak-trough pattern that indicates a north-easterly-directed resultant magnetic vector, which lies between the present earth field (PEF; 350° NW) and a more eastward-directed remanence vector (Schnetzler and Taylor, 1984; Dentith and Mudge, 2014). The dipole anomaly corresponds with the northwest-southeast contact between the more magnetized layer 3 amphibolite gneiss ($\kappa = 0.09$, $J_r = 3.0$ Am^{-1}) and layer 1 orthogneiss ($\kappa = 0.04$, $J_r = 1.0$ Am^{-1}). The dipole anomaly was employed to estimate the resultant and remanence vector directions in Modelvision (see section 4.4.3) (Pratt et al., 2014; Clark, 2014). Several previous studies have employed remote remanence estimation (RRE) in modelling complex geology, particularly for banded-iron formations (BIF's) (Guo et al.,2011; Foss and McKenzie 2011; Pratt et al. 2014; Clark, 2014).

The vertical magnetic gradient map (Fig. 4.5C) shows northwest-trending magnetic lineaments that extend from the southeastern lake shoreline below the central basin. The lineaments parallel the regional strike of the Mesoproterozoic bedding and are continuous with linear shear zones that have been mapped in the southeastern shore (Fig. 4.2). The lineaments are also present in the ASA (Fig. 4.5D). The lineaments are still visible, though attenuated in the lake basin (Fig. 4.5C). In the SW-NW profile in Fig. 4.6C, lineaments are indicated by low-amplitude attenuated signals at the northeastern side of the lake. The lineaments are interpreted as the attenuated signals of through-going basement shear zones that are present at depth below the lake basin (Fig. 4.5C, 4.6C,

4.6D). This finding is important, as it provides strong evidence for the continuity of Mesoproterozoic basement strata below the Skeleton Lake structure.

The profiles in Fig. 4.6 compare the lake basin bathymetry with the magnetic signal. The TMI drops steeply drop to the southwest, then increasing relatively smoothly to the northeast. The TMI changes correspond with the change in bathymetry in the northeast, but less so at the southwestern edge of the lake (Fig. 4.6A, B). The inflection line of the dipole (Fig. 4.5A) shows an orientation that is the same as the high susceptibility unit (Fig. 4.2

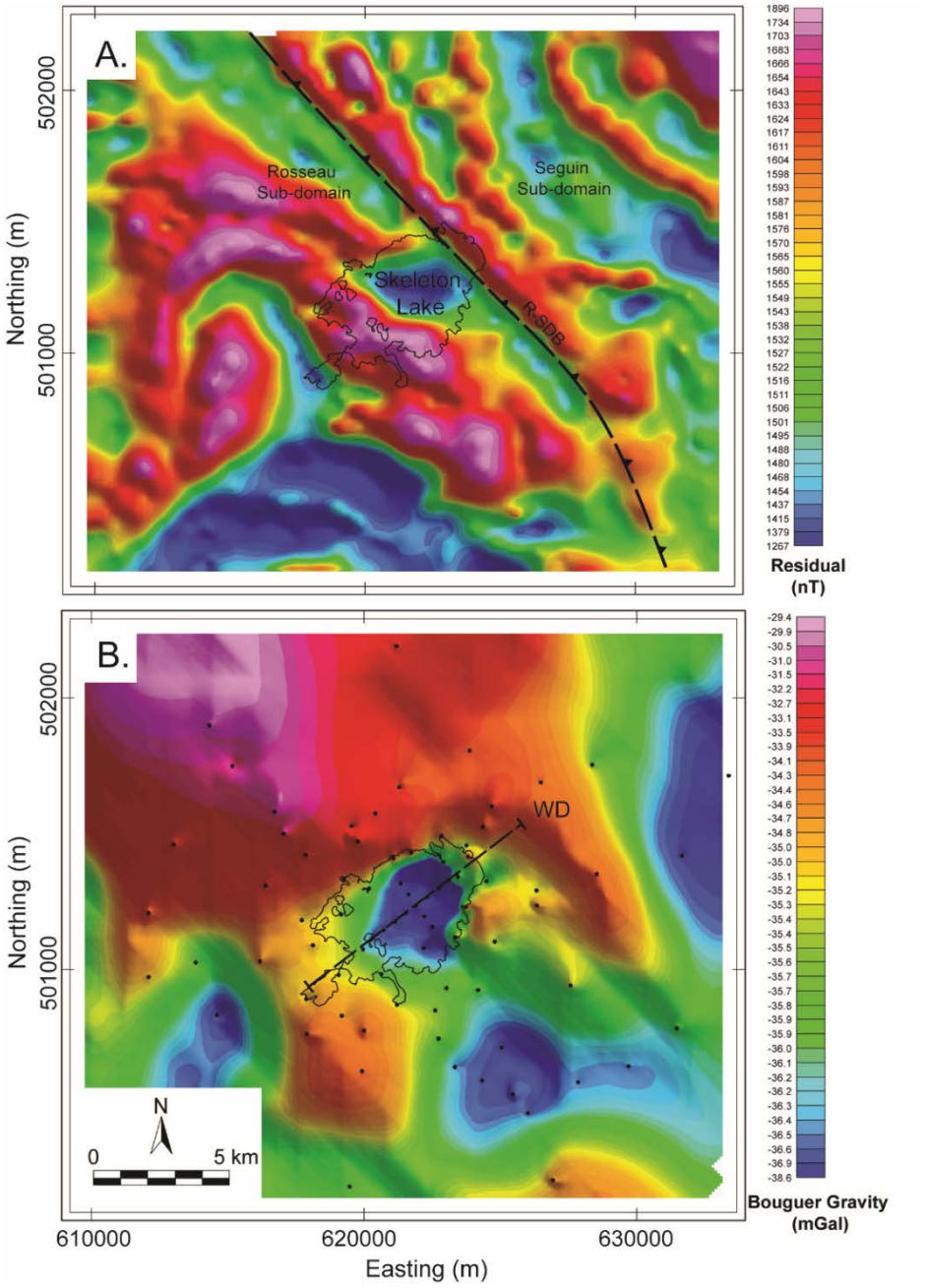

Figure 4.4. A. Residual aeromagnetic map showing dominant northwest-southeast trending shear zone at the Rosseau and Seguin sub-domains boundary (R-SDB) of the Muskoka Terrane (data source: OGS, 1999). Note interruption of NW-SE magnetic trend by >300 nT magnetic anomaly. B. Bouguer gravity map with gravity station locations and Bouguer profile (WD) shown in Figure 4.14 (data source: CGS, 2021).

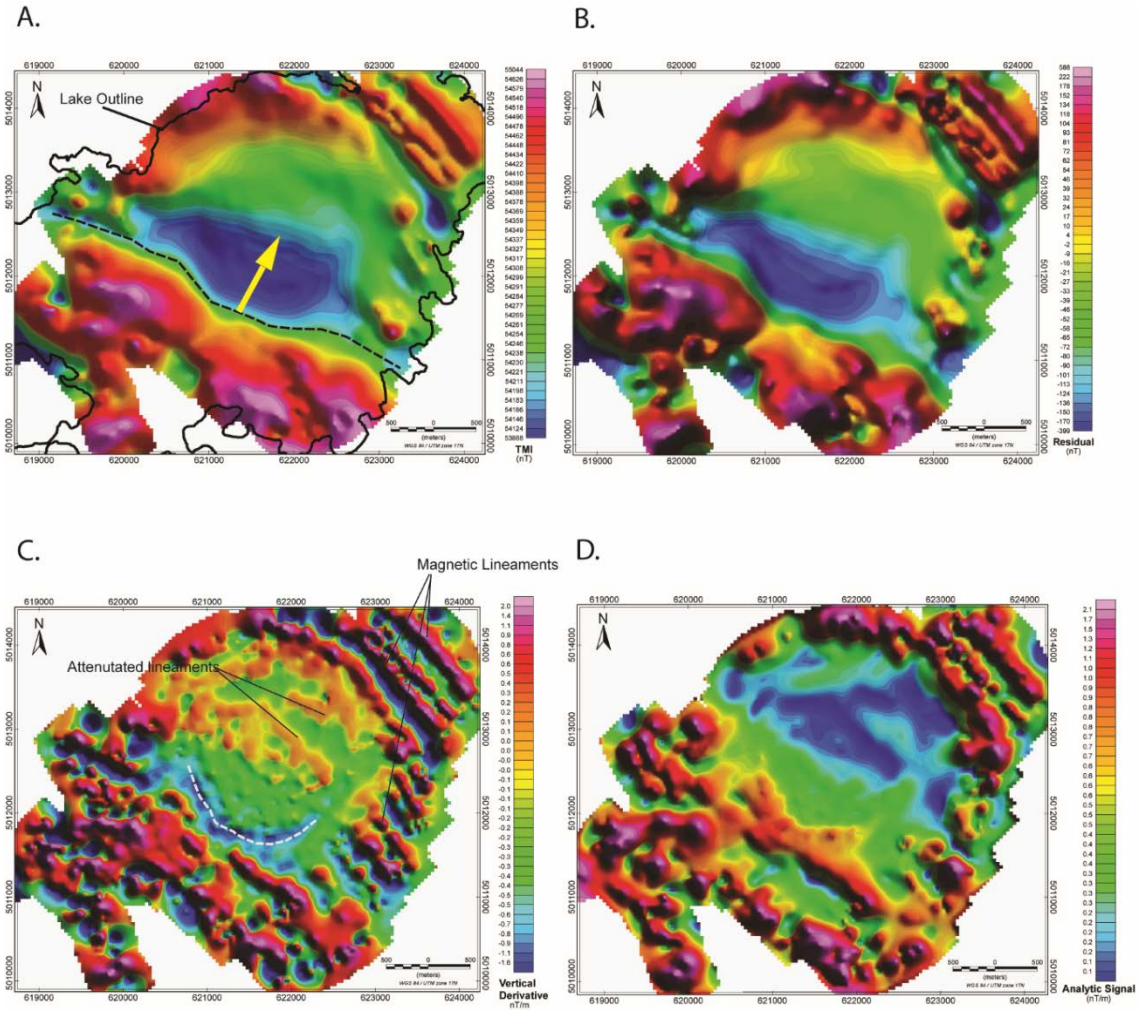

Figure 4.5. Magnetic survey results. A. Total magnetic intensity (TMI) map. Black dashed line indicates inflection point of southwest-northeast oriented magnetic dipole; yellow arrow shows estimated direction of dipole (resultant vector with D ~ 16°). B. Residual magnetic intensity. C. 1st vertical derivative. White dashed line shows arcuate anomaly low that corresponds with the arcuate bedrock ridge in Fig 4.3A. Magnetic lineaments appear as spikes in Figure 4.6 C D. Analytic signal amplitude (ASA).

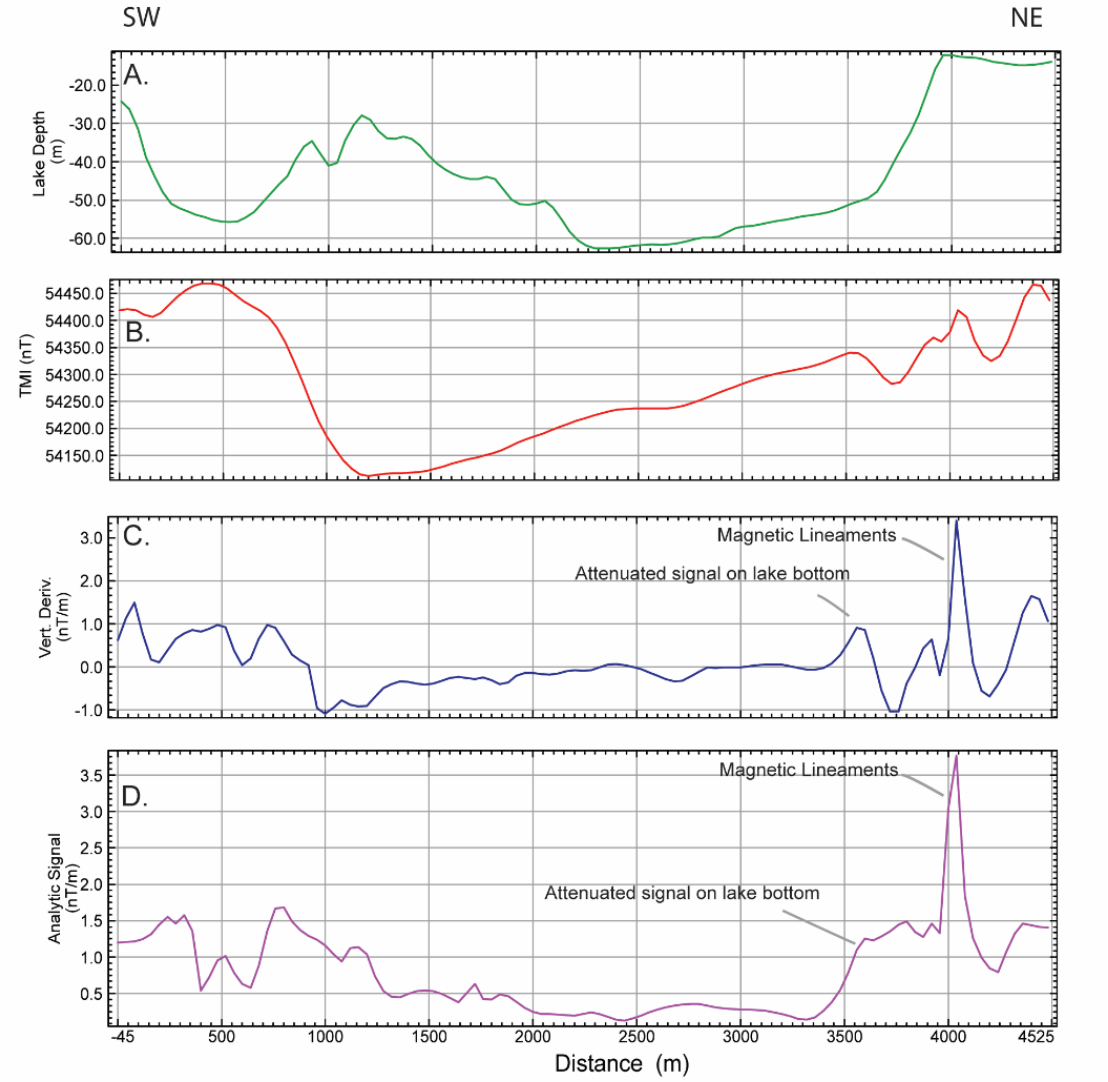

Figure 4.6. SW-NE profiles across basin centre. A. Water depth, B. Total magnetic intensity (TMI). C. 1st vertical derivative. D. Analytic signal amplitude (ASA). Note high-frequency anomalies at northeastern ends of profiles in C and D, indicating continuity of high magnetic susceptibility model layer 3 below the lake basin. See also magnetic lineaments in Fig. 4.5C, 4.6C.

4.4.3 Magnetic properties

Magnetic susceptibility measurements show a broad range of values (0.001 – 0.096 SI; Table 4.1) corresponding with lithological changes in Mesoproterozoic rocks (Fig. 4.1B, 4.2). The largest susceptibility values (κ ~0.09 SI) were associated with amphibolite gneiss (layer 3). The horneblende-rich layers within the gneiss have a relatively high content of magnetite relative to the other basement lithologies, which accounts for its high κ and NRM intensity (J_r = 3 Am^{-1}). Grey orthogneiss units (layer 1), which are the predominant lithology in the lake basin had highly variable κ values (~0.001 to 0.014 SI), while the monzonite and quartzo-feldspathic gneisses (layer 2) were of relatively low values (mean κ < 0.007 SI) (Table 4.1). The mean susceptibility values (Table 4.1) were employed in the assignment of the initial κ values of model layers and optimized using inversion. The optimized κ values for layers 2, 3 were consistent with measured values (Tables 4.1, 4.2). For layer 1 however, the model could not be fitted using the average magnetic susceptibility (κ ~0.004 SI) - the inversion produced an optimized value (0.04 SI) that was about 10 times higher than measured in-situ. The much higher value indicates that the orthogneiss (layer 1) has a higher bulk magnetic susceptibility than predicted by field measurements. This likely results from the heterogeneous composition of the layer 1 orthogneiss as noted by Lumbers and Vertolli (2000). The larger model-derived magnetic susceptibility of model layer 1 may be explained by the presence of mafic-rich amphibolite interbeds within the orthogneiss that were not captured by field measurements at the 9 sampled outcrop locations. Field measurements were restricted to accessible outcrops, and the measured ranges apparently underestimate susceptibility of the orthogneiss.

Remanence estimation using Helbig analysis was unsuccessful as the body was not compact enough to establish a remanent vector direction (Pratt et al., 2014). For the induction-remanence model, direct inversion of the NRM produced a stable remanence vector for layer 3 with D = 048°, I = -69° and remanence intensity of ~3 Am^{-1} (Table

4.2). The layer 3 NRM vector was aligned with the general dip direction of Mesoproterozoic units (055°; Fig. 4.2). The inverted NRM directions for model layer 1 were more variable but produced a best fit with D = 200°, I= -69° (NRM <1 Am^{-1}). For the low magnetic susceptibility layer 2, the remanence inversion was unstable and the NRM vector was set to the same values as model layer 3.

A model of simple dipping slab with strike of 50° NW-SE and dip 60° using magnetic susceptibilities from model layers 1 and 3 (Table 4.2, Fig. 4.7) could replicate the dipole (Fig. 4.7B) from Fig. 4.5A. Two approaches were used in inverting for the model. Direct inversion of the slab model (SM) produced a NRM vector with D = 050° and inclination I = -67° (Table 4.3). Inversion on the resultant vector (SMR) estimated D = 045° and I = -73°. The estimated NRM directions were then tilt corrected and translated to virtual geomagnetic poles (VGP), which plot with a resulting direction of 240° E and -61°N. (Table 4.3, Fig 4.8A)

Figure 4.8A plots the VGP from modelling results (Table 4.3) with pole directions of the APWP for rocks ages 1.1Ga to 700Ma (Brown and McEnroe, 2012). This shows that the VGP from the tilt-correct NRM vectors fall on the southern loop of the APWP of Hyodo and Dunlop (1993) with an age ~980 Ma. Figure 4.8 B shows the remanent vector direction mean values for the Muskoka, Rousseau and Huntsville terranes in the region around Skeleton Lake, as well as the tilt-corrected Skeleton Lake NRM values.

A. Alvarez and Dunlop (1988)	VGP ⇨		NRM vector	
	D (°E)	I (°N)	D (°E)	I (°N)
Huntsville domain (H)	154	-12	289	-54
Rosseau domain (R)	130	-22	304	-72
Muskoka domain (M)	147	-33	273	-70
	VGP		⇦NRM vector	
B. Skeleton Lake (Model inversion)	D (°E)*	I (°N)*	D (°E)	I (°N)
Direct inversion (DI)	73	-16	48	-69
Slab model (SM)	72	-17	50	-67
Slab model resultant vector (SMR)	78	-20	45	-73
C. Skeleton Lake (Tilt-corrected)	D (°E)*	I (°N)*	D (°E)	I (°N)
Direct inversion (DI)	173	-47	240	-61
Slab model (SM)	173	-48	239	-61
Slab model resultant vector (SMR)	178	-45	240	-57

Table 4.3. A. Virtual geomagnetic poles (VGP's) from Alvarez and Dunlop (1998) for Muskoka, Rosseau domains and estimated NRM directions. B. NRM vector direction determined for Skeleton Lake using model inversion and the corresponding VGP's. C. Bedding tilt-corrected NRM vectors and corresponding VGP's. Following bedding tilt correction, the Skeleton Lake model-derived VGP's plot on the southern loop of the Hyodo and Dunlop (1993) APWP (Fig. 8A).

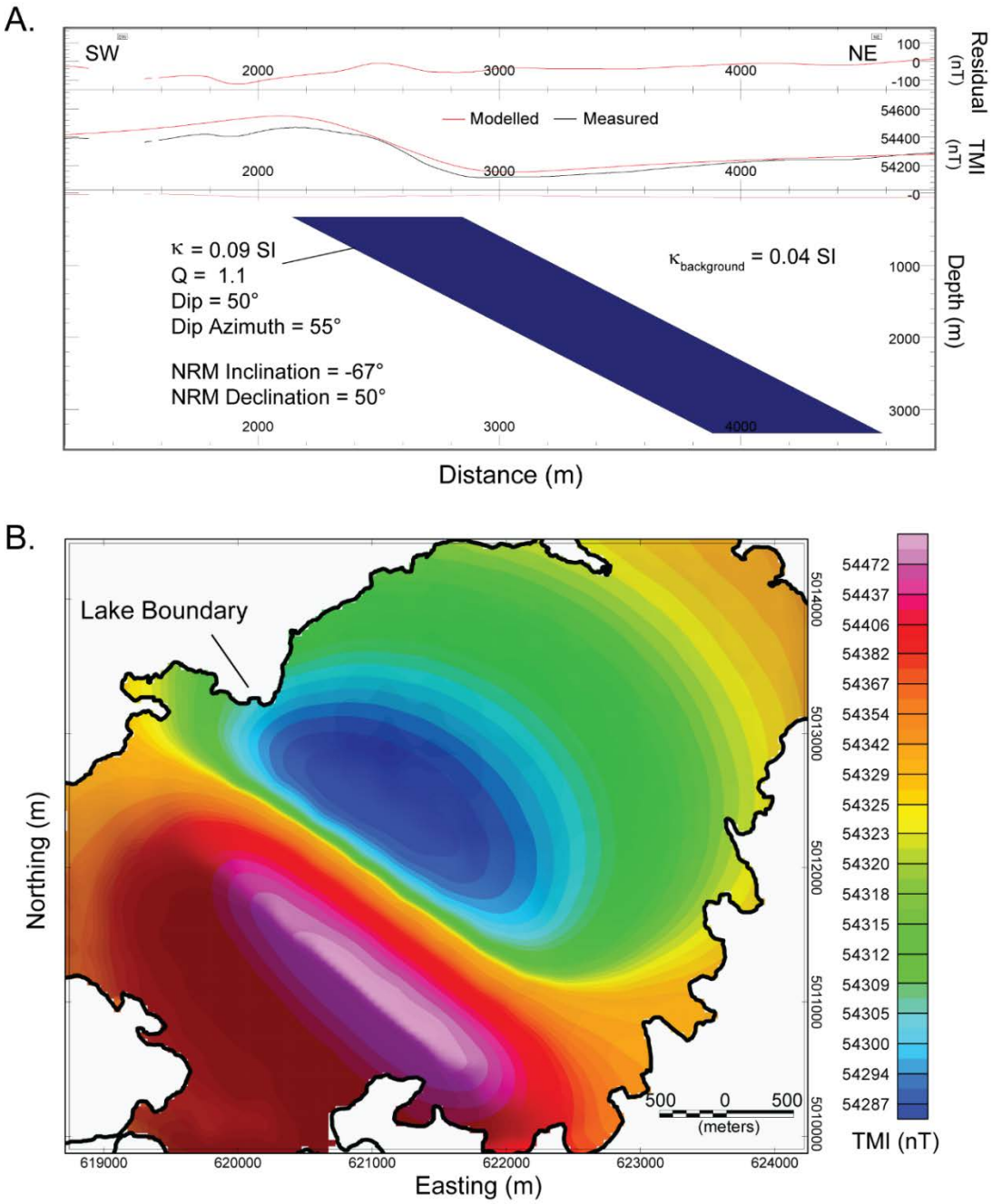

Fig. 4.7. A. 2-D profile model of amphibolite slab (κ=0.09; layer 3) dipping 50° northwestward towards 55° NE. Background magnetic susceptibility κ=0.04, (layer 1). Modelled TMI map showing dipole and northeast-directed resultant magnetic vector.

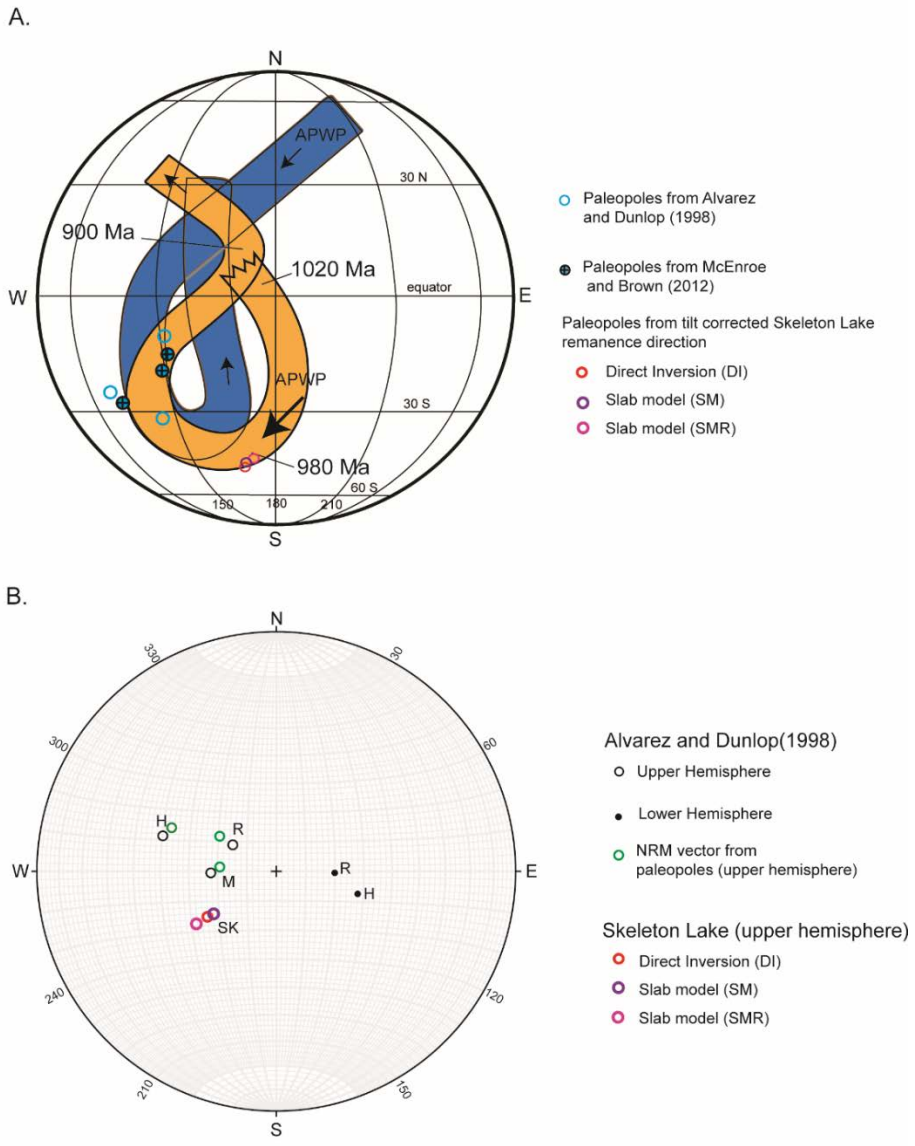

Fig. 4.8. A. Apparent polar wander paths (APWP) for Late Proterozoic (ca. 1100-700 Ma) Laurentian rocks in southern Ontario and Adirondacks (modified from McEnroe and Brown, 2012). Counter-clockwise APWP path (blue) from McEnroe and Brown (2012) and clockwise path (orange) from Hyodo and Dunlop (1993). Tilt-corrected poles for Skeleton Lake dipolar anomaly plot on the southern loop of the APWP of Alvarez and Dunlop (1998). B. Lower hemisphere stereonet showing NRM vectors from Alvarez and Dunlop (1998) for Muskoka (M), Huntsville (H) and Rousseau (R) lithotectonic domains and tilt-corrected NRM vectors for Skeleton Lake (SK) (see Table 4.3).

4.4.4 3-D Models

4.4.4.1 Volcanic intrusive

The volcanic intrusive model (Fig. 4.9) simulates a ~1.2 km diameter volcanic plug with remanence properties modelled on the Early Cambrian (575 <Ma) Callander Bay complex (Symons and Chiasson, 1991). Several trials were attempted with cylindrical pipes with a range of diameters (0.5 to 3 km), but a simple, straight-sided cylinder could not be fitted to the observed TMI anomaly. An elliptical pipe with a diameter of ~1.2 km and remanence intensity of 1.0 Am^{-1} reproduced some aspects of the TMI anomaly but required a steeply dipping western contact that paralleled the dip of Mesoproterozoic units (Fig.4. 9). The pipe model had a much poorer fit (> 20 nT RMS along profile) with the observed magnetic anomaly when compared with the impact crater models (Fig. 4.9, 4.10, 4.11).

4.4.4.2 Impact crater models

Modelling reveals a roughly circular crater form basin with no distinct rim and a possible central uplift or ring structure. The structure is slightly elongated with an across-strike diameter of >4.2 km and ~ 4.0 km diameter along strike (Fig. 4.12). The estimated diameters for both the induction and induction-remanence models should be taken as a lower limit of the rim-rim diameter of the structure. In both models, the southern structure rim appears heavily eroded with no evidence of a crater wall or rim (Fig. 4.10C, 4.11C, 4.12). The northern and eastern edges (Fig. 4.12) of the basin are clearly circular, with a basement surface that dips steeply into the basin centre. Lineaments visible in the vertical derivative (Fig. 4.5C) northeast of the basin centre, correspond to higher susceptibility amphibolites (model layer 3). At the northern eastern edge of the basin, magnetic lows are associated with low susceptibility units (model layer 2). (Fig. 4.10, 4.11).

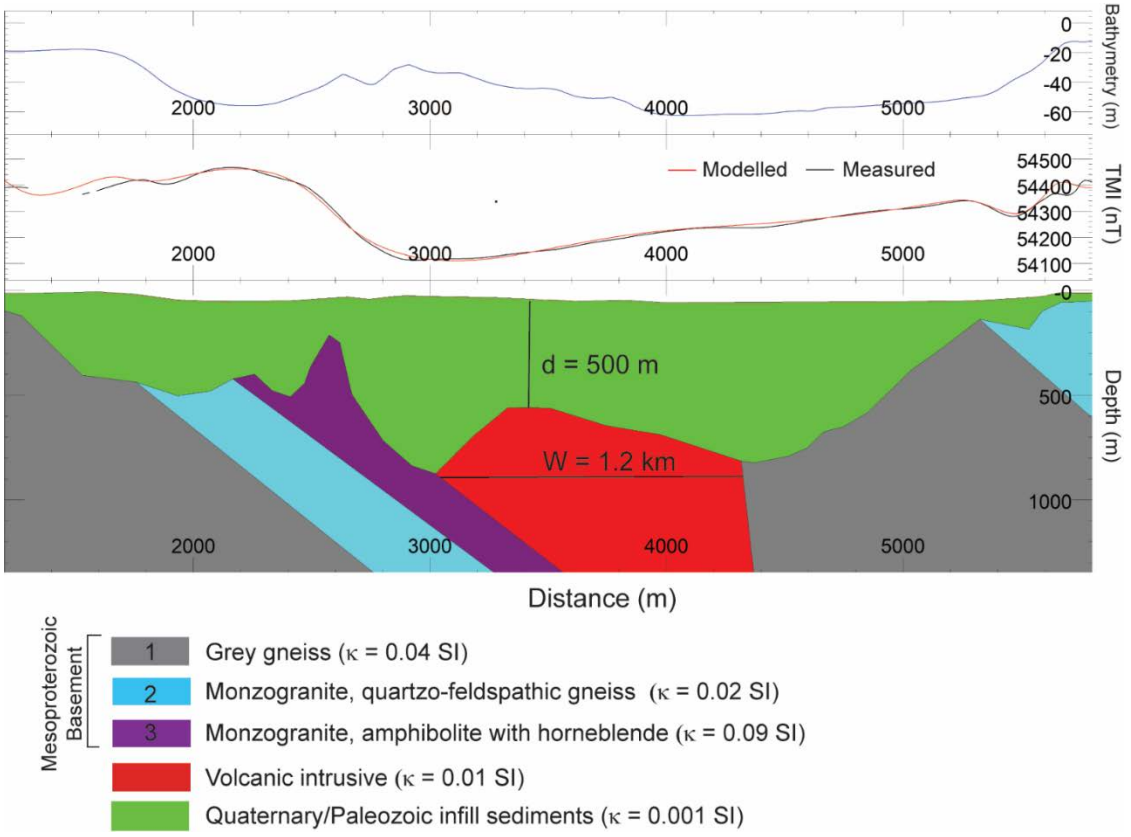

Figure 4.9. Cross-strike (SW-NE) 2-D profile model for a volcanic intrusive plug (κ = 0.01 SI). Plug is elliptical in plan view and ~1.2-1.4 km in diameter.

In the basin centre, the maximum depth to basement for the induction and induction-remanence models is at the contact between the thickest model layer 3 element and model layer 1 (Fig. 4.10B, 4.11B). As the pre-impact elevation of ground surface can not be determined, the minimum d_t (depth from pre-impact ground surface) for the structure is taken to be the depths measured from lake surface to basement.

In both models, though more distinct in the induction-remanence model, a channel-like structure is present in the western edge of the basin. This apparently marks the location of a trough in basement related to either a shear zone and/or glacial erosion of the basement surface. The channel can be traced a a northwest-southeast trending trough in the topography surrounding the lake (Fig. 4.12) and is also visible as an area of thicker basin fill in the isochore maps (Fig. 4.13)

For the induction model the channel feature at the boundary between model layer 3 and 1 may not be impact related. The deep channel results from the dipole in the TMI (next to high of possible 'terrace' or 'uplift' in Fig 4.10B) has a depth of ~1000 m. Ignoring the channel at the model layer boundary would give a depth to basement of ~ 800 m. The bottom morphology shows elements of possible terraces or central uplift, more consistent with a complex crater (Fig. 4.10 B, C). The low in the basement appears in this model to align with the dipole in the TMI (Fig. 4.5A). The fill (Fig. 4.13A) also seems to follow the trend of the dipole in the TMI.

For the induction-remanence model, the overall depth to basement is greater than the induction model at ~1200 m and occurs at the boundary between model layers 1 and 3 near the basin centre. In this model a curved raised ridge to the southwest (Fig. 4.12B) is more distinct than in the induction model and follows the arcuate low in the vertical 1st derivative map (Fig. 4.5C). The basin shape in this model is notably more circular, with a well-defined central basin and a steeply dipping basement surface at the northern edge of the structure. In the isochore map (Fig. 4.13B) the basin fill shows a distinct thickening of the infill to > 1000 m at the basin centre.

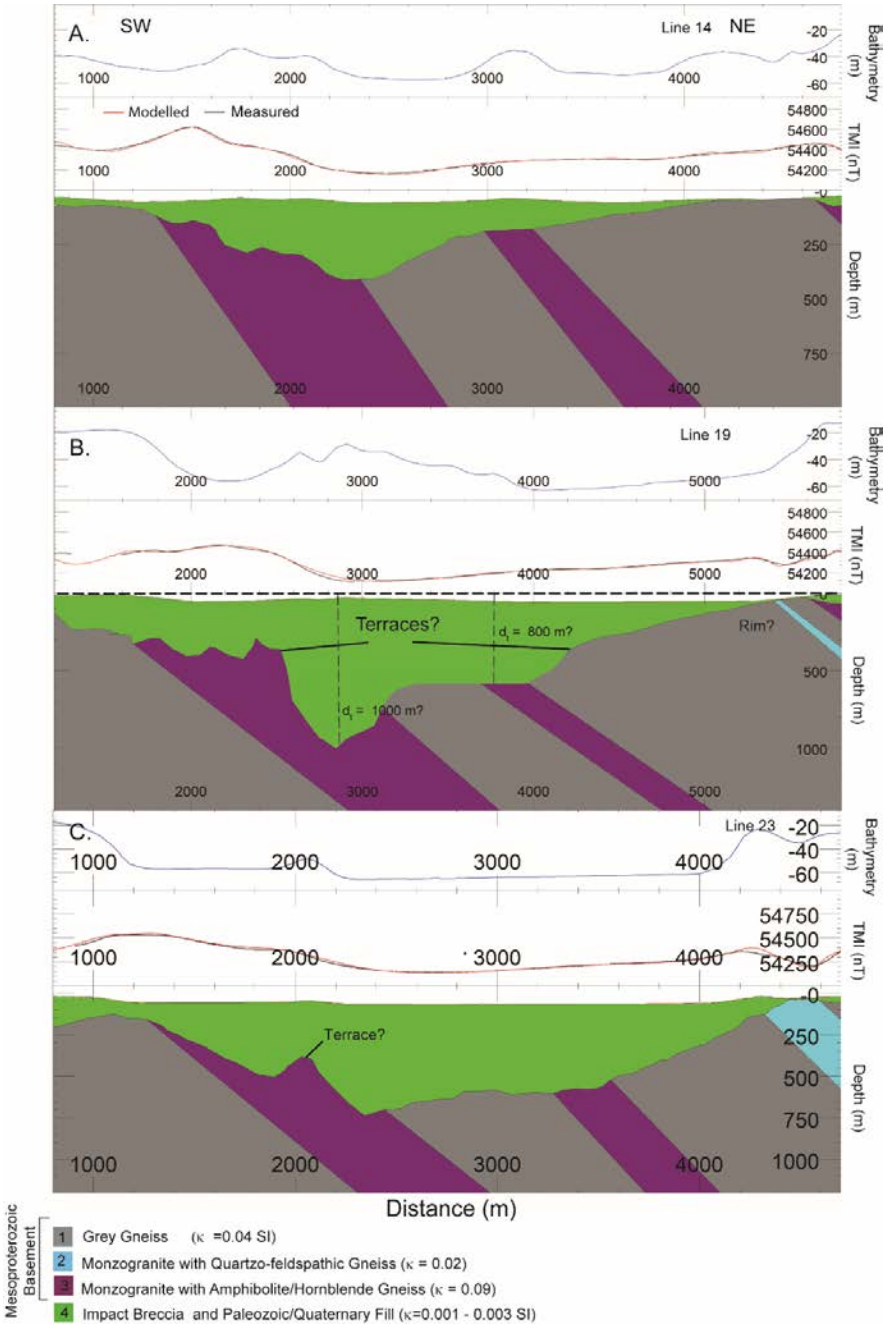

Figure 4.10. Cross-strike (SW-NE) 2-D profile models for impact crater with induction only magnetization. A. Profile line along northwest of the structure, 1 km northwest of profile in B. B. Profile across centre of structure. C. Profile along southeast of structure 1 km southeast of profile in B.

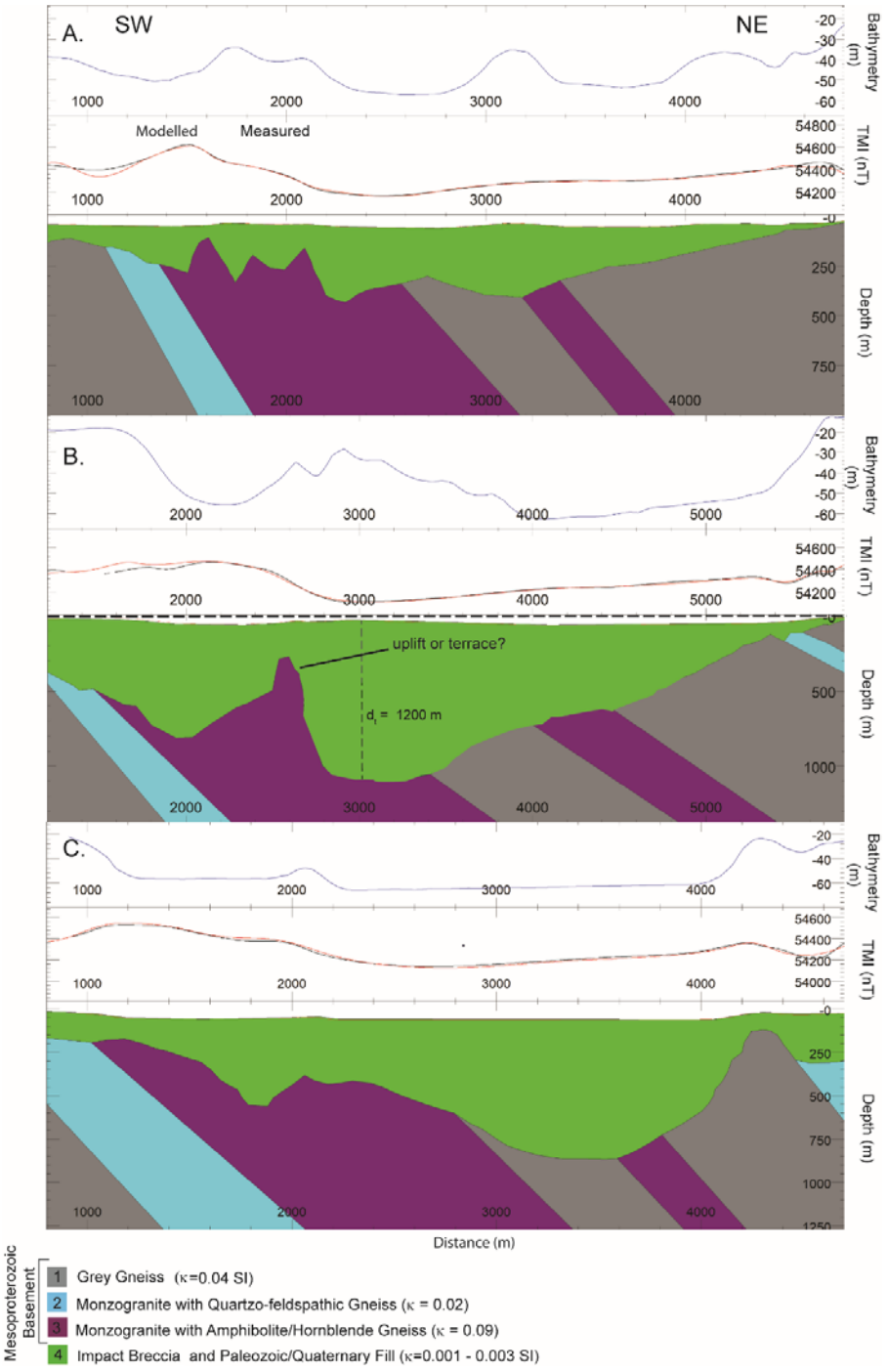

Figure 4.11. Cross-strike (SW-NE) 2-D profile models for impact crater with induction and remanence magnetization. A. Profile line along northwest of structure, 1 km northwest of profile in B. B. Profile across centre of structure. C. Profile along southeast of structure 1 km southeast of profile in B.

Model	**χ^2 Full Model**	**χ^2 Central profiles**	**RMS central profiles**
Volcanic	670	4.6	13.5
Induction	654	3.6	8.1
Induction-Remanence	560	2.3	8.4

Table 4.4 - Chi-squared (χ^2) statistic and RMS error values from three model scenarios.

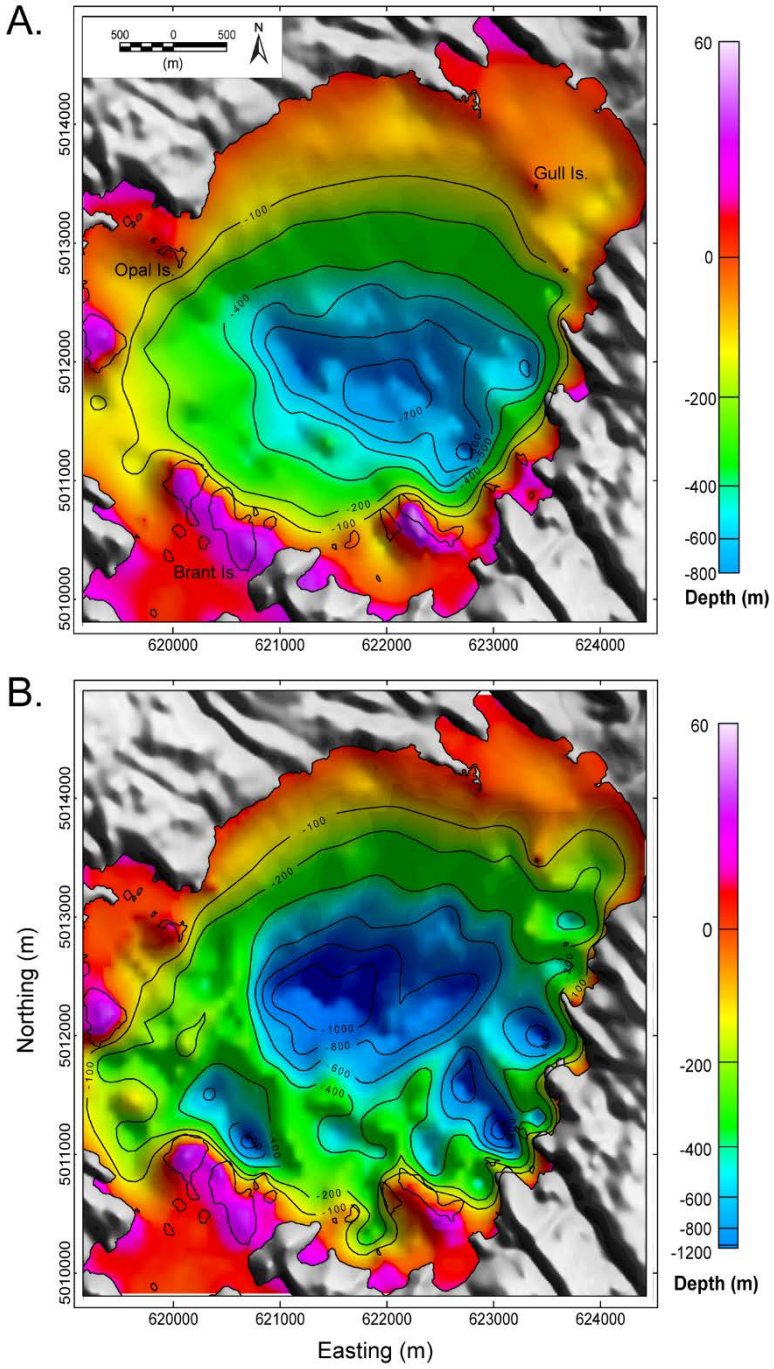

Figure 4.12. Reconstructed crater basin morphology and true depth (d_t) for: A. Induction only model. B. Induction-remanence model. Depths and terrain height in metres relative to modern lake level (280 m asl).

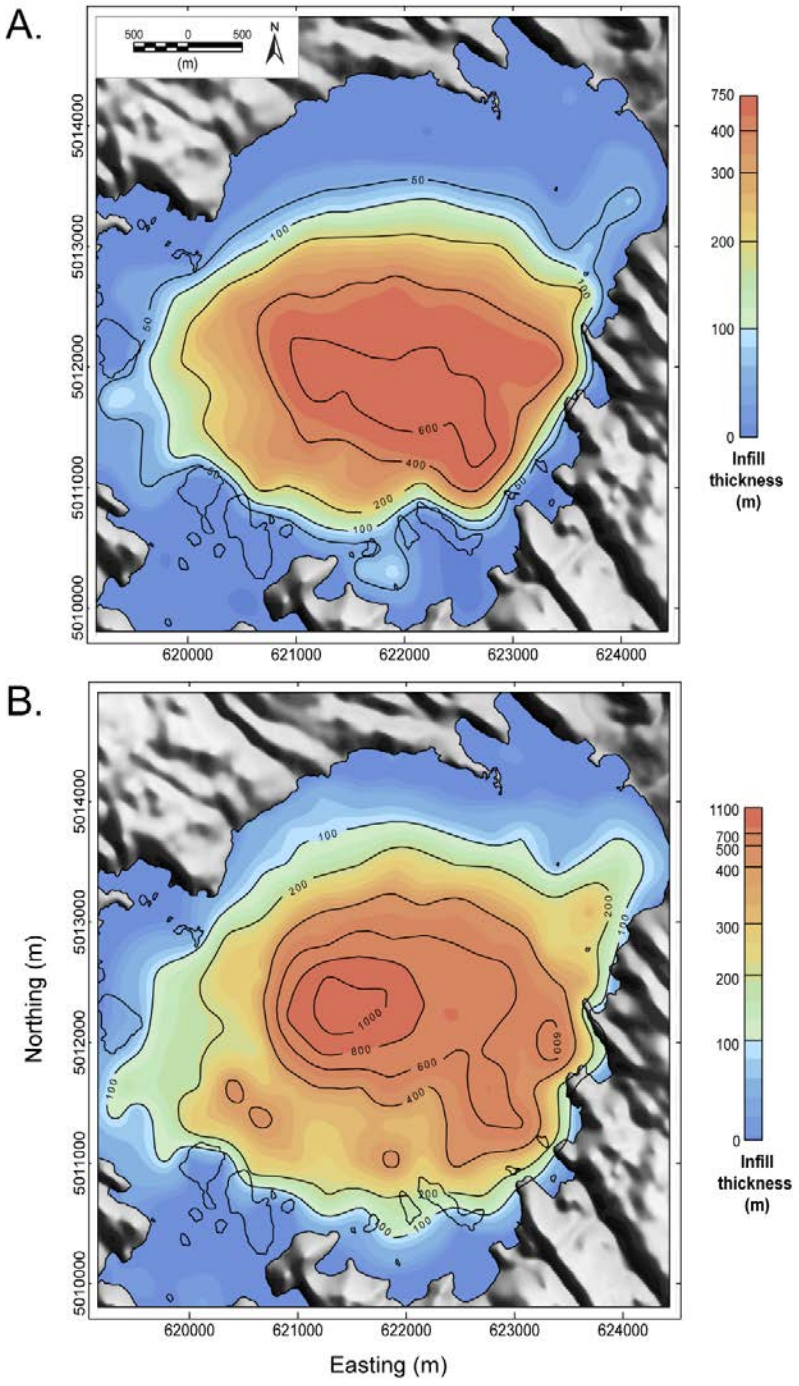

Figure 4.13. Isochore maps of total infill thickness overlying basement obtained by subtraction of reconstructed basement surface (Fig. 4.12) from DBM (Fig. 4.3). A. Induction model. B. Induction-remanence model.

Figure 4.14A shows a gravity profile across the central basin from Waddington and Dence (1979) for comparison with a forward-modelled gravity (Fig 4.14B). The forward-modelled gravity was constructed using the model layers from the induction model. Based on the central profiles, (Fig. 4.10B shown) a single gravity profile (Fig. 4.14 B) was created using the mass deficit calculations of Waddington and Dence (1979). This profile shows a distinct low (~5 mGal) over the structure, with a high on the northeast edge.

4.5. Discussion

4.5.1 Volcanic origin?

The northwest-trending magnetic lineaments in the vertical derivative map show that Mesoproterozoic shear zones and basement rocks are continuous below Skeleton Lake (Fig. 4.5C, 4.6C). The continuity of basement below the structure rules out a volcanic origin, as a pipe structure cross-cutting the basement units would obliterate all basement magnetic fabric (L'Heureux et al., 2005). A simple vertical-sided cylindrical volcanic stock was tested in modelling but could not reproduce the observed magnetic anomaly low. An elliptical pipe structure (e.g., Fig. 4.9) can reproduce some aspects of the anomaly but requires a steeply dipping western margin that parallels the dip of the amphibolite gneiss (layer 3). From Table 4.4 we also see that this model has the poorest fits with the data with the highest chi-squared values for both the full model (670) and the central profile (4.6), and an RMS for the central profile of 13.5. The values of the chi-squared for the induction model are somewhat lower at 654 for the full model, and 3.6 for the central profile, with and RMS of 8.1. The RMS of the induction-remanence model is similar to that of the induction model (8.4), but still lower than the volcanic intrusive. The chi-squared of the model is also lower than both the intrusive and induction only model, with a full model value of 560 and central profile of 2.3.

The magnetic and gravity anomaly lows at Skeleton Lake are also inconsistent with the typical geophysical signatures of carbonatite-alkaline intrusives in the region (e.g., Callander Bay, Burritt Island). The 3 km diameter Callander Bay complex, for example, is characterized by a central magnetic high of a few hundred nT (Satterly, 1970; OGS, 1999). Alkaline-carbonatite complexes tend to have well-defined gravity highs (10's of mGal) due to the high density of the intrusive body (2840-3090 kg/m^3) when compared with Precambrian host rocks (typical densities of 2700-2750 kg/m^3) (Gittens and Lumbers,1972; Thomas et al, 2016). For example, the Oka carbonatite at the eastern end of the OBG near Montreal, has a central Bouguer gravity high of about 15 mGal (Thomas et al, 2016). Skeleton Lake in contrast, has a well-defined (~ 3 mGal) Bouguer gravity low (Waddington and Dence, 1979) (Fig. 4.4B, 4.14A).

A volcanic origin is also problematic because there is no evidence for thermal metamorphism and alteration (i.e., fenitization) of basement rocks at Skeleton Lake (Waddington and Dence, 1979). Marginal dikes and meso-somatic alteration are common features of ultrabasic-alkaline intrusive suites in the region (Symons and Chiasson, 1991). None of the 12 outcrops sampled as part of this study (Fig. 4.2) showed any evidence for hydrothermal alteration or fenitization of Mesoproterozoic units. It is also notable that the Skeleton Lake breccias (e.g., Opal Island) lacked meso-somatic alteration or carbonatite inclusions that accompany fenitization and breccia formation around carbonatite intrusions (Tuttle and Gittins, 1966; Elliot et al., 2018). Overall, the geological context, magnetic and gravity anomaly patterns and the new modelling results do not support a volcanogenic origin.

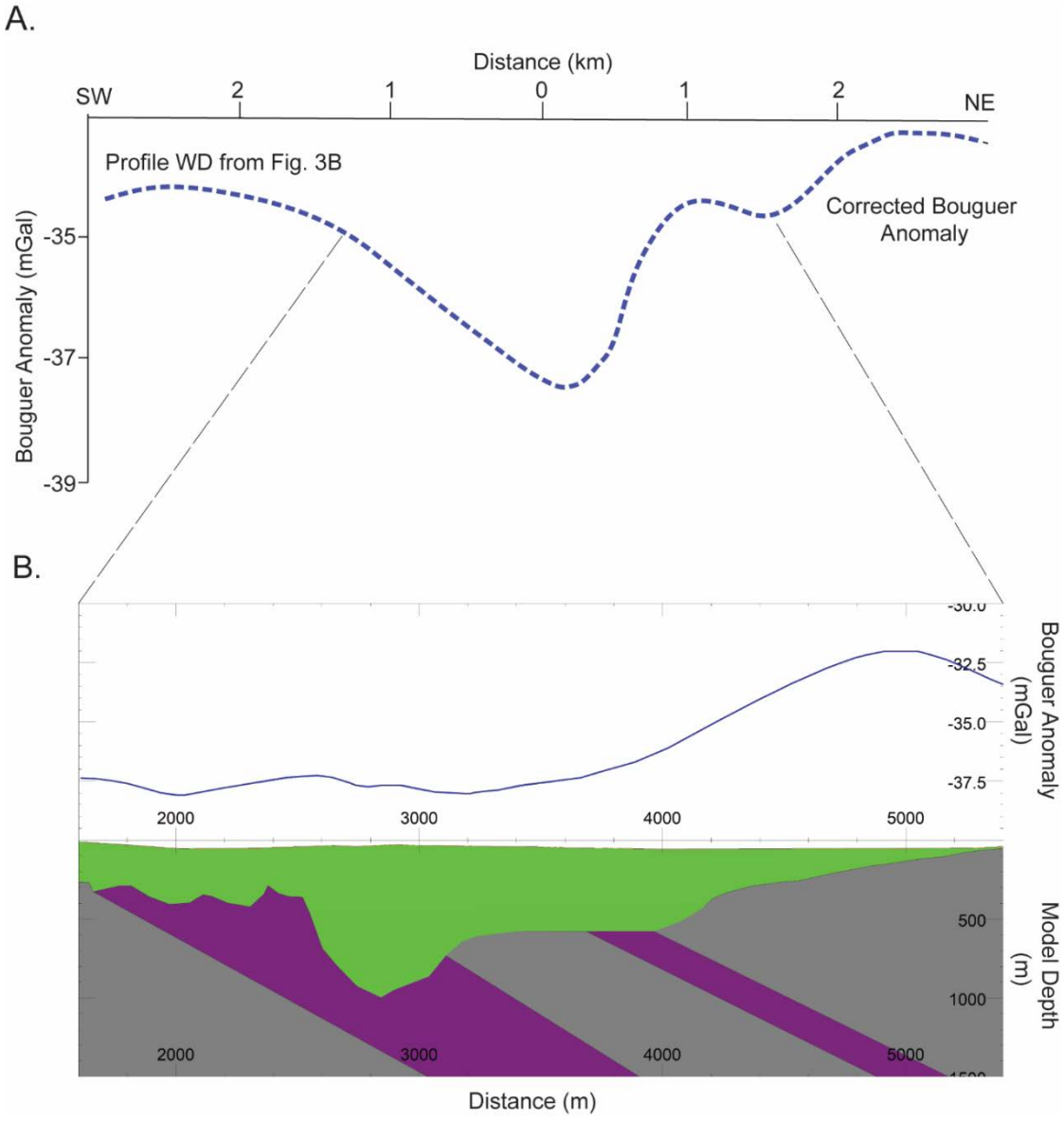

Figure 4.14. A. SW-NE Bouguer gravity profile (WD, Fig. 4.4), corrected for water depth, across approximate centre of lake, redrawn from Waddington and Dence (1979). B. Forward-modelled Bouguer gravity profile (centre profile Fig. 4.8B) along approximately same line as WD and using the same gravity contrasts.

4.5.2 Impact origin?

The >700 nT circular magnetic anomaly and a ~ -3 mGal gravity anomaly are consistent with the geophysical expression of a buried impact crater (Waddington and Dence, 1979; Pilkington and Grieve, 1992). High-resolution magnetic surveys reveal through-going, low-amplitude magnetic lineaments, showing the continuity of basement shear zones below the basin, (Fig. 4.5C) which is consistent with excavation of the basement by an impact. For both these models, the chi-squared values and RMS as seen in Table 4.4 are lower than that of the volcanic intrusive.

Both models show a ~4.2 km diameter structure with a depth of 1200 m (Fig. 4.12B). The diameter and depth to basement estimates should be considered as lower limits of possible values, as the both the location of the rim and the pre-impact ground surfaces are estimates (Fig. 4.10B, 4.11B). The presence of breccias on Opal Island and on the northwest shoreline (Fig. 4.2) indicate that the structure rim has been deeply eroded and was originally above the elevation of the lake surface (~ 280 masl). Similar autochthonous breccia outcrops are also exposed around the edges of the Brent impact structure (Millman et al.,1960), which is known to be heavily eroded (Grieve and Cintala, 1981).

The impact crater models indicate a complex, high-relief basement surface (Fig. 4.10, 4.11, 4.12). The deepest part of the basin with the adjacent upraised feature may represent part of a ring structure or off-centre central uplift (Fig. 4.10B, 4.11B, 4.12) that are found in complex or transitional (Osinski et al, 2019; Kenkmann, 2021) structures. The presence of this ‘ring’ structure is also visible in the vertical 1st derivative, (Fig 4.5C). The upstanding ridge in the bathymetric data (Fig. 4.3) seems to follow this basement high. (Fig. 4.11B). Modelling indicates the bathymetric high is clearly not due to the presence of basement rock (Fig. 4.11B) but may represent expression of the basement surface in Ordovician age carbonate deposits.

The circular shape of the northern lake shoreline suggests a possible structural control which may indicate the presence of shock-induced fracturing of basement rocks beyond the lake basin. The southern and western shorelines in contrast, are more complex, and the shoreline is controlled by the alternation of more resistant quartzo-feldspathic and monzonitic gneiss with amphibolite gneiss units (Fig. 4.2,4.12, 4.13). The denuded southern shore, with little or no evidence of a steeply dipping rim also shows the headlands extending into the lake. (Fig. 4.12) and a possible erosional channel (Fig. 4.12, 4. 13)

Waddington and Dence (1979) previously estimated a depth to basement of ~1.2 km and a diameter of ~ 4.0 km using gravity modelling. Their model indicated a total mass deficit of 6.5×10^{14} g, which they attributed to the lower density of breccias and fractured basement rocks in the impact crater base. For comparison, we calculated a forward gravity model using their density values and the basement layer thickness from the induction-only crater model (Fig. 4.14). The profile model produces a ~ -5 mGal anomaly (Fig. 4.14B) over the central basin that conforms generally with the observed gravity anomaly. For comparison, the gravity anomaly at Brent Crater is ~ -6 mGal. (Millman et al., 1960)

There are a number of differences between the basement morphology produced by the induction-only and induction-remanence models with the remanence model having the best fit overall (Table 4.4) The induction remanence model has a slightly higher RMS (8.4) than the induction model (8.1), but a lower chi-squared value of 560 for the full model and 2.3 for the central profile as compared to the induction model which has chi-squared values of 654 for the full model and 3.6 for the central profile.

The remanence model provides an estimated maximum depth at the structure centre of ~1200 m (Fig. 4.11) versus ~800 m for the induction-only model (Fig. 4.10). The induction-remanence model also produced a more regular shaped structure (Fig. 4.12B) than the induction-only model (Fig. 4.12A), with the induction-remanence model

having an elliptical basin with a major axis that parallels the strike of Mesoproterozoic basement (Fig. 4.12B). The apparent irregular basin in the induction-only model (Fig. 4.12A) is a distortion produced by the dipole component of the remanent magnetization of layer 3, which is not accounted for in the induction-only model. The results demonstrate the remanent magnetization is a key element and ignoring remanence can lead to significant error in the crater depth estimates and geometry (Clark, 2014).

The range of remanence intensities for the different model layers (0.14-3 A/m, Table 2) are lower than the regional estimates for Grenville basement rocks (0.02 to 7 A/m; Alvarez and Dunlop, 1998; Brown and McEnroe, 2012). The reduced NRM intensity was required for the model to produce a reasonable fit with the observed TMI signal (Fig. 4.11). The model derived reduced NRM intensity of the basement relative to the Muskoka Domain values may indicate some level of shock demagnetization of basement rock below the structure, consistent with results from Kärdla (Plado et al., 1996) that demonstrate a reduction of remanence intensity in shocked target rocks. Shock demagnetization can occur when shock pressures reach ~1 GPa (Pilkington and Grieve, 1992).

Direct inversion estimated a repeatable and stable NRM vector for the high susceptibility amphibolite layer 3 (I= -69°, D = 48°). Inversion of the slab model (Fig. 4.7) produced similar directions (Table 4.3). The stability of the remanent vector through all 3 approaches indicates this approach can reasonably reproduce the remanent vector of the geology at SLS (Clark, 2014; Pratt et al., 2014).

When the remanent vector was tilt corrected, the NRM directions are consistent with values obtained by Alvarez and Dunlop (1998) (Table 4.3). This tilt corrected NRM, produces a virtual geomagnetic pole direction of 240° E and -61°N, which places this pole on the southern edge of the APWP of Hyodo and Dunlop (1993) (Fig. 4.8A). This location on the APWP, indicates that the remanence was acquired around 980 Ma ago. Tilting of the bedding would have taken place after this remanent vector was acquired.

Rivers and Schwerdtner (2015) looked at the evolution of the Muskoka domain after the peak of Ottawa metamorphism. Their work indicates that the dominant amphibolite-facies metamorphic assemblages, fabrics, and structures of the Muskoka domain, (such as those found at Skeleton Lake) developed in large part after the peak of Ottawan metamorphism (~1060-1020 Ma). This is consistent with the tilting of the beds found at Skeleton Lake occurring after acquisition of their remanent magnetization (980 Ma). This also put an upper limit on the age of the impact structure of ~980 Ma.

4.5.3 Terrestrial analogs?

There are few examples of terrestrial impact craters in crystalline target rocks in the 4 km diameter range for comparison with Skeleton Lake (PASSC, 2022). The Kärdla impact crater (Estonia) and Gow crater (Saskatchewan, Canada) may provide possible terrestrial analogues. The 4 km diameter Kärdla structure has been interpreted as a transitional crater with distinct central uplift and ring depression (Suuroja et al., 2002). Seismic studies show an asymmetric crater basin with a central uplift that is offset by 300-400 m from the basin (Jöeleht and Plado, 2010; Jöeleht et al., 2018). The morphology of Kärdla suggests a transitional impact crater between complex and simple morphologies (Jöeleht et al., 2018). The central raised basement topography at Skeleton Lake (Fig. 4.11B) may represent the eroded remnants of a central uplift, offset from the basin centre similar to what is seen at Kärdla (Jöeleht and Plado, 2010; Jöeleht et al., 2018)

The ~5 km Gow impact structure in Saskatchewan, Canada is a further example of a heavily eroded complex crater with an elliptical central island that marks the remnants of a central uplift and impact melt sheet (Thomas and Innes, 1977; Grieve 2006; Osinski et al., 2012). Gow is one of the smallest known complex craters in crystalline target rocks (Grieve, 2006). The crater has a ~ -3 mGal central gravity

anomaly (Thomas and Innes, 1977) comparable with gravity anomaly of Skeleton Lake (Waddington and Dence, 1979).

4.5.4 Structure morphology

The basement surface below Skeleton Lake is high-relief and not easily interpreted. The crater form depression in the upper surface of the basement is slightly elliptical and elongated along a southwest to northeast direction, perpendicular with the strike of Mesoproterozoic strata (Fig. 4.12). The elliptical shape of the impact basin could have several possible origins: 1) low angled impact (Krohn et al., 2014; Davidson et al., 2011), 2) target rock heterogeneity (i.e., structural controls) (Kenkmann, 2021; Kumar and Kring, 2008) or 3) post-impact tectonic modification. (e.g., Sudbury Impact Structure, Spray et al., 2004; Riller, 2010).

In addressing a possibly more elliptically shaped crater at Skeleton Lake, low angle impacts are known from Davidson et al. (2011), to result in decreased crater size and the along-range crater profile becoming asymmetric. The elliptical shape may also relate to pre-existing topography. The high surface relief and complexity of the basement surface may indicate an impact into a pre-existing high relief terrain, (Krohn et al., 2014). Folding and faulting in the area may control the overall shape of the SLS basin, similar to the almost square shape of Meteor crater, Arizona, which is known to be controlled from pre-existing faults. (Kumar and Kring, 2008).

4.6. Summary and Conclusions

This study confirms that the Skeleton Lake structure is a deep-seated (> 1200 m), crater-form depression in the Mesoproterozoic basement rocks of the Muskoka Domain (Fig. 4.12). High-resolution magnetic surveys reveal through-going, low-amplitude magnetic lineaments, showing the continuity of basement shear zones below the basin (Fig. 4.5C). Basement shear zones and magnetic and gravity anomaly lows are incompatible with an endogenic origin as a volcanic intrusive. The geophysical survey results, 3-D modelling, and geological context (e.g., lack of fenitization, dikes) favour an impact origin for Skeleton Lake, as proposed by Waddington and Dence (1979). Our 3-D modelling better resolves the subsurface structure, indicating a crater-form basin with diameter of ~4.2 km and depth of ~1200 m at the basin centre. The complex basement topography and structure size suggest that Skeleton Lake is a heavily modified transitional impact crater, similar to the Kärdla structure (Estonia) and the heavily denuded Gow crater in central Canada (Suuroja et al., 2002; Osinski et al., 2012). The presence of autochthonous breccias on the north shore (Tomelin Bluffs; Fig. 4.2) and the absence of an identifiable rim in the basement surface suggests that the crater rim has been completely removed by erosion. The structure therefore may represent the remnants of the crater floor of a much larger and heavily denuded impact structure (i.e., > 4.2 km diameter).

The distinct dipole character of the Skeleton Lake magnetic anomaly indicates a strong component of remanent magnetization in basement rocks (Layer 3; Fig. 4.5). Remanent vector inversion using three different approaches produced a NE resultant vector and a stable (reversed) NRM with a mean D = 47.7 and I = -70 (Table 4.3). The induction-remanence model yielded a deeper and more circular basin morphology when compared with the induction-only model (Fig. 4.12). The VGP's estimated from the dipole lie on the Mesoproterozoic APWP of Hyodo and Dunlop (1993) (Fig. 4.8A), which suggests that NRM was acquired prior to regional folding and tilting of the Mesoproterozoic bedding. The VGP position on the APWP also suggests an upper limit

of ~980 Ma for the structure age. The modelled NRM vectors are generally consistent with the regional reversed paleomagnetic directions determined for the Muskoka, Rosseau and Huntsville Domains by Alvarez and Dunlop (1998), which implies an absence of shock-remanent magnetization (SRM) and at most, only minimal demagnetization effects at Skeleton Lake (Pilkington and Grieve, 1992; Ugalde et al., 2005). The lack of such shock effects is also indicated by preservation of basement linear magnetic anomalies (shear zones) below the eastern basin (Fig. 4.5C). Our models provide only a bulk estimate of the NRM of the Mesoproterozoic basement rocks; site-specific paleomagnetic investigations are required to test for possible shock and thermal re-magnetization or demagnetization effects in target rocks (e.g., Quesnel et al., 2013).

Shock metamorphic effects have not been identified in breccias at Skeleton Lake (Waddington and Dence, 1979) but this does not rule out an impact origin. Shock effects are not generally observed in the rim of simple impact craters due to rapid shock attenuation beyond the impact point (Robertson and Grieve, 1977). At the Brent impact crater (D ~3.8 km), shock indicators are present in target rocks in the basin centre but not in the structure rim (Robertson and Grieve, 1977; Grieve, 2006). We also note that the Skeleton Lake monomict breccias are the only known occurrence of Mesoproterozoic-age breccias within the Muskoka region (Lumbers and Vertolli, 2000). The lack of Paleozoic sedimentary clasts within the breccias, supports a Late Proterozoic to early Paleozoic (Cambrian?) age for the structure as proposed by Waddington and Dence (1979).

The digital bathymetric model reveals upstanding (> 30 m high) arcuate ridges on the lake floor, which are interpreted as bedrock scarps. The ridges likely represent erosional remnants of a Paleozoic basin fill, similar to the (Silurian-Devonian age) outlier preserved within the Brent impact crater (Millman et al., 1960). The bedrock ridges are coincident with highs in the underlying basement, indicating possible structural controls on lake bottom relief (Fig. 4.3) by the underlying basement topography (Fig. 4.10, 4.11, 4.12). Future planned work at Skeleton Lake will include marine seismic investigations using a low frequency seismic source (e.g., airgun, boomer plate) to determine the Quaternary and Paleozoic sediment thickness and depth to basement for comparison with

model estimates. Marine seismic studies could also determine the thickness and extent of the breccia layer, which could not be resolved by potential field modelling.

Confirmation of an impact origin for the Skeleton Lake structure will ultimately require deep drilling and recovery of samples with evidence for shock metamorphism. Lake-based drilling (i.e., on the ice surface) would be difficult due to the water depth and changeable winter ice conditions on the lake (Waddington and Dence, 1979); angled boreholes will likely be required to sample the basement rocks below the central basin. Systematic sampling and detailed petrographic analysis of breccias and the underlying Mesoproterozoic basement from exposures along the north shore and Opal Island may provide further insights into the processes of breccia formation and a possible impact origin.

4.7 References

Alvarez V. C. and Dunlop D. J. 1998. A regional paleomagnetic study of lithotectonic domains in the Central Gneiss Belt, Grenville Province, Ontario. *Earth and Planetary Science Letters*, 157(1-2): 89-103. https://doi.org/10.1016/S0012-821X(98)00028-4

Beals C.S. 1960. A probable meteorite crater of Precambrian age at Holleford, Ontario. *Publications of the Dominion Observatory* 24:6 (Ottawa) https://doi.org/10.4095/8727

Briggs I. C. 1974. Machine contouring using minimum curvature. *Geophysics*, 39(1):39-48.

Brown L. L. and McEnroe S. A. 2012. Paleomagnetism and magnetic mineralogy of Grenville metamorphic and igneous rocks, Adirondack Highlands, USA. *Precambrian Research* 212: 57-74. https://doi.org/10.1016/j.precamres.2012.04.012

Cady J. W. 1980. Calculation of gravity and magnetic anomalies of finite-length right polygonal prisms. *Geophysics*, 45(10):1507-1512. http://dx.doi.org/10.1190/1.1441045

Canadian Geodetic Survey (CGS). 2021. Canadian Gravity Database (CGDB).

Clark D.A. 2014. Methods for determining remanent and total magnetisations of magnetic sources – a review, *Exploration Geophysics*, 45(4):271-304 https://doi.org/10.1071/EG14013

Clark J. F. 1982. Earth Physics Branch, Geomagnetic Report 81-2, 25 pages https://doi.org/10.4095/226536

Cordell L. 1985. Techniques, applications, and problems of analytical continuation of New Mexico aeromagnetic data between arbitrary surfaces of very high relief. *Inst*. Geophys., Univ. Lausanne, Switz. Bull. 7: 96-99.

Cullers R. L. and Medaris G. 1977. Rare Earth elements in carbonatite and cogenetic alkaline rocks: examples from Seabrook Lake and Callander Bay, Ontario. *Contributions to Mineralogy and Petrology*, 65:143-153 https://doi.org/10.1007/BF00371054

Currie K.L. and Shafiqullah M. 1967. Carbonatite and alkaline igneous rocks in the Brent Crater, Ontario. *Nature,* 215:725–726. https://doi.org/10.1038/215725a0

Currie K. L. and Ferguson J. 1971. A study of fenitization around the alkaline carbonatite complex of Callander Bay, Ontario, Canada. *Canadian Journal of Earth Sciences*, 8: 498-517.

Davidson T. M., Collins G. S., Elbeshausen D., Wuennemann K. and Kearsley A. 2011. Numerical modeling of oblique hypervelocity impacts on strong ductile targets. *Meteoritics & Planetary Science* 46(10): 1510-1524. https://doi.org/10.1111/j.1945-5100.2011.01246.x

Dence M. R., Innes M. J. S. and Robertson, P. B. 1968. Recent geological and geophysical studies of Canadian craters. *Contributions from the Dominion Astrophysical Observatory in Victoria* 8(25). https://ui.adsabs.harvard.edu/abs/1968CoDAO...8Q....D

Dentith M. and Mudge S.T. 2014. Geophysics for the mineral exploration geoscientist. Cambridge University Press.

Dickin A., Strong J., Arcuri G., Van Kessel A. and Krivankova-Smal L. 2017. A revised model for the crustal structure of the SW Grenville Province, Ontario, Canada. *Geological Magazine* 154(4):903-913.https://doi.org/10.1017/S001675681700005X

Easton R.M. 1992 The Grenville Province and Proterozoic History of Central and Southern Ontario Geology of Ontario Special Volume 4 Part 2: 715-906.

French B.M. and Koeberl C. 2010. The convincing identification of terrestrial meteorite impact structures: What works, what doesn't, and why. *Earth-Science Reviews 98*: 123-70 https://doi.org/10.1016/j.earscirev.2009.10.009

Elliott H.A.L., Wall F., Chakhmouradian A.R., Siegfried P.R., Dahlgren S., Weatherley S., Finch A.A., Mark, M.A.W., Dowman E. and Deady E. 2018. Fenites associated with carbonatite complexes: A review. *Ore Geology Reviews*, 93:38-59. https://10.1016/j.oregeorev.2017.12.003

Foss C. and McKenzie B. 2011. Inversion of anomalies due to remanent magnetisation: an example from the Black Hill Norite of South Australia. *Australian Journal of Earth Sciences*, 58(4);391-405. https://doi.org/10.1080/08120099.2011.581310

Gittens J. and Lumbers S.B. 1972. Alkalic rock complexes and carbonatites of Ontario and part of Quebec. *24th International Geological Congress, Montreal, Guidebook, Field Excursion* A53-C53 p. 41

Grieve R. A. F. 2006. Impact structures in Canada (p. 210).

Grieve R.A.F. and Cintala M.J., 1992. An analysis of differential impact melt-crater scaling and implications for the terrestrial impact record. *Meteoritics*, 27(5):526-538. https://doi.org/10.1111/j.1945-5100.1992.tb01074.x

Guo W. W., Li Z. X. and Dentith M. C. 2011. Magnetic petrophysical results from the Hamersley Basin and their implications for interpretation of magnetic surveys. *Australian Journal of Earth Sciences*, 58(4):317-333. https://doi.org/10.1080/08120099.2011.552984

Hewitt D. F. 1967. Geology and mineral deposits of the Parry Sound-Huntsville area. Department of Mines and Resources, 52.

Hogarth D. D., Rushforth P. and McCorkell R. H. 1988. The Blackburn carbonatites, near Ottawa, Ontario; dikes with fluidized emplacement. *The Canadian Mineralogist* 26(2): 377-390.

Hyodo H. and Dunlop D. J. 1993. Effect of anisotropy on the paleomagnetic contact test for a Grenville dike. *Journal of Geophysical Research: Solid Earth*, 98(B5):7997-8017. https://doi.org/10.1029/92JB02915

Jõeleht A. and Plado J. 2010. Architecture of the northeastern rim of the Kärdla impact crater, Estonia, based on ground-penetrating radar studies. *Large Meteorite Impacts and Planetary Evolution IV* :133-140.

Jõeleht A., Plado J. and Sarv K. 2018. Kärdla impact crater–transitional from simple to complex based on reflection seismics. *EPSC Abstracts*, 12.

Kamo S. L., Krogh T. E. and Kumarapeli P. S. 1995. Age of the Grenville dyke swarm, Ontario–Quebec: implications for the timing of lapetan rifting. *Canadian Journal of Earth Sciences* 32(3), 273–280. https://doi.org/10.1139/e95-022

Kenkmann T. 2021. The terrestrial impact crater record: A statistical analysis of morphologies, structures, ages, lithologies, and more. *Meteoritics &Planetary Science* 56(5): 1024-1070. https://doi.org/10.1111/maps.13657

Krohn K., Jaumann R., Elbeshausen D., Kneissl, T., Schmedemann, N., Wagner R., Voigt J., Otto K., Matz K.D., Preusker F., Roatsch T., Stephan K., Raymond C.A. and Russell C. T. 2014. Asymmetric craters on Vesta: Impact on sloping surfaces. *Planetary and Space Science* 103:36-56. https://doi.org/10.1016/j.pss.2014.04.011

Kumar P.S. and Kring D.A. 2008. Impact fracturing and structural modification of sedimentary rocks at Meteor Crater, Arizona. *Journal of Geophysical Research: Planets* 113: E09009 https://doi.org/10.1029/2008JE003115

Kumarapeli P. S. and Saull V. A. 1966. The St. Lawrence valley system: a North American equivalent of the East African rift valley system. *Canadian Journal of Earth Sciences*, 3(5): 639-658. https://doi.org/10.1139/e66-045

L'Heureux E., Ugalde H., Milkereit B., Boyce J.I., Morris W.A., Eyles N. and Artemieva N. 2005. Using vertical dikes as a new approach to constraining the size of buried craters: An example from Lake Wanapitei, Canada. Large meteorite impacts III: Geological Society of America Special Paper, 384:43-50.

LIO. 2019. Ontario digital surface model (imagery-derived). Land Information Office Ontario.

Lumbers S.B. and Vertolli V.M. 2000. Precambrian geology, Bracebridge area; Ontario Geological Survey, Preliminary Map P.3411 -3414, scale 1:50 000.

Millman P. M., Liberty B. A., Clark J. F. Willmore P. L. and Innes M. J. S. 1960. Publications of the Dominion Observatory vol. 24, no. 1, https://doi.org/10.4095/8722

Morris B., Ugalde H. and Thomson V. 2007. Magnetic remanence constraints on magnetic inversion models. *The Leading Edge*, 26(8):960-964. https://doi.org/10.1190/1.2769548

O'Dowd C. and Eaton D. 2005. Field and laboratory measurements of magnetic properties and density, Central Metasedimentary Belt, Ontario. Natural Resources Canada, Geological Survey of Canada.

Oldenburg D.W. and Pratt D.A. 2007. Geophysical Inversion for Mineral Exploration: A Decade of Progress in Theory and Practice Proceedings of Exploration: 5th Decennial International Conference on Mineral Exploration. 7(5):61-95. https://911metallurgist.com/blog/wp-content/uploads/2015/10/Geophysical-Inversion-for-Mineral-Exploration.pdf

Ontario Geological Survey (OGS), 1999. Single Master Gravity and Aeromagnetic Data for Ontario. ERLIS Data Set GDS1035. http://www.geologyontario.mndm.gov.on.ca/mndmaccess/mndm_dir.asp?type=pub&id=GDS1035

Osinski G. R., Singleton A. C., Ozaruk A. and Hansen J. R. 2012. New investigations of the Gow Lake impact structure, Saskatchewan, Canada: Impact melt rocks, astronaut training, and more. In *Lunar and Planetary Science Conference* (No. 1659, p. 2367).

Osinski G. R., Silber E. A., Clayton J., Grieve R. A. F., Hansen K., Kalynn J. and Tornabene L. 2019.Transitional impact craters on the Moon: Insight into the effect of target lithology on the impact cratering process. *Meteoritics and Planetary Science* 54:573–591. https://doi.org/10.1111/maps.13226

PASSC, 2022. Earth Impact Database 2022. Planetary and Space Science Centre, University of New Brunswick, Fredericton NB. http://passc.net/EarthImpactDatabase/New%20website_05-2018/Index.html

Paterson N.R., Reford S.W. and Kwan K.C. 1990. Continuation of magnetic data between arbitrary surfaces: Advances and applications. In *Society of Exploration Geophysicists, Technical Program*, Expanded Abstracts, 666-669. https://doi.org/10.1190/1.1890296

Pearson K. 1900. On the criterion that a given system of deviations from the probable in the case of a correlated system of variables is such that it can be reasonably supposed to have arisen from random sampling. *Philosophical Magazine*, 50, 157–172. https://doi.org/10.1080/14786440009463897

Pilkington M. and Grieve R. A. F. 1992. The geophysical signature of terrestrial impact craters. *Reviews of Geophysics*, 30(2), 161. https://doi.org/10.1029/92RG00192

Plado J., Pesonen L. J., Elo S., Puura V. and Suuroja K. 1996. Geophysical research on the Kärdla impact structure, Hiiumaa Island, Estonia. *Meteoritics & Planetary Science*, 31(2):289-298. https://doi.org/10.1111/j.1945-5100.1996.tb02025.x

Pratt D. A., McKenzie K. B. and White T. S. 2014. Remote remanence estimation (RRE). Exploration Geophysics, 45(4):314-323. https://doi.org/10.1071/EG14031

Pratt D. A., White A. S., Parfrey K. L. and McKenzie K. B. 2020. ModelVision 17.0 User Guide. Tensor Research Pty Ltd., Greenwich, NSW, Australia, 596 p.

Quesnel Y., Gattacceca J., Osinski G.R. and Rochette P. 2013. Origin of the central magnetic anomaly at the Haughton impact structure, Canada. *Earth and Planetary Science Letters*, 367: 116-122. https://doi.org/10.1016/j.epsl.2013.02.032

Riller U. 2010. Structural characteristics of the Sudbury impact structure, Canada: Impact-induced versus orogenic deformation—A review. *Meteoritics & Planetary Science*, 40(11):1723-1740. https://doi.org/10.1111/j.1945-5100.2005.tb00140.x

Rimando R. E. and Benn K. 2005. Evolution of faulting and paleo-stress field within the Ottawa graben, Canada. *Journal of Geodynamics*, 39(4):337-360. https://doi.org/10.1016/j.jog.2005.01.003

Rivers T. and Schwerdtner W. 2015. Post-peak evolution of the Muskoka domain, western Grenville Province: ductile detachment zone in a crustalscale metamorphic core complex. *Geoscience Canada: Journal of the Geological Association of Canada/Geoscience Canada: journal de l'Association Géologique du Canada*, 42(4):403-436. https://id.erudit.org/iderudit/1034681ar

Robertson P.B. and Grieve R.A.F. 1977. Shock attenuation at terrestrial impact structures. In: *Impact and Explosion Cratering*. Pergamon, New York, pp. 687-702.

Satterly J. 1970. Aeromagnetic maps of carbonatitie-alkalic Ontario Geological Survey, preliminary map no. 452 (revised)

Schnetzler C. C. and Taylor P. T. 1984. Evaluation of an observational method for estimation of remanent magnetization. *Geophysics*, 49(3): 282-290. https://doi.org/10.1190/1.1441660

Schwerdtner W. M., Rivers T., Tsolas J., Waddingtion D., Page S. and Yang J. 1987. Interplay between folding and ductile shearing in the Proterozoic crust of the Muskoka – Parry Sound region, central Ontario. *Canadian Journal of Earth Sciences*, 24(8):1507–1525. https://doi.org/10.1139/e87-148

Schwerdtner W. M., Rivers T., Tsolas J., Waddington D. H., Page S. and Yang J. 2016. Transtensional origin of multi-order cross-folds in a high-grade gneiss complex, southwestern Grenville Province: formation during post-peak gravitational collapse. Canadian *Journal of Earth Sciences*, 53(12): 1511-1538. https://doi.org/10.1139/cjes-2015-0212

Sonnenburg E. P., Boyce J. I. and Suttak P. 2012. Holocene paleoshorelines, water levels and submerged prehistoric site potential of Rice Lake (Ontario, Canada). *Journal of Archaeological Science*, 39(12): 3553-3567. https://doi.org/10.1016/j.jas.2012.05.035

Spray J. G., Butler H. R. and Thompson, L. M. 2004. Tectonic influences on the morphometry of the Sudbury impact structure: Implications for terrestrial cratering and modeling. *Meteoritics & Planetary Science*, 39(2),:287-301. https://doi.org/10.1111/j.1945-5100.2004.tb00341.x

Suuroja K., Suuroja S. All T. and Floden T. 2002. Kärdla (Hiiumaa Island, Estonia)—the buried and well-preserved Ordovician marine impact structure. Deep Sea Research Part II: Topical *Studies in Oceanography* 49(6): 1121-1144. https://doi.org/10.1016/S0967-0645(01)00145-X

Symons D. T. A. and Chiasson A. D. 1991. Paleomagnetism of the Callander Complex and the Cambrian apparent polar wander path for North America. *Canadian Journal of Earth Sciences* 28:355–363 https://doi.org/10.1139/e91-032

Talwani M. and Heirtzler J. R. 1964. Computation of Magnetic Anomalies Caused by Two Dimensional Bodies of Arbitrary Shape. In G. A. Parks (Ed.), *Computers in the Mineral Industries*, 1: 464-480. Stanford Univ. Publ., Geological Sciences 9.

Thomas M. D. and Innes M. J. S. 1977. The Gow Lake impact structure, northern Saskatchewan. *Canadian Journal of Earth Sciences*, *14*(8):1788-1795. https://doi.org/10.1139/e77-152

Thomas M. D., Ford K. L. and Keating P. 2016. Review paper: Exploration geophysics for intrusion-hosted rare metals. *Geophysical Prospecting* 64(5):1275–1304. https://doi.org/10.1111/1365-2478.12352

Tsikalas F. and Eldholm O., 2018. Malvinas (Falkland) Plateau Structure versus Mjolnir crater: Geophysical workflow template for proposed marine impact structures. *Meteoritics & Planetary Sciences* 54(3): 544-55 https://doi.org/10.1111/maps.13227

Tuttle O. F. and Gittens J. 1966. Carbonatites. New York: Interscience Publishers, 591 p.

Ugalde H.A., Artemieva N. and Milkereit B. 2005. Magnetization on impact structures - constraints from numerical modeling and petrophysics, in Kenkmann, T., Hörz, F., Deutsch, A., Large Meteorite Impacts III, GSA special paper 384: 25-42.

Waddington E. D. and Dence M. R. 1975. Skeleton Lake - a Paleozoic impact crater in central Canada. *Meteoritics:* 10:503.

Waddington E. D. and Dence M. R. 1979. Skeleton Lake, Ontario: evidence for a Paleozoic impact crater. *Canadian Journal of Earth Science*16(2) :256–263. https://doi.org/10.1139/e79-025

Chapter 5: Summary and Conclusions

5.1 Summary

The overall aim of this thesis was to evaluate 3-D geophysical modelling as a tool for investigating the subsurface geology of impact craters in south-central Ontario. The subsurface geology of the confirmed Holleford crater and two suspected impact structures (Charity Shoal, Skeleton Lake) were investigated using multi-parameter geophysical studies and 3-D potential field modelling. The models incorporated a broad range of geophysical data (i.e., magnetic, gravity, seismic, bathymetry, LiDAR, and photogrammetric digital elevation) and geological constraints (boreholes, geological maps) to construct detailed, 3-D subsurface geological models. As summarized in this chapter, the application of 3-D geophysical modelling techniques provides important new details of the subsurface geology of the Holleford impact crater and better resolves the geological origins of Charity Shoal and Skeleton Lake. It has also been demonstrated that modelling can provide useful geophysical constraints for evaluating the origin of suspected impact craters where definitive physical evidence is lacking (Stewart, 2003). As discussed below, 3-D geophysical modelling, constrained by borehole and rock physical property measurements is an approach that can be applied broadly in impact geology in the investigation of terrestrial impact craters.

5.1.1 Holleford Crater

Chapter 2 provides new details of the subsurface geology of Holleford crater and the post-impact modification and sedimentation history of the structure. The 3-D modelled basement surface (Fig. 5.1A) demonstrates a discontinuous, heavily-eroded crater rim with an estimated basement rim-to-rim diameter of ~1.8-2.0 km. The crater diameter is smaller than the 2.35 km of Beals (1960), which was based on the surface

crater rim outcrop pattern. The new results show the apparent crater at surface may not accurately reflect the actual subsurface dimensions of the structure. The model yields a true depth from the estimated pre-existing ground surface to basement of ~430 and a total depth to basement of ~580 m. This is consistent with the resistivity results of Andrieux and Clark (1969) that suggest a depth of 800 m +/-15%. The modelled rim height (~30 m) is less is < 50% of the estimated 80 m rim height for 2.0 km diameter, simple impact crater (Table 2.2). Comparison of the crater depth and rim height with scaling equations suggests a heavily eroded impact crater.

Erosion of the structure and deposition due to fluvial activity is evidenced by the modelled sand deposits and outflow channel on the eastern edge. This indicates significant erosion of the structure occurred prior to the deposition of Late Cambrian sandstones. The erosional channel is interpreted as an outflow channel from a paleolake impounded within the crater basin (St. John, 1968). This region was later flooded during the Ordovician, with Paleozoic cover of up to 200 m being deposited over the structure. Later glaciation has removed some of this cover and deposited a layer of Quaternary sediments within the basin, that although it was not modelled, does extend to a depth of a few metres as seen in the core sections.

Modelling indicates that the pre-impact basement surface that dips to the southeast, has influenced the geometry of the structure in the direction of strike. The heterogeneity and variable strength characteristics of the Mesoproterozoic basement rocks may also have imparted a structural control on the crater form and dimensions.

5.1.2 Charity Shoal

Geophysical surveys at Charity Shoal demonstrate a >1400 nT TMI anomaly and confirm the continuity of Middle Ordovician carbonate bedrock below the structure. The continuity of Paleozoic strata below the central basin rules out a volcanic plug intruded into Paleozoic cover rocks as proposed by Suttak (2013). Multi-beam and seismic data

show that the Trenton Group carbonate strata in the bedrock rim are complexly folded. Similar antiformal and synformal folding is present in exposed Middle Ordovician strata in Prince Edward County (Fig. 3.6), demonstrating that the low amplitude, three-dimensional folding is a regional feature of Trenton-Black River Group sediments. Syn-sedimentary folding has been described in Trenton-Black River sediments elsewhere in the Appalachian Basin and is likely the result of sediment mass movements on the tectonically-active Trenton shelf margin (McLaughlin and Brett, 2004).

Holcombe et al. (2013) interpreted the CSS as an impact into Middle Ordovician (Trenton Group) marine sediments and the exposed bedrock rim as a 'ring-anticline' structure, which was modified by glacial erosion. Re-analysis of high-resolution, multi-beam data in this study (Fig. 5.2B), demonstrates that the bedrock topography and rim structure is much more complex, consisting of low-amplitude, antiforms and synforms with evidence for extensional faults. The complex folding of the rim rules out a simple ring antiform produced by the successive draping of carbonate sediment across a raised crater rim as suggested by Holcombe et al. (2013). The large (>1400 nT) magnetic anomaly at Charity Shoal is not compatible with a simple impact basin seated in Paleozoic sediments as suggested by Holcombe et al. (2013), as the magnetic contrast of these sediments is too low to produce this large an anomaly. The new modelling results confirm the work of Suttak (2013), showing that Charity Shoal is a deep-seated structure with a base in Mesoproterozoic basement at a depth of >450 m.

A volcanogenic origin for Charity Shoal was also considered. The annular magnetic anomaly (>1400 nT) can be fitted to a zoned volcanic plug model, which simulates a carbonatite-alkalic intrusion below the Paleozoic cover (Thomas et al., 2016). The magnetic and gravity signatures are, however, inconsistent other known alkaline-carbonatite complexes in the region. Callander Bay at the eastern end of Lake Nipissing, for example, has a magnetic high (Satterly, 1970; OGS, 1999). The gravity anomaly (~-1.7 mGal) is also at odds with positive gravity anomalies typical of carbonatite-type intrusives in the region (Gittens and Lumbers, 1997; Thomas et al., 2016). The annular magnetic anomaly and gravity low at Charity Shoal are more consistent with an impact

origin (Pilkington and Grieve, 1992). The Bouguer gravity anomaly is similar in magnitude and form to the gravity signature of the Holleford impact crater (-3 mGal).

The basement surface model for Charity Shoal indicates a ~1.2 km diameter crater, with a 20-30 m high raised rim and depth to basement of ~450 m. The thickness of the modelled breccia layer at Charity Shoal is uncertain, as the breccia magnetic susceptibility can only be estimated. The modelled basement surface reveals a possible outflow channel in the southwest corner of the structure with a depth of about 50 m.

Based on the weight of available evidence, Charity Shoal is interpreted as a deeply buried ~1.2-km-diameter simple impact crater seated in Mesoproterozoic basement rocks as proposed by Suttak (2013). A marine impact crater with a base in Middle Ordovician sediments (Holcombe et al., 2013) can be excluded based on the magnetic modelling. The continuity of Middle Ordovician Trenton Group sediments below the basin centre suggests a Late Proterozoic to early Paleozoic (Cambrian-Early Ordovician) age for the structure.

5.1.3 Skeleton Lake

Geophysical surveys and 3-D modelling confirm that the Skeleton Lake is a crater-form depression in Grenville Province (Mesoproterozoic; ca. 1.45 Ga) rocks with a depth >1200 m. The complexity of the basement surface and structure diameter (~ 4.2 km) suggests that Skeleton Lake may be a ‘transitional’ impact structure (Kenkmann, 2021), which is elongated along a southwest-northeast major axis. The basin asymmetry may reflect structural heterogeneities and differences in the strength of the Mesoproterozoic basement rocks. The high-relief crater-form basin may record the eroded remnants of a ring or central uplift for an impact structure on the transition boundary from simple to complex crater (Osinski et al., 2019; Kenkmann, 2021;).

Magnetic survey data rule out a volcanic intrusive origin, demonstrating through-going magnetic lineaments that are continuous below the structure base. A volcanic intrusive model with an Early Ordovician remanence magnetization similar to Callander Bay can be fitted to the anomaly but cannot account for many aspects of the magnetic signature. Geological evidence for volcanism is also lacking - there is no evidence for hydrothermal metamorphism (fenitization) or dyke intrusions in the Mesoproterozoic target rocks (Waddington and Dence, 1979) and a central gravity low rules out a denser volcanic intrusive body (Thomas et al., 2016).

The basement remanence is an important magnetic parameter for modelling of the Skeleton Lake structure. The induction-remanence model produced a depth to basement of 1200 m and a central circular basin that better reproduces the basement magnetic lineaments. This is consistent with the results of Waddington and Dence (1979), which predict a deep (1.2 km) crater basin, up to 4 km in diameter. Clark's (1982) estimate of the crater depth (750 m), based on an induction only model underestimates the structure depth.

The lake-based magnetic surveys resolved subsurface details such as a possible central uplift that was not possible with earlier low-resolution aeromagnetic data (Clark, 1982). The merged DEM and bathymetric model (Figs. 4.3, 5.2C) also clearly demonstrates that the ridge-and-swale topography is interrupted by the structure.

The geophysical and modelling results support an impact origin for Skeleton Lake (Waddington and Dence, 1979) and provide new constraints on the structure depth and subsurface geology. The reconstructed basement surface shows a heavily-eroded, > 4 km diameter crater-form basin with complex basement topography that indicates a likely transitional impact crater seated in Mesoproterozoic rocks.

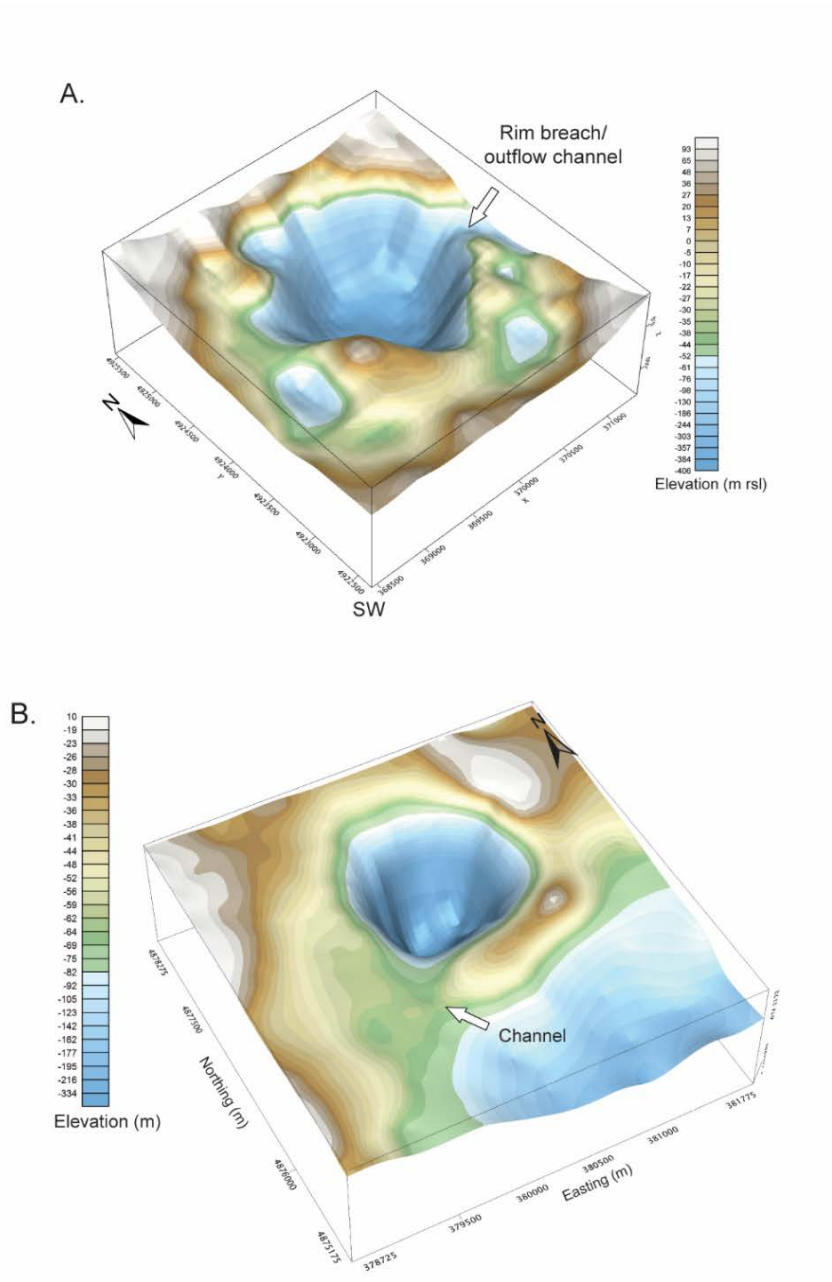

Figure 5.1. 3-D model reconstructions of basement surfaces for: A. Holleford impact crater. B. Charity Shoal. Note remnants of rim structures and erosional channels at Holleford and Charity Shoal recording possible fluvial dissection of rim by outflows. The complex basement topography below Skeleton Lake may indicate a heavily eroded crater basin of a transitional impact structure.

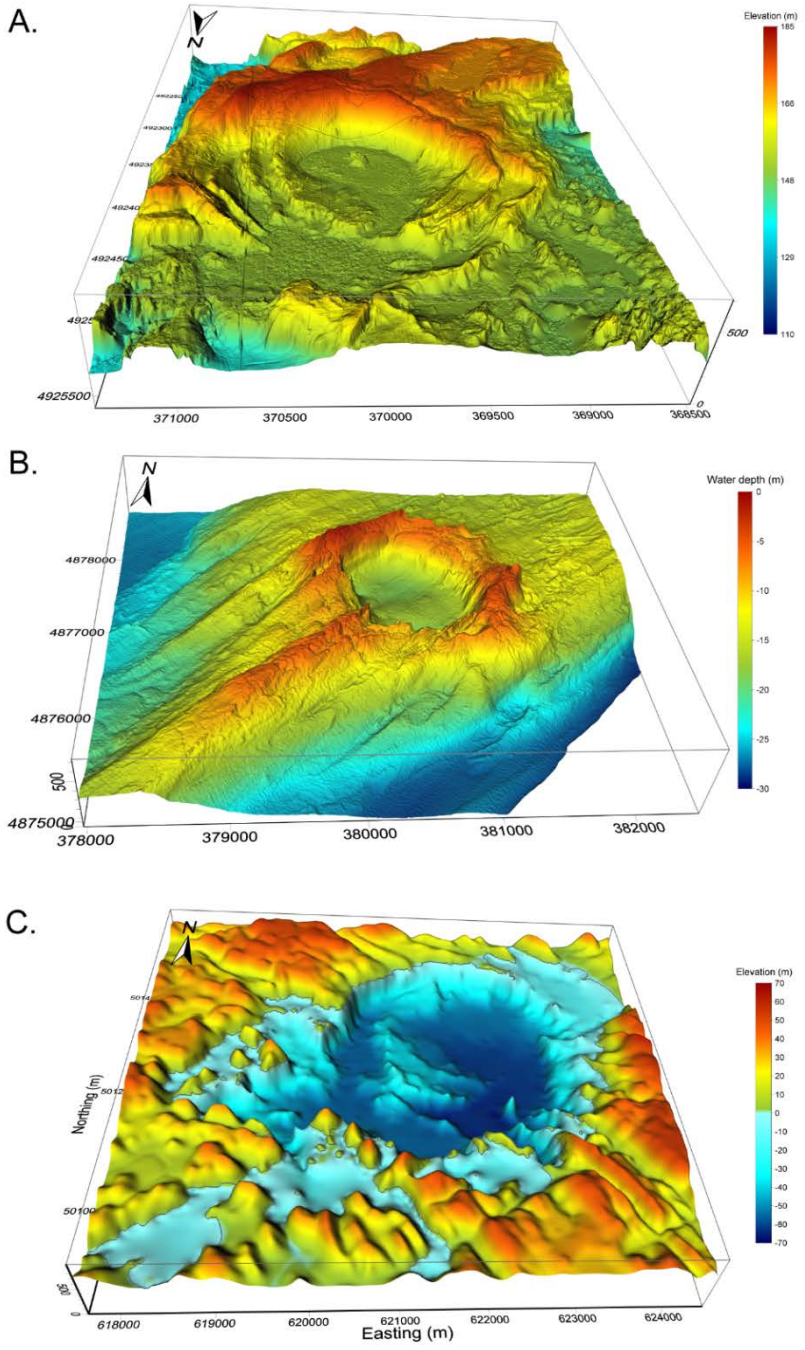

Figure 5.2. 3-D digital elevation and bathymetric models for: A. Holleford impact structure (DEM, 2-m resolution), B. Charity Shoal (DBM- multi-beam data, 2-m resolution). C. Skeleton Lake (merged DEM/DBM, 30-m resolution).

5.2 Identification of Suspected Impact Structures

To date the identification of terrestrial impact structures has relied on shock metamorphic evidence (e.g., planar deformation features, PDFs, polymorphs) or other physical evidence (e.g., shatter cones, impactites) as proof of an impact origin (French 1998; French and Koeberl, 2010). It has been demonstrated in this thesis that 3-D modelling of geophysical data (gravity, magnetics) with geological constraints can provide additional data for evaluation of a possible impact origin. Geophysical data from Charity Shoal and Skeleton Lake, strongly support an impact origin and provide evidence that can be used to rule out an endogenic (volcanic) origin for both structures. The results show that detailed modelling when combined with other geological evidence, can assist in evaluating a possible impact origin (Tsikalas and Eldhom, 2018). 3-D geophysical models can also provide a means for investigating deeply buried impact structures where drilling is unlikely due to economic or other reasons and where physical evidence (e.g. PDF's, shatter cones) may have been removed by post-emplacement modification.

3-D modelling demonstrates similarities in the morphology and subsurface geology of the confirmed Holleford crater and Charity Shoal structures (Fig. 5.1). Both structures are buried below thick (> 200 m) Paleozoic sediments but have a well-defined expression in surface outcrop patterns (Fig. 5.2A, B). The morphology of Holleford crater shows a striking similarity to Charity Shoal. Both structures have craig-and tail landforms, formed by glacial erosion and streamlining of bedrock. The crater rim in both structures, mimics the underlying basement topography (Fig. 5.2 A, B) indicating a basement structural control on the Trenton-Black River Group carbonate strata. The sediment infill thickness at Holleford suggests conformal deposition of carbonate sediments across the basement surface to form a central synclinal basin. At Charity Shoal, the rim is more complex, consisting of 3-D antiforms and synforms. The folding is a regional feature of the Trenton Group in eastern Lake Ontario, and likely records syndepositional folding of carbonate sediments. The sediment deformation may have

been triggered by mass movements on the seismically active (Taconic) intracontinental basin margin (Wallace and Eyles, 2015).

A template for investigation and modelling of suspected marine impact structures was proposed by Tsikalas and Eldhom (2018) (Fig. 5.3). They break the workflow into two main components. Component A addresses the geophysical signature of a structure and initial assessment of whether it is a possible impact structure. Component B provides guidelines for the use of physical evidence such as shock features to confirm the origin of the structure. In Part A, they outline the steps of first collecting geophysical data (A1), while in A3 data is analyzed. If the data and models do not support an impact structure, other possible origins considered (A2). In step A4, the physical evidence parameters for a possible impact structure are evaluated. Part A of the workflow of Tsikalas and Eldhom (2018) could be refined by using 3-D modelling to rule out other possible origins for suspected impact structures, with this being incorporated into step A3 (Fig. 5.3). Step A4 could also be enhanced by evaluating subsurface features that result from the model, in particular where modelling indicates post-modification of impact structures.

An opportunity exists for 3-D modelling of confirmed impact structures (i.e., Brent crater, Ontario), where borehole data are available, that could further refine the process of modelling impact structures and provide analogs for comparison with suspected structures as was done here with Holleford. 3-D subsurface models of existing structures could also be combined with hydrocode modelling (e.g., iSale; Vasconcelos et al., 2012) to allow comparison of the hypothetical crater depth and geometry with sub-surface geometry and morphology. Vasconcelos et al. (2012) note that for models of the 3.8 km diameter Steinem crater, the amount of erosion is difficult to determine, and the current form will result from either a smaller impact energy, or a greater level of erosion since formation. Modelling could help to establish the level of post-emplacement modification that has taken place.

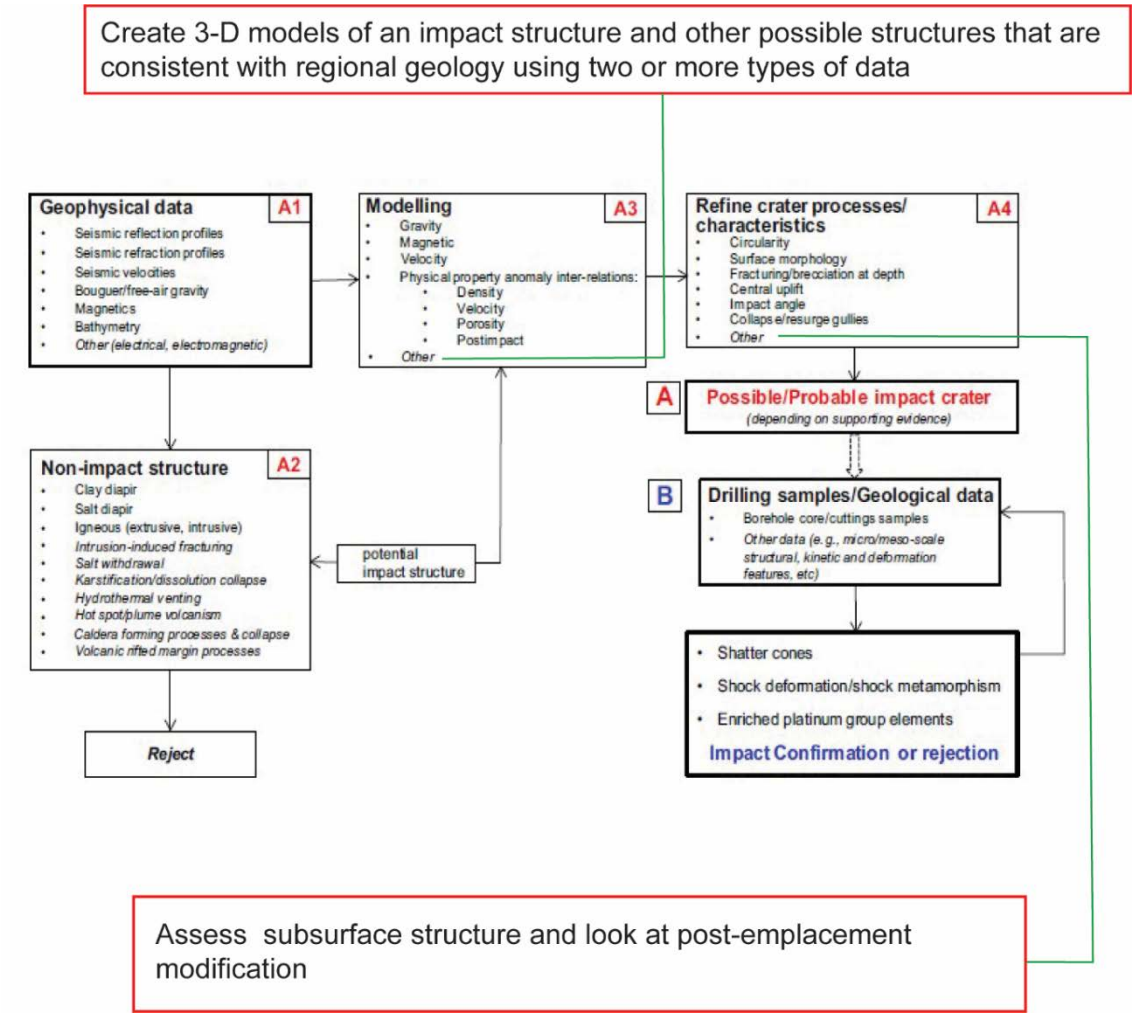

Figure 5.3. Workflow template for investigation of marine impact structures (from Tsikalas and Eldhom (2018). A) Workflow process and iterative steps (A1–4; workflow starts at step A1) to be followed in the absence of drilling samples/geological data when only geophysical data are available. B) Workflow process to be followed when drilling samples/geological data are initially available or became available at a later stage following the evaluation of geophysical data. Suggested enhancements (red boxes) are included to address modelling of buried or submerged structures.

The post-emplacement modification of impact structures on Earth will have a significant effect on the existing morphology of a structure, and their parameters may vary significantly from values that might be expected from scaling equations or hydrocode modelling (Vasconcelos, 2012). 3-D modelling allows for the evaluation of post-emplacement infill and overlying deposition of material as well as erosional features. The modelling approach in this thesis has applications in evaluating the post-impact alteration of terrestrial impact sites, as structures will be altered from the pristine crater very rapidly as has been seen at younger structures like Tamelzane. (Grant and Schultz, 1993; Indu et al., 2021).

5.3 Future Work

5.3.1 Charity Shoal and Skeleton Lake

The weight of geological and geophysical evidence from Charity Shoal and Skeleton Lake supports an impact origin for both structures. Confirmation will ultimately require exploration drilling and recovery of samples with shock metamorphic effects (French and Koeberl, 2010). At Charity Shoal drilling may be feasible on the structure rim (< 2-5 m water depth) using a barge-mounted drill rig but is unlikely due to regulatory issues; exploratory drilling is allowed in Ontario for natural gas but has been banned by US federal regulations since 2005 (Hall, 2011). Exploration drilling at Skeleton Lake would be a technical challenge due to the water depth (> 65 m) and estimated depth to basement (~1200 m). Drilling on the lake ice is likely infeasible due to variable winter ice conditions (Waddington and Dence, 1979). Land-based drilling of angled boreholes from the shoreline is possible but would be very costly due to the depth to basement (~1200 m).

At both sites, a more likely strategy for future work is marine seismic surveys using low-frequency, high-energy sources (e.g., sparker, airgun arrays), which would allow penetration of Quaternary sediments and underlying bedrock to depths of several hundred metres. Marine seismic surveys at Charity Shoal using a low-frequency source type, for example, could confirm the thickness of Middle Ordovician sediments and geometry of the buried structure for comparison with the results potential field geophysical modelling. At Skeleton Lake, marine seismic surveys are needed to confirm the depth to basement and the nature of arcuate bedrock ridges revealed by bathymetry surveys and their relation to the basement surface. Seismic studies could also assist in determining the breccia thickness and details of the basin geometry. High-resolution land-based and airborne magnetic surveys at Skeleton Lake could also assist in determining the structure diameter. Several unmanned aerial vehicle (UAV) platforms are now available (e.g., GEM systems) that allow collection of aeromagnetic data at low flight elevations and with high survey line density (Bell, 2021). Drone surveys would be the most efficient way to acquire new magnetic data beyond the existing lake survey grid. Land-based and airborne vector magnetic data could also be employed, to determine the resultant magnetic vector, allowing the remanence of the basement rocks to be estimated within Modelvision (Pratt et al., 2012). Paleomagnetic studies of the breccia and Mesoproterozoic basement are also required to provide constraints on the NRM and other magnetic properties (e.g., Koenigsberger ratio, Q) for refinement of the existing magnetic models.

5.3.2 Regional Search for Impact Structures

Hergarten and Kenkmann (2015) suggest that globally up to 90 impact structures in the 1-6 km range may yet remain to be discovered. The Holleford DEM (Fig. 5.2A) shows that the buried crater structure has a clear surface topographic expression even though the infill sediments are >200 m in thickness (Fig. 2.1A). Likewise, the Charity

Shoal suspected impact structure is a crater-form depression formed by draping of Paleozoic sedimentary strata over a buried crater-form basin in Mesoproterozoic basement rocks (Fig, 5.2B). The DEMs suggest that examination of digital topographic and multi-beam bathymetric data could be helpful in identifying the surface expression of buried impact structures (e.g., Beals, 1960; Herd et al., 2008). This process can be aided by automated routines that search DEM's for evidence of surface crater expression and may lead to the discovery of impact sites (Krøgli et al., 2007; Mu et al.,2020).

The three structures investigated in this thesis are located in the Precambrian Shield (Skeleton Lake) or close to the limits of the St. Lawrence Paleozoic platform, where the average thickness of the sediment cover is <300 m thick (Holleford, Charity Shoal). Kenkmann (2021) and others (e.g., Beals, 1960) have argued that continental Precambrian shields areas are the most likely locations for discovery of new impact structures, with burial below Paleozoic sediments better preserving these structures. This thesis demonstrates that areas of relatively thin Paleozoic cover sediments have a high potential for preservation of buried impact structures, that have surface topographic expression (Fig. 5.2). High-resolution DEMs (e.g., Fig. 5.2A) are now available for large parts of Ontario and other regions of Canada. LiDAR surveys with resolutions of 1-2 m are currently being conducted province-wide in Ontario (LIO, 2014). Previous workers have used aerial photography (Beals, 1960) to identify structures, but this recognition on airphotos requires a clear view of the structure, unaffected by ground vegetation or cloud cover. Newly available DEMs collected with LiDAR imaging provide the possibility of detecting impact crater that were obscured in aerial photos. The search for undiscovered impact craters can also be aided by airborne geophysical surveys collected for mineral exploration. High-resolution airborne gravity and magnetic surveys are becoming increasingly available in public databases. Ontario for example has in the last two decades acquired high-resolution aeromagnetic datasets for selected regions of the province with line spacings of < 400 m (Miles and Oneschuk, 2016). The magnetics and gravity data available in these public databases could be combined with the DEM and ground-based surveys and modelled using the approach here.

5.3.2 3-D Geophysical modelling

The modelling techniques demonstrated in this thesis can be employed broadly in investigation of deeply buried impact craters and for evaluating suspected impact structures. Robertson and Grieve (1975) in their review of Canadian impact structures, identified several probable impact craters, including Skeleton Lake. Some of these structures, such as Slate Island and Eagle Butte have now been confirmed as impact structures through field studies (PASSC, 2022). Other suspected impact structures, such as the Merewether structure, a small circular crater-form basin in Northern Labrador (Meen, 1957), have not been further examined. In southern Ontario, 3-D modelling could provide new insights into the depth and subsurface geometry of the CAN-AM structure, a >100 km circular magnetic feature in the Precambrian basement below southern Lake Huron (Forsyth et al., 1990). The Earth Impact Database is currently working to produce a listing of suspected structures which could be used to identify targets for geophysical modelling (PASSC, 2022).

An important area for future work is to evaluate the model uncertainty in forward and inversion modelling of impact structures using potential field data. It is widely recognized that potential field models are non-unique and may generate many equiprobable solutions to the inverse problem (Saltus and Blakely, 2011; Wellman and Caumon, 2018), but there are currently few guidelines on how to handle model uncertainty. Future work should include an examination of model uncertainty by investigations of known impact craters, where the subsurface geology is well-constrained by borehole data. A primary candidate for future 3-D geophysical modelling is Brent Crater, located some 130 km northeast of Skeleton Lake (Fig. 1.1). Brent is a ~3.8 km diameter structure with a ~6 mGal gravity anomaly and a small magnetic low over the centre of the structure (Millman et al., 1960). Borehole data at Brent have determined the crater infill stratigraphy, breccia thickness and presence of a melt lens (Millman et al., 1960; Grieve, 1978; McGregor et al., 2020). Two boreholes at Brent near the crater centre penetrated through the breccia layer to basement, which would provide an

important depth constraint for evaluating depth to basement estimates that could be obtained by modelling this structure. Given its size, Brent may also be a transitional crater (Kenkmann, 2021). Another possible candidate for 3-D modelling is the Kärdla (Estonia) impact structure, which has been investigated extensively by drilling and geophysical surveys (Puura and Suuroja,1992; Suuroja et al, 2002; Jõeleht et al., 2018).

5.4 References

Andrieux P. and Clark J.F. 1969. Application des méthodes électriques de prospection à l'étude du cratère d'Holleford. *Canadian Journal of Earth Sciences* 6(6): 1325-1337. https://doi.org/10.1139/e69-135

Beals C. S. 1960. A probable meteorite crater of Precambrian age at Holleford, Ontario. *Publications of the Dominion Observatory* 24(6). https://doi.org/10.4095/8727

Bell R.S. 2021. UAS magnetic surveys over the Crestone Crater. *In* Symposium on the Application of Geophysics to Engineering and Environmental Problems, Society of Exploration Geophysicists and Environment and Engineering Geophysical Society, p. 322. https://doi.org/10.4133/sageep.33-174

Clark J. F. 1982 Earth Physics Branch, Geomagnetic Report 81-2, 25 pages https://doi.org/10.4095/226536

Forsyth D. A., Pílkington M., Grieve R.A.F and Abbinett D.1990. Major circular structure beneath southern Lake Huron defined from potential field data. *Geology* 18 (8): 773–777. https://doi.org/10.1130/0091-7613(1990)018<0773:MCSBSL>2.3.CO;2

French B.M. 1998. Traces of Catastrophe: A Handbook of Shock-Metamorphic Effects in Terrestrial Meteorite Impact Structures. *LPI Contribution No.954,* Lunar and Planetary Institute, Houston. 120 p.

French B.M. and Koeberl C. 2010. The convincing identification of terrestrial meteorite impact structures: What works, what doesn't, and why. *Earth-Science Reviews* 98: 123-70 https://doi.org/10.1016/j.earscirev.2009.10.009

Miles W. and Oneschuk. D. 2016 Magnetic Anomaly Map Canada Geological Survey of Canada (GSC). Open File 77991 sheet, https://doi.org/10.4095/297337

Gittens J. and Lumbers S.B. 1972 Alkalic rock complexes and carbonatites of Ontario and part of Quebec. 24th International Geological Congress, Montreal, Guidebook, Field Excursion A53-C53 p. 41

Grant J. A. and Schultz P. H. 1993. Degradation of selected terrestrial and Martian impact craters. *Journal of Geophysical Research: Planets* 98(E6):11025-11042. https://doi.org/10.1029/93JE00121

Grieve R.A. 1978. The melt rocks at Brent crater, Ontario, Canada. In Lunar and Planetary Science Conference Proceedings, 9: 2579-2608.

Hall N.D. 2011. Oil and freshwater don't mix: transnational regulation of drilling in the Great Lakes. *Environmental Affairs and Law Review*, 38: 305-314.

Hergarten S. and Kenkmann T. 2015. The number of impact craters on Earth: Any room for further discoveries? *Earth and Planetary Science Letters*, 425:187-192. https://doi.org/10.1016/j.epsl.2015.06.009

Herd C. D. K., Froes D. G., Walton E. L., Kofman, R. S., Herd E. P. K. and Duke M. J. M. 2008. Anatomy of a young impact event in central Alberta, Canada: Prospects for the missing Holocene impact record. *Geology* 36(12):955-958. https://doi.org/10.1130/G25236A.1

Holcombe T.L., Youngblut S. and Slowey N. 2013 Geological structure of Charity Shoal crater, Lake Ontario, revealed by multi beam bathymetry. *Geo-Marine Letters* 33 (4): 245-252. https://doi.org/10.1007/s00367-013-0322-6

Indu G. K., James S., Chandran S. R., Aneeshkumar V., Keerthy S., Oommen T. and Sajinkumar K. S. 2022. Deriving a denudation index for terrestrial meteorite impact craters using drainages as proxies. *Geomorphology* 397:108007. https://doi.org/10.1016/j.geomorph.2021.108007

Jõeleht A., Plado J. and Sarv K. 2018. Kärdla impact crater–transitional from simple to complex based on reflection seismics. *EPSC Abstracts*, 12.

Kenkmann T. 2021. The terrestrial impact crater record: A statistical analysis of morphologies, structures, ages, lithologies, and more. *Meteoritics &Planetary Science*, *56*(5):1024-1070. https://doi.org/10.1111/maps.13657

Krøgli S. O., Dypvik H. and Etzelmüller B. 2007. Automatic detection of circular depressions in digital elevation data in the search for potential Norwegian impact structures. *Norwegian Journal of Geology/Norsk Geologisk Forening*, 87. https://foreninger.uio.no/ngf/ngt/pdfs/NJG_87_157-166.pdf

LIO 2014. Digital Raster Acquisition Project Eastern (DRAPE) Ontario (2014). Land Information Ontario, Ontario. https://geohub.lio.gov.on.ca/documents/digital-raster-acquisition-project-eastern-ontario-drape-2014/about

McGregor M., Dence M.R., McFarlane C.R. and Spray J.G. 2020. U–Pb geochronology of apatite and zircon from the Brent impact structure, Canada: a Late Ordovician Sandbian–Katian boundary event associated with L-Chondrite parent body disruption. *Contributions to Mineralogy and Petrology*, 175(7): 1-21. https://doi.org/10.1007/s00410-020-01699-9

McLaughlin P. I. and Brett C. E. 2004. Eustatic and tectonic control on the distribution of marine seismites: examples from the Upper Ordovician of Kentucky, USA. *Sedimentary Geology*, 168(3-4):165-192. https://doi.org/10.1016/j.sedgeo.2004.02.005

Millman P. M., Liberty B. A., Clark J. F. Willmore P. L. and Innes M. J. S. 1960. Publications of the Dominion Observatory 24:1 https://doi.org/10.4095/8722

Meen V.B. 1957. Merewether crater as a possible impact crater. *Proceedings of the Geological Association of Canada* (9):49-67

Mu Y., Zhang X., Xie W. and Zheng Y. 2020. Automatic detection of near-surface targets for unmanned aerial vehicle (UAV) magnetic survey. *Remote Sensing*, 12(3), 452. https://doi.org/10.3390/rs12030452

Ontario Geological Survey (OGS) 1999. Single Master Gravity and Aeromagnetic Data for Ontario. ERLIS Data Set GDS1035. http://www.geologyontario.mndm.gov.on.ca/mndmaccess/mndm_dir.asp?type=pub&id=GDS1035

Osinski G. R., Silber E. A., Clayton J., Grieve R. A. F., Hansen K., Kalynn J. and Tornabene L. L. 2019.Transitional impact craters on the Moon: Insight into the effect of target lithology on the impact cratering process. *Meteoritics & Planetary Science* 54:573–591. https://doi.org/10.1111/maps.13226

PASSC, 2022. Planetary and Space Science Centre, University of New Brunswick, Fredericton NB http://passc.net/EarthImpactDatabase/New%20website_05-2018/Index.html

Pilkington M. and Grieve R.A.F. 1992. The geophysical signature of terrestrial impact craters. *Reviews of Geophysics* 30: 161-81. https://doi.org/10.1029/92RG00192

Puura V. and Suuroja K. 1992. Ordovician impact crater at Kärdla, Hiiumaa Island, Estonia. *Tectonophysics*, 216(1-2):143-156. https://doi.org/10.1016/0040-1951(92)90161-X

Pratt D. A., McKenzie K. B. and White A. S. 2012. The remote determination of magnetic remanence. *ASEG Extended Abstracts*, 2012(1):1-5.

Robertson P. B. and Grieve R. A. F. 1975. Impact structures in Canada - heir recognition and characteristics. *Journal of the Royal Astronomical Society of Canada* 69:1-21.

Saltus R. W. and Blakely R. J. 2011. Unique geologic insights from" non-unique" gravity and magnetic interpretation. *GSA Today*, 21(12):4-11. https://doi.org/10.1130/G136A.1

Satterly J. 1970. Aeromagnetic maps of carbonatitie-alkalic Ontario Geological Survey, preliminary map no. 452 (revised)

St. John B. E. 1968. Paleolacustrine arenites in the Holleford meteorite crater, Ontario. *Canadian Journal of Earth Sciences* 5(4): 935-943. https://doi.org/10.1139/e68-090

Stewart S.A. 2003. How will we recognize buried impact craters in terrestrial sedimentary basins? Geology 31: 929-32, 31. https://doi.org/10.1130/G19853.1

Suttak P.A. 2013. High-resolution lake-based magnetic mapping and modeling of basement structures, with examples from Küçükçekmece Lagoon, Turkey and Charity Shoal, Lake Ontario. unpublished MS thesis, School of Geography and Earth Sciences, McMaster University, Hamilton, Ontario. 113 pp. http://hdl.handle.net/11375/13532

Suuroja K, Suuroja S, All T. and Floden T. 2002. Kärdla (Hiiumaa Island, Estonia) - the buried and well-preserved Ordovician marine impact structure. Deep Sea Research Part II: Topical Studies in Oceanography 49(6): 1121-1144. https://doi.org/10.1016/S0967-0645(01)00145-X

Thomas M. D., Ford K. L. and Keating P. 2016. Review paper: Exploration geophysics for intrusion-hosted rare metals. *Geophysical Prospecting* 64(5):1275–1304. https://doi.org/10.1111/1365-2478.12352

Tsikalas F. and Eldholm O. 2018. Malvinas (Falkland) Plateau Structure versus Mjolnir crater: Geophysical workflow template for proposed marine impact structures. *Meteoritics & Planetary Sciences* 54(3): 544-557 https://doi.org/10.1111/maps.13227

Vasconcelos M.A.R., Wünnemann K., Crósta, A.P., Molina E.C., Reimold W.U. and Yokoyama E. 2012. Insights into the morphology of the Serra da Cangalha impact structure from geophysical modeling. *Meteoritics & Planetary Science* 47: 1659-1670. https://doi.org/10.1111/maps.12001

Wallace K. and Eyles N., 2015. Seismites within Ordovician–Silurian carbonates and clastics of Southern Ontario, Canada and implications for intraplate seismicity. *Sedimentary Geology*, 316:80-95. https://doi.org/10.1016/j.sedgeo.2014.12.004

Waddington E. D. and Dence M. R. 1979. Skeleton Lake, Ontario: evidence for a Paleozoic impact crater. *Canadian Journal of Earth Sciences* 16(2):256-263. https://doi.org/10.1139/e79-025

Wellmann F. and Caumon G. 2018. 3-D Structural geological models: Concepts, methods, and uncertainties. *Advances in Geophysics*, 59:1-121. https://doi.org/10.1016/bs.agph.2018.09.001